Analyse von Fe65/Fe65L1 an Knockout Mausmodellen

vom Fachbereich Biologie der Universität Kaiserslautern zur Verleihung des

akademischen Grades „Doktor der Naturwissenschaften" genehmigte Dissertation,

vorgelegt von

Dipl. Biol. Paul Strecker

Kaiserslautern, im Oktober 2017

Datum der wissenschaftlichen Aussprache: 1.12.17

Prüfungskommission

Vorsitzender: Prof. Dr. Thorsten Stoeck, Technische Universität Kaiserslautern

Gutachter: 1. Prof. Dr. Stefan Kins, Technische Universität Kaiserslautern

2. Prof. Dr. Claus Pietrzik, Johannes Gutenberg-Universität Mainz

Die vorliegende Arbeit wurde in der Abteilung Humanbiologie und Humangenetik im Fachbereich Biologie der Technischen Universität Kaiserslautern unter Anleitung von Prof. Dr. Stefan Kins durchgeführt.

Declaration

I hereby declare that I have produced the present dissertation independently. The use of other sources or auxiliary material has been properly and fully acknowledged. Furthermore, I declare that the present dissertation has not been presented complete or partial to any other institution or university with the aim to obtain an academic degree.

Statement of own contribution to publications

Paul Strecker, Susann Ludewig, Marco Rust, Tabea A. Mundinger, Andreas Görlich, Elisa G. Krächan, Christina Mehrfeld, Joachim Herz, Martin Korte, Suzanne Y. Guénette & Stefan Kins (2016) FE65 and FE65L1 share common synaptic functions and genetically interact with the APP family in neuromuscular junction formation. Scientific Reports | 6:25652 | DOI: 10.1038/srep25652

Author contribution: I designed the study, performed behavioral, immunohistochemical and statistical analysis, interpreted the results, prepared figures, wrote and revised the paper.

Lukas P. Feilen, Kevin Haubrich, **Paul Strecker**, Sabine Probst, Simone Eggert, Gunter Stier, Irmgard Sinning, Uwe Konietzko, Stefan Kins, Bernd Simon and Klemens Wild (2017) Fe65-PTB2 Dimerization Mimics Fe65-APP Interaction. Front. Mol. Neurosci. 10:140. doi: 10.3389/fnmol.2017.00140

Author contribution: I contributed and analyzed data, prepared figures, reviewed drafts of the manuscript and revised the paper.

Uta-Mareike Herr [†], **Paul Strecker** [†], Steffen E. Storck, Carolin Thomas, Verena Rabiej, Anne Junker , Sandra Schilling , Nadine Schmidt , C. Marie Dowds , Simone Eggert , Claus U. Pietrzik and Stefan Kins (2017) LRP1 Modulates APP Intraneuronal Transport and Processing in Its Monomeric and Dimeric State. Front. Mol. Neurosci. 10:118. doi: 10.3389/fnmol.2017.00118

[†] These authors have contributed equally to this work.

Author contribution: I contributed and analyzed data, performed live cell imaging, protein-biochemical and statistical analysis, interpreted the results, prepared figures, wrote and revised the paper.

Kaiserslautern, den 27.10.2017

_____

Paul Strecker

Contens

Introduction

The Fe65 protein family

The conserved mammalian Fe65 multi-adaptor protein family consists of three members, namely Fe65, Fe65 like 1 and 2 (Fe65L1, Fe65L2). Thereby, Fe65 is enriched in brain (in dependence of its splice variant, see below) while Fe65L1 as well as Fe65L2 are more widely expressed (Bressler et al. 1996, Guénette et al. 1996, Tanahashi & Tabira 2002). The first member of this protein family was initially identified by F. Esposito and co-workers and named after its discoverer and the clone number 65 of the cDNA library (Esposito et al. 1990). It was originally described as a transcriptional activator with homology to the DNA binding domain of retroviral integrases (Duilio et al. 1991). However, two database searches identified a WW domain and two phosphotyrosine-binding domains indicating a function in membrane- as well as receptor-associated signal transduction (Bork & Margolis 1995, Bork & Sudol 1994). This assumption was further supported by the finding that Fe65 interacts with the amyloid precursor protein (APP) (Fiore et al. 1995, McLoughlin & Miller 1996), a type I transmembrane protein, which plays an important role in Alzheimers Disease (AD) (see below), placing Fe65 in the focus of AD research. Soon after this study, both homologues Fe65L1 and Fe65L2 were characterized and reported to bind to APP as well (Guénette et al. 1996, Duilio et al. 1998, Tanahashi & Tabira 1999). Due to this interaction with APP, the Fe65 gene was called *APBB* (APP binding family B; *APBB1,2,3* encoding for Fe65, Fe65L1 and Fe65L2, respectively (Blanco et al. 1998)). Intensive investigations during the last 20 years mainly focused on Fe65. Studies of the Fe65 interactome revealed up to date more than 20 putative protein interaction partners (Nensa et al. 2013 and recently reviewed in Chow et al. 2015), which bind to the three domains of the Fe65 protein family and influencing a diversity of cellular functions including cytoskeletal remodeling (Ermekova et al. 1997, Ikin et al. 2007, Cheung et al. 2014), calcium homeostasis (Nensa et al. 2013), nuclear signaling (Cao & Südhof 2001) and synaptic vesicular loading and release (Nensa et al. 2013).

Structural properties of the Fe65 protein family

The Fe65 protein family is evolutionary conserved from worms to human. In mammals it includes the two paralogs Fe65L1 and Fe65L2, harboring all three a WW domain and C-terminally two phosphotyrosine-binding domains 1 and 2 (PTB1 and PTB2), schematically illustrated in Figure 1 (Meiyappan et al. 2007, Radzimanowski et al. 2008a, Radzimanowski et al. 2008b).
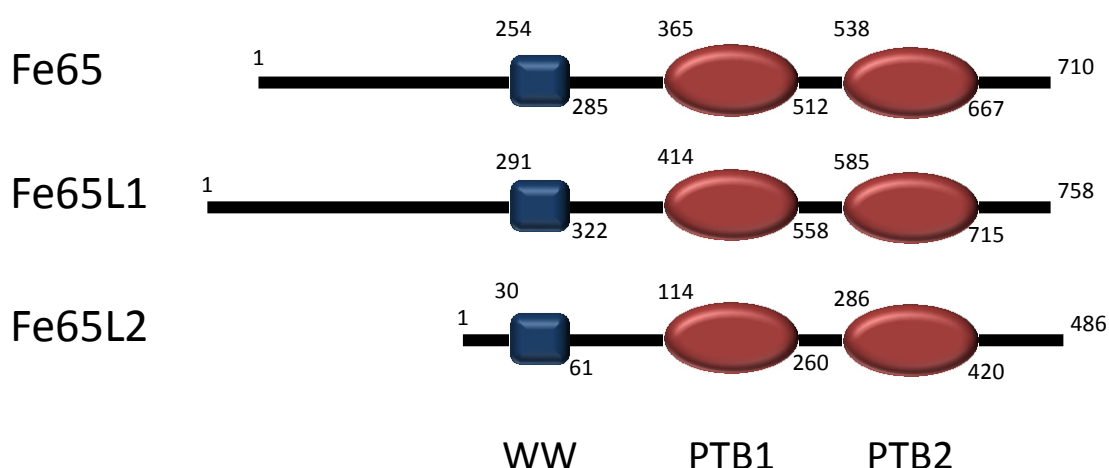

Figure 1: Schematic structure of the human Fe65 protein family.

The amino acid numbering for the WW (blue squares) as well as the PTB 1 and PTB 2 (red oval) domain is depicted for all members of the Fe65 protein family. WW (tryptophan, tryptophan) protein interaction domain; PTB, phosphotyrosine binding domain.

All three proteins share a remarkable amino acid as well as domain homology but diverge in their N-termini. Human Fe65 has an N–terminal 253 amino acid long sequence before the WW domain, while the according regions in Fe65L1 and Fe65L2 are 290 and 29 amino acids long. Additionally, Fe65L2 harbours a 23 amino acids longer C-terminus compared to its two paralogs.

Fe65 expression is highly regulated during mouse brain development with increasing levels in early phase and declining levels in late phase of embryogenesis followed by an increased expression after postnatal day 10 (Kesavapany et al. 2002). Detailed analysis of Fe65L1 and Fe65L2 expression during development are lacking.

Splicing of Fe65 leads to different isoforms in mouse brain resulting in a full length isoform p97Fe65 mainly expressed in neuronal tissues or a shorter p60Fe65 isoform (Wang et al. 2004, Cool et al. 2010) occurring especially in non-neuronal cells of the cerebral cortex, cerebellum, hippocampus and the amygdala (Hu et al. 1999, Domingues et al. 2011). Furthermore, Fe65 undergoes proteolytic cleavage leading to the product p65Fe65 with an increased affinity for APP compared to full length p97Fe65 (Hu et al. 2005, Saeki et al. 2011). Moreover, further increasing the complexity, also polymorphisms of Fe65 have been identified leading to an altered PTB2 domain lacking the amyloid precursor protein (APP) binding site (Hu et al. 2002) and is speculated to be responsible for resistance to the very late onset of AD (Hu et al. 2002). Similarly, for F65L1 and Fe65L2 different splice variants have been described, which have an influence on cell cycle control, DNA damage response and Aβ production (a small peptide resulting after APP cleavage and main component of senile plaques, see below) (Penna et al. 2013, Tanahashi & Tabira 2002). Further, in a study of Golanska and co-workers a polymorphism of Fe65L1 was analyzed where an association with severe cognitive impairments in centenarians has been described (Golanska et al. 2013). How these different splice variants, polymorphisms and cleavage products exactly influence Fe65 protein family´s function or localization *in vivo* is still not well determined and needs to be examined in the future to shed light on the physiological relevance of the Fe65 protein family.

Interaction partners and function of the Fe65 protein family

The most prominent interaction partners of the Fe65 protein family are the amyloid precursor protein (APP) and its homologs, APP like protein 1 and 2 (APLP1, APLP2) playing an important function in diverse cellular processes, including cell adhesion, neurite outgrowth and synaptogenesis (recently reviewed in (Guénette et al. 2017, Sosa et al. 2017, Muller et al. 2017)). All Fe65 family members interact via their PTB2 domains with the NPTY motif of the different APP/APLPs intracellular domains (ICDs) (Fiore et al. 1995, Borg et al. 1996, Bressler et al. 1996, Guénette et al. 1996, McLoughlin & Miller 1996, Duilio et al. 1998, Tanahashi & Tabira 1999). The precise interaction between Fe65 PTB2 and the intracellular domain of APP has been characterized in detail by co-crystallization of the Fe65 PTB2 domain and AICD, via

Nuclear Magnetic Resonance (NMR) experiments and Molecular Replacement methods, showing that the interaction is phophotyrosine independent (Radzimanowski et al. 2008b). Interestingly, the NPTY motif is recognized in a β-augmentation manner placing the PTB-relevant tyrosine in its binding pocket. Further, the AICD/Fe65- PTB2 complex is capped by the T^{668}PEE-motif of the N-terminal binding helix αN within the AICD (Radzimanowski et al. 2008b) whose threonine T^{668} phosphorylation was shown to regulate the interaction (Ando et al., 2001). This interplay might lead to different functions in the aspect of processing and intracellular signaling/transactivation of genes by the APP family on the one hand and to cellular movement and actin cytoskeleton remodeling on the other hand (see below). The APP protein family members are all type I membrane glycoproteins and processed mainly by the α-,β- and γ-secretases, resulting in the cytosolic release of the ICDs illustrated in Figure 2 (Eggert et al. 2004, Haass et al. 2012).
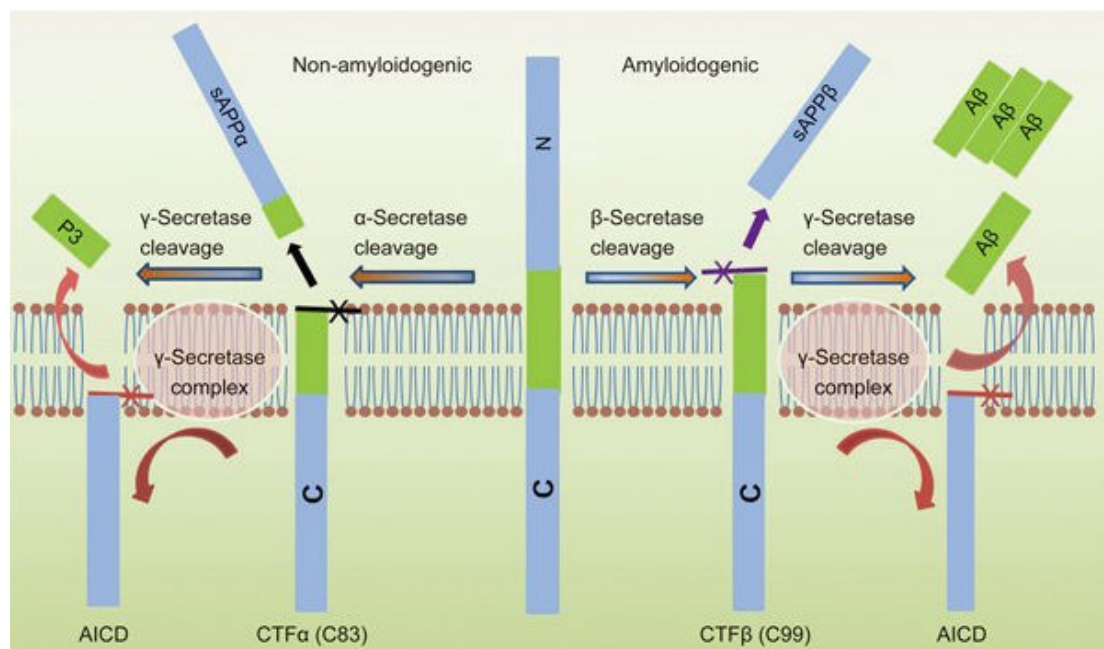

Figure 2: Processing of human APP (adopted from Chen et al. 2017).

Non-amyloidogenic and amyloidogenic processing of human APP. Non-amyloidogenic processing is initiated by the α-secretase, cleaving APP within the Aβ-sequence leading to the release of sAPPα (soluble APP after α-secretase cleavage) and a membrane bound CTFα (C-terminal fragment after α-secretase cleavage). CTFα is further processed by γ-secretases to generate extracellular P3 and the APP intracellular domain (AICD). The amyloidogenic pathway is initiated by the β-secretase cleaving APP at the N-terminus of the Aβ sequence leading to the release of sAPPβ (soluble APP after β-secretase cleavage) and a membrane bound CTFβ. CTFβ is afterwards processed by γ-secretases to generate extracellular the Aβ peptide which in the case of Alzheimers Disease accumulates to Aβ plaques and the APP intracellular domain (AICD).

Interestingly, only interconnected with Fe65 ICDs of APP and APLP2 can translocate to the nucleus, which was not observed for the ICD of APLP1 (Gersbacher et al. 2013). Furthermore, although Fe65, Fe65L1 and Fe65L2 are mainly present in the nucleus (Bruni et al. 2002), solely Fe65 in complex with APP is capable to regulate gene expression (Cao & Südhof 2001, Telese et al. 2005). In contrast, co-expression of APP together with Fe65L1 or Fe65L2 prevents their nuclear translocation (Bruni et al. 2002).

The Aβ peptide arises only in the so called amyloidogenic pathway of APP processing especially by proteolytic shedding of the β- and ɣ-secretase (Figure 2) resulting in the formation of senile plaques in AD patients (Aleksis et al. 2017, Chen et al. 2017). The influence of the Fe65 protein family on APP processing and Aβ generation provided contradictory results. Initial *in vitro* studies showed that Fe65 promotes Aβ generation (Sabo et al. 1999), whereas following analysis reported an inhibition in Aβ production (Ando et al. 2001). For Fe65L1 and Fe65L2 also an enhanced production of Aβ species was reported (Tanahashi & Tabira 2002, Chang et al. 2003). Also *in viv*o as well as *ex viv*o analysis demonstrated inconsistent findings. Analysis of primary neurons of transgenic APPswe mice expressing human APP with a familiar Alzheimer causing mutation (swe, Swedish; carrying an APP mutation which leads to higher amounts of APP; for detailed overview of APP mouse models in AD research see (Sasaguri et al. 2017)) and a partial Fe65 Knock Out (KO) double mutant mice exhibited less Aβ compared to neurons of APPswe mutant mice (Wang et al. 2004). Further, investigations of young male Fe65/Fe65L1 Double KO (DKO) mice showed a moderate reduction in the cerebral Aβ amount (Guénette et al. 2006). On the other hand overexpression of Fe65 in APP transgenic mice leads to lowered levels of cerebral Aβ (Santiard-Baron et al. 2005). Also the influence of Fe65 on sAPP secretion is yet unclear, as several studies reported contradictory results (Hu et al. 2005, Hoe et al. 2006). Possibly, to unravel the influence of the Fe65 protein family on APP processing and Aβ production further studies will be necessary considering the different isoforms, splice and cleavage products as well as phosphorylation status of the APP and Fe65 protein family.

Besides APP/APLPs that are bound by the PTB2 domain, several PTB1 domain interacting proteins were reported (Muller et al. 2017), including the histone acetyltransferase Tat-interacting protein 60 kDa (Tip60) and the transcription factor Alpha-globin transcription factor CP2/Late SV40 Factor/Lipopolysaccharide Binding

Protein 1 (CP2/LSF/LBP1) (Zambrano et al. 1998, Cao & Südhof 2001). Thereby, a tripartite complex of Fe65/AICD and one of the mentioned transcription factors might translocate to the nucleus regulating gene activation by forming nuclear aggregates, called spheres or speckles (recently reviewed in Bukhari et al. 2017). The precise mechanism of complex formation and translocation to the nucleus still remains elusive, but a general consensus has been built that initially Fe65 is tethered to the plasma membrane and membrane-bound AICD directly interconnects with Fe65 by forming an APP/Fe65 complex (Cao and Sudhof 2004, Goodger et al. 2009, Nensa et al. 2014, Bukhari et al. 2016). This interaction leads to a conformational change and subsequently to Fe65 activation. After activation, the AICD/Fe65 complex translocates to the nucleus, interacts with Tip60 and leads to the formation of a nuclear APP/Fe65/Tip60 complex (Cao and Sudhof, 2004).

However, despite intensive examination various results have been described regarding the influence on gene regulation of the Fe65/AICD complex. For example, Hebert and co-workers showed in a luciferase-based reporter assay the activation of gene transcription of KAI, APP, Hes1 or SV40 (Hebert et al. 2006), while others could demonstrate that increased AICD/Fe65-complex formation does not influence gene activation of KAI and APP (Waldron et al. 2008).

Another finding addressing the nuclear function of Fe65 is the interaction with the Bloom syndrome protein (BLM), which plays a role in DNA replication and repair mechanisms, by forming nuclear Fe65/BLM containing spheres exclusively occuring in neurons (Schrötter et al. 2013, Kolbe et al. 2016). These Fe65/BLM spheres are postulated to regulate cell cycle re-entry in neurons of AD patients (Schrötter et al. 2013). Intriguingly, it was shown that Fe65 plays a pivotal role in DNA damage response in the cell after X-ray treatment of mouse embryonic fibroblasts isolated from Fe65 KO mice (Minopoli et al. 2007).

Further, Fe65 PTB1 domain was shown to interact with members of the low density lipoprotein receptor (LDLR) family (Figure 3), for instance with the Low density lipoprotein receptor-related protein 1 (LRP1) (Trommsdorff et al. 1998), very-low-density-lipoprotein receptor (VLDLR) (Dumanis et al. 2012), Megalin/LRP2 (Alvira-Botero et al. 2010) and ApoEr2 (Hoe et al. 2006) which all of them harboring at least one NPxY motif in their intracellular domains (Pohlkamp et al. 2017). All members of the LDLR family are, likewise the members of APP protein family, type I

transmembrane proteins, mainly involved in lipid metabolism and take part in a broad range of pre- and post-developmental functions in brain (Pohlkamp et al. 2017).
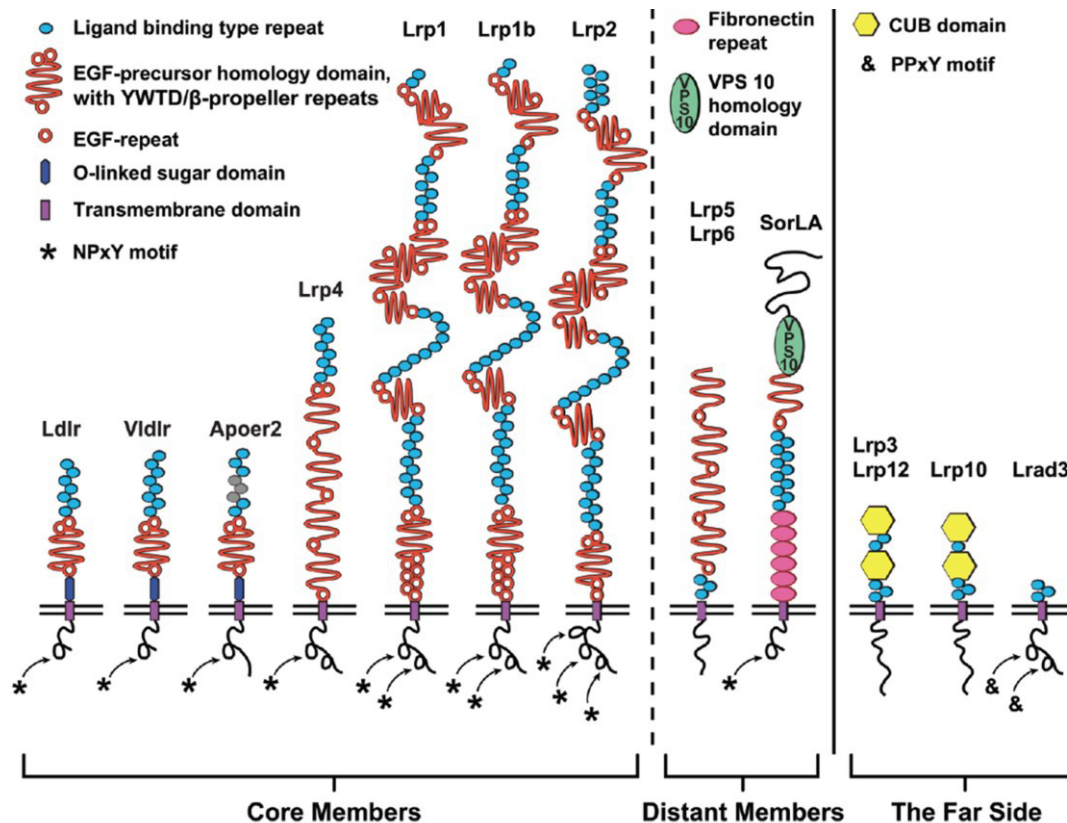

Figure 3: The low-density lipoprotein (LDL) receptor family (adopted from Pohlkamp et al. 2017).

Schematic drawing of the domain structure of the LDL receptor family members grouped in "Core Members", "Distant Members" and "The Far Side". The seven "Core Members" are LDL receptor (Ldlr), very-LDL receptor (Vldlr), Apolipoprotein E (ApoE) receptor 2 (Apoer2/Lrp8), LDL receptor related protein (Lrp)-4 (Lrp4), Lrp1, Lrp1b and Lrp2 and are classified by at least one NPxY domain (asterix) and a combination of two LDL receptor domains, namely the ligand binding domain (blue) and an epidermal growth factor (EGF)-precursor homology domain (orange). Ldlr, Vldlr and Apoer2 contain an additional extracellular O-linked sugar (OLS) domain. The two "Distant Members" include the NPxY-lacking Lrp5/Lrp6 and the hybrid SorLA with additional Fibronectin repeats (pink) and the VPS10p-sorting motif (green). The three "far side" proteins solely express ligand binding-type repeats. Lrp3, Lrp10 and Lrp12 also encoding a typical CUB-domain (binds Complement, Uegf and Bmp1). In addition alternative splicing of Apoer2 produces splice variants lacking N-terminal ligand binding type repeats.

Beside this physiological relevant functions the LDLR family plays a key role in AD by influencing APP processing in neurons and astrocytes as well as Aβ clearance in endothelial cells of the blood brain barrier (BBB) and ependymal cells of the blood cerebrospinal fluid (CSF) (Wagner & Pietrzik 2012, Lane-Donovan et al. 2014). Interestingly, the members of the LDLR family are processed by the same secretases

as the APP family thereby partially competing with the latter (Wasser et al. 2014, Nakajima et al. 2013, Zurhove et al. 2008, von Arnim et al. 2005, von Einem et al. 2010, Irizarry et al. 2004). In this manner, Fe65 links the proteins of the LDLR family with APP forming a tripartite complex and regulates APP processing and/or Aβ production by among others changing the endocytosis rates or trafficking of APP (Pietrzik et al. 2004,Dumanis et al. 2012, Alvira-Botero et al. 2010). Whether Fe65L1 or Fe65L2 are also involved in modulating LRP1 function is yet unclear. However, due to the high homology between the different protein family members in the PTB1 domain, an interconnection appears well feasible.

ADP-ribosylation factor 6 (ARF6), an intriguing Fe65 PTB1 binding partner was recently described to influence the endocytosis and membrane trafficking of APP in neurons by probably forming a Fe65/APP/ARF6 complex (Cheung et al. 2014, Tang et al. 2015). Further, this interaction of Fe65 and ARF6 was reported to affect Rac1 signaling, involved in regulation of spine formation as well as neurite outgrowth (Cheung et al. 2014). Both, ARF6 and Rac1 belong to the family of small Rho GTPases involved in synaptic function and plasticity during NMDA receptor mediated long term potentiation (LTP) and long term depression (LTD) (Haditsch et al. 2009, Oku & Huganir 2013, Scholz et al. 2017). The impact of Fe65 in LTP and hippocampus dependent learning and memory formation has already been described (discussed in more detail below) (Wang et al. 2009) and might partially include signaling via ARF6 or Rac1. Interestingly, a direct influence of the AICD on LTP was reported by controlling GluN2B-containing NMDA receptors at immature excitatory synapses including AICD/Fe65 binding (Pousinha et al. 2017). Further, Fe65 is also able to directly interact with Rac1 (Wang et al. 2011) and thereby possibly regulates actin skeleton remodeling. A recent study showed the influence of the Fe65/Rac1 pathway and its impact on APP mediated axon guidance and neural circuit formation during mouse brain development by activating the intracellular Pak1 complex (Wang et al. 2017).

Studies of Fe65 WW domain identified an interaction with the proline rich motif of mammalian enabled (Mena) (Ermekova et al. 1997) and thereby modulating actin polymerization and cell movement in complex with APP (Sabo et al. 2001). Indeed, recovery of the tripartite complex of Mena/Fe65/APP and the co-localization of these proteins in growth cones and synapses implies such a function in neurons (Sabo et al. 2003, Ikin et al. 2007). Consistent with this hypothesis that Fe65 might regulate

APP dependent neuronal growth and/or migration, Fe65/Fe65L1 DKO, APP/APLP1/APLP2 Triple KO (TKO) mice as well as Mena KO mice exhibit similar phenotypes regarding the occurrence of ectopic cortical neurons and axonal pathfinding defects (discussed in more detail below) (Herms et al. 2004, Guénette et al. 2006, Goh et al. 2002). Besides this role in actin remodeling via binding to Mena, the WW domain was found to interact with Abl tyrosine kinase and the nucleosome assembly factor SET, which plays an intriguing role in nuclear signaling and transcriptional activation (Zambrano et al. 2001, Perkinton et al. 2004, Telese et al. 2005). Furthermore, it was shown to bind to the P2X2 receptor subunits at excitatory synapses and modulate receptor function (Masin et al. 2006).

Here, only the best known Fe65 binding partners are introduced. In fact the current picture of the Fe65 interactome is much more complex, involving a variety of interaction partners with very diverse cellular functions (Muller et al. 2017), including regulation of gene expression, actin polymerization/remodeling and endocytosis. Most of the findings originated from *in vitro* experiments. However, to gain a deeper understanding of the function *in vivo* several mouse models were generated to examine its function in a complex living organism.

Fe65 protein family KO mice

Two independently generated Fe65 KO mouse models have provided a deeper understanding of the biological function of the Fe65 protein family (Wang et al. 2004, Guénette et al. 2006). Since Fe65 is mainly expressed in the cerebral cortex and hippocampus (Kesavapany et al. 2002) which are the brain regions important for memory acquisition and learning, the first described Fe65 KO mouse, a p97Fe65 isoform specific KO, provided important evidences in this field. p97Fe65 KO mice are viable and showed no obvious physical or histopathological abnormalities, but revealed impairments in learning and memory (Wang et al. 2004). They showed deficits in the passive avoidance test and in the hidden platform task of the Morris Water Maze (MWM) test indicating disturbances in spatial learning properties. Interestingly, only older mice (>14 month) displayed the observed phenotypes whereas younger animals (2-4 months) performed normal in comparison to wildtype (WT) mice (Wang et al. 2004, Wang et al. 2009). Further analysis examining the LTP

features *in vivo* uncovered deficits only in the early phase of LTP after a single 100 Hz train (Wang et al. 2009) implicating a potential role in short-term plasticity but affecting spatial memory formation only to a lower extend. However, these mice exhibit a five-fold upregulation of the N-terminal truncated isoform p60Fe65 which might compensate the loss of the p97Fe65 isoform and therefore reasoning the only minor detected defects.

The second Fe65 KO mouse model was generated by Guénette and co-workers lacking both isoforms p97Fe65 as well as p60Fe65. Additionally, they generated the first Fe65L1 KO mouse model and by crossing with the Fe65KO mice the Fe65/Fe65L1 DKO mouse model (Guénette et al. 2006). Histological examination of both single KO mice revealed no gross defects in brain or organ formation. Also initial observations revealed no abnormal behavior in housing cages but detailed analyses are missing. However, deficits in the hanging wire task have been described for Fe65 KO as well as Fe65L1 KO mice (Suh et al. 2015). Moreover, in older Fe65L1 KO mice (>14 months) lens degradation and cataract phenotypes have been detected. In contrast to single KO mice Fe65/Fe65L1 DKO mice displayed abnormal circling behavior in housing cages, aggravated impairments in the hanging wire task as well as lens degradation and cataract phenotypes in all examined older mice (Guénette et al. 2006, Suh et al. 2015). In addition, centralized nuclei in muscle cells, an indication for muscle degeneration (Bassez et al. 2008), of the quadriceps were found possibly explaining the poor performance in the hanging wire test. The most remarkable observation has been made in the Fe65/Fe65L1 DKO mice brain after histological examination. Those brains displayed deficits in neuronal positioning and axon outgrowth in the cortex (Figure 4) as well as disruptions of the pial-meningeal basement membrane with altered laminin organization (Guénette et al. 2006).
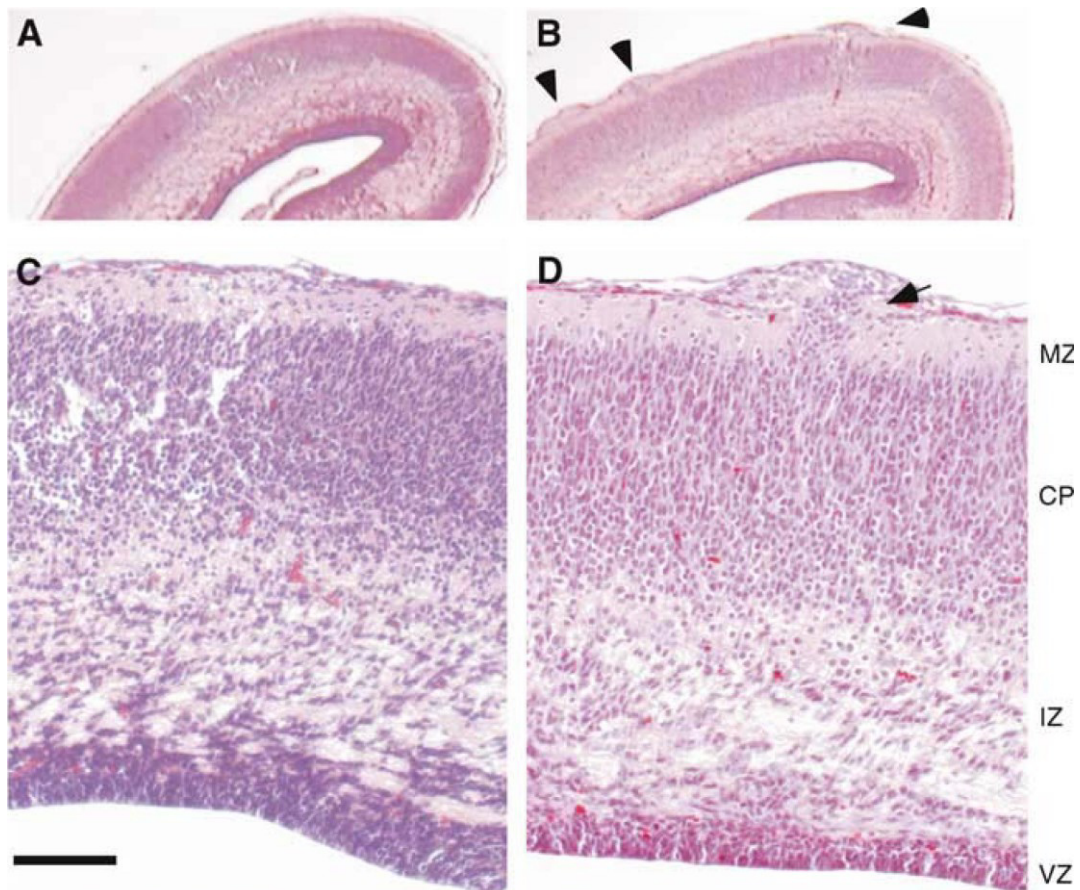
Figure 4: Cortical abnormalities in Fe65/Fe65L1 DKO mice (adoptted from Guénette et al. 2006).

H&E staining of coronal sections of embryonal stage E18.5 mouse cortices of WT littermates (A,C) and Fe65/Fe65L1 DKO (B,D) mice. Arrowheads point to ectopic cells on the surface of the E18.5 cortex of Fe65/Fe65L1 DKO mice (B) and arrows indicate ectopic neurons which have invaded the marginal zone (MZ) of E18.5 cortex (D). Scale bar, 100 mm. CP, cortical plate; IZ, intermediate zone; VZ, ventricular zone.

Interestingly, similar phenotypes have been described in mice lacking all three members of the APP protein family (see below) (Herms et al. 2004).

APP protein family KO mice

Single disruption of APP, APLP1 or APLP2 caused only minor abnormalities in APP KO mice, namely reduced body as well as reduced brain weights and no significant changes in APLP1 KO or APLP2 KO mice (Müller et al. 1994, Zheng et al. 1995, von Koch et al. 1997, Heber et al. 2000, Weyer et al. 2011, Midthune et al. 2012). However, aged APP KO mice showed impairments in behavior, LTP measurements and spine density (Müller et al. 1994, Ring et al. 2007, Seabrook et al. 1999, Weyer et al. 2014). Recent studies of aged APLP1 KO mice revealed reduced spine density and impairments in synaptic transmission as well (Schilling et al. 2017).
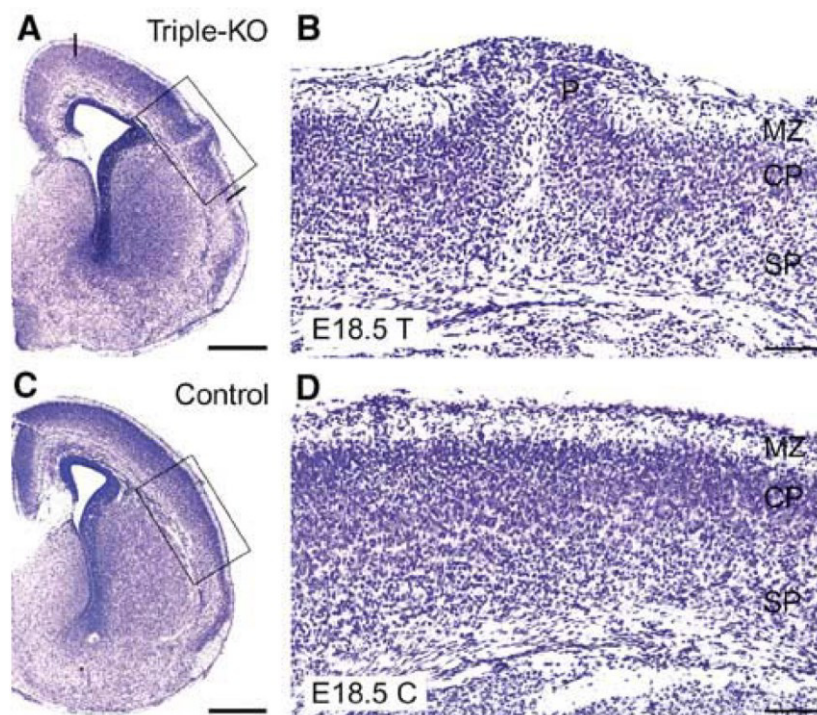

Figure 5: Cortical dysplasia in APP/APLP1/APLP2 TKO mice (adopted from Herms et al. 2014)

Cresyl violet staining of coronal sections of a triple knockout mouse brain (A,B) at E18.5 in comparison to littermate control (APP$^{-/-}$, APLP1$^{-/+}$, APLP2$^{-/-}$, C,D). Compared to the region of littermate controls boxed in (C) and enlarged in (D) a protrusion (P) of the right hemispheric cortical plate boxed in (A) and enlarged in (B) is shown. Ectopias were restricted to dorsal cortical areas as indicated in (A) and neurons disrupt the subplate (SP) and cortical plate (CP) by overmigrating into the marginal zone (MZ). Scale bars, 500 mm.

In contrast, combined KO mice with loss of APP and APLP2 or APLP1 and APLP2 showed an early perinatal lethal phenotype (Heber et al. 2000), which might be

explained by deficits in neuromuscular junction (NMJ) formation, comprising improper positioning of the pre- and postsynaptic site (Wang 2005, Klevanski et al. 2014). An intriguing finding was made after crossing APPΔCT (lacking the last 15 amino acids including the Fe65 interaction motive YNPTY) mice with APLP2 KO mice thereby partially rescuing the lethal phenotype of the DKO mice without ameliorating the NMJ defects (Klevanski et al. 2015). This implies an important function of the binding partners of the intracellular domain of APP in NMJ formation and pre- and postsynaptic apposition. However, APP/APLP1 DKO mice are viable and show no aggravated phenotypes compared to single APP KO or APLP1 KO mice (Heber et al. 2000), thus indicating an important key role of APLP2 in physiological function and a functional redundancy between the homologs. Interestingly, TKO mice lacking all three APP family members die directly after birth (Herms et al. 2004). In comparison to the lethal APP/APLP2 DKO or APLP1/APLP2 DKO mice histological examination of the brain of the TKO mice revealed cranial abnormalities like focal dysplasia and partial loss of Caja-Retzius cells, resembling human type II lissencephaly. Within the affected areas neuronal cells migrated beyond their usual position and disrupted the marginal zone layering (Figure 5). Compared to the observed cranial phenotype in brains of Fe65/Fe65L1 DKO mice a remarkable correlation is noticeable indicating a pivotal role for the APP protein family members in neuronal adhesion and positioning, very likely mediated by the members of the Fe65 protein family.

Outline of this thesis

The main goal of my thesis was to characterize the Fe65 KO, Fe65L1 KO and Fe65/Fe65L1 DKO mouse model generated by Guénette and co-workers (Guénette et al. 2006) in various behavioral experiments focusing on locomotion, strength as well as learning and memory formation. Furthermore, I intended to examine the influence of the Fe65 protein family on LRP and/or APP fast axonal transport and checked the dimerization properties of Fe65 *in vitro*.

My thesis comprises three main chapters, which are presented hereafter with the corresponding publications.

I) The first part of my thesis, addressed the influences of the Fe65 protein family on mouse behavior by using different approaches measuring learning and memory consolidation as well as locomotion and grip strength. Furthermore I extended the NMJ analysis in Fe65 protein family KO mice during my diploma thesis (Strecker, 2012) by comparing the NMJ formation of Fe65/APLP2 KO and Fe65L1/APLP2 KO mice to NMJ of single Fe65 KO and Fe65L1 KO mice, respectively.

Paul Strecker, Susann Ludewig, Marco Rust, Tabea A. Mundinger, Andreas Görlich, Elisa G. Krächan, Christina Mehrfeld, Joachim Herz, Martin Korte, Suzanne Y. Guénette & Stefan Kins. *Scientific Reports* | 6:25652 | DOI: 10.1038/srep25652

II) Fe65 with its two phosphotyrosine domains interacts with a variety of intracellular proteins and builds a functional linker. A way to control this interaction is the phosphorylation of Fe65 or the binding partners. The dimerization of Fe65 as an additional control mechanism and thereby a possible influence on APP binding was analyzed in the second part of my thesis by *in vitro* co-immunoprecipitation experiments and Blue Native Gel analysis.

Lukas P. Feilen, Kevin Haubrich, **Paul Strecker**, Sabine Probst, Simone Eggert, Gunter Stier, Irmgard Sinning, Uwe Konietzko, Stefan Kins, Bernd Simon & Klemens Wild. *Front. Mol. Neurosci*. 10:140. doi: 10.3389/fnmol.2017.00140

III)   The third part of my thesis concentrated on the function of Fe65 as scaffolding protein linking APP and LRP1. Here, the influence of APP on LRP1 and LRP1 on APP in absence/presence of Fe65 was investigated. Moreover, the first characterization of LRP1 axonal transport was examined.

References

Aleksis, R. et al., 2017. Structural studies of amyloid-β peptides: Unlocking the mechanism of aggregation and the associated toxicity. Biochimie, 140, pp.176–192.

Alvira-Botero, X. et al., 2010. Megalin interacts with APP and the intracellular adapter protein FE65 in neurons. Molecular and Cellular Neuroscience, 45(3), pp.306–315.

Ando, K. et al., 2001. Phosphorylation-dependent Regulation of the Interaction of Amyloid Precursor Protein with Fe65 Affects the Production of Aβ-Amyloid. Journal of Biological Chemistry, 276(43), pp.40353–40361.

Von Arnim, C.A.F. et al., 2005. The low density lipoprotein receptor-related protein (LRP) is a novel β-secretase (BACE1) substrate. Journal of Biological Chemistry, 280(18), pp.17777–17785.

Bassez, G. et al., 2008. Type 2 Myotonic Dystrophy Can Be Predicted by the Combination of Type 2 Muscle Fiber Central Nucleation and Scattered Atrophy. Journal of Neuropathology & Experimental Neurology, 67(4), pp.319–325.

Blanco, G. et al., 1998. Mapping of the human and murine X11-like genes (APBA2 and Apba2), the murine Fe65 gene (Apbb1), and the human Fe65-like gene (APBB2): Genes encoding phosphotyrosine-binding domain proteins that interact with the Alzheimer's disease amyloid precursor prote. Mammalian Genome, 9(6), pp.473–475.

Borg, J.P. et al., 1996. The phosphotyrosine interaction domains of X11 and FE65 bind to distinct sites on the YENPTY motif of amyloid precursor protein. Molecular and cellular biology, 16(11), pp.6229–6241.

Bork, P. & Margolis, B., 1995. A phosphotyrosine interaction domain. Cell, 80(5), pp.693–694.

Bork, P. & Sudol, M., 1994. The WW domain: A signaling site in dystrophin? Trends in Biochemical Sciences, 19(12), pp.531–533.

Bressler, S.L. et al., 1996. cDNA cloning and chromosome mapping of the human Fe65 gene: interaction of the conserved cytoplasmic domains of the human beta-amyloid precursor protein and its homologues with the mouse Fe65 protein. Human molecular genetics, 5(10), pp.1589–98.

Bruni, P. et al., 2002. Fe65, a ligand of the Alzheimer's Aβ-amyloid precursor protein, blocks cell cycle progression by down-regulating thymidylate synthase expression. Journal of Biological Chemistry, 277(38), pp.35481–35488.

Bukhari, H. et al., 2017. Small things matter: Implications of APP intracellular domain AICD nuclear signaling in the progression and pathogenesis of Alzheimer's disease. Progress in Neurobiology, 156(Supplement C), pp.189–213.

Cao, X. & Südhof, T.C., 2001. A transcriptionally [correction of transcriptively] active complex of APP with Fe65 and histone acetyltransferase Tip60. Science (New York, N.Y.), 293(5527), pp.115–120.

Chang, Y. et al., 2003. Generation of the beta-amyloid peptide and the amyloid precursor protein C-terminal fragment gamma are potentiated by FE65L1. The Journal of biological chemistry, 278(51), pp.51100–7.

Chen, G. et al., 2017. Amyloid beta: structure, biology and structure-based therapeutic development. Acta Pharmacol Sin, 38(9), pp.1205–1235.

Cheung, H.N.M. et al., 2014. FE65 interacts with ADP-ribosylation factor 6 to promote neurite outgrowth. FASEB journal : official publication of the Federation of American Societies for Experimental Biology, 28(1), pp.337–49.

Chow, W.N.V. et al., 2015. FE65: Roles beyond amyloid precursor protein processing. Cellular & molecular biology letters, 20(1), pp.66–87.

Domingues, S.C. et al., 2011. Identification and characterization of a neuronal enriched novel transcript encoding the previously described p60Fe65 isoform. Journal of neurochemistry, 119(5), pp.1086–98.

Duilio, A. et al., 1991. A Rat Brain mRNA Encoding a Transcriptional Activator Homologous to the DNA Binding Domain of Retroviral Integrases. Nucleic Acids Research, 19(19), pp.5269–5274.

Duilio, A. et al., 1998. Fe65L2: a new member of the Fe65 protein family interacting with the intracellular domain of the Alzheimer's beta-amyloid precursor protein. The Biochemical journal, 330 Pt 1, pp.513–9.

Dumanis, S.B. et al., 2012. FE65 as a link between VLDLR and APP to regulate their trafficking and processing. Molecular neurodegeneration, 7, p.9.

Eggert, S. et al., 2004. The proteolytic processing of the amyloid precursor protein gene family members APLP-1 and APLP-2 involves α-, β-, γ-, and ε-Like cleavages: Modulation of APLP-1 processing by N-glycosylation. Journal of Biological Chemistry, 279(18), pp.18146–18156.

von Einem, B. et al., 2010. The role of low-density receptor-related protein 1 (LRP1) as a competitive substrate of the amyloid precursor protein (APP) for BACE1. Experimental Neurology, 225(1), pp.85–93.

Ermekova, K.S. et al., 1997. The WW domain of neural protein FE65 interacts with proline-rich motifs in Mena, the mammalian homolog of Drosophila enabled. Journal of Biological Chemistry, 272(52), pp.32869–32877.

Esposito, F. et al., 1990. Isolation of cDNA fragments hybridizing to rat brain-specific mRNAs. Developmental neuroscience, 12(6), pp.373–381.

Fiore, F. et al., 1995. The Regions Of the Fe65 Protein Homologous to the Phosphotyrosine Interaction Phosphotyrosine Binding Domain Of Shc Bind the Intracellular Domain Of the Alzheimers Amyloid Precursor Protein. Journal of Biological Chemistry, 270(52), pp.30853–30856.

Gersbacher, M.T. et al., 2013. Turnover of Amyloid Precursor Protein Family Members Determines Their Nuclear Signaling Capability. PLoS ONE, 8(7).

Goh, K.L. et al., 2002. Ena/VASP Proteins Regulate Cortical Neuronal Positioning. Current Biology, 12(7), pp.565–569.

Golanska, E. et al., 2013. APBB2 genetic polymorphisms are associated with severe cognitive impairment in centenarians. Experimental Gerontology, 48(4), pp.391–394.

Guénette, S. et al., 2006. Essential roles for the FE65 amyloid precursor protein-interacting proteins in brain development. The EMBO journal, 25(2), pp.420–431.

Guénette, S., Strecker, P. & Kins, S., 2017. APP Protein Family Signaling at the Synapse: Insights from Intracellular APP-Binding Proteins. Frontiers in Molecular Neuroscience, 10(March), p.87.

Guénette, S.Y. et al., 1996. Association of a novel human FE65-like protein with the cytoplasmic domain of the beta-amyloid precursor protein. Proceedings of the National Academy of Sciences of the United States of America, 93(20), pp.10832–7.

Haass, C. et al., 2012. Trafficking and proteolytic processing of APP. Cold Spring Harbor Perspectives in Medicine, 2(5), pp.1–25.

Haditsch, U. et al., 2009. A central role for the small GTPase Rac1 in hippocampal plasticity and spatial learning and memory. Molecular and cellular neurosciences, 41(4), pp.409–419.

Heber, S. et al., 2000. Mice with combined gene knock-outs reveal essential and partially redundant functions of amyloid precursor protein family members. The journal of neuroscience, 20(21), pp.7951–7963.

Hebert, S. et al., 2006. Regulated intramembrane proteolysis of amyloid precursor protein and regulation of expression of putative target genes. EMBO reports.

Herms, J. et al., 2004. Cortical dysplasia resembling human type 2 lissencephaly in mice lacking all three APP family members. The EMBO journal, 23(20), pp.4106–15.

Hoe, H.-S. et al., 2006. FE65 Interaction with the ApoE Receptor ApoEr2. Journal of Biological Chemistry, 281(34), pp.24521–24530.

Hu, Q. et al., 2002. A candidate molecular mechanism for the association of an intronic polymorphism of FE65 with resistance to very late onset dementia of the Alzheimer type. Human molecular genetics, 11(4), pp.465–475.

Hu, Q. et al., 2005. Endoproteolytic cleavage of FE65 converts the adaptor protein to a potent suppressor of the sAPP?? pathway in primates. Journal of Biological Chemistry, 280(13), pp.12548–12558.

Hu, Q. ai et al., 1999. Alternatively spliced isoforms of FE65 serve as neuron-specific and non- neuronal markers. Journal of Neuroscience Research, 58(5), pp.632–640.

Ikin, A.F. et al., 2007. A macromolecular complex involving the amyloid precursor protein (APP) and the cytosolic adapter FE65 is a negative regulator of axon branching. Molecular and Cellular Neuroscience, 35(1), pp.57–63.

Irizarry, M.C. et al., 2004. Apolipoprotein E modulates γ-secretase cleavage of the amyloid precursor protein. Journal of Neurochemistry, 90(5), pp.1132–1143.

Kesavapany, S., Banner, S., et al., 2002. Expression of the Fe65 adapter protein in adult and developing mouse brain. Neuroscience, 115, pp.951–960.

Kesavapany, S., Banner, S.J., et al., 2002. Expression of the Fe65 adapter protein in adult and developing mouse brain. Neuroscience, 115(3), pp.951–60.

Klevanski, M. et al., 2014. Differential role of APP and APLPs for neuromuscular synaptic morphology and function. Molecular and Cellular Neuroscience, 61, pp.201–210.

Klevanski, M. et al., 2015. The APP Intracellular Domain Is Required for Normal Synaptic Morphology, Synaptic Plasticity, and Hippocampus-Dependent Behavior. Journal of Neuroscience, 35(49), pp.16018–16033.

von Koch, C.S. et al., 1997. Generation of APLP2 KO Mice and Early Postnatal Lethality in APLP2/APP Double KO Mice. Neurobiology of Aging, 18(6), pp.661–669. Available at: http://dx.doi.org/10.1016/S0197-4580(97)00151-6.

Lane-Donovan, C.E., Philips, G.T. & Herz, J., 2014. More Than Cholesterol Transporters: Lipoprotein Receptors in CNS Function and Neurodegeneration. Neuron, 83(4), pp.771–787.

Masin, M. et al., 2006. Fe65 interacts with P2X2 subunits at excitatory synapses and modulates receptor function. Journal of Biological Chemistry, 281(7), pp.4100–4108.

McLoughlin, D.M. & Miller, C.C., 1996. The intracellular cytoplasmic domain of the Alzheimer's disease amyloid precursor protein interacts with phosphotyrosine-binding domain proteins in the yeast two-hybrid system. FEBS Lett, 397(2–3), pp.197–200. Meiyappan, M., Birrane, G. & Ladias, J.A.A., 2007. Structural Basis for Polyproline Recognition by the FE65 WW Domain. Journal of Molecular Biology, 372(4), pp.970–980.

Midthune, B. et al., 2012. Deletion of the amyloid precursor-like protein 2 (APLP2) does not affect hippocampal neuron morphology or function. Molecular and Cellular Neuroscience, 49(4), pp.448–455.

Müller, U. et al., 1994. Behavioral and anatomical deficits in mice homozygous for a modified beta-amyloid precursor protein gene. Cell, 79(5), pp.755–765.

Muller, U.C., Deller, T. & Korte, M., 2017. Not just amyloid: physiological functions of the amyloid precursor protein family. Nat Rev Neurosci, 18(5), pp.281–298.

Nakajima, C. et al., 2013. Low Density Lipoprotein Receptor-related Protein 1 (LRP1) Modulates N-Methyl-d-aspartate (NMDA) Receptor-dependent Intracellular Signaling and NMDA-induced Regulation of Postsynaptic Protein Complexes. The Journal of Biological Chemistry, 288(30), pp.21909–21923.

Nensa, F.M. et al., 2013. FE65 interactomics revealed SV2A and SERCA2 as new binding proteins in the human brain. Molecular & cellular proteomics : MCP, pp.1–46.

Oku, Y. & Huganir, R.L., 2013. AGAP3 and Arf6 Regulate Trafficking of AMPA Receptors and Synaptic Plasticity. The Journal of Neuroscience, 33(31), pp.12586–12598.

Penna, I. et al., 2013. A novel snRNA-like transcript affects amyloidogenesis and cell cycle progression through perturbation of Fe65L1 (APBB2) alternative splicing. Biochimica et Biophysica Acta - Molecular Cell Research, 1833(6), pp.1511–1526.

Perkinton, M.S. et al., 2004. The c-Abl tyrosine kinase phosphorylates the Fe65 adaptor protein to stimulate Fe65/amyloid precursor protein nuclear signaling.

Pietrzik, C.U. et al., 2004. FE65 constitutes the functional link between the low-density lipoprotein receptor-related protein and the amyloid precursor protein. The Journal of Neuroscience, 24(17), pp.4259–65.

Pohlkamp, T., Wasser, C.R. & Herz, J., 2017. Functional Roles of the Interaction of APP and Lipoprotein Receptors. Frontiers in Molecular Neuroscience, 10(March), pp.1–22.

Pousinha, P.A. et al., 2017. Physiological and pathophysiological control of synaptic GluN2B-NMDA receptors by the C-terminal domain of amyloid precursor protein I. Slutsky, ed. eLife, 6, p.e25659.

Radzimanowski, J. et al., 2008. Crystal structure of the human Fe65-PTB1 domain. Journal of Biological Chemistry, 283(34), pp.23113–23120.

Radzimanowski, J. et al., 2008. Structure of the intracellular domain of the amyloid precursor protein in complex with Fe65-PTB2. EMBO Reports, 9(11), pp.1134–1140.

Ring, S. et al., 2007. The Secreted β-Amyloid Precursor Protein Ectodomain APPsα Is Sufficient to Rescue the Anatomical, Behavioral, and Electrophysiological Abnormalities of APP-Deficient Mice. , 27(29), pp.7817–7826.

Sabo, S. et al., 2001. The Alzheimer amyloid precursor protein (APP) and FE65, an APP-binding protein, regulate cell movement. The Journal of Cell Biology, 153(7), pp.1403–1414.

Sabo, S.L. et al., 1999. Regulation of ??-amyloid secretion by FE65, an amyloid protein precursor-binding protein. Journal of Biological Chemistry, 274(12), pp.7952–7957.

Sabo, S.L. et al., 2003. The amyloid precursor protein and its regulatory protein, FE65, in growth cones and synapses in vitro and in vivo. The Journal of neuroscience : the official journal of the Society for Neuroscience, 23(13), pp.5407–5415.

Saeki, K. et al., 2011. Amyloid precursor protein binding protein Fe65 is cleaved by caspases during DNA damage-induced apoptosis. Biological & pharmaceutical bulletin, 34(2), pp.290–294.

Santiard-Baron, D. et al., 2005. Expression of human FE65 in amyloid precursor protein transgenic mice is associated with a reduction in beta-amyloid load. Journal of neurochemistry, 93(2), pp.330–8.

Sasaguri, H. et al., 2017. APP mouse models for Alzheimer's disease preclinical studies. The EMBO Journal, 36(17), pp.2473–2487.

Schilling, S. et al., 2017. APLP1 Is a Synaptic Cell Adhesion Molecule, Supporting Maintenance of Dendritic Spines and Basal Synaptic Transmission. The Journal of Neuroscience, 37(21), p.5345 LP-5365.

Scholz, R. et al., 2017. AMPA Receptor Signaling through BRAG2 and Arf6 Critical for Long-Term Synaptic Depression. Neuron, 66(5), pp.768–780.

Schrötter, A. et al., 2013. FE65 Regulates and Interacts with the Bloom Syndrome Protein in Dynamic Nuclear Spheres - Potential Relevance to Alzheimer's Disease. Journal of Cell Science, 126(11), pp.2480–2492.

Seabrook, G.R. et al., 1999. Mechanisms contributing to the deficits in hippocampal synaptic plasticity in mice lacking amyloid precursor protein. Neuropharmacology, 38(3), pp.349–359.

Sosa, L.J. et al., 2017. "The physiological role of the Amyloid Precursor Protein (APP) as an adhesion molecule in the developing nervous system." Journal of Neurochemistry, pp.11–29.

Strecker, P. Diplomarbeit, 2012. Analyse der Fe65-Proteinfamilie; Auswirkungen auf die neuromuskuläre Endplatte des Triangularis sterni, sowie die Synaptosomenzusammensetzung im Gehirn und das Aktinzytoskelett in MEF-Zellen

Suh, J. et al., 2015. FE65 and FE65L1 amyloid precursor protein-binding protein compound null mice display adult-onset cataract and muscle weakness. FASEB Journal, 29(6), pp.2628–2639.

Tanahashi, H. & Tabira, T., 2002. Characterization of an amyloid precursor protein-binding protein Fe65L2 and its novel isoforms lacking phosphotyrosine-interaction domains. The Biochemical journal, 367(Pt 3), pp.687–95.

Tanahashi, H. & Tabira, T., 1999. Molecular cloning of human Fe65L2 and its interaction with the Alzheimer's beta-amyloid precursor protein. Neuroscience Letters, 261(3), pp.143–146.

Tang, W. et al., 2015. Arf6 controls beta-amyloid production by regulating macropinocytosis of the Amyloid Precursor Protein to lysosomes. Molecular Brain, 8(1), p.41.

Telese, F. et al., 2005. Transcription regulation by the adaptor protein Fe65 and the nucleosome assembly factor SET. EMBO reports, 6(1), pp.77–82.

Trommsdorff, M. et al., 1998. Interaction of cytosolic adaptor proteins with neuronal apolipoprotein E receptors and the amyloid precursor protein. Journal of Biological Chemistry, 273(50), pp.33556–33560.

Wagner, T. & Pietrzik, C.U., 2012. The role of lipoprotein receptors on the physiological function of APP. Experimental Brain Research, 217(3), pp.377–387.

Waldron, E. et al., 2008. Increased AICD generation does not result in increased nuclear translocation or activation of target gene transcription. Experimental Cell Research, 314(13), pp.2419–2433.

Wang, B. et al., 2004. Isoform-specific knockout of FE65 leads to impaired learning and memory. Journal of neuroscience research, 75(1), pp.12–24.

Wang, B. et al., 2017. The Amyloid Precursor Protein Is a Conserved Receptor for Slit to Mediate Axon Guidance. eNeuro, 4(3), p.ENEURO.0185-17.2017.

Wang, P., 2005. Defective Neuromuscular Synapses in Mice Lacking Amyloid Precursor Protein (APP) and APP-Like Protein 2. Journal of Neuroscience, 25(5), pp.1219–1225.

Wang, P.-L. et al., 2011. Functional and molecular interactions between Rac1 and FE65. Neuroreport, 22(14), pp.716–20.

Wang, Y. et al., 2009. The APP-Interacting Protein FE65 is Required for Hippocampus-Dependent Learning and Long-Term Potentiation. Learning & Memory, 16(9), pp.537–544.

Wasser, C.R. et al., 2014. Differential splicing and glycosylation of Apoer2 alters synaptic plasticity and fear learning. Science Signaling, 7(353), p.ra113--ra113.

Weyer, S.W. et al., 2011. APP and APLP2 are essential at PNS and CNS synapses for transmission, spatial learning and LTP. The EMBO journal, 30(11), pp.2266–80.

Weyer, S.W. et al., 2014. Comparative analysis of single and combined APP/APLP knockouts reveals reduced spine density in APP-KO mice that is prevented by APPsα expression. Acta Neuropathologica Communications, 2, p.36.

Zambrano, N. et al., 1998. The Fe65 adaptor protein interacts through its PID1 domain with the transcription factor CP2/LSF/LBP1. Journal of Biological Chemistry, 273(32), pp.20128–20133.

Zambrano, N. et al., 2001. The β-Amyloid Precursor Protein APP is Tyrosine-Phosphorylated in Cells Expressing a Constitutively Active Form of the Abl Protoncogene. The Journal of Biological Chemistry, 276(23), pp.19787–19792.

Zheng, H. et al., 1995. ??-Amyloid Precursor Protein-Deficient Mice Show Reactive Gliosis and Decreased Locomotor Activity. Cell, 81(4), pp.525–531.

Zurhove, K. et al., 2008. γ-Secretase Limits the Inflammatory Response Through the Processing of LRP1. Science Signaling, 1(47), p.ra15 LP-ra15.

Chapter I

Behavioral and electrophysiological analysis of Fe65 KO, Fe65L1 KO and Fe65/Fe65L1 DKO mice and the influence of the Fe65 protein family on neuromuscular junction formation

Background

The members of the mammalian Fe65 protein family, consisting of Fe65 itself and its two homologues Fe65L1 and Fe65L2, are scaffolding proteins forming numerous complexes with a widespread range of proteins (Chow et al. 2015). The first identified Fe65 interacting protein was the Amyloid Precursor Protein (APP) (Fiore et al. 1995), which plays a major role in Alzheimers Disease (John & Gerald 1992). Few years later its homologues APP-like-proteins 1 and 2 (APLP1 and APLP2) were described to interact with Fe65 as well (Guénette et al. 1996, Duilio et al. 1998). To characterize the function of Fe65 in more detail different Fe65 knockout (KO) mouse models were generated, using different targeting vectors (Wang et al. 2004, Guénette et al. 2006). Behavioral analysis of the first KO, the isoform specific p97Fe56-KO, resulted in deficits in non-spatial learning tasks, classical fear conditioning and only in older (>14 months) mice impairments in the Morris Water Maze Test, whereas younger animals (2-4 months) showed no changes (Wang et al. 2004, Y. Wang et al. 2009). Although deficits in the hanging wire task have been described for the second Fe65 KO, lacking both isoforms p97 and p60, and Fe65L1 KO mice (Suh et al. 2015) detailed behavioral analysis were missing. Furthermore no detailed electrophysiological analysis of both single Fe65 KO and Fe65L1 KO and the Fe65/Fe65L1 double-KO (DKO) had been performed.

Interestingly, the lack of Fe65 and its homologue Fe65L1 leads to similar phenotypes observed in APP/APLP1/APLP2 triple-KO (TKO) mouse brains, exhibiting ectopic neurons and axonal pathfinding defects (Guénette et al. 2006, Herms et al. 2004).

Therefore, the goal of this study was to perform a set of behavioral tests, electrophysiological and histochemical analysis of the central and peripheral nervous system to characterize single Fe65 KO and Fe65L1 KO as well as Fe65/Fe65L1 DKO mice in more detail on the one hand and to provide further information of the interplay of the Fe65 and the APP protein families at the neuromuscular junction (NMJ) on the other hand.

Methods

According to the SHIRPA guidelines (Rogers et al. 1997) different behavioral tests were used to characterize the phenotypes of Fe65 KO, Fe65L1 KO and Fe65/Fe65L1 DKO mice in comparison to wildtype (WT) mice (C57BL/6j) at an age of 4-6 months. In this study we focused especially on locomotor, learning and memory analysis. First evidences on phenotypical changes of Fe65/Fe65L1 DKO mice have been provided by Guénette and co-workers who described abnormal circling behavior of the Fe65/Fe65L1 DKO mice in home cages (Guénette et al. 2006) as well as deficits in the Hanging Wire test of older (>12 months) Fe65 KO and Fe65L1 KO mice (Suh et al. 2015). Therefore, first the general behavior and locomotion was analyzed by an Open Field experiment followed by a Rota-Rod test, a Hanging Wire test to verify the findings of Suh and co-workers and a grip strength test. Interestingly, during the Open Field analysis Fe65/Fe65L1 DKO mice showed no indication of anxiety which leads us to check the anxiety behavior via an Elevated Plus Maze experiment. To examine the spatial learning and memory behavior the Morris Water Maze (MWM) test was used which was originally invented to study the learning abilities of rats (Morris 1984).

After the behavioral analyses the mice were subjected for electrophysiological studies. Field excitatory postsynaptic potentials (fEPSPs) from acute hippocampal slices were recorded in the CA1 region following stimulation of CA3 Schaffer collateral axons. The longterm potentiation (LTP), paired-pulse facilitation (PPF) and the basal synaptic transmission were measured. Furthermore, a detailed histological investigation of the spine density of the hippocampal CA1 region was performed.

The *triangularis sternii* muscle with its thin structure of only five muscle layers and no sensory innervation, as all neurites branching into the muscle are motor axons, is a model tissue to study NMJ formation. Therefore, the *triangularis sternii* muscle of six to eight month old mice was dissected and analyzed by histochemical stainings of the NMJ to examine the area covered by the pre- and postsynapse, its apposition and postsynaptic fragmentation.

Results and Discussion

Analyses of Fe65 KO, Fe65L1 KO and Fe65/Fe65L1 DKO mice showed impairments in locomotion, grip strength, anxiety, learning and memory as well as NMJ formation deficits in comparison to WT mice. Single Fe65 KO and Fe65L1 KO mice exhibited an overall mild phenotype in our experimental setups whereas Fe65/Fe65L1 DKO mice displayed a strongly aggravated phenotype. This shows that Fe65 or Fe65L1 can functionally compensate each other, indicating redundant or overlapping functions. However, loss of both Fe65 and Fe65L1 has a dramatic influence on the performance in grip strength and Rota-Rod analysis. This finding was underpinned by the histological examination of the NMJs of *triangularis sternii* muscles, where the total area of the pre- and postsynapse and the apposition of the pre- and postsynapse of Fe65/Fe65L1 DKO mice was significantly reduced compared to single Fe65 KO and Fe65L1 KO mice. Interestingly, the putative loss of anxiety of Fe65/Fe65L1 DKO mice might be explained by the observed cataract phenotype in older Fe65/Fe65L1 DKO mice (Suh et al. 2015) thus leading to disorientated and increased movement in the Open Fiel and Elevated Plus Maze experiment. These findings weren´t detectable for single KO mice.

In both probe trials as well as in the reversal paradigm of the Morris Water Maze test impairments in spatial learning and memory were observed for Fe65 KO as well as Fe65L1 KO mice which were exacerbated in Fe65/Fe65L1 DKO mice too. In contrast, for p97Fe65 KO mice none of the described phenotypes were detected (Wang et al., 2009). These findings suggest a compensatory influence of the p60Fe65 isoform which was upregulated in p97Fe65 KO mice (Wang et al., 2009). Intriguingly, electrophysiological analyses only partially reflect these results. While Fe65 KO mice showed only a trend towards post titanic potentiation (PTP) deficits and Fe65/Fe65L1 DKO mice exhibited significant impairments in the late phase of LTP measurements Fe65L1 KO mice displayed no differences compared to measurements of WT mice. This speaks against a redundant and overlapping function of Fe65 and Fe65L1 and the outcome of the Morris Water Maze experiments might depend on two different mechanisms for Fe65 and Fe65L1. However, limitation of interpretation of MWM data of Fe65/Fe65L1 DKO mice analyses due to altered anxiety, activity and possibly visual ability which have also been described for older Fe65L1 KO mice (Suh et al., 2015) cannot be directly linked to LTP deficits and the

impairments in the MWM experiments.

Notably, no significant changes have been observed in the paired-pulse ratio, the basic synaptic transmission measurements and spine density analysis for all tested genotypes, arguing for a dominant postsynaptic function of Fe65/Fe65L1.

Interestingly, impairments in grip strength of Fe65 KO as well as Fe65L1 KO mice described by Suh and co-workers (Suh et al., 2015) weren´t detectable in our analysis, which might be explained by the progressed age (>14 month old vs. 4-6 month old mice) of mice examined. Only Fe65/Fe65L1 DKO mice displayed impairments in the grip strength as well as hanging wire test. Accordingly, analysis of the NMJ exhibited an aggravated phenotype of decreased pre- and postsynaptic areas as well as impairments in apposition of the pre- and postsynapse in Fe65/Fe65L1 DKO mice compared to single Fe65 or Fe65L1 KO mice which might correspond to the muscle strength deficits (Suh et al., 2015). Further a higher fragmentation of the postsynaptic area of the NMJs of Fe65 KO, Fe65L1 KO and Fe65/Fe65L1 DKO mice compared to WT mice were measurable. Thus, loss of Fe65 and/or Fe65L1 which are present both at the pre- and postsynapse as well as in neurons and in muscle cells leading to NMJ defects and subsequently to muscle denervation indicated by centralized nuclei and subsequently to muscle strength deficits (Guénette et al., 2006, Suh et al., 2015).

Testing the influence of the Fe65 protein family in dependence of APLP2 on NMJ formation showed a further decrease in size of the area of the pre- and postsynapse of NMJs of Fe65/APLP2 DKO and Fe65L1/APLP2 DKO mice compared to NMJs of Fe65 KO and Fe65L1 KO mice. This genetic interaction strongly suggests a functional role of the Fe65 protein family in APP protein family signaling required for NMJ formation. This finding is further affirmed by the analysis of knockin mice expressing APP lacking the Fe65/Fe65L1 interaction site on an APLP2 KO background, exhibiting similar defects of NMJ formation, in locomotion and grip strength (Weyer et al. 2011, Klevanski et al. 2015). Additionally it was shown that APP interacts with LRP4 (Choi et al. 2013), a key component of the LRP4/Musk/Agrin complex, which is involved in Acetyl-Choline Receptor (AChR) patterning and thereby stabilizing postsynaptic sites (Wu et al. 2012). A participation of the Fe65 protein family in this pathway appears well plausible.

Conclusion

In this study we could show that the Fe65 protein family is involved in and essential for CNS and PNS function and formation as well as learning and memory consolidation. Moreover, we were able to demonstrate that the interaction with the APP protein family is crucial for NMJ formation. Together, these data suggest that the Fe65 protein family is the main interaction partner for the APP protein family in the CNS as well as PNS.

Reference

Caldwell, J.H. et al., 2012. Roles of the amyloid precursor protein family in the peripheral nervous system. Mechanisms of development, 130(6–8), pp.433–46.

Chow, W.N.V. et al., 2015. FE65: Roles beyond amyloid precursor protein processing. Cellular & molecular biology letters, 20(1), pp.66–87.

Choi, H.Y. et al., 2013. APP interacts with LRP4 and agrin to coordinate the development of the neuromuscular junction in mice. eLife, 2, p.e00220.

Duilio, A. et al., 1998. Fe65L2: a new member of the Fe65 protein family interacting with the intracellular domain of the Alzheimer's beta-amyloid precursor protein. The Biochemical journal.

Fiore, F. et al., 1995. The regions of the Fe65 protein homologous to the phosphotyrosine interaction/phosphotyrosine binding domain of Shc bind the intracellular domain of the Alzheimer's amyloid precursor protein. Journal of Biological Chemistry, 270(52), pp.30853–30856.

Guénette, S. et al., 2006. Essential roles for the FE65 amyloid precursor protein-interacting proteins in brain development. The EMBO journal, 25(2), pp.420–431.

Herms, J. et al., 2004. Cortical dysplasia resembling human type 2 lissencephaly in mice lacking all three APP family members. The EMBO journal, 23(20), pp.4106–15.

John, A. & Gerald, A., 1992. Alzheimers Disease : The Amyloid Cascade Hypothesis.

Klevanski, M. et al., 2014. Differential role of APP and APLPs for neuromuscular synaptic morphology and function. Molecular and Cellular Neuroscience, 61, pp.201–210.

Klevanski, M. et al., 2015. The APP Intracellular Domain Is Required for Normal Synaptic Morphology, Synaptic Plasticity, and Hippocampus-Dependent Behavior. Journal of Neuroscience, 35(49), pp.16018–16033.

Morris, R., 1984. Developments of a water-maze procedure for studying spatial learning in the rat. Journal of Neuroscience Methods, 11(1), pp.47–60.

Rogers, D.C. et al., 1997. Behavioral and functional analysis of mouse phenotype: SHIRPA, a proposed protocol for comprehensive phenotype assessment. Mammalian genome : official journal of the International Mammalian Genome Society, 8(10), pp.711–3.

Suh, J. et al., 2015. FE65 and FE65L1 amyloid precursor protein-binding protein compound null mice display adult-onset cataract and muscle weakness. FASEB Journal, 29(6), pp.2628–2639.

Weyer, S.W. et al., 2011. APP and APLP2 are essential at PNS and CNS synapses for transmission, spatial learning and LTP. The EMBO journal, 30(11), pp.2266–80.

Wang, B. et al., 2004. Isoform-specific knockout of FE65 leads to impaired learning and memory. Journal of neuroscience research, 75(1), pp.12–24.

Wang, P. et al., 2005. Defective neuromuscular synapses in mice lacking amyloid precursor protein (APP) and APP-Like protein 2. The Journal of neuroscience : the official journal of the Society for Neuroscience, 25(5), pp.1219–25.

Wang, Y. et al., 2009. The APP-interacting protein FE65 is required for hippocampus-dependent learning and long-term potentiation. Learning & memory (Cold Spring Harbor, N.Y.), 16(9), pp.537–44.

Wang, Z. et al., 2009. Presynaptic and postsynaptic interaction of the amyloid precursor protein promotes peripheral and central synaptogenesis. The Journal of neuroscience : the official journal of the Society for Neuroscience, 29(35), pp.10788–801.

Wu, H. et al., 2012. Distinct Roles of Muscle and Motoneuron LRP4 in Neuromuscular Junction Formation. Neuron, 75(1), pp.94–107.

FE65 and FE65L1 share common synaptic functions and genetically interact with the APP family in neuromuscular junction formation

Paul Strecker[1], Susann Ludewig[3], Marco Rust[2,4], Tabea A. Mundinger[5], Andreas Görlich[2], Elisa G. Krächan[2], Christina Mehrfeld[1], Joachim Herz[6], Martin Korte[3], Suzanne Y. Guénette[7,*] & Stefan Kins[1,5,*]

[1]Division of Human Biology and Human Genetics, Erwin-Schrödinger-Straße13, 67663 Kaiserslautern, Germany. [2]Division of Animal Physiology, University of Kaiserslautern, Erwin-Schrödinger-Straße 13, 67663 Kaiserslautern, Germany. [3]Department of Cellular Neurobiology, Technical University of Braunschweig, Spielmannstraße 7, 38106 Braunschweig, Germany. [4]Institute of Physiological Chemistry, University of Marburg, Karl-von-Frisch-Straße 1, 35032 Marburg, Germany. [5]Centre for Molecular Biology (ZMBH) University of Heidelberg, Im Neuenheimer Feld 282, 69120 Heidelberg, Germany. [6]Center for Translational Neurodegeneration Research, UT Southwestern, Dallas, TX, USA. [7]Genetics and Aging Research Unit, MassGeneral Institute for Neurodegenerative Disease, Department of Neurology, Massachusetts General Hospital, Harvard Medical School, Boston, MA, USA.

*These authors contributed equally to this work.

ABSTRACT

The FE65 adaptor proteins (FE65, FE65L1 and FE65L2) bind proteins that function in diverse cellular pathways and are essential for specific biological processes. Mice lacking both FE65 and FE65L1 exhibit ectopic neuronal positioning in the cortex and muscle weakness. p97FE65-KO mice, expressing a shorter FE65 isoform able to bind amyloid precursor protein family members (APP, APLP1, APLP2), develop defective long-term potentiation (LTP) and aged mice display spatial learning and memory deficits that are absent from young mice. Here, we examined the central and peripheral nervous systems of FE65-KO, FE65L1-KO and FE65/FE65L1-DKO mice. We find spatial learning and memory deficits in FE65-KO and FE65L1-KO mice. Severe motor impairments, anxiety, hippocampal LTP deficits and neuromuscular junction (NMJ) abnormalities, characterized by decreased size and reduced apposition of pre- and postsynaptic sites, are observed in FE65/FE65L1-DKO mice. As their NMJ deficits resemble those of mutant APP/APLP2-DKO mice lacking the FE65/FE65L1 binding site, the NMJs of APLP2/FE65-DKO and APLP2/FE65L1-DKO mice were analyzed. NMJ deficits are aggravated in these mice when compared to single FE65- and FE65L1-KO mice. Together, our data demonstrate a role for FE65 proteins at central and peripheral synapses possibly occurring downstream of cell surface-associated APP/APLPs.

INTRODUCTION

The FE65 protein family members, FE65 and FE65 like proteins (FE65L1, FE65L2) are scaffolding proteins containing two PTB domains and a WW domain that mediate complex formation with a diverse set of proteins[1]. These include Amyloid Precursor Protein (APP) family members, lipoprotein receptors[2–4], proteins that regulate cellular processes such as cytoskeletal remodeling[5–7], synaptic vesicular loading and release[8], calcium homeostasis[8], signal transduction[9,10], nuclear signaling[11] and DNA repair[12].

Characterization of two FE65 knockout (KO) mouse models, generated using different targeting vectors, have provided insights into the biological roles of the FE65 protein[13,14]. The isoform specific p97FE65-KO mice results in loss of the p97 isoform and a 5-fold upregulation of an N- terminal truncated soluble isoform (p60), believed to be derived from the same transcript, that is expressed in the cortex at low levels under normal physiological conditions[13,14]. Locomotor activity and behavior in the open field test were normal, but deficits in cognitive behavior using non-spatial learning tasks such as temporal dissociative passive avoidance[13,15] and classic fear conditioning[15] were noted for these mice. In the Morris water maze spatial learning test, only older p97FE65-KO mice (>14 months old) revealed a significant decline in task performance in the training phase and probe trial of the reversal paradigm, whereas young (2–4 months old) mice showed no impairments[13,15]. The p97FE65-KO mice also display early-phase long-term potentiation (LTP) deficits elicited *in vivo* by a single 100 Hz train[15]. These data indicate that the p97 isoform of FE65 plays only a minor role in spatial memory formation and may be involved in short-term plasticity. Possible compensation by elevated p60 levels or shared function with related family members may obscure more severe cognitive deficits.

The second FE65 knockout mouse model, lacking both the p97 and p60 isoforms displays deficits in the hanging wire task that are also observed in FE65L1-KO mice[16]. In contrast to the FE65/FE65L1 double knockout (DKO) mice, which exhibit deficits in neuronal positioning and axon outgrowth in the developing cortex, there are no overt morphological abnormalities present in FE65-KO and FE65L1-KO mouse brains[14].

Thus, a systematic assessment of the contribution of FE65 protein family members to cognitive and motor functions is lacking. Here, we report severe deficits in motor and cognitive behaviors in mice lacking FE65 protein family members. These are associated with neuromuscular junction abnormalities and altered LTP, respectively. Thus, establishing FE65 family proteins as essential synaptic components in mice.

RESULTS

Functional redundancy of FE65 and FE65L1 in motor behavior, control of anxiety and activity.

For comparative analysis of FE65-KO, FE65L1-KO, and FE65/FE65L1 -DKO mice, we used offspring from FE65^{+/−} and FE65L1^{+/−} heterozygous mouse crossings. Behavior analyses were conducted with a cohort of male FE65-KO (n = 12), FE65L1-KO (n = 12) and FE65/FE65L1-DKO (n = 10) mice aged 4–6-month. These behavioral studies initially included 12 FE65/FE65L1-DKO mice, but we found that two mice had developed unilateral eye lens opacity shortly after performing the behavioral tests. We did not detect eye lens opacity in any other mice by visual inspection. Therefore, only these two mice were excluded retrospectively from data analysis for all behavioral studies.

Limb clasping in mice briefly held by the tail in an inverted position[17] showed that the vast majority of FE65/ FE65L1-DKO mice (8/10) were unable to adopt the characteristic splayed limb position observed in WT mice (Fig. 1a). The intermediate phenotype, a single set of clasped limbs (position 1)[17], was observed for the majority of FE65 (9/12) and half of the FE65L1 single KO mice (Fig. 1a). These data are suggestive of motor deficits that may be due to changes in the central nervous system (CNS)[17], peripheral abnormalities in muscle spindle inner-vation[18] or myopathy[19] . No changes in limb position were observed when FE65/FE65L1-DKO mice were held in an inverted position for up to 30 seconds, nor did these mice have difficulty recovering once placed back on a horizontal surface (data not shown). Difficulty with the latter would also be suggestive of CNS deficits[20]. The rotarod test requiring balance and coordination, revealed statistically significant motor deficits only for the FE65/ FE65L1-DKO mice (Fig. 1b, $p < 0.041$). Furthermore in the hanging wire grip test requiring strength and coordination the FE65/FE65L1-DKO mice had a significantly lower latency to fall compared to WT mice, while single KOs, which also showed a trend towards a lower latency to fall, were not significantly different from WT mice (Fig. 1c, $p = 0.0001$). To directly assess whether motor deficits might involve a peripheral motor defect, the grip strength test was used. Significantly reduced grip strength was observed for the FE65/FE65L1-DKO mice when compared to WT mice, indicating a peripheral motor function deficit in these

mice (Fig. 1d, p = 0.00013). Single KO mice showed a trend towards reduced grip strength that was not significantly different from WT (Fig. 1d).

Although FE65/FE65L1-DKO mice showed severe motor deficits, the total traveling distance measured during 1 hour in the open field arena was 2-fold higher than in WT controls, FE65-KO or FE65L1-KO mice (Fig. 1e, DKO vs. WT, p = 0.013; DKO vs. FE65-KO, p = 0.002; DKO vs. FE65L1-KO, p = 0.0001). In contrast to the control and single KO mice, FE65/FE65L1-DKO mice failed to show habituation to this novel environment. Furthermore, FE65/FE65L1- DKO mice crossed the center region more often than the other three genotypes studied (Fig. 1f, DKO vs. WT, p = 0.024; DKO vs. FE65-KO, p = 0.0002; DKO vs. FE65L1-KO, p = 0.0001) (Supplementary Video S1). Given that mice have a natural aversion to open spaces, open field behaviors of the FE65/FE65L1-DKO mice are suggestive of reduced anxiety. To further examine anxiety-like behaviors in these mice, the elevated plus-maze behavioral test was performed[21]. In this test, rodents are exposed to an approach–avoidance conflict between exploratory behavior and their aversion to heights and open spaces. The numbers of visits to the open arm were not significantly different between genotypes (Fig. 1g, p = 0.09). However, FE65/ FE65L1-DKO mice displayed a 7-fold increase in the time spent in the open arm of the elevated plus maze compared to WT, FE65- or FE65L1-KO mice (Fig. 1h, DKO vs. WT, p = 0.026; DKO vs. FE65-KO, p = 0.003; DKO vs. FE65L1-KO, p = 0.118). Collectively, these data show that FE65/FE65L1-DKO mice have deficits in peripheral motor function and reduced anxiety. The data also clearly show that FE65 and FE65L1 are functionally redundant in these contexts.
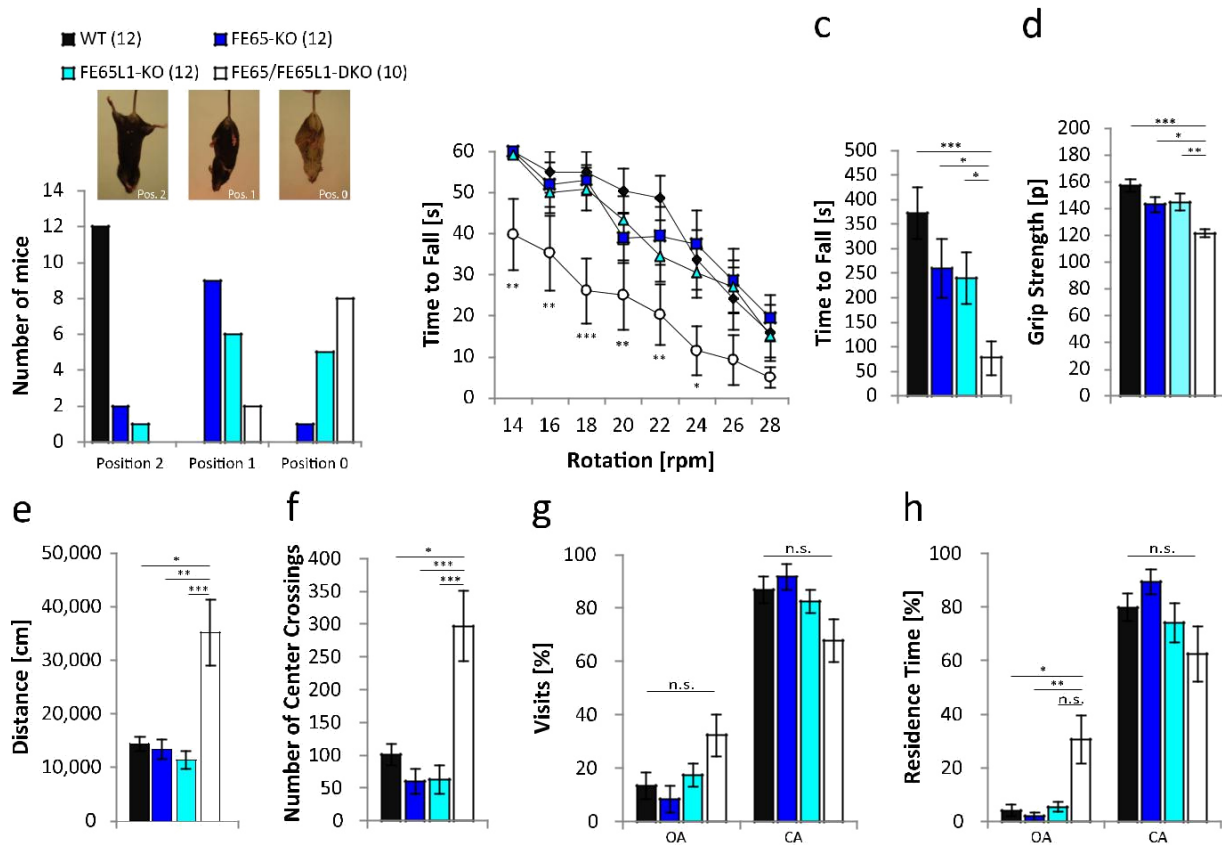
Figure 1. Severe abnormalities in locomotor and anxiety behaviors for FE65/FE65L1-DKO mice.

Male FE65-KO (n = 12), FE65L1-KO (n = 12) and FE65/FE65L1-DKO (n = 10) mice (4–6 months-old) were used for all behavioral tests. (a) Paw-clasping response: Mice were lifted by the tail and the position of their limbs (normal limb position (Pos. 2), front or hind limb clasping (Pos. 1), front and hind limb clasping (Pos. 0) were recorded. (b) Mouse-rotarod: Mice were placed on a rotating cylinder with different speeds of rotation and the time to fall was measured. Shown is the significance between WT and FE65/FE65L1-DKO mice, since no difference was observed between WT and FE65- or WT and FE65L1-KO mice. (c) During the Hanging Wire Grip Test the time to fall was measured. (d) Grip strength measurements of all limbs with a Grip Strength Meter. (e,f) Open-field behavior recorded for 1 h. (e) The distance traveled and (f) the number of times mice crossed the center area were measured. (g,h) Elevated Plus Maze was used to assess anxiety levels. Mice were placed in the closed arm of the plus maze and (g) the number of visits in the open arms (OA) and closed arms (CA), as well as (h) the residence time was measured over a period of five minutes. Data were analyzed using Kruskal-Wallis-Test followed by Dunn´s Multiple Comparison Test due to differences in normal distribution. Error bars are given as s.e.m. *p < 0.05; **p < 0.01; ***p < 0.001; n.s. for not significant.

Learning and memory deficits in FE65/FE65L1-DKO mice.

To assess cognitive function, we used the Morris Water Maze (MWM) test. Male FE65-, FE65L1-KO and FE65/FE65L1-DKO mice (4–6-month-old) were initially assessed in the MWM with a visible platform to exclude confounding factors such as

deficits in visual perception or swimming performance (Supplementary Video S2). Under these conditions, no differences in procedural learning (Fig. 2a, p = 0.34) or swim speeds (Fig. 2b, p = 0.57) were observed between FE65 and FE65L1 single KOs when compared to WT controls. In contrast, FE65/FE65L1-DKO mice showed normal swim speed but did not learn the task (Fig. 2a, p = 0.042) and appeared disoriented (Supplementary Video S2). We observed strong deficits for the FE65/FE65L1-DKO mice in the MWM tasks. Since interpretation of the cognitive deficits observed for these mice is confounded by altered anxiety, activity and possibly visual abilities[16] the analyzed data are not further discussed, but are presented in Supplementary Fig. S1.

The FE65- and FE65L1-KO mice were trained for 5 days (4 trials per day) and no significant changes in escape latencies were measured between genotypes (p = 0.56) (Fig. 2c). In the probe trial, WT mice showed a preference for the target quadrant, whereas both FE65- and FE65L1-KO mice lacked a respective preference (Fig. 2d quadrant 3 (target), WT, p = 0.0085; FE65-KO, p = 0.23; FE65L1-KO, p = 0.46). These data show that genetic deletion of either FE65 or FE65L1 causes spatial memory deficits. After one day without training, the hidden platform was moved to the opposite quadrant of the MWM for the Reverse Hidden Platform test and mice were again trained for 4 days (4 trials per day). During this training phase, the times required to find the platform were now significantly longer for both FE65- and FE65L1-KO mice when compared to WTs (Fig. 2e, p = 0.048). After removal of the platform, FE65- and FE65L1-KO mice lacked a preference for the new target quadrant (Fig. 2f, quadrant 1 (target), WT, p = 0.035, FE65-KO, p = 0.09, FE65L1-KO, p = 0.15). These data indicate that loss of either FE65 or FE65L1 causes deficits in spatial memory retrieval and impaired learning or consolidation in the reversal paradigm.
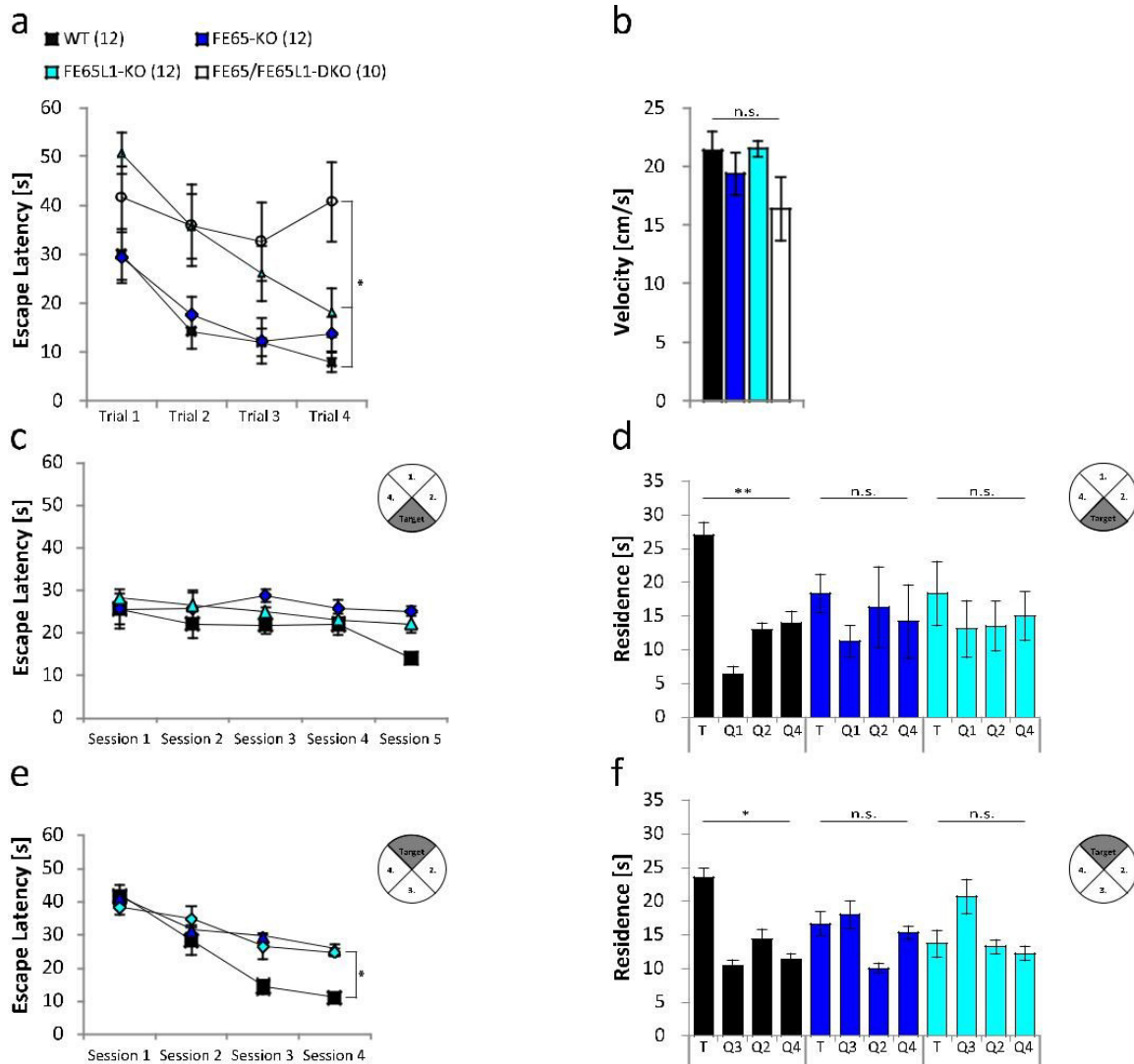
Figure 2. Spatial learning is impaired in FE65-KO and FE65L1-KO mice.

The Morris Water Maze (MWM) test was used to examine spatial learning. (a,b) FE65-KO, FE65L1-KO and FE65/FE65L1-DKO mice (4–6 months-old) were first trained using a platform placed 0.5 cm beneath the water surface and marked with a black pencil in a pool filled with opaque water. (a) Time to find the platform was measured. (b) Swim speeds were measured for each mouse by dividing path length by escape time. Shown is the mean velocity of each genotype tested. (c) WT, FE65-KO and FE65L1-KO mice were trained for five days in the hidden platform test and the time to find the platform was measured. (d) On the 6th day the platform was removed for the probe trial and the time of residence in each quadrant was measured. (e) After one day without training, the platform was placed in the opposite quadrant for the reversal paradigm test and the mice were retrained for four days and the time to find the platform was measured. (f) On the last day, the platform was removed and the time of residence in each quadrant was measured. The number of male mice (4–6 months-old) is given in brackets. Statistical analysis: (a,b) one-way ANOVA with Bonferroni´s post-hoc test. (d,f) two-way ANOVA with Bonferroni´s post-hoc test. (c,e) two-way repeated measures ANOVA (Greenhouse-Geisser correction). Error bars are given as s.e.m. *p< 0.05; **p < 0.01; n.s. for not significant.

Pyramidal neuron spine densities are similar for all FE65 genotypes.

To investigate whether the observed cognitive deficits are due to altered spine density, we performed Golgi staining of brains isolated from 4–6 month-old WT, FE65-KO, FE65L1-KO, and FE65/FE65L1-DKO mice (see Fig. 3a for representative images). Spine density analyses of second-order CA1 pyramidal neuron dendrites showed a slight reduction compared to WT, but were not statistically significant (Fig. 3b; WT vs. FE65-KO, p = 0.16; WT vs. FE65L1-KO, p = 0.19; WT vs. DKO, p = 0.21). These data suggest that loss of FE65 and/or FE65L1 does not substantially affect neuronal connectivity of hippocampal CA1 neurons.

LTP, PTP and PPF deficits in hippocampi of FE65 protein family KO mice.

The possibility that impaired spatial learning and memory may be due to functional network deficits in the CA3-CA1 synapses was also explored. Extracellular field recordings were performed on acute hippocampal slices obtained from the same cohort of WT, FE65-KO, FE65L1-KO, and FE65/FE65L1-DKO mice used in the behavioral studies. Field excitatory postsynaptic potentials (fEPSPs) were recorded in the CA1 region upon stimulating Schaffer collateral axons in the CA3 at a frequency of 0.1 Hz. LTP was induced via theta burst stimulation (TBS) after 20 min of baseline stimulation and was recorded for 60 min. During these sixty minutes of LTP recording, acute slices of FE65/ FE65L1-DKO mice (n = 16/4, corresponding to 16 slices from 4 mice) exhibited lower potentiation compared to WT (p = 0.023, n = 13/3) or FE65L1-KO mice (p = 0.023, n = 25/6) (Fig. 3c). The overall shape of potentiation after TBS application (LTP curve) of FE65L1-KO was similar to that of WT mice (Fig. 3c). The post-tetanic potentiation values (PTP, 5 min after TBS) and the stable phase of LTP were averaged for each genotype. Significantly reduced PTP was observed in FE65/FE65L1-DKO mice when compared to WT mice (184.34 ± 13.97% vs. 277,74 ± 29,15%, p = 0.013) Fig. 3d). FE65-KO mice also showed reduced PTP compared to WT mice, but this was not statistically significant (205.69 ± 10.52% vs. 277,74 ± 29,15%). A significant reduction in the maintenance of LTP, obtained from the mean slope of field potentials during the last 30 min of LTP recording, was observed for FE65/FE65L1-DKO mice in comparison to WT (137.67 ± 4.53% vs. 173.42 ± 12.98%; p = 0.023) (Fig.3d). Importantly, for FE65-KO mice, only a reduction in PTP was observed, whereas the overall LTP level 60 min

after TBS application was only significantly affected in FE65/FE65L1-DKO mice, suggesting partial overlapping functions of FE65 and FE65L1 in synaptic plasticity.

In order to further elucidate whether the LTP defect and lowered PTP observed in FE65/FE65L1-DKO and FE65-KO mice, respectively, were due to altered synaptic transmission, we probed the excitability of hippocampal neurons by increasing the fiber volley (FV) amplitude (Fig. 3e) or the stimulus intensity (Fig. 3f). Analyzing the Input- Output (IO) strength of FE65 protein family deficient mice yielded no alterations between genotypes at any FV amplitude. Although not significant, a trend towards hindered excitability was observed in FE65/FE65L1-DKO FV measurements, with the lowest IO curve of all genotypes (Fig. 3e). Pre-synaptic functionality and short-term plasticity was assessed using the paired-pulse facilitation (PPF) paradigm. Here, none of the analyzed genotypes exhibited any significant difference in PPF values (Fig. 3g). Collectively, these data show that aside from the FE65/FE65L1-DKO mice none of the other FE65 genotypes display significant alterations in basal synaptic transmission.
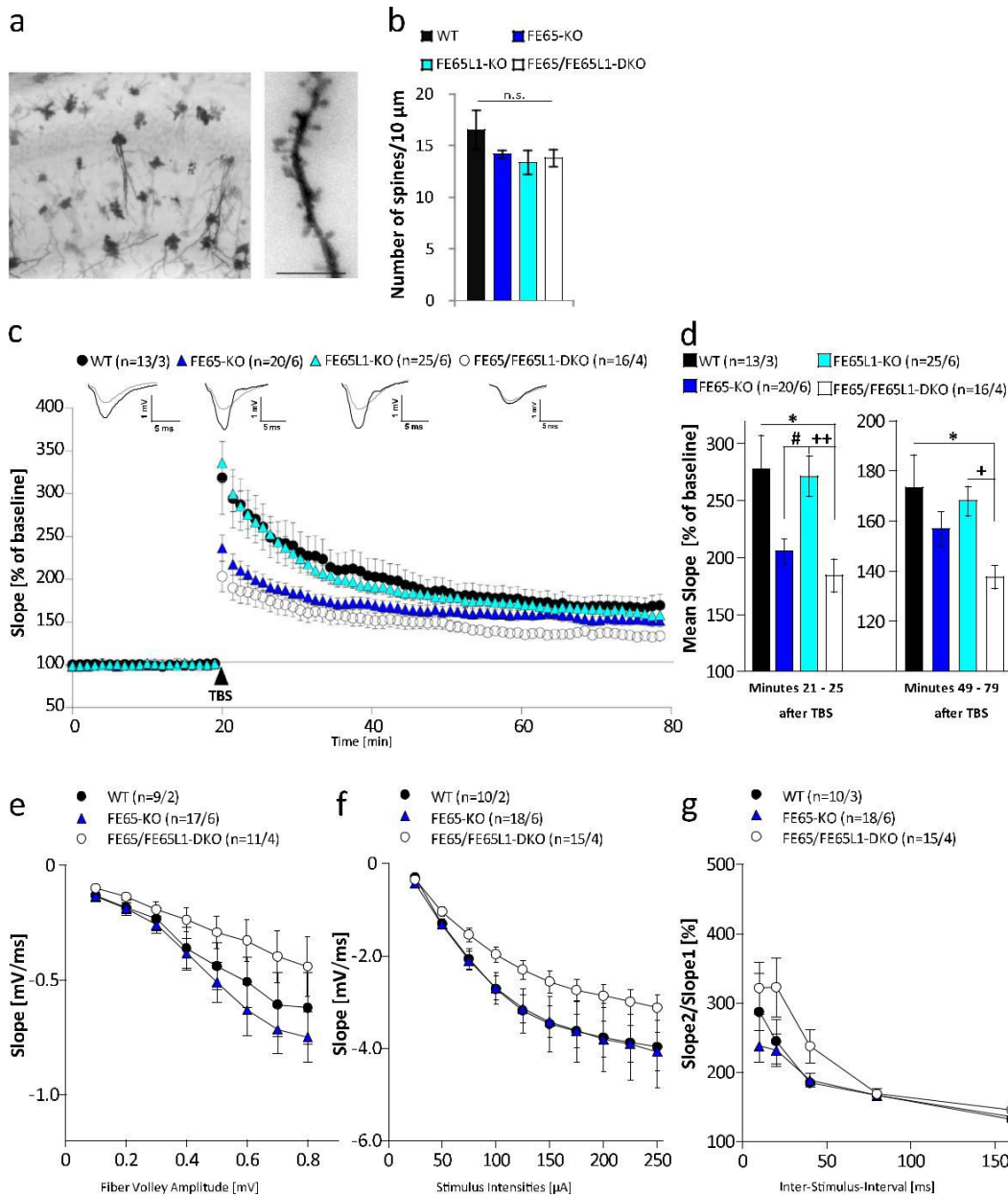
Figure 3. FE65 family KO mice have impaired synaptic plasticity.

Coronal slices (100 µm) were used for spine density analysis. (a) Overview of Golgi stained neurons in the hippocampal CA1 region of a WT mouse brain. Scale bar represents 10 µm. (b) Quantification of total spine density on secondary dendrites of hippocampal CA1 neurons for all genotypes. More than 30 secondary dendrites from three male mice (4–6 months-old) were analyzed for each genotype. (c–g) Field excitatory postsynaptic potentials (fEPSPs) from acute hippocampal slices of indicated genotypes were recorded in the CA1 region following stimulation of CA3 Schaffer collateral axons at a frequency of 0.1 Hz. (c) LTP was induced by application of theta burst stimulus (TBS) after a 20 min baseline stimulation (arrowhead). The LTP induction rate is shown as percentage (%) of the mean baseline slope. Data points were averaged over 6 time points and error bars indicate s.e.m., n = number of recorded slices/ number of animals. (d) PTP values represent averaged potentiation values for the 5 minutes after TBS and the maintenance phase of LTP was calculated from the mean slope of field potentials during the last 30 min of LTP recording. (e) Analysis of the Input-Output (IO) strength of FE65 protein family deficient mice. (f) Neuronal excitability was tested

for all genotypes at increasing stimulus intensities (50–200 µA). (g) PPF behavior using 50 ms inter-stimulus-intervals (ISI) was examined for all mouse genotypes. Male mice between four and six month of age were used for spine density analysis and between 8 and 10 month of age for electrophysiology measurements respectively. Data were analyzed using one-way ANOVA with Bonferroni's post-hoc test. Differences between FE65-KO and FE65L1-KO, between FE65L1-KO and FE65/FE65L1-DKO, and between WT and FE65/FE65L1-DKO mice are marked with #, +, and *, respectively. Error bars are given as s.e.m. */ + /#p < 0.05; ++p < 0.01; n.s. for not significant.

FE65 and FE65L1 proteins are required for normal apposition and sizes of pre- and post-synaptic specializations at the NMJ.

We observed deficits in motor behavior and more specifically in grip strength for FE65/FE65L1-DKO mice that may result from malformations in the motor cortex, spinal cord or NMJ. Heterotopic neurons were previously found in layer 1 of the motor cortex in the more severely affected adult mice (unpublished data). It is possible that this motor cortex phenotype contributes to the observed motor behavior deficits in a subset of FE65/FE65L1 DKO mice. In contrast, Nissl staining of spinal cord morphology revealed no gross morphological differences between genotypes (Supplementary Fig. S2).

NMJ morphology was examined in the *triangularis sterni*. In comparison to other muscle types it offers several advantages: reproducible staining due to its thinness, with fewer than five muscle fiber layers, and the absence of sensory innervation i.e. all neurites branching into this muscle are motor axons[22]. FE65-KO, FE65L1-KO and FE65/FE65L1-DKO mice (6–8 month-old) were examined by staining the pre-synaptic site with an anti-synaptophysin antibody and the post-synaptic site with bungarotoxin, which recognizes nicotinergic acetylcholine receptors (mAChR) (Fig. 4a). Quantification of the pre- and postsynaptic staining showed that the surface area covered by both synaptophysin and AChR were significantly reduced in FE65-KO, FE65L1-KO and FE65/FE65L1-DKO mice compared to WT mice (Fig. 4b, WT vs. FE65 -KO, p = 0.0001; WT vs. FE65L1-KO, p = 0.0001; WT vs. DKO, p = 0.0001 and 4c, WT vs. FE65-KO, p = 0.008; WT vs. FE65L1-KO, p = 0.048; WT vs. DKO, p = 0.0008). Pre- and postsynaptic marker apposition was also reduced in the single KO and DKO mice (Fig. 4d, WT vs. FE65-KO, p = 0.002; WT vs. FE65L1-KO, p = 0.0006; WT vs. DKO, p = 0.0002). In addition, the relative number of fragmented NMJs were significantly increased in the FE65- and FE65L1-KOs, and very pronounced in FE65/FE65L1-DKO mice (Fig. 4e, WT vs. FE65-KO, p = 0.0006; WT

vs. FE65L1-KO, p = 0.0005; WT vs. DKO, p = 0.00001). Additive effects for FE65 and FE65L1 protein loss were noted for the presynaptic area and the post-synapse fragmentation (Fig. 4b,e). These data suggest that the NMJ morphological defects in FE65 family protein KO mice may be responsible for the muscle strength deficits described above.
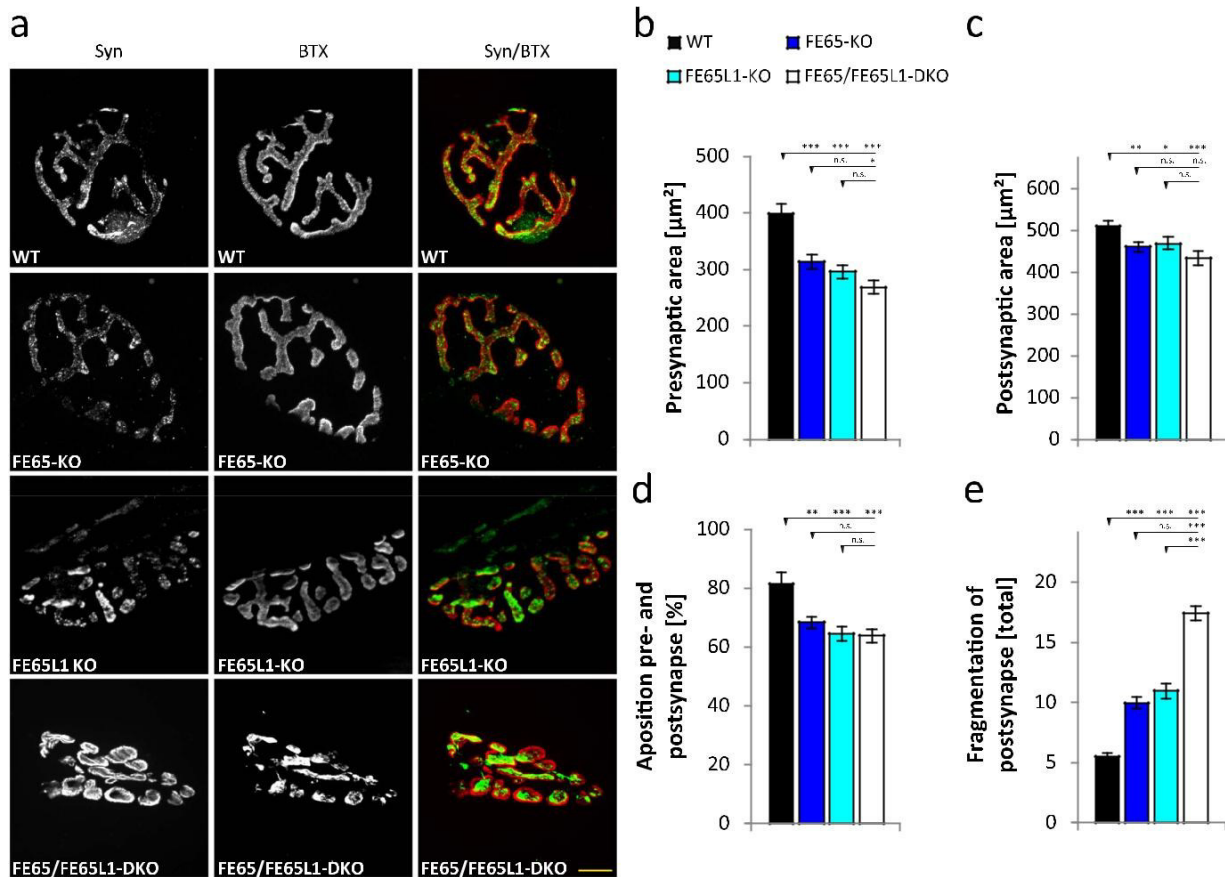

Figure 4. Morphological abnormalities in FE65 family KO Neuromuscular Junctions (NMJs).

WT, FE65-KO, FE65L1-KO, FE65/FE65L1-DKO mice were decapitated, the *triangularis sterni* muscle was dissected and the pre- and postsynaptic areas of NMJs were stained using antibodies against Synaptophysin as a presynaptic marker and Bungarotoxin as a postsynaptic marker, respectively. (**a**) Representative pictures of stained presynaptic (Synaptophysin, Syn, green) and postsynaptic areas (Bungarotoxin, BTX, red) in NMJs of *triangularis sterni* muscle for all mouse genotypes studied. Scale bar represents 10 µm. (**b**) Quantification of synaptophysin positive presynaptic areas of *triangularis sterni* NMJs in all FE65 protein family mouse genotypes. (**c**) Quantification of bungarotoxin positive postsynaptic areas of *triangularis sterni* in NMJs of these mice. (**d**) Quantitative analysis of the apposition of synaptophysin and AChR covered areas of *triangularis sterni* NMJs for all FE65 genotypes studied. (**e**) Quantification of postsynaptic fragmentation in *triangularis sterni* NMJs for all FE65 genotypes studied. In total over 30 NMJs from four animals (6–8 months-old) of age of each genotype were analyzed. Statistical analyses were performed using one-way ANOVA followed with Bonferroni´s post-hoc test. Error bars are given as s.e.m. *p < 0.05; **p < 0.01; ***p < 0.001; n.s. for not significant.

APLP2 deficiency aggravates NMJ deficits in FE65- and FE65L1-KO mice.

APP, APLP1 and APLP2 single KO mice showed no changes in NMJ morphology[23,24]. Likewise, no change was described for NMJs of APPsα or APP CT15 KI mice[25,26]. However, when expressed on an APLP2-KO background, the APP, APLP1 null[24,27] as well as APP mutant genotypes lacking the FE65 binding site all produced deficits at the NMJ[24,28–30]. To determine whether a similar genetic interaction can be found between APP and FE65 protein family members, we examined the NMJ morphologies in 8-month old FE65/APLP2- (Fig. 5a–d) and FE65L1/APLP2-DKO (Fig. 5e–h) mice. Staining of *triangularis sterni* muscles was performed as described above, with the addition that axonal tracks were visualized with an anti-Neurofilament H antibody (Fig. 5a,e). Quantitation of NMJ specializations revealed significantly smaller surface area staining for the pre- and post-synaptic sites of FE65/APLP2-DKO when compared to FE65-KO mice (Fig. 5b,c; 32%, p = 0.000071 and 28%, p = 0.000018, respectively) and for FE65L1/APLP2-DKO when compared to FE65L1-KO mice (Fig. 5f,g; 30%, p = 0.000016 and 36%, p = 0.000011, respectively) . Apposition of pre- and post- synaptic markers (Fig. 5d,h) was also reduced in these mice when compared to WT (p = 0.044), but not when compared to FE65 or FE65L1 single KO mice (p = 0.27and p = 0.25, respectively; data not shown). The existence of a genetic interaction between APLP2 and FE65 or FE65L1 null alleles for NMJ deficits suggests that the physical interaction of these proteins is physiologically relevant at the NMJ.
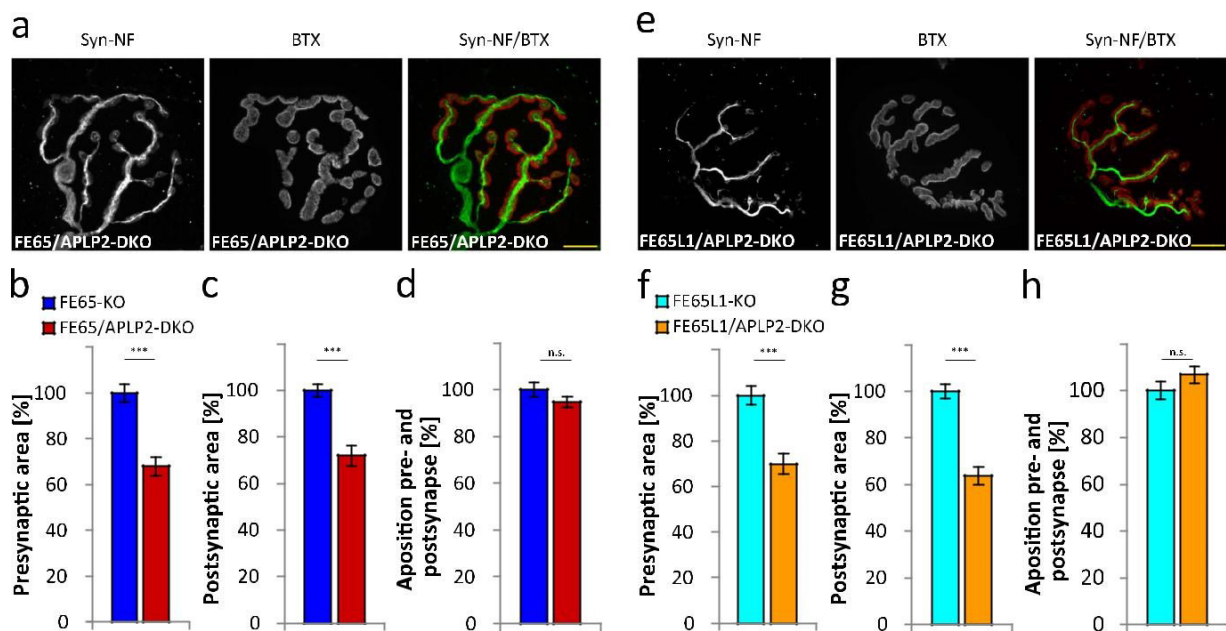
Figure 5. Genetic interaction of FE65 and FE65L1 with APLP2 at the NMJ.

FE65-KO, FE65/APLP2-DKO, FE65L1-KO and FE65L1/APLP2-DKO mice were decapitated, the *triangularis sterni* muscle was dissected and the pre- and postsynaptic areas of NMJs were stained using antibodies against synaptophysin as a presynaptic marker, bungarotoxin as a postsynaptic marker and neurofilament H as a marker for axonal tracks, respectively. (**a**) Representative images of stained presynaptic areas, axonal tracks (Synaptophysin and Neurofilament H, Syn-NH, green) and postsynaptic areas (Bungarotoxin, red) of FE65/APLP2-DKO NMJs of *triangularis sterni* muscle. Scale bar represents 10 µm. (**b**) Quantification of synaptophysin-positive presynaptic areas of *triangularis sterni* NMJs in FE65/APLP2-DKO and FE65-KO mice. (**c**) Quantification of bungarotoxin-positive postsynaptic areas of *triangularis sterni* NMJs in FE65/APLP2-DKO and FE65-KO mice. (**d**) Quantitative analysis of the apposition of synaptophysin and AChR covered areas of *triangularis sterni* NMJs in FE65-KO and FE65/APLP2-DKO mice. (**e**) Representative images of stained FE65L1/APLP2-DKO NMJs of *triangularis sterni* muscle. Scale bar represents 10 µm. (**f**) Quantification of synaptophysin-positive presynaptic areas of *triangularis sterni* NMJs in FE65L1/APLP2-DKO and FE65L1-KO mice. (**g**) Quantification of bungarotoxin-positive postsynaptic areas of *triangularis sterni* NMJs in FE65L1/APLP2-DKO and FE65L1-KO mice. (**h**) Quantitative analysis of the apposition of synaptophysin and AChR covered areas of *triangularis sterni* NMJs in FE65L1-KO and FE65L1/APLP2-DKO mice. In total over 30 NMJs from four animals (8 months-old) of each genotype were analyzed. Statistical analyses were performed using the Student´s t-test. Error bars are given as s.e.m. ***p < 0.001; n.s. for not significant.

DISCUSSION

In this study, we show that mice with genetic deletions of both FE65 and FE65L1 exhibit severe neurological phenotypes, including motor deficits, reduced anxiety, NMJ malformations and LTP impairments. In addition, loss of either FE65 or FE65L1 is sufficient to produce significant spatial learning deficits and NMJ abnormalities. These data suggest widely overlapping functions for FE65 and FE65L1 at central and peripheral synapses. Finally, we demonstrate a genetic interaction between APLP2 and either FE65 or FE65L1 for pre- and post-synaptic NMJ sizes suggesting that the physical interaction of FE65 proteins with APLP2 has functional significance for peripheral synapse structure.

In contrast to the p97FE65- KO, FE65-KO mice have impaired spatial memory[15]. These data suggest that the p60 isoform, which bears both PTB protein-protein interaction domains and a truncated WW domain, is able to compensate for loss of the FE65 protein function involved in spatial memory consolidation or retrieval. Thus, one or more of the 20 proteins with known binding sites in the WW, PTB1 and PTB2 protein-protein interaction domains[31], such as APP or LRP, may participate in FE65-directed cognitive function (Fig. 6).
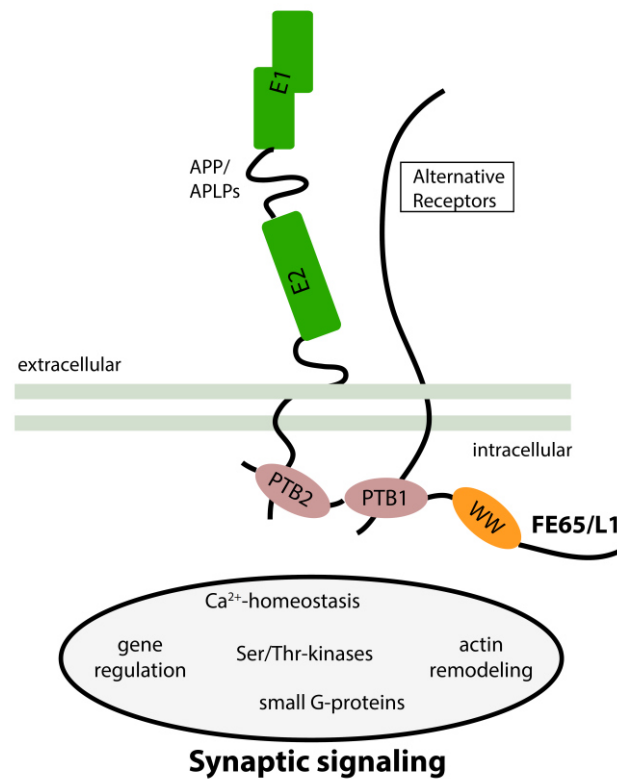
Figure 6. Model summarizing putative FE65/FE65L1 synaptic function.

FE65 and FE65L1 are adaptor proteins that bind different receptors (APP, APLP1, APLP2, ApoER2, LRP1, LRP8, VLDLR, Alcadein/ calsyntenin, P2x$_2$ and others) possibly linking these to pathways that impact synaptic function through molecular interactions with intracellular binding partners, such as calcium signaling (e.g. via DEXRAS1) or actin remodeling (e.g. via Mena) (for a recent review see Chow *et al.*[31]). Based on the remarkable phenotypic similarity of FE65/FE65L1-DKO and APP/APLPs mutants lacking the Fe65 binding site as well as the genetic interaction between APLP2 and FE65/FE65L1 documented in this study, we hypothesize that FE65 and FE65L1 are key components of APP/APLPs synaptic function.

FE65L1-KO mice also displayed spatial memory deficits in the MWM. Yet, only FE65/FE65L1-DKO mice showed deficits in the maintenance phase of LTP and only FE65-KO mice showed a trend towards PTP deficits.

A subset of aged FE65L1 KO mice (16–20 months old) demonstrated cataract and corneal ulcerations[16]. Thus, we cannot formally exclude the possibility that younger FE65L1 KO mice have some visual acuity deficit that interferes with their performance in the MWM tasks. However, since FE65L1-KO mice behaved similarly to littermate controls in the visible platform task and in the initial training, it appears

more likely that loss of FE65L1 affects learning in a manner independent of LTP or visual ability.

A significant difference in the stable phase of LTP (between 50 and 80 min) is only apparent for FE65/ FE65L1-DKO mice. Such deficits in the physiological correlate of memory (LTP) are often presented as a cellular mechanism for spatial memory deficits[32], such as those observed in the MWM for all the KO mice examined in this study. However, since interpretation of the cognitive deficits of FE65/FE65L1-DKO mice is confounded by altered activity (Fig. 1e,f), anxiety (Fig. 1g,h), and possibly visual abilities[16], LTP deficits in these mice cannot be unequivocally linked to the spatial memory deficits observed in the MWM.

FE65 is reported to play a role in the nucleus that includes regulation of gene transcription[1,11,33]. Yet, FE65L1 is unable to induce the transcriptional activation of reporter constructs that served to demonstrate this role for FE65[31,34]. These data suggest that the molecular mechanism by which FE65 and FE65L1 mediate their effect on LTP is not dependent on gene transcription, since both deletion of FE65 and FE65L1 is required to produce LTP deficits.

A presynaptic role for FE65 and FE65L1 is supported by the observation that expression of both FE65 and FE65L1 is upregulated in mature cortical neurons lacking the three Mint/X11 proteins, which play a critical role in presynaptic neurotransmitter release[35]. However, neither PPF nor basal neurotransmission were significantly affected in FE65-KO or FE65/FE65L1-DKO mice, indicating that neurotransmitter release is unaffected.

Impairments in several motor tasks, rotarod, limb clasping, hanging wire and grip strength tests, were observed in FE65/FE65L1-DKO mice (4–6 months old). FE65- and FE65L1-KO mice also showed a similar trend for deficits that did not reach statistical significance. Notably, significant impairments in the hanging wire test were found in a previous study of 14 months old FE65- and FE65L1-KO mice[16]. The difference between our results and those of Suh and co-workers[16] may be explained by an additional impact of aging on motor abilities or may be due to different genetic backgrounds. Furthermore, we observed that the size and apposition of NMJ pre- and postsynaptic sites were significantly reduced in FE65- and FE65L1-KO mice and that these deficits were more pronounced in FE65/FE65L1-DKO mice. Thus, the

severity of morphological NMJ defects in FE65 family KO mice parallel the muscle strength deficits. Defects at the NMJ may result from loss of function of FE65 and/or FE65L1 at pre- or postsynaptic sites since FE65 and FE65L1 are expressed in neurons and skeletal muscle[14,16,36].

As FE65/FE65L1-DKO mice develop brain abnormalities that include cortical heterotopias and hippocampal malformations, which are absent in FE65- and FE65L1-KO mice, it is possible that the brain abnormalities in FE65/FE65L1 DKO mice contribute to the increased latency to fall in the rotarod task[37], a phenotype unique to FE65/FE65L1 DKO mice.

Histological analyses of the mouse quadriceps muscle from 14 month-old FE65/FE65L1-DKO mice showed an absence of severe muscle degeneration. Notably, 14% of the muscle fiber cells harbor centralized nuclei, usually found in immature myofibers[16]. The decreased apposition of pre- and post-synaptic terminals in FE65 family KO mice may produce partial denervation and subsequent myofiber regeneration that contributes to muscle dysfunction in these mice. Together, our data suggest that the observed motor deficits are predominantly due to NMJ abnormalities, particularly since the severity of NMJ deficits correlate with the extent of the motor deficits.

The phenotypes of FE65/FE65L1-DKO mice resemble those observed for mice expressing APP lacking the FE65/FE65L1 interaction site or carrying a mutation in the FE65/FE65L1 binding site (APPY682G) on an APLP2-KO background[26,28,38,39], namely impaired locomotor abilities associated with deficits in NMJ formation. Our data showing aggravation of NMJ defects in FE65/APLP2 or FE65L1/APLP2 compound KO mice provide genetic evidence to support the hypothesis that the FE65/APP protein family interactions are essential for NMJ formation. Interestingly, APP interacts biochemically and genetically with LRP4, a key component of the post-synaptic LRP4/MUSK/Agrin complex[40] mediating signals essential for AChR patterning and stabilization at post-synaptic sites[41–43]. The FE65 protein family members may play a role in modulating LRP4/MuSK/Agrin complex function at the NMJ.

The synaptic function of Mint/X11 proteins[35] led others to propose a role for these proteins in the manifestation of APP- dependent NMJ phenotypes [28]. However, since

the Mint/X11 knockout mice[35] do not exhibit the same synaptic phenotypes as APP/APLP2 or APLP1/APLP2 knockout mice, and a genetic interaction exists between FE65 or FE65L1 and APLP2, we postulate that of the APP-binding proteins that bind the NPTY motif, it is the FE65 proteins that are primarily responsible for APP/APLP function at the NMJ.

Together our data suggest a pivotal role for FE65/FE65L1 in the central and peripheral nervous systems, possibly downstream of APP/APLP-dependent signaling at the synapse (Fig. 6). These data now form a basis for determining which partners of the FE65/FE65L1 interactome[31] are involved in these neuronal processes. These may include proteins implicated in nuclear signaling[11,44], actin cytoskeleton regulation[5,45,46], or those critically involved in FE65/FE65L1 synaptic function[8]. Alternatively, phosphorylation of FE65 which regulates proteasomal degradation of APP and possibly other binding partners may be responsible for its effects at the synapse[31].

METHODS

Animals.

FE65- and FE65L1-KO mice[14] were backcrossed a minimum of ten times on the C57/BL6J (Janvier) mouse background prior to this study. Mice were genotyped as previously described[14]. Ten to twelve male mice (4–6 month-old) of each genotype were used for behavioral studies. WT mice were littermates from crosses set up to generate FE65-KO or FE65L1-KO mice. Mouse husbandry was performed according to local and National Institutes of Health (NIH) guidelines using groups of 4–5 mice per breeding cage, maintained under constant temperature, humidity and a 12 h light/dark cycle, with food and water *ad libitum*. One week before behavioral studies were performed, mice were separated and kept single in breeding cages. Treatment of mice was in accordance with the German law for conducting animal experiments and followed the NIH guide for the care and use of laboratory animals. All experimental protocols were carried out in accordance with the European Communities Council Directive of 24 November 1986 (86/609/EEC). Animal housing, breeding, behavioral studies and euthanasia were approved by the Landesuntersuchungsamt Rheinland-Pfalz,Germany.

Behavioral studies.

All behavioral studies were performed in a blinded fashion.

The Tail Hanging Test[17] was performed by recording the limb position five seconds after suspending each mouse by the tail. Three different positions were distinguished: Position 2, all limbs were stretched out; Position 1, front or back limbs were tucked; Position 0, all limbs were tucked.

For the Hanging Wire Test, the edges of a home cage wire lid were masked with tape to prevent mice from climbing over the rim onto the top of the wire lid during the experiment. Mice were placed on the middle of the wire lid, which was carefully inverted to ensure that mice had a proper grip on the wires and the latency to fall was measured.

For each mouse, the grip strength was measured for all limbs using a Grip Strength Meter 303500 ®(TSE Systems, v.2.32). Mice were put on a special grip mounted on

a force sensor and slowly pulled by the tail. The maximum force exerted was shown on a connected control unit after the animals released their grip.

Movement coordination was analyzed using the Mouse Rota Rod (Ugo Basil, type 7600). Mice were trained for two days at the slowest rotation speed (14 rpm). Two training sessions were performed on each day with a 15 min break in between. On the third day, mice were placed on the Rota Rod and tested using a stepwise increase in rotation speed from 14 to 28 rpm with 2 rpm increases every 60 s and time to fall was measured.

For open field analysis mice were put in a box with an area of 60 cm × 60 cm (TSE Systems) for one hour. Their movement, traveled distance and residence time in the center and in the periphery of the open field were recorded and evaluated with the TSE VideoMot 2 software over the entire 60 min time period[21].

For the Elevated Plus Maze test[21] mice were placed on a 50 cm high cross-shaped table (TSE Systems) with two closed and two open arms. Mouse behavior in the maze was recorded for 5 min and the time spent in the open arms was evaluated using the TSE VideoMot2 software.

For Morris Water Maze experiments (TSE Systems)[21,47], mice were first tested for their ability to climb onto the platform and become familiar with the task, mice were trained for one day using a visible platform, identified by a black pencil fixed to the platform in a vertical position. For each trial a single mouse was placed in the water at different locations. On the next day the platform was moved to another quadrant, the pencil was removed and four symbols of different shapes and color were placed on the pool wall for orientation. Mice were trained for five days, 4 trials/day, in a pool filled with opaque water containing a platform placed 0.5 cm beneath the water surface. The probe trial was performed on the sixth day and involved removing the platform and recording the residence time of mice in each quadrant for 60 s. Training for the reverse hidden platform test was started on the eight day after one day of rest. In this test the hidden platform was moved to the opposite quadrant and mice were trained for four days, 4 trials/day. The probe trial for this test involved removing the platform on day 12 and recording the residence time of mice in each quadrant over 60 s. Training and probe trials were recorded and analyzed using the TSE VideoMot

2 Software. The time required for each mouse to find the platform and the residence time in each quadrant was evaluated for the two probe trials.

Spine density analysis.

Male mice (4–6 month old) were deeply anesthetized with 4% chloral hydrate/PBS with 100 µl/10 g bodyweight and perfused with 50 ml PBS followed by 50 ml 4% PFA/PBS to fix the tissues. Brains were dissected and fixed overnight at 4 °C in 4% PFA/PBS. Golgi staining was performed with the FD Rapid Golgi-Staining™ Kit on 100 µm thick coronal slices obtained using a vibratome (Campden Instruments Ltd.). Spines were counted on 10 µm long secondary dendrites of hippocampal neurons of the CA1 basal and apical region.

Histological analysis.

Triangularis sterni muscle of male mice (6–8 months-old) were dissected as described[22]. Mice were decapitated after CO_2 treatment and the muscle was dissected and stored in PBS for sub-sequent staining. Muscle tissue was incubated with an antibody against synaptophysin (Invitrogen) to stain pre-synaptic vesicles, anti-neurofilament H (Chemicon) to visualize axons and Alexa594 conjugated bungarotoxin (Invitrogen) to stain nicotinic acetylcholine receptors in the postsynapse.

For spinal cord analysis mice (6–8 months old) were deeply anesthetized with 4% chloral hydrate/PBS using 100 µl/10 g bodyweight and perfused with 50 ml PBS followed by 50 ml 4% PFA/PBS for tissue fixation. Spinal cords were carefully dissected as described [48] and fixed overnight at 4 °C in 4% PFA/PBS followed by another incubation overnight in 30% Sucrose/PBS at 4 °C. 30 µm thick frozen coronal sections of the ~C8-C6 region were prepared according to Harrison and co-workers[49] using a freezing microtome (Microm KS 34, Thermo Scientific) and mounted on slides for further analyses. Sections of the spinal cord were Nissl stained for morphological evaluation or sections were immunostained with an antibody against choline acetyltransferase (#178850, Abcam) according to the manufacturer´s protocol to visualize motor neurons in the mouse cervical spinal cord anterior horn[48].

Images of Nissl stained spinal cord sections were generated with an Olympus SZX7 microscope, an Olympus DP20 camera and the CellF software (Olympus, Hamburg,

Germany). Microscopic images for NMJ and spine density analysis were recorded using a Zeiss Axio Observer Z.1 and the corresponding Axio Vision Rel.4.8 software. For quantification of areas, apposition and fragmentation ImageJ software was used.

Electrophysiology.

Acute hippocampal transversal slices were prepared from individual 8 to 10 month-old mice. Mice were anesthetized with isoflurane and decapitated. The brain was removed and quickly transferred into ice-cold carbogenated (95% O_2, 5% CO_2) artificial cerebrospinal fluid (ACSF) containing 125 mM NaCl, 2 mM KCl, 1.25 mM NaH_2PO_4, 2 mM $MgCl_2$, 26 mM $NaHCO_3$, 2 mM $CaCl_2$, 25 mM glucose. Hippocampi were dissected and cut into 400 µm thick transversal slices with a vibratome (Leica, VT1200S). Slices were maintained in carbonated ACSF at room temperature for at least 1.5 h before transferred into a submerged recording chamber. Slices were placed in a submerged recording chamber and perfused with carbonated ACSF (32 °C) at a rate of 1 to 1.5 ml/min. Field excitatory postsynaptic potentials (fEPSPs) were recorded in stratum radiatum of CA1 region with a borosilicate glass micropipette (resistance 3–15 MΩ) filled with 3 M NaCl at a depth of ~ 150–200 µm.

Monopolar tungsten electrodes were used for stimulating the Schaffer collaterals at a frequency of 0.1 Hz. Stimulation intensity was adjusted to ~40% of the maximum fEPSP slope for the 20 minutes baseline recordings. LTP was induced by applying theta-burst stimulation (TBS: 10 trains of 4 pulses at 100 Hz in a 200 ms interval, repeated 3 times). Properties of baseline synaptic transmission were analyzed via input-output (IO) -measurements and short -term plasticity was probed via paired pulse facilitation (PPF). The IO- measurements were performed either by application of a defined current values (25–250 µA) or by adjusting the stimulus intensity to certain fiber volley (FV) amplitudes (0.1–0.8 mV). PPF was performed by applying a pair of two closely spaced stimuli in different inter-stimulus-intervals (ISI) ranging from 10 to 160 ms.

All experiments were performed in a blinded manner. Electrophysiological data were collected, stored and analyzed with LABVIEW software (National Instruments, Austin, TX). The initial slope of fEPSPs elicited by stimulation of the Schaffer collaterals was measured over time, normalized to baseline and plotted as average ± SEM. Analysis

of the PPF data was performed by calculating the ratio of the slope of the second fEPSP divided by the slope of the first one and multiplying by 100.

Statistical analyses.

In general one-way ANOVA (Microsoft Office, Excel 2010) was used to assess statistical differences between the four genotypes given that data were normally distributed (Shapiro-Wilk -Test) and variance (Levene-Test) was not significantly (α= 0.05) different. The Bonferroni method was used as a post hoc test (GraphPrism Software, www.graphpad.com). The Kruskal-Wallis- Test followed by Dunn´s Multiple Comparison Test was used to assess statistical differences between the four genotypes given that data weren´t normally distributed or variance was significantly different. MWM probe trials data were analyzed using two-way ANOVA (Microsoft Office, Excel 2010) to compare residence times in different quadrants for all tested genotypes. Escape latencies data during Visible, Hidden and Reversed Platform trials were analyzed by two-way repeated measures ANOVA (Greenhouse-Geisser correction, α = 0.05) using the Real Statistics Resource Packsoftware (Release 3.8, Copyright (2013–2015) Charles Zaiontz. www.real- statistics.com) for comparison of learning over time for all tested genotypes. The unpaired two-tailed Student's t-test (Microsoft Office, Excel 2010) was used when comparing only two sets of data with normal distributions. All data are shown as standard error of the mean (s.e.m.). Significance was set at $*p < 0.05$ $**p < 0.01$ and $***p < 0.001$, n.s. for not significant.

REFERENCES

1) McLoughlin, D. M. & Miller, C. C. The FE65 proteins and Alzheimer's disease. *J Neurosci Res* **86,** 744–754, doi: 10.1002/jnr.21532 (2008).

2) Hoe, H. S. *et al.* FE65 interaction with the ApoE receptor ApoEr2. *J Biol Chem* **281,** 24521–24530, doi: 10.1074/jbc.M600728200 (2006).

3) Trommsdorff, M., Borg, J. P., Margolis, B. & Herz, J. Interaction of cytosolic adaptor proteins with neuronal apolipoprotein E receptors and the amyloid precursor protein. *J Biol Chem* **273,** 33556–33560 (1998).

4) Dumanis, S. B. *et al.* FE65 as a link between VLDLR and APP to regulate their trafficking and processing. *Molecular neurodegeneration* **7,** 9, doi: 10.1186/1750-1326-7-9 (2012).

5) Ermekova, K. S. *et al.* The WW domain of neural protein FE65 interacts with proline-rich motifs in Mena, the mammalian homolog of Drosophila enabled. *J Biol Chem* **272,** 32869–32877 (1997).

6) Ikin, A. F., Sabo, S. L., Lanier, L. M. & Buxbaum, J. D. A macromolecular complex involving the amyloid precursor protein (APP) and the cytosolic adapter FE65 is a negative regulator of axon branching. *Molecular and cellular neurosciences* **35,** 57–63, doi: 10.1016/j.mcn.2007.02.003 (2007).

7) Cheung, H. N. *et al.* FE65 interacts with ADP-ribosylation factor 6 to promote neurite outgrowth. *FASEB journal: official publication of the Federation of American Societies for Experimental Biology* **28,** 337–349, doi: 10.1096/fj.13-232694 (2014).

8) Nensa, F. M. *et al.* Amyloid beta a4 precursor protein-binding family B member 1 (FE65) interactomics revealed synaptic vesicle glycoprotein 2A (SV2A) and sarcoplasmic/endoplasmic reticulum calcium ATPase 2 (SERCA2) as new binding proteins in the human brain. *Molecular & cellular proteomics : MCP* **13,** 475–488, doi: 10.1074/mcp.M113.029280 (2014).

9) Sumioka, A. *et al.* Role of 14-3-3gamma in FE65-dependent gene transactivation mediated by the amyloid beta-protein precursor cytoplasmic fragment. *J Biol Chem* **280,** 42364–42374 (2005).

10) Lau, K. F. *et al.* Dexras1 interacts with FE65 to regulate FE65-amyloid precursor protein-dependent transcription. *J Biol Chem* **283,** 34728–34737, doi: 10.1074/jbc.M801874200 (2008).

11) Cao, X. & Sudhof, T. C. A transcriptionally [correction of transcriptively] active complex of APP with Fe65 and histone acetyltransferase Tip60. *Science* **293,** 115–120 (2001).

12) Minopoli, G., Gargiulo, A., Parisi, S. & Russo, T. Fe65 matters: new light on an old molecule. *IUBMB life* **64,** 936–942, doi: 10.1002/ iub.1094 (2012).

13) Wang, B. *et al.* Isoform-specific knockout of FE65 leads to impaired learning and memory. *J Neurosci Res* **75,** 12–24, doi: 10.1002/ jnr.10834 (2004).

14) Guenette, S. *et al.* Essential roles for the FE65 amyloid precursor protein-interacting proteins in brain development. *The EMBO journal* **25,** 420–431, doi: 10.1038/sj.emboj.7600926 (2006).

15) Wang, Y. *et al.* The APP-interacting protein FE65 is required for hippocampus-dependent learning and long-term potentiation. *Learning & memory* **16,** 537–544, doi: 10.1101/lm.1499309 (2009).

16) Suh, J. *et al.* FE65 and FE65L1 amyloid precursor protein-binding protein compound null mice display adult-onset cataract and muscle weakness. *FASEB journal : official publication of the Federation of American Societies for Experimental Biology*, doi: 10.1096/ fj.14-261453 (2015).

17) Lalonde, R. & Strazielle, C. Brain regions and genes affecting limb-clasping responses. *Brain Res Rev* **67,** 252–259, doi: 10.1016/j. brainresrev.2011.02.005 (2011).

18) Newbern, J. M. *et al.* Specific functions for ERK/MAPK signaling during PNS development. *Neuron* **69,** 91–105, doi: 10.1016/j. neuron.2010.12.003 (2011).

19) Hayward, L. J. *et al.* Targeted mutation of mouse skeletal muscle sodium channel produces myotonia and potassium-sensitive weakness. *J Clin Invest* **118,** 1437–1449, doi: 10.1172/JCI32638 (2008).

20) Auerbach, W. *et al.* The HD mutation causes progressive lethal neurological disease in mice expressing reduced levels of huntingtin. *Human molecular genetics* **10,** 2515–2523 (2001).

21) Zimmermann, A. M. *et al.* Attention-Deficit/Hyperactivity Disorder-like Phenotype in a Mouse Model with Impaired Actin Dynamics. *Biol Psychiatry*, doi: 10.1016/j.biopsych.2014.03.011 (2014).

22) Kerschensteiner, M., Reuter, M. S., Lichtman, J. W. & Misgeld, T. *Ex vivo* imaging of motor axon dynamics in murine triangularis sterni explants. *Nat Protoc* **3,** 1645–1653, doi: 10.1038/nprot.2008.160 (2008).

23) Wang, P. *et al.* Defective neuromuscular synapses in mice lacking amyloid precursor protein (APP) and APP-Like protein 2. *J Neurosci* **25,** 1219–1225 (2005).

24) Klevanski, M. *et al.* Differential role of APP and APLPs for neuromuscular synaptic morphology and function. *Molecular and cellular neurosciences* **61,** 201–210, doi: 10.1016/j.mcn.2014.06.004 (2014).

25) Ring, S. *et al.* The secreted beta-amyloid precursor protein ectodomain APPs alpha is sufficient to rescue the anatomical, behavioral, and electrophysiological abnormalities of APP-deficient mice. *J Neurosci* **27,** 7817–7826 (2007).

26) Barbagallo, A. P., Wang, Z., Zheng, H. & D'Adamio, L. A single tyrosine residue in the amyloid precursor protein intracellular domain is essential for developmental function. *J Biol Chem* **286,** 8717–8721, doi: 10.1074/jbc.C111.219873 (2011).

27) Wang, Z. *et al.* Presynaptic and postsynaptic interaction of the amyloid precursor protein promotes peripheral and central synaptogenesis. *J Neurosci* **29,** 10788–10801, doi: 29/35/10788 (2009).

28) Weyer, S. W. *et al.* APP and APLP2 are essential at PNS and CNS synapses for transmission, spatial learning and LTP. *The EMBO journal* **30,** 2266–2280, doi: 10.1038/emboj.2011.119 (2011).

29) Li, H. *et al.* Soluble amyloid precursor protein (APP) regulates transthyretin and Klotho gene expression without rescuing the essential function of APP. *Proc Natl Acad Sci USA* **107,** 17362–17367, doi: 1012568107 (2010).

30) Klevanski, M. *et al.* The APP Intracellular Domain Is Required for Normal Synaptic Morphology, Synaptic Plasticity, and Hippocampus-Dependent Behavior. *J Neurosci* **35,** 16018–16033, doi: 10.1523/JNEUROSCI.2009-15.2015 (2015).

31) Chow, W. N., Cheung, H. N., Li, W. & Lau, K. F. FE65: Roles beyond amyloid precursor protein processing. *Cell Mol Biol Lett* **20,** 66–87, doi: 10.1515/cmble-2015-0002 (2015).

32) Lynch, M. A. Long-term potentiation and memory. *Physiol Rev* **84,** 87–136, doi: 10.1152/physrev.00014.2003 (2004).

33) Konietzko, U. AICD nuclear signaling and its possible contribution to Alzheimer's disease. *Curr Alzheimer Res* **9,** 200–216 (2012).

34) Cool, B. H., Zitnik, G., Martin, G. M. & Hu, Q. Structural and functional characterization of a novel FE65 protein product upregulated in cognitively

impaired FE65 knockout mice. *J Neurochem* **112,** 410–419, doi: 10.1111/j.1471-4159.2009.06456.x (2010).

*35)*Ho, A. *et al.* Genetic analysis of Mint/X11 proteins: essential presynaptic functions of a neuronal adaptor protein family. *J Neurosci* **26,** 13089–13101, doi: 10.1523/JNEUROSCI.2855-06.2006 (2006).

36)Suh, J., Lyckman, A., Wang, L., Eckman, E. A. & Guenette, S. Y. FE65 proteins regulate NMDA receptor activation-induced amyloid precursor protein processing. *J Neurochem* **119,** 377–388, doi: 10.1111/j.1471-4159.2011.07419.x (2011).

37)Scholz, J., Niibori, Y., Frankland, P. W. & Lerch, J. P. Rotarod training in mice is associated with changes in brain structure observable with multimodal MRI. *Neuroimage* **107,** 182–189, doi: 10.1016/j.neuroimage.2014.12.003 (2015).

*38)*Li, H. *et al.* Genetic dissection of the amyloid precursor protein in developmental function and amyloid pathogenesis. *J Biol Chem* **285,** 30598–30605, doi: M110.137729/jbc.M110.137729 (2010).

39)Klevanski, M. *et al.* The APP Intracellular Domain Is Required for Normal Synaptic Morphology, Synaptic Plasticity, and Hippocampus-Dependent Behavior. *J Neurosci* **35,** 16018-16033, doi: 10.1523/JNEUROSCI.2009-15.2015 (2015).

40)Choi, H. Y. *et al.* APP interacts with LRP4 and agrin to coordinate the development of the neuromuscular junction in mice. *eLife* **2,** e00220, doi: 10.7554/eLife.00220 (2013).

*41)*Kim, M. L. *et al.* O-fucosylation of muscle agrin determines its ability to cluster acetylcholine receptors. *Molecular and cellular neurosciences* **39,** 452–464, doi: 10.1016/j.mcn.2008.07.026 (2008).

42)Zhang, W., Coldefy, A. S., Hubbard, S. R. & Burden, S. J. Agrin binds to the N-terminal region of Lrp4 protein and stimulates association between Lrp4 and the first immunoglobulin-like domain in muscle-specific kinase (MuSK). *J Biol Chem* **286,** 40624–40630, doi: 10.1074/jbc.M111.279307 (2011).

43)Wu, H. *et al.* Distinct roles of muscle and motoneuron LRP4 in neuromuscular junction formation. *Neuron* **75,** 94–107, doi: 10.1016/j.neuron.2012.04.033 (2012).

44)Kimberly, W. T., Zheng, J. B., Guenette, S. Y. & Selkoe, D. J. The intracellular domain of the beta-amyloid precursor protein is stabilized by Fe65 and translocates to the nucleus in a notch-like manner. *J Biol Chem* **276,** 40288–40292 (2001).

45) Lambrechts, A. *et al.* cAMP-dependent protein kinase phosphorylation of EVL, a Mena/VASP relative, regulates its interaction with actin and SH3 domains. *J Biol Chem* **275,** 36143–36151, doi: 10.1074/jbc.M006274200 (2000).

46) Sabo, S. L., Ikin, A. F., Buxbaum, J. D. & Greengard, P. The amyloid precursor protein and its regulatory protein, FE65, in growth cones and synapses *in vitro* and *in vivo*. *J Neurosci* **23,** 5407–5415 (2003).

47) Morris, R. Developments of a water-maze procedure for studying spatial learning in the rat. *J Neurosci Methods* **11,** 47–60 (1984).

48) Gunther, R. *et al.* Clinical testing and spinal cord removal in a mouse model for amyotrophic lateral sclerosis (ALS). *J Vis Exp*, doi: 10.3791/3936 (2012).

49) Harrison, M. *et al.* Vertebral landmarks for the identification of spinal cord segments in the mouse. *Neuroimage* **68,** 22–29, doi: 10.1016/j.neuroimage.2012.11.048 (2013).

Chapter II

Analysis of Fe65 dimerization properties *in vitro*

Background

The conserved eukaryotic Fe65 protein family contains C-terminal two phosphotyrosine-binding domains (PTB) followed by an N-terminal WW domain. These adaptor proteins are involved in many cellular pathways acting as a functional linker among various interaction partner (McLoughlin & Miller 2008, Chow et al. 2015). The WW domain was shown to bind proline riche sequences, e.g. Mena and thereby influencing actin cytoskeleton remodeling, cell movement and cell adhesion (Sabo et al. 2001). Based on its interaction via the PTB2 domain with the APP intracellular domain (AICD) (Russo et al. 1998), Fe65 was shown to play an essential role in the pathogenesis of Alzheimers Disease by modulating APP processing and Aβ generation (Müller et al. 2008). Fe65-PTB1 domain was mainly shown to bind to the histone acetyltransferase Tip60, forming a trimeric complex of Fe65/Tip60/AICD involved in nuclear signaling and influencing transcriptional activity (Cao & Südhof 2001). Interaction of the PTB1 domain with the transcription factor CP2/LSF/LBP1 further underlines the importance of Fe65 in regulating transactivation of a yet not well characterized set of genes (Zambrano et al. 1998).

The Fe65-PTB2 domain binds to the NPTY motif within the AICD in a phosphotyrosine-independent (Uhlik et al. 2005) maner capturing the canonical PTB-relevant tyrosine in the hydrophobic binding pocket (J Radzimanowski et al. 2008a).

Here we analyzed the structure and functions of the Fe65-PTB2 in more detail and could show *in vitro* as well as *ex vivo* that the Fe65-PTB2 domain is capable to form homodimers. Interestingly, dimer formation leads to an unfolding of the C-terminus of one Fe65 molecule (donor) and thereby mimicking the AICD NPTY motif by binding in a competitive fashion to the second Fe65 molecule (acceptor).

Methods

Human Fe65-PTB2 domain was expressed and purified via size exclusion chromatography (SEC) followed by multi angle light scattering (MALS) measurements and finally crystallized in liquid nitrogen for X-ray structure analysis. X-ray data, collected at the European Synchrotron Radiation Facility, was subsequently integrated, merged and the structure was solved by molecular replacement method using known monomeric Fe65-PTB2 structure out of Fe65-PTB2/AICD complex (Radzimanowski et al. 2008). For dimer analysis in solution, purified proteins were spin labeled with 3-(2-Iodoacetamido)-proxyl or ^{15}N- or ^{13}C/^{15}N respectively and further examined by small angle X-ray scattering (SAXS) as well as Nuclear magnetic resonance (NMR) and Paramagnetic Relaxation Enhancements (PRE) measurements.

To verify Fe65 dimer formation ex vivo, pull down experiments were carried out by transfecting HEK cells with vectors co-expressing either m-cherry tagged full length Fe65 or deletion mutants lacking Fe65-PTB2 domain, -PTB1 domain, -WW domain or lacking the Fe65PTB2 and WW domain together with full length Fe65 harboring a streptavidin-binding peptide and a myc-tag. The influence of APP on Fe65 dimerization was analyzed by Co-Immunoprecipitation studies via cells lysates of co-transfected HEK cells expressing HA- and Flag-tagged Fe65 as well as myc-tagged APP and by subcellular fractionation experiments.

Results and Discussion

During purification of the Fe65-PTB2 domain via size exclusion chromatography (SEC) monomeric as well as dimeric and even trimeric complexes of Fe65-PTB2 domain were detected. Further, multi-angle light scattering measurements (MALS) and analysis via SDS-Page confirmed the finding of oligomerized PTB2 domain. X-ray structure analysis and molecular replacement modeling using the known Fe65-PTB2/AICD complex (Radzimanowski et al. 2008b) revealed that Fe65-PTB2 can form a dimer of dimers induced by structural transformation of the C-terminal α3-helix into a β-strand. To exclude possible artificial properties leading to dimer formation in crystal, small angle X-ray scattering (SAXS) measurements in solution were performed. Model refinement and fitting of the acquired data by calculating the theoretical scattering curves of monomers, dimers and tetramers revealed that most of Fe65-PTB2 is dimerized corroborating the results of the crystal structure analysis.

High resolution structural information was gained by detailed NMR characterization. Thereby, incorporated ^{15}N, achieved during protein assembly by growing *E.Coli* in ^{15}N-containing M9 media, leads to chemical shifts during NMR spectroscopy predicting a partially stable α3-helix and increasing flexibility of the c-terminus of the latter. Interestingly, analysis of the ^{15}N relaxation experiments suggest higher percentage of monomers than dimers in solution by comparing the rotational correlation time of 10.6 ns to 8.9 ns (for complementing subunit) and 15.7 ns (for crystallographic dimer). However, since the flexible part of the α3-helix mediates the dimer formation and is further supported by observed quickly reducing backbone order parameters S^2 for the C-terminus of the α3-helix a dimeric form of Fe65-PTB2 seems to be favorable. This dimer formation in solution was afterwards characterized by measuring paramagnetic relaxation enhancements (PREs) after introducing nitro-oxide spin labels which covalently bind cysteine residues. A prerequisite for the PRE analysis is a solely single spin-label attached to each peptide. Therefore, a series of consecutive mutation of all six cysteines harboured in the Fe65-PTB2 was performed to define the available solvent exposed cysteine which was afterwards paramagnetically labeled. The C663E mutant with its uniquely labeled cysteine on position 661 was used for further detailed PRE measurements. Due to the correlation of the induced relaxation and bleaching (Clore 2015), the structure and the specific complex could be determined.

Exploring the dimer formation of two Fe65-PTB2 peptides and comparing the binding between the AICD and Fe65-PTB2 (Radzimanowski et al. 2008) we found an interesting correlation. While in AICD (GYENTPY)/Fe65-PTB2 complex formation the glycine at position 681 plays an essential role in placing the αN-helix in a vertical position to the α3-helix of Fe65-PTB2 it is the cysteine at position 661 of F65-PTB2 which takes over this binding without introduction of a similar hinge. In Addition, an intramolecular salt bridge between Glutamate E^{683} of AICD and a lysine K^{688} (following the GYENTPY sequence) is replaced by Fe65-PTB2 leucine L^{662} and arginine R^{665} forming an identical AICD-Fe65-PTB2 intramolecular salt bridge. Thus, the Fe65-PTB2 dimer formation mimics the AICD/Fe65-PTB2 complex by effectively capping the binding region and shielding the AICD binding.

Having shown that Fe65-PTB2 dimer formation occurs *in vitro* in crystal as well as in solution we analyzed in a next step the dimerization properties of Fe65 *ex vivo* using pull down and co-immunoprecipitation experiments. Thereby analysis of different deletion mutants revealed that Fe65 indeed is able to form dimers *ex vivo* and that the PTB2 domain is responsible for the dimer formation. Interestingly, although deletion of the WW domain alone leads to no significant change in dimer formation, loss of the WW and PTB2 domain further decreased dimerization properties of Fe65. Further, examination of the native state of Fe65 via Blue Native Gel analyses of cytosolic and membrane fractions of transfected HEK cell lysates revealed that Fe65 migrates in the gel as a single band at a molecular weight of approximately 240 kDa underlining a mostly dimerized form of Fe65. While solely expressed Fe65 was prominently detected in the cytosolic fraction, co-expression of APP caused a shift of Fe65 localisation from the cytosol to the membrane fraction. Furthermore, the influence of APP expression on Fe65 dimer formation was analyzed via co-immunoprecipitation studies. These experiments indicated that Fe65 can still dimerize in the presence of APP and that even trimeric complexes might be formed. The details of this complex are yet unknown, but might involve besides intermolecular interactions between two PTB2 domains also Fe65 dimerization via the WW and PTB1-PTB2 linker domain, previously described as an intramolecular interaction (Cao & Südhof 2004).

Conclusion

In our study we could show that Fe65 is able to form dimers *in vitro* as well as *ex vivo* via its PTB2 domain. Further, we could demonstrate that the flexible α3-helix of Fe65-PTB2 mimics AICD/Fe65 complex formation leading to efficient shielding of AICD binding to Fe65 suggesting a regulatory function of the multiprotein-adapter protein in intracellular APP signaling pathway.

References

Cao, X. & Südhof, T.C., 2001. A transcriptionally [correction of transcriptively] active complex of APP with Fe65 and histone acetyltransferase Tip60. Science (New York, N.Y.), 293(5527), pp.115–20.

Chow, W.N.V. et al., 2015. FE65: Roles beyond amyloid precursor protein processing. Cellular & molecular biology letters, 20(1), pp.66–87.

Clore, G.M., 2015. Practical Aspects of Paramagnetic Relaxation Enhancement in Biological Macromolecules. Methods in Enzymology, 564, pp.485–49.

McLoughlin, D.M. & Miller, C.C.J., 2008. The FE65 proteins and Alzheimer's disease. Journal of neuroscience research, 86(4), pp.744–54.

Müller, T. et al., 2008. The amyloid precursor protein intracellular domain (AICD) as modulator of gene expression, apoptosis, and cytoskeletal dynamics-Relevance for Alzheimer's disease. Progress in Neurobiology, 85(4), pp.393–406.

Radzimanowski, J. et al., 2008a. Structure of the intracellular domain of the amyloid precursor protein in complex with Fe65-PTB2. EMBO Reports, 9(11), pp.1134–1140.

Radzimanowski, J. et al., 2008b. Structure of the intracellular domain of the amyloid precursor protein in complex with Fe65-PTB2. EMBO Rep, 9(11), pp.1134–1140.

Radzimanowski, J. et al., 2008. Structure of the intracellular domain of the amyloid precursor protein in complex with Fe65-PTB2. EMBO reports, 9(11), pp.1134–40.

Russo, T. et al., 1998. Fe65 and the protein network centered around the cytosolic domain of the Alzheimer â€™ s L -amyloid precursor protein. , 434, pp.1–7.

Sabo, S.L. et al., 2001. The Alzheimer amyloid precursor protein (APP) and FE65, an APP-binding protein, regulate cell movement. The Journal of cell biology, 153(7), pp.1403–14.

Uhlik, M.T. et al., 2005. Structural and evolutionary division of phosphotyrosine binding (PTB) domains. Journal of Molecular Biology, 345(1), pp.1–20.

Zambrano, N. et al., 1998. The Fe65 adaptor protein interacts through its PID1 domain with the transcription factor CP2/LSF/LBP1. Journal of Biological Chemistry, 273(32), pp.20128–20133.

Fe65-PTB2 Dimerization Mimics Fe65-APP Interaction

Lukas P. Feilen [1†], Kevin Haubrich [1,2†], **Paul Strecker** [3], Sabine Probst [4], Simone Eggert [3], Gunter Stier [1], Irmgard Sinning [1], Uwe Konietzko [4], Stefan Kins [3], Bernd Simon [2] and Klemens Wild [1]*

[1]Heidelberg University Biochemistry Center (BZH), University of Heidelberg, Heidelberg, Germany, [2]European Molecular Biology Laboratory (EMBL), Structural and Computational Biology, Heidelberg, Germany, [3]Division of Human Biology and Human Genetics, University of Kaiserslautern, Kaiserslautern, Germany, [4]Institute for Regenerative Medicine (IREM), University of Zurich, Zurich, Switzerland

†These authors have contributed equally to this work.

ABSTRACT

Physiological function and pathology of the Alzheimer's disease causing amyloid precursor protein (APP) are correlated with its cytosolic adaptor Fe65 encompassing a WW and two phosphotyrosine-binding domains (PTBs). The C-terminal Fe65-PTB2 binds a large portion of the APP intracellular domain (AICD) including the GYENPTY internalization sequence fingerprint. AICD binding to Fe65-PTB2 opens an intramolecular interaction causing a structural change and altering Fe65 activity. Here we show that in the absence of the AICD, Fe65-PTB2 forms a homodimer in solution and determine its crystal structure at 2.6 Å resolution. Dimerization involves the unwinding of a C-terminal α-helix that mimics binding of the AICD internalization sequence, thus shielding the hydrophobic binding pocket. Specific dimer formation is validated by nuclear magnetic resonance (NMR) techniques and cell-based analyses reveal that Fe65-PTB2 together with the WW domain are necessary and sufficient for dimerization. Together, our data demonstrate that Fe65 dimerizes via its APP interaction site, suggesting that besides intra- also intermolecular interactions between Fe65 molecules contribute to homeostatic regulation of APP mediated signaling.

INTRODUCTION

The Fe65s (Fe65, Fe65L1 and Fe65L2) are a family of conserved eukaryotic adaptor proteins involved in a variety of biological processes (Russo et al., 1998; McLoughlin and Miller, 2008; Minopoli et al., 2012). Special attention has been given to the brain-enriched Fe65 as its expression pattern parallels the amyloid precursor protein (APP; Guenette et al., 2006). Accordingly, the physiological functions of the two proteins are interdependent and knockout studies resulted in markedly similar phenotypes (Zambrano et al., 2002; Guenette et al., 2006; Strecker et al., 2016). APP is a single-spanning type-1 transmembrane protein (Coburger et al., 2014) with numerous neuronal functions especially in the developing brain (Müller and Zheng, 2012). Sequential regulated proteolysis of APP by different secretases (Lichtenthaler et al., 2011; Haass et al., 2012) results in multiple break-down products including soluble ectodomains, the Aβ-peptides forming the amyloids in Alzheimer's disease, and the APP intracellular domain (AICD) that is released into the cytosol (Selkoe and Hardy, 2016). The AICD is an intrinsically disordered peptide of 47 residues (Ramelot et al., 2000) and includes the GYENPTY internalization sequence that besides Fe65 binds also to many other adaptor proteins (Russo et al., 1998) with a variety of physiological functions and pathological implications (Müller et al., 2008; Pardossi-Piquard and Checler, 2012).

Fe65 determines localization and nuclear signaling of APP and modulates APP processing and Aβ-peptide generation (McLoughlin and Miller, 2008). Fe65 is a multidomain protein including an N-terminal α-helical domain and three protein-protein interaction modules: a WW domain and two consecutive C-terminal phosphotyrosine-binding (PTB) domains (Figure 1A). The WW domain binds to the Mena protein (Ermekova et al., 1997) involved in actin dynamics and cell motility thus regulating neuronal positioning in the developing brain. Fe65-PTB1 has been mainly implicated as central module of a ternary AICD/Fe65/Tip60 complex responsible for transcriptional activity of APP (Cao and Südhof, 2001), with the histone acetyltransferase Tip60 being a key regulator of genome expression and stability. Further data suggested Fe65 to provide a dominant role for nuclear signaling (Yang et al., 2006). The analysis of the AICD/Fe65/Tip60 interaction revealed that only membrane-bound AICD in context of APP and not on its own is a potent transactivator of transcription (Cao and Südhof, 2004). The distinction had been

interpreted by a membrane association dependent transition of Fe65 from a closed to an open and active conformation, involving its WW and PTB2 domain.

Most attention has been given to Fe65-PTB2 as it directly interacts with the AICD and thus functionally joins the two proteins (Borg et al., 1996). The interaction is phosphotyrosine-independent and untypically for PTB-interactions (Uhlik et al., 2005) includes an extended interface of 28 AICD residues including two α-helices (αN and αC; Figure 1B; Radzimanowski et al., 2008c). The GYENPTY internalization sequence is recognized in a rather hydrophobic crevice with GYE involved in a PTB-typical β-augmentation manner and NPTY starting helix αC and placing the canonical PTB-relevant tyrosine in its binding pocket. Unique for the AICD/Fe65-PTB2 complex is the N-terminal binding helix αN within AICD that is capped by the T^{668}PEE-motif. Phosphorylation of threonine T^{668} regulates the interaction and has been identified as sensitive checkpoint switching between physiological and pathological APP related pathways (Ando et al., 2001).
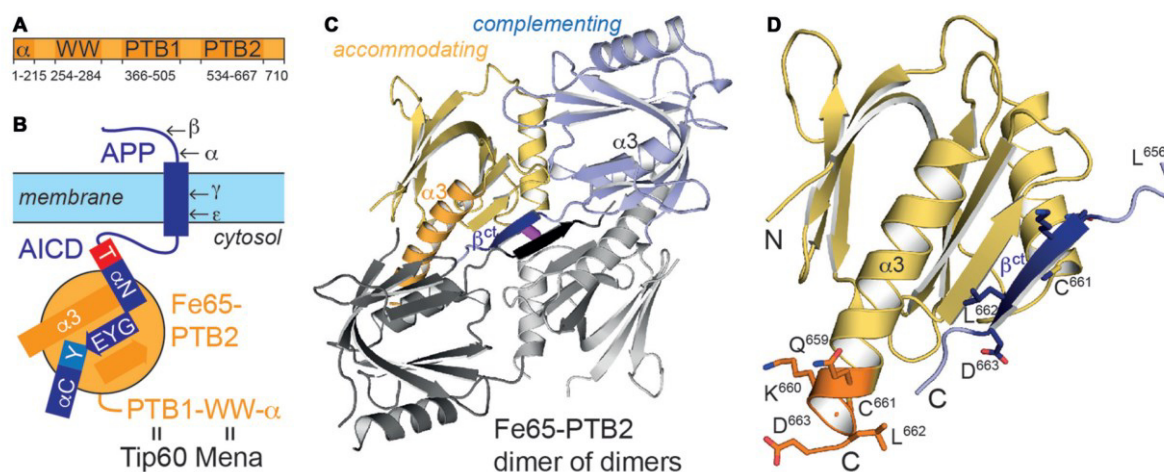
FIGURE 1 | Fe65 and amyloid precursor protein (APP).

(A) Domain architecture of human Fe65 with numbering of domain boundaries. (B) Schematic for Fe65-mediated APP-signaling by the APP intracellular domain (AICD)/Fe65-phosphotyrosine-binding domains 2 (PTB2) complex at the cell membrane. Structural details for the interaction are depicted as follows: αN and αC: AICD helices; T and Y: AICD sequence fingerprints (T: $T^{668}PEE$, Y: $N^{684}PTY$) as part of AICD helices, GYE: AICD region involved in β-augmentation with Fe65-PTB2. APP-cleavage sites by secretases are indicated by Greek symbols. (C) X-ray structure of the Fe65-PTB2 dimer of dimers. The dimer is constituted by a "complementing" subunit (blue) with a transition of the C-terminus to strand $β^{ct}$ (dark blue), while the "accommodating" subunit (yellow) contains the entire helix α3 (orange). The second dimer symmetrically attached by β-augmentation is shown with gray subunits. The central disulfide bond connecting the dimer of dimers is shown in magenta. (D) Close-up on the C-terminal Fe65-transition. According regions (L^{656}-D^{663}) of the complementing (dark blue, $β^{ct}$) and accommodating (orange, α3) subunits are given with side chains and numbering.

Here we present structural and functional data on Fe65-PTB2 revealing the domain as flexible module forming a homodimer in vitro and ex vivo in the absence of APP. Dimerization mimics the AICD-interaction and at the same time shields the hydrophobic crevice. The interaction competes with AICD binding and therefore with APP signaling depending on its cellular context.

MATERIALS AND METHODS

Protein Production and Characterization for X-ray Structure Analysis

Human Fe65-PTB2 (residues 534-667; UniPROTKB: APBB1_HUMAN, O00213) was expressed and purified for crystallization as described previously (Radzimanowski et al., 2008a). To avoid precipitation of concentrated and pure Fe65-PTB2, 5% (v/v) glycerol was added in the final size exclusion chromatography (SEC) buffer. Multi angle light scattering (MALS) was performed in line with SEC and monitored by refractive index measurements (Wyatt technology). The protein (5–20 mg/mL) was crystallized within 3 days in an automated platform at 18 C by mixing equal amounts (200 nL) of protein solution and a reservoir containing 1.6 M ammonium sulfate, 0.08 M sodium acetate pH 4.6 and 20% (v/v) glycerol in a sitting drop setup. The high glycerol concentration allowed direct flash-cooling in liquid nitrogen for X-ray structure analysis. X-ray data collection was done at beamline ID29 of the European Synchrotron Radiation Facility (ESRF). Data was integrated with program XDS (Kabsch, 2010) and scaled and merged with program AIMLESS (Evans and Murshudov, 2013) from the CCP4-package (Winn et al., 2011). The structure was solved by the Molecular Replacement method (PHENIX package; Adams et al., 2010) using a monomeric Fe65-PTB2 molecule taken out of the Fe65-PTB2/AICD complex (PDB entry: 3dxc). Iterative model building, refinement and validation were performed with programs COOT (Emsley et al., 2010) and PHENIX. All structural figures were prepared using PyMOL

(Molecular Graphics System, Version 1.5.0.4 Schrödinger, LLC).

NMR Measurements

Sequences for wildtype (wt) Fe65-PTB2 and the C633E mutant were cloned into a pETHis vector using NcoI/BamHI restriction enzymes. The proteins were expressed in *E. coli* BL21(DE3) Rosetta pLysS grown in LB media or for ^{15}N- or ^{13}C/^{15}N-labeling in M9 media by induction with 0.5 mM IPTG overnight at 22 C. Pellets were lysed by sonication in 20 mM Tris pH 8.0, 150 mM NaCl, 0.2% (v/v) Nonidet P-50 and 2 mM DTT, and the proteins purified by nickel affinity chromatography. Spin-labeling of the C633E mutant was performed by incubation with a five-fold molar excess of 3-(2-Iodoacetamido)-proxyl free radical dissolved in methanol over night at 4 C. Free spin-

label was removed by buffer exchange or SEC into 20 mM Na_2HPO_4 pH 6.5 and 150 mM NaCl. Nuclear magnetic resonance (NMR) spectra were acquired on Bruker Avance III 600 and 800 spectrometers with a cryogenic triple resonance probe and a Bruker Avance III 700 with a triple resonance probe at concentrations of 0.1–0.5 mM in the same buffer at 300 K. Data where processed with NMRPipe (Delaglio et al., 1995) and analyzed using NMRView (Johnson and Blevins, 1994). The transfer of backbone assignment from the wt protein (Dietl et al., 2014) was confirmed by analyzing HNCA, HNCACB and CBCA(CO)NH spectra of the C633E mutant. Chemical shift based secondary structure predictions and structure based chemical shift predictions where done using the programs TALOS+ (Shen et al., 2009) and SPARTA+ (Shen and Bax, 2010). Model-free Liparai-Szabo parameters derived from the ^{15}N relaxation data of the C633E mutant were analyzed and compared to hydrodynamic diffusion tensors using the programs ROTDIF and ELM (Berlin et al., 2013). Paramagnetic Relaxation Enhancements where measured and analyzed as described (Simon et al., 2010). SAXS measurements were carried out at the BM29 beamline at ESRF in Grenoble (Pernot et al., 2013). Samples were measured in NMR buffer (20 mM Na2HPO4 pH 6.5, 150 mM NaCl, 2 mM DTT) at concentrations between 0.25 and 6 mg/mL, a temperature of 300 K and a wavelength of 1 Å. Data was processed using the ATSAS suite (Petoukhov et al., 2012).

Pull-Down Experiments

The coding sequence for full-length human Fe65 was inserted into the pUKBK vector system (Kohli et al., 2012) by standard cloning techniques in order to attach either a streptavidin-binding peptide (SBP) together with a myc-tag or a mCherry (mChe)-tag to the protein N-terminus. Thereof, the following deletion constructs were generated: ΔPTB2 (Fe65(1-532)-(665-710)), ΔWW (Fe65(1-253)-(286-710)), and ΔWW-DPTB2 (Fe65(1-253)-(286-532)-(665-710)). After transfection with Lipofectamine 2000 (ThermoFisher Scientific) for 22 h, HEK293 cells were lysed in homogenization buffer consisting of 140 mM KCl, 20 mM HEPES pH 7.2, 10 mM NaCl, 5% (v/v) glycerol, 2 mM MgSO4, 1% (v/v) Triton-X100, 2 mM DTT, EDTA-free Protease-Inhibitor Cocktail (Roche), and 2 mM Phenantrolen. Pull-down assays were performed with Dynabeads® M-280 Streptavidin (ThermoFisher Scientific) and bound proteins were eluted with biotin and further separated on Novex™ 10%–20% Tricine Protein Gels. Antibodies used for detection were the c-myc antibody (1:1000, 9E10, Roche),

mCherry antibody (1:1000, 5F8, Chromotek), and GAPDH antibody (1:5000, Meridian Life Science). ECL detection was performed with the ImageQuant LAS 4000 (GE Healthcare Life Sciences). Quantification was done on the latest exposure before saturation of the brightest band on the blot, using the ImageQuant TL software.

Co-Immunoprecipitation

Co-Immunoprecipitation (Co-IP) experiments were performed as described before (Baumkotter et al., 2014). Briefly, HEK293 cells were transfected with pcDNA3.1 constructs containing FE65-HA, FE65-Flag or APP-myc using JetPRIME (Polyplus transfection). Twenty to twenty-two hours after transfection cells were harvested and lysed in 150 mM NaCl2, 50 mM Tris/HCl pH 7.5, 2 mM EDTA, 1% (v/v) NP40 and freshly added Complete Protease Inhibitor mix (Roche) for 20 min on ice. After centrifugation at 16,000 g for 10 min the supernatant was pre-cleared with protein A Sepharose beads (GE Healthcare). Then the supernatant was incubated over night with anti-HA agarose beads (Roche) to allow binding of HA-tagged FE65. After washing bound proteins were eluted by denaturation with SDS sample buffer at 95 C. Samples were separated on 8% Tris/glycine gels and probed via immunoblotting for HA-, Flag-and myc-tagged constructs.

Subcellular Fractionation

Subcellular fractionation was performed according to Abcams subcellular fractionation protocol. HEK293 cells were transfected as described before. Twenty to twenty-two hours post transfection cells were resuspended in 1 mL of fractionation buffer (250 mM Sucrose, 20 mM HEPES, 10 mM KCl, 2 mM MgCl2, 1 mM EDTA and 1 mM EGTA with freshly added Complete Protease Inhibitor mix (Roche)) and passed 10 times through a 27 gauge needle. After differential centrifugation at 720 g and 10,000 g for 5 min and 100,000 g for 1 h the supernatant (cytosolic fraction) was transferred and kept on ice for further analysis. The sediment (membrane fraction) was resuspended by pipetting and pass through 10 times a 27-gauge needle. Protein concentration of membrane and cytosolic fraction was determined using the BCA assay (Sigma).

Blue Native Gel Electrophoresis

For Blue Native Gel analysis 100 mg protein of the cytosolic and membrane fraction was diluted in 1.5 M amino caproic acid, 0.05 M Bis-Tris, pH 7, 1.25% (w/v) dodecyl maltosidase and 5% (w/v) Coomassie Brilliant Blue G250, as described in detail before (Eggert et al., 2009). Afterwards, samples were separated on a 4%–15% (w/v) Tris-HCl gel (Biorad), transferred on a PVDF membrane and probed via immunoblotting for HA- and myc-tagged constructs.

RESULTS

Fe65-PTB2 Dimerization

Recombinantly expressed human Fe65-PTB2 (residues 534-667) is difficult to purify as it precipitates at higher protein concentrations in the mg/mL range. Instability is related to the exposure of a hydrophobic crevice that corresponds to the AICD binding site and complex formation dramatically enhances solubility about a 100-fold (Radzimanowski et al., 2008c). When purified via SEC, Fe65-PTB2 partitions in monomeric, dimeric and tetrameric species as validated by multi-angle light scattering (MALS) and on SDS-PAGE the protein appears as detergent-resistant dimer (Supplementary Figure S1). Unspecific aggregation of Fe65-PTB2 at concentrations in the mg/mL range can be prevented by the addition of glycerol and we subsequently crystallized the domain and solved its crystal structure by molecular replacement at 2.6 Å resolution (Table 1).

TABLE 1 | Data collection and refinement statistics.

Data collection	
Space group	P 1 21 1
Cell dimensions	
a, b, c (Å)	56.6 104.3 60.6
α, β, γ (°)	90 112.0 90
Resolution (Å)	49.44–2.6 (2.74–2.6)
R_{pim} (%)	7.3 (39.5)
Wilson B-factor (Å^2)	39.0
I/σ(I)	9.0 (2.3)
CC1/2	99.1 (83.5)
Completeness (%)	99.3 (98.3)
Redundancy	6.6 (6.2)
Wavelength (Å)	1.033
Refinement	
No. reflections	19931 (1993)
R_{work} (%)	19.3 (29.6)
R_{free} (%)*	24.1 (40.6)
No. atoms	3970
protein	3832
ligand/ion	60
Protein residues	501
B-factors (Å^2)	50.4
R.m.s. deviations	
bond lengths (Å)	0.002
bond angles (°)	0.60
Ramachandran plot	
allowed (%)	99.8

for 5% of all data. Statistics for the highest-resolution shell are shown in parentheses.

Fe65-PTB2 crystallizes as dimer of dimers with a continuous central β-sheet (Figure 1C). Dimerization occurs via a structural transition of the C-terminal α-helix α3 within one Fe65-PTB2 subunit (the ''complementing'' subunit) in respect to the conformation as seen in the previously solved AICD/Fe65-PTB2 complex (rmsd of 0.85 Å for 123 Cα-atoms; Figure 1D, Supplementary Figure S2; Radzimanowski et al., 2008c). The last two helical turns dissolve (starting at L^{656}) and adopt an extended β-conformation that complements the ''accommodating'' subunit in trans (dimer interface: 585 Å2). The interface is classified just about stable (Krissinel and Henrick, 2007). The newly formed β-strand (defined here as β^{ct}) quasi-symmetrically mediates also the dimer of dimer contact with the tetrameric assembly being stabilized by a disulfide bridge between respective cysteine (C^{661}) residues (Figure 1C).

Fe65-PTB2 Dimer Structure in Solution

Having solved the crystal structure of Fe65-PTB2, we had to make sure that the observed interactions did not represent a crystallographic artifact and are also present in solution. We therefore first performed concentration dependent (0.25–6 mg/mL) small angle X-ray scattering (SAXS) measurements under reducing conditions to avoid the covalent and likely non-physiological cysteine bridge. The data showed a sharp increase in intensity at very small scattering angles that becomes more pronounced with higher concentrations and thus confirming the observation of the presence of aggregation (Figure 2A). Accordingly, the deduced molecular masses showed a strong concentration dependence that reflects the monomer-dimer transition. Calculating the theoretical scattering curves of the monomer, dimer and tetramer structures and fitting them against the experimental data, revealed the best fit to correspond to the crystallographic dimer (Supplementary Figure S3A), which holds true for the whole concentration range and also when the data are interpolated to zero concentration. Calculations of monomer and dimer content based on fitting linear combinations of two structures range from more than 20% of monomer to almost exclusively dimer at higher concentrations, but should be taken as rough estimates with the given data quality and the insecurity of especially the dimer structural model. In accordance with these data, a dissociation constant could be estimated by preliminary isothermal titration calorimetry (ITC) measurements to be in the low micromolar range (data not shown). In order to obtain high resolution structural information for Fe65-PTB2 dimerization in solution, we performed an extended NMR characterization. Overall, we observe a high consistency between the backbone chemical shift data and the dihedral angles observed in the crystal structure (Figures 2B, Supplementary Figure S3B). For the C-terminus, the chemical shifts predict the existence of a helix until Y^{658} and indicate an increase in backbone flexibility starting from M^{655}. Interestingly, the observed secondary Cα-Cβ chemical shift differences for the C-terminus are in between the values predicted for the accommodating (long C-terminal α-helix) and complementing (β-sheet augmentation) subunits of the crystal structure.

A more detailed picture for the internal dynamics and dimerization was obtained by the analysis of ^{15}N relaxation data. The average ratio of transverse and longitudinal relaxation rates measured at 300 K indicated a rotational correlation time

T_c of 10.6 ns. This value compares to 8.9 ns (for complementing subunit) and 15.7 ns (for crystallographic dimer) as calculated from the coordinates. Assuming a rapid exchange between rigid monomers and dimers the experimental value would suggest a high percentage of monomers in solution. However, since the intermolecular interaction is mediated by the flexible C-terminus, we envision a dimer with a rather flexible connection between the monomers and thus with faster effective rotational correlation time than expected for a rigid dimer. This model is supported by the observation of quickly reducing backbone order parameters S^2 for the C-terminal residues starting from Y^{658} (Figure 2C, Supplementary Figure S3C).

To further characterize the oligomerization in solution, we introduced nitroxide spin-labels covalently attached to cysteine residues to measure paramagnetic relaxation enhancements (PREs). The presence of the electron spin leads to signal broadening of nuclear spins in spatial proximity (less than ~ 20 Å) to the nitroxide and can assist NMR protein structure determination. Due to the r^{-6} dependence of the induced relaxation, the signal bleaching can also be used to structurally and dynamically characterize specific encounter complexes (Clore, 2015). Since Fe65-PTB2 contains six native cysteines and the evaluation of the experiment requires a single spin-label attached to each molecule, we performed an extensive mutational analysis to determine the accessibility and structural importance of all native cysteines. In the end, only two cysteines (C^{633} and C^{661}) were solvent exposed to be efficiently paramagnetically labeled. Of particular interest are the PRE results for the C633E mutant, which positions the spin-label solely on C^{661} at the C-terminus in the center of the oligomerization region. We measured the intensity ratios in ^{15}N-^{1}H heteronuclear correlation spectra (HSQC) between the paramagnetic and diamagnetic state of the molecule (Supplementary Figures S3D,E). Due to the instability and precipitation of the molecule in solution during the measurements, a number of intensity ratios larger than one for residues that are not in proximity of the nitroxide were observed. Therefore, and because of the difficulties to accurately model the spin-label being attached to a flexible C-terminus, we resign from a detailed quantitative analysis of the data. A qualitative picture however can be obtained by plotting the experimental I_{para}/I_{dia} ratios onto the X-ray structure. The lowest ratios are observed for residues in the C-terminal helix and the loops and secondary structure elements in the vicinity of the C-terminus. To disentangle intra- and inter-molecular contributions, we performed a second experiment with a mixed sample of ^{14}N-paramagnetic and ^{15}N-diamagnetic

molecules. The observed PREs are exclusively due to inter-molecular proximity of the radical. Bleaching was observed for patches adjacent to the hydrophobic crevice and on surface loops consistent with the presence of the dimer and tetrameric species in solution (Figure 2D). Strongest bleaching with I_{para}/I_{dia} ratios below 0.3 occurred for residues L^{609} and F^{611} that also are in closest contact within the crystallographic dimer and for C^{661} itself that also bridges the observed dimer of dimers.
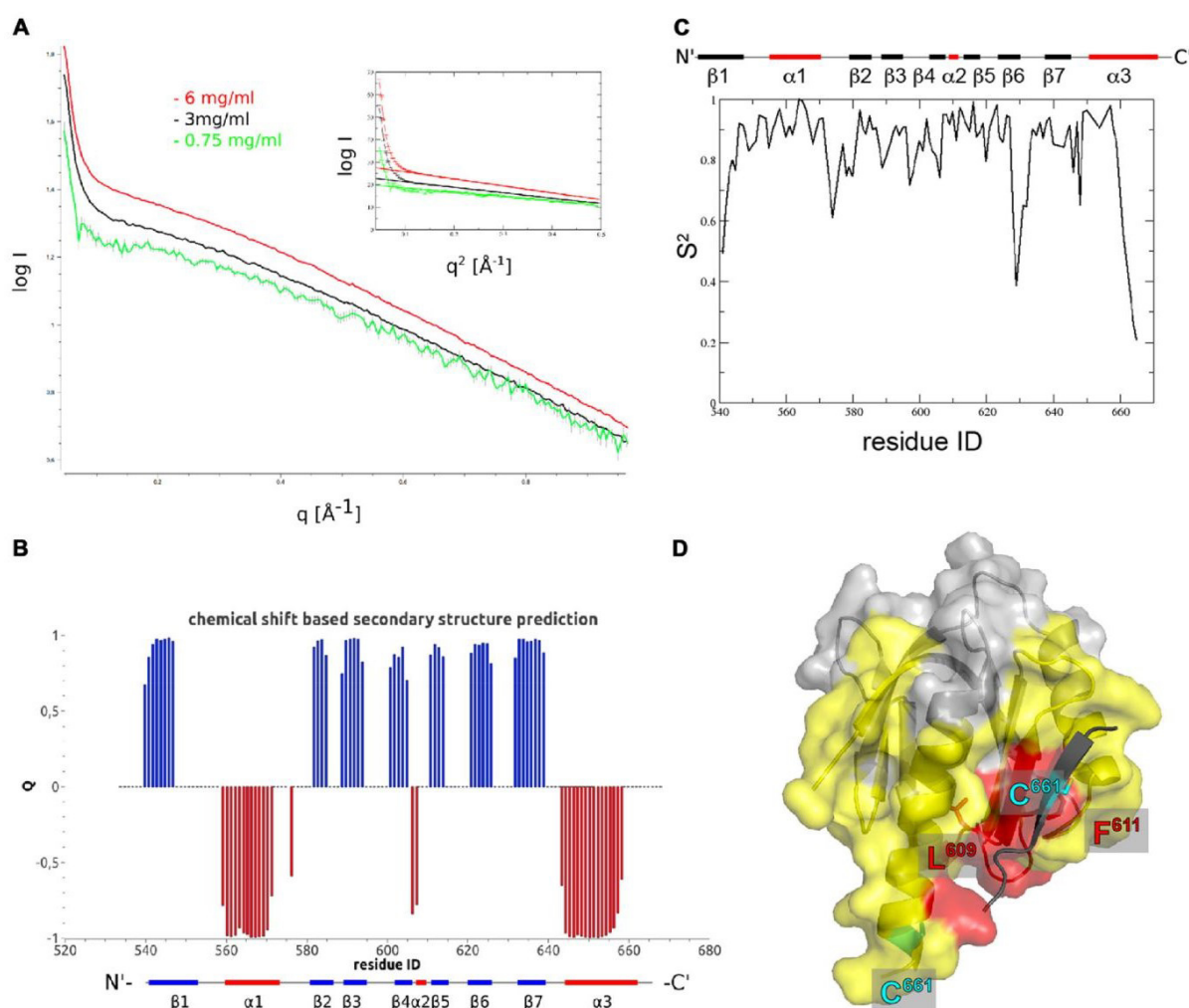
FIGURE 2 | The Fe65-PTB2 dimer in solution.

(A) Small angle scattering data measured at three different protein concentrations. The presence of self-aggregation leads to a pronounced increase in scattering intensity at low angles. The radius of gyration extracted from the Guinier plot (inset) is slightly higher than expected for a dimer and the initial intensity values almost reaches the expected value for the dimer. (B) Secondary structure predicted from backbone chemical shifts with positive blue bars indicating β-sheets and negative red bars α-helices. The secondary structure of the accommodating subunit (long α3 helix) is shown below for comparison.(C) Backbone order parameters S^2 derived from ^{15}N nuclear magnetic

FIGURE 2 continued

resonance (NMR) spin-relaxation data. The decrease of the order parameter for the C-terminal residues indicates the unfolding of the α-helix in this region resulting in a rapid reorientation of the N-H bond vectors on a ns to ps timescale. (D) Residues experiencing paramagnetic relaxation enhancements at the backbone NH when a nitroxide spin-label is attached to C^{661}. The protein surface of the complementing subunit is shown in color if the average intensity ratio of the observed ^{1}H-^{15}N peak in the paramagnetic and diamagnetic NMR spectra of the corresponding residue and its two neighbors is smaller than 0.7 and thus identifies amino acids that are close to the paramagnetic center. Residues in yellow are bleached for molecules that are simultaneously ^{15}N and nitroxide labeled, while residues in red are also bleached when exclusively ^{15}N and nitroxide labeled proteins are mixed. The spin-label carrying C^{661} residues are highlighted for the monomer (on the C-terminal α-helix) and the crystallographic dimer (on the extra β-strand).

Taken all NMR measurements together, a transient dimer formation as seen in the crystal structure is validated as homotypic interaction in solution. The tetrameric and covalent linkage of two dimers seems to be favored only under high concentrations and oxidizing conditions as seen in the crystallographic array.

Fe65-PTB2 Mimics the AICD

The central part within the AICD/Fe65-PTB2 interface has been previously shown to be constituted by antiparallel β-augmentation of the PTB domain with the G^{681}YE sequence fingerprint of the AICD (APP695 numbering; Figure 3A, left panel; Radzimanowski et al., 2008c). The glycine presents an essential hinge that places the N-terminally located helix αN of the AICD almost perpendicular to the C-terminal helix α3 of Fe65-PTB2 whereas the tyrosine residue (Y^{682}) is imbedded in a hydrophobic pocket formed by residues of helix α3. Glutamate E^{683} is involved in an intramolecular salt bridge with a lysine (K^{688}) following the NPTY^{687} sequence. In the crystal structure of the Fe65-PTB2 dimer, the induced strand β^{ct} with the C^{661}LD sequence directly matches to the AICD strand (Figure 3A, right panel). Cysteine C^{661} occupies the glycine position although due to the restrained main chain flexibility it does not introduce a similar hinge. The hydrophobic leucine L^{662} superposes with the tyrosine and aspartate D^{663} forms an AICD-equivalent intramolecular salt-bridge with arginine R^{665}. Thus, the complementing Fe65-PTB2 mimics the interacting AICD in space and charge. Of note, the accommodating Fe65-PTB2 subunit does not show the structural transition. The hydrophobic crevice of the complementing subunit is therefore still available, however, the adjacent C-terminal binding site for helix αC of

the AICD is destroyed by the helical unwinding and the respective space is occupied by the accommodating subunit (Supplementary Figure S2C). In summary, Fe65-PTB2 dimerization results in a structural change that blocks the AICD binding site either fundamentally in the accommodating subunit or partially in the complementing subunit.
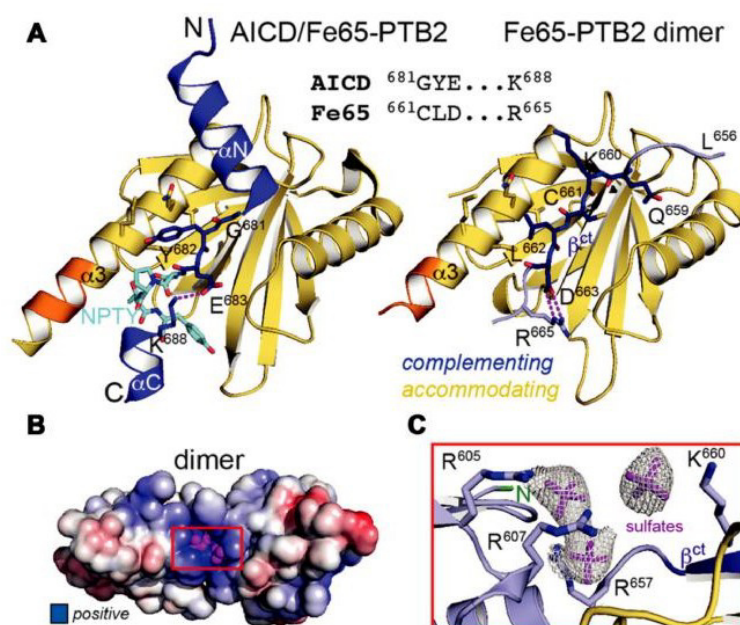
FIGURE 3 | Fe65 mimicry of AICD binding.

(A) Left: X-ray structure of the AICD/Fe65-PTB2 complex (PDB: 3dxc; Radzimanowski et al., 2008c). The central interacting part of the AICD is detailed: G681YE in dark blue, N684PTY in cyan. Right: same view and coloring of the Fe65 dimer with the AICD replaced by the accommodating subunit. The geometry and type of interactions mimic the AICD/Fe65-PTB2 complex. Matching sequences are given in the alignment. Coloring as in Figure 1D. (B) Surface potential (5 kBT/e; blue: positive, red: negative) of the Fe65-PTB2 dimer. Dimerization results in an extended positively charged groove with tightly bound sulfate ions originating from crystallization. (C) Coordination and electron densities (2mFo-DFc, 1.0 s) for the centrally bound sulfate ions (magenta). Binding occurs next to strand bct and the N-terminus of Fe65-PTB2 (green). Same orientation as in Panel B as indicated by the red rectangle.

A Basic Cluster Next to the Dimerization Site

In order to evaluate changes of the surface properties due to dimerization we calculated surface charge potentials. The analysis revealed a pronounced positively charged patch (R^{605},R^{607}, R^{657}, K^{660} and R^{665}) in the center of the dimer directly located at the transition site of the C-terminal helix (Figures 3B,C). Due to its location, the shape of the patch differs between an extended (complementing subunit with extended strand β^{ct}) and a condensed form (accommodating subunit with folded C-terminal helix; Supplementary Figure S4). Fe65-PTB2 was crystallized in sulfate conditions and we find sulfate ions bound to both the condensed and extended patches. Most strikingly, in the elongated patch next to the dimer interface we find three adjacent sulfate ions (Figures 3B,C). The spatial arrangement of the ions

perfectly match to the three phosphoryl-groups of the head-group (IP3) of phosphatidyl-inositol-4,5-bisphosphate (PIP2; Supplementary Figure S4), which has been found earlier to bind to Fe65 by liposome flotation assays (Cao and Südhof, 2004). PIP_2-binding is a recurrent and functionally important feature of many PTB domains due to their juxtamembrane location and always occurs in similar basic clusters (Uhlik et al., 2005). Of note, also the N-terminus of Fe65-PTB2, and thus the PTB1-PTB2 linker region implicated in the intramolecular closure by binding to the WW-domain (Cao and Südhof, 2004), locates next to the basic cluster.

Fe65 Dimerization In Vivo

All structural studies have been performed in vitro with isolated Fe65-PTB2 at rather high protein concentrations and they do not necessarily reflect the in vivo situation in context of the full-length protein and the cellular environment. We therefore set out to determine its relevance by testing Fe65 dimerization in the cellular context. HEK293 cells expressing Fe65 full-length protein fused N-terminally to a SBP and deletion variants missing either the WW domain (Fe65ΔWW), the PTB2 (Fe65ΔPTB2) domain or both (Fe65ΔWW/PTB2; Figure 4), were subjected to streptavidin-based isolation. Indeed, all precipitates of SBP-tagged Fe65 also recovered mCherry-tagged Fe65 in the eluate, and thus proving Fe65 dimerization in a cellular context (Figures 4A,B). Deletion of exclusively the PTB2 domain resulted in a strong reduction of the interaction with full-length Fe65 and the same was true for a Fe65 deletion mutant lacking the PTB2 and WW domains. In contrast, deletion of solely the WW domain did not significantly interfere with Fe65 dimerization. The negative control of the input of SBP- and mCherry-tagged Fe65 validates the dimerization event (Figures 4C,D). These results show that Fe65 dimerization takes place in a cellular environment and implement the PTB2 domain being mainly responsible for dimer formation.
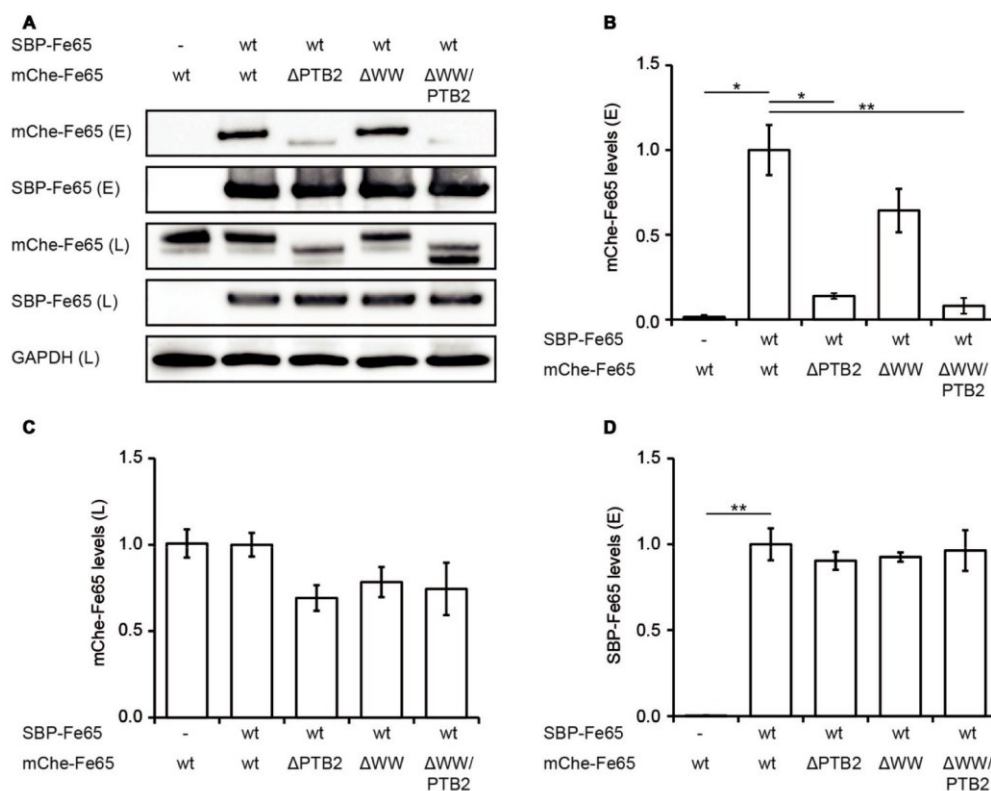
FIGURE 4 | Deletion of the PTB2 domain impairs Fe65 dimerization in cells.

(A) HEK293 cells expressing streptavidin-binding peptide (SBP)-myc-Fe65 (SBP-Fe65) and mCherry-Fe65 (mChe-Fe65) as wildtype (wt) or deletion constructs were subjected to pulldown analyses. Total cell lysates (L) and eluates (E) were analyzed with antibodies against myc, mCherry and GAPDH. (B) Levels of co-precipitated mChe-Fe65 constructs in the eluate are significantly reduced in both constructs harboring a deletion of the PTB2 domain. (C) Confirmation of similar levels of mChe-Fe65 in the lysate. (D) Similar amounts of SBP-Fe65 are eluted in all experiments. No GAPDH signal is seen in the eluate (not shown). Mean SEM of n = 3 are shown (p < 0.05, p < 0.01, t-test).

Furthermore, we tested via Blue Native Gel analyses, if Fe65 migrates as a dimer. The analyses revealed a single band with a molecular weight of about 200 kDa pointing indeed to a full-length Fe65 dimer (Figure 5A). In HEK cells, Fe65 partitions into a major cytosolic and a minor membrane-bound fraction, whereas co-expression of APP caused a strong repartitioning of Fe65 towards the membrane fraction. Co-expression of APP did not alter electromobility of Fe65 in the native gel analysis. However, as APP and Fe65 have very similar molecular weights, the native gel analysis does not allow for differentiating homotypic from heterotypic complexes. In the next step we tested, if APP co-expression might affect Fe65 dimerization. For this purpose, we analyzed HEK293 cells expressing Flag- and HA-tagged Fe65 and myc-tagged APP and performed co-immunoprecipitation studies with anti-HA antibodies

from total cell extracts (Figure 5B). For control we used cells expressing Flag-Fe65 and myc-APP only. The analyses revealed interactions of HA-Fe65 with both Flag-Fe65 and myc-APP.
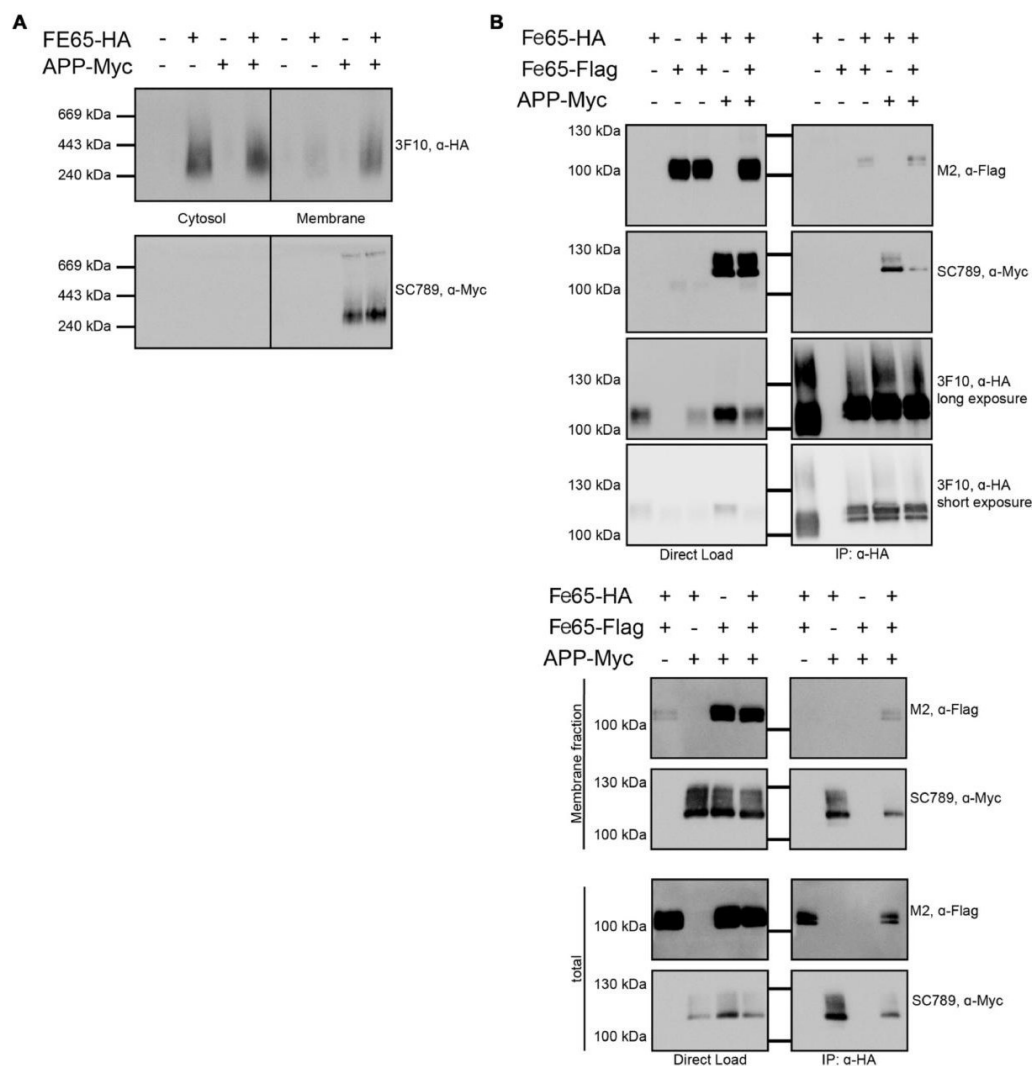

FIGURE 5 | Influence of APP on Fe65 dimerization.

HEK cells expressing exogenous Fe65-HA, Fe65-Flag or APP-myc were subjected for subcellular fractionation. (A) The cytosolic and membrane fractions were separated on a BlueNative-Gel and analyzed by Western Blotting using 3F10 (anti HA) and SC789 (anti myc) antibodies. Note the shift of Fe65 from the cytosolic to the membrane fraction when co-expressed with APP. (B) Co-Immunoprecipitation (Co-IP) analysis of whole cell lysates (upper panel) and whole cell lysates and membrane fraction (lower panel) of HEK293 cells expressing Fe65-HA and Fe65-Flag alone or together with APP-myc. Cells expressing Fe65-HA and APP-myc served as positive and cells lacking Fe65-HA as negative control. For direct load 4% of the total extracts were loaded. Immunoprecipitation was carried out with anti-HA antibody covered beads. Immunoprecipitates were eluted by denaturation and probes were subjected for PAGE (8% Tris/glycine gels) and Western analysis using 3F10 (anti HA), SC789 (anti myc) and M2 (anti Flag) antibodies.

No clear reduction was observed for HA-Fe65/Flag-Fe65 interaction upon co-expression with myc-APP. However, these data again did not allow for differentiating between a trimeric complex of APP with dimeric Fe65 and two separate dimeric complexes either consisting of HA-and Flag-tagged Fe65 or HA-Fe65 and myc-APP. Therefore, we repeated the Co-IP of Fe65-HA, Fe65-Flag and mycAPP from HEK293 cell extracts from the membrane fraction. In this fraction only minor Fe65 amounts are present and we could not detect any Fe65 dimer. Upon co-expression of APP, Fe65 was shifted into the membrane fraction as expected from the known and strong APP-Fe65 interaction (Radzimanowski et al., 2008c). Interestingly, under these conditions we succeeded to precipitate the two differently tagged Fe65 molecules (HA and Flag) and APP (Figure 5B). These data show that Fe65 at least to some extend can still dimerize in presence of APP and even a trimeric species might be formed.

DISCUSSION

Fe65 is a versatile protein-adaptor with an interactome list of increasing size and complexity. It participates in various neuronal processes, including neurogenesis, neuronal migration and positioning, neurite outgrowth, synapse formation and plasticity, and finally in learning and memory (McLoughlin and Miller, 2008; Minopoli et al., 2012; Strecker et al., 2016). The most studied function concerns the gene transactivation complex together with APP and the histone acetyltransferase Tip60, although the pathway that at least in parts parallels Notch signaling and its gene targets are far from being understood (Cao and Südhof, 2001; Pardossi-Piquard and Checler, 2012). However, it is possible that in ageing and sporadic Alzheimer's disease there is an increase of nuclear signaling concomitant with amyloidogenic processing of APP and the accumulation of the Aβ-peptide (Fukumoto et al., 2002; Yang et al., 2003; Goodger et al., 2009). Inline, it was found that an alternate splice variant of Fe65 (Fe65a2 isoform) lacking the last exon confers resistance against very late onset of AD (Hu et al., 2002). The exon codes for residues starting at the C-terminal end of helix α3 of Fe65-PTB2 and therefore is impaired in AICD binding. Soon after the first description of the signaling pathway, it was found that complex formation with APP includes a membrane-associated initiation process that enables Fe65 to act as transactivator of transcription once the AICD is cleaved-off (Cao and Südhof, 2004). This process was associated with an opening of Fe65 by the release of a WW-PTB2 domain interaction eventually triggered by a membrane-associated factor.

The AICD/Fe65-PTB2 contact is of hydrophobic character and recombinant expressed Fe65-PTB2 is aggregation prone (Radzimanowski et al., 2008a). Here we show by X-ray crystallography and extended NMR measurements including spin-labeling PRE techniques that homotypic dimerization of the Fe65-PTB2 domain mimics AICD binding and effectively shields the hydrophobic surface. The shielding may reflect the physiological need of chaperoning this surface in case the binding partner is not present or binding is to be prevented for functional reasons. This intermolecular protection does not contradict the predicted intramolecular WW-PTB2 interaction, which involves the PTB1-PTB2 boundary and could occur at the same time inhibiting downstream signaling via the WW-domain (Cao and Südhof, 2004). Interestingly, the interaction of the Fe65 WW domain and full length Fe65 is inhibited

by excess of AICD, indicating that AICD binding to the PTB2 domain affects the interaction of PTB1-PTB2 boundary with the WW domain (Cao and Südhof, 2004). Homotypic dimerization might also impact pathological pathways including the AICD/Fe65 interaction. Of note, the Fe65a2 isoform conferring very late onset AD resistance (Hu et al., 2002) lacks the dimerization sequence and thus excludes the self-association. However, all interactions of Fe65 distinct to the dimerization site and independent of APP binding are likely to be unaffected by the homotypic Fe65-PTB2 interaction.

We demonstrate by co-immunoprecipitation assays performed in transfected HEK293 cells in the presence of Fe65/APP overexpression that at the membrane a Fe65-dimer complex still co-exists with APP, which could correlate with the previously described Fe65-activating state of a "primed complex" (Cao and Südhof, 2004). While there is no indication yet for an additional membrane-associated protein factor, activation seems to be guided by the lipid PIP_2, which plays an important role in many endocytic events. PIP_2-binding most likely occurs via the epitope identified by multiple sulfate ion binding in our dimeric Fe65 crystal structure and/or via Fe65-PTB1 (Radzimanowski et al., 2008b). As the epitope is in direct proximity to the dimer interface, membrane association could also have a direct influence on the monomer-dimer equilibrium. As also the PTB1-PTB2 linker region is directly adjacent, the WW-domain is likely be involved in this process as also indicated by our pull-down assays, which show at least some influence of the WW-domain on Fe65 dimerization. The WW-domain recognizes polyproline stretches (Meiyappan et al., 2007) and might bind to two proline residues close to Fe65-PTB2 and therefore to the PIP_2-epitope. Inline, it had been found that the AICD and the WW-domain cannot bind simultaneously to the PTB-domains including the linker (Cao and Südhof, 2004).

We therefore propose the following integrated scenario for Fe65-mediated gene transactivation (Figure 6): Fe65 is the central adaptor for APP nuclear signaling as validated earlier. Without its upstream signal, consisting of the AICD in context of membrane-associated APP, Fe65 resides in a closed conformation. This conformation occurs in the cytosol and might avoid futile cycles and ensure efficient recycling of Fe65 pools from the nucleus back to the endomembrane system or the cell membrane. The closed conformation favors homotypic dimerization via the structural transition of the C-terminal helix $\alpha 3$ to strand β^{ct} that performs substrate-

mimicry. At the membrane, APP and potentially other protein and lipid factors like PIP$_2$, induce an opening of Fe65 and the homodimer finally dissociates. Therefore, membrane association via the basic cluster and subsequent APP binding would also result in the opening and activation of Fe65. Similarly, it appears well feasible that other functions of Fe65, involving interaction via the WW-domain with Mena or via the PTB1 domain with other surface receptors such as LRP1 might also go along with changes in the Fe65 monomer/dimer equilibrium. Further research will be required to understand these processes in more detail.
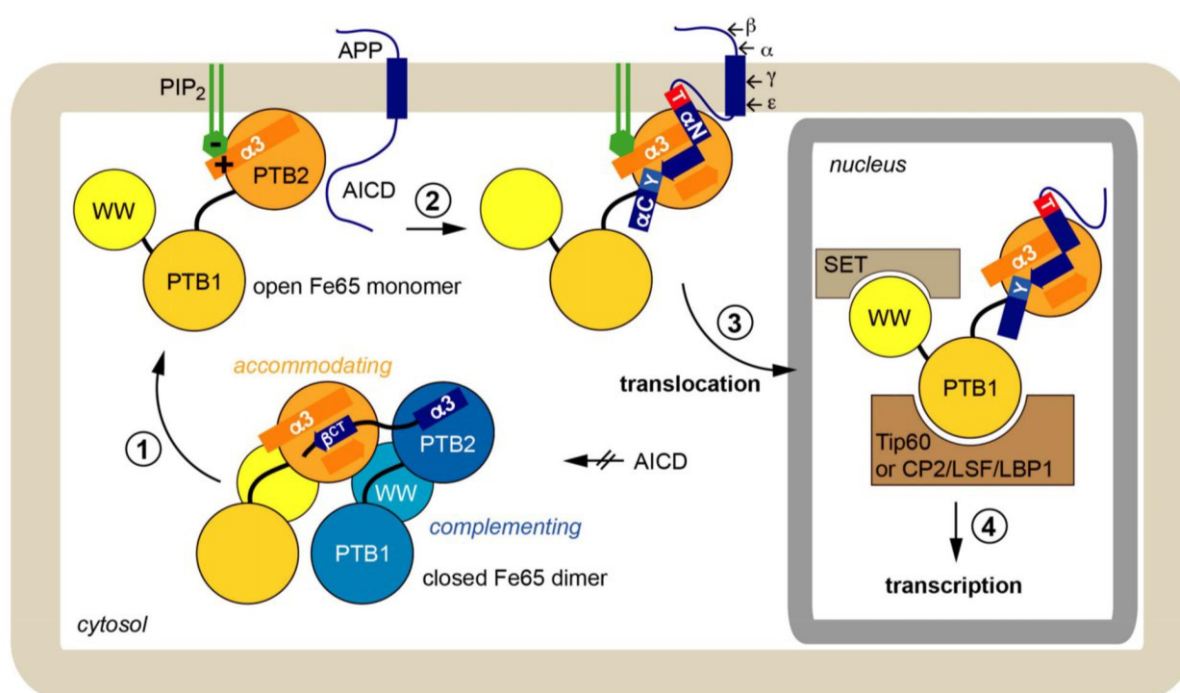
FIGURE 6 | Physiological function of Fe65 dimerization.

In a schematic model Fe65-mediated APP signaling is divided into four steps: (1) In the cytosol Fe65 forms a closed dimer by mimicking the AICD and thereby shielding the binding epitope. (2) APP binding at the cell membrane, putatively induced by phosphatidyl-inositol-4,5-bisphosphate (PIP$_2$)-mediated recruitment, opens the dimer and the AICD/Fe65-PTB2 interaction is formed. The AICD changes from a disordered to a structured conformation. (3) Upon secretase cleavage of APP, AICD-Fe65 signaling complexes translocate to the nucleus. (4) Respective transcription activation processes are initiated.

Upon ε-cleavage of APP by ɣ-secretase, the AICD is released from the membrane into the cytosol and the Fe65-AICD complex translocates to the nucleus. Very recent results indicate that the PTB2 rather than the WW domain is important for the nuclear localization of Fe65 (Koistinen et al., 2017). Secretase cleavage is influenced by

various aspects like APP cellular localization (Haass et al., 2012), APP dimerization (Winkler et al., 2015) and APP and Fe65 phosphorylation (Bukhari et al., 2016). Due to the tight and extended interaction involving 2/3 of the AICD (Radzimanowski et al., 2008c) and co-localization studies (von Rotz et al., 2004), we favor co-migration without degradation of the AICD. Fe65-PTB1 then binds to Tip60 or other transcription factors like CP2/LSF/LBP1 (Zambrano et al., 1998). The WW-domain in the open Fe65 conformation could finally engage with downstream components as found for the nucleosome assembly factor SET (Telese et al., 2005) or the AICD might interact with Med12 from the transcriptional mediator complex (Xu et al., 2011) essential for starting transcriptional activation processes.

In summary, our structural and biochemical dissection of the molecular properties of the multiprotein-adapter Fe65 reveal the details of an essential regulatory circuit of APP signaling. The importance of APP signaling in health and disease make it worth revisiting Fe65 and its different functional conformations as target for further pharmacological investigations.

REFERENCES

1) Adams, P. D., Afonine, P. V., Bunkóczi, G., Chen, V. B., Davis, I. W., Echols, N., et al. (2010). PHENIX: a comprehensive Python-based system for macromolecular structure solution. Acta Crystallogr. D Biol. Crystallogr. 66, 213–221. doi: 10.1107/S0907444909052925

2) Ando, K., Iijima, K. I., Elliott, J. I., Kirino, Y., and Suzuki, T. (2001). Phosphorylation-dependent regulation of the interaction of amyloid precursor protein with Fe65 affects the production of b-amyloid. J. Biol. Chem. 276, 40353–40361. doi: 10.1074/jbc.M104059200

3) Baumkotter, F., Schmidt, N., Vargas, C., Schilling, S., Weber, R., Wagner, K., et al. (2014). Amyloid precursor protein dimerization and synaptogenic function depend on copper binding to the growth factor-like domain. J. Neurosci. 34, 11159–11172. doi: 10.1523/JNEUROSCI.0180-14.2014

4) Berlin, K., Longhini, A., Dayie, T. K., and Fushman, D. (2013). Deriving quantitative dynamics information for proteins and RNAs using ROTDIF with a graphical user interface. J. Biomol. NMR 57, 333–352. doi: 10.1007/s10858-013-9791-1

5) Borg, J. P., Ooi, J., Levy, E., and Margolis, B. (1996). The phosphotyrosine interaction domains of X11 and FE65 bind to distinct sites on the YENPTY motif of amyloid precursor protein. Mol. Cell. Biol. 16, 6229–6241. doi: 10.1128/mcb.16.11.6229

6) Bukhari, H., Kolbe, K., Leonhardt, G., Loosse, C., Schröder, E., Knauer, S., et al. (2016). Membrane tethering of APP c-terminal fragments is a prerequisite for T668 phosphorylation preventing nuclear sphere generation. Cell Signal. 28, 1725–1734. doi: 10.1016/j.cellsig.2016.08.007

7) Cao, X., and Südhof, T. C. (2001). A transcriptionally correction of transcriptively active complex of APP with Fe65 and histone acetyltransferase Tip60. Science 293, 115–120. doi: 10.1126/science.1058783

8) Cao, X., and Südhof, T. C. (2004). Dissection of amyloid-b precursor protein-dependent transcriptional transactivation. J. Biol. Chem. 279, 24601–24611. doi: 10.1074/jbc.m402248200

9) Clore, G. M. (2015). Practical aspects of paramagnetic relaxation enhancement in biological macromolecules. Meth. Enzymol. 564, 485–497. doi: 10.1016/bs.mie. 2015.06.032

10) Coburger, I., Hoefgen, S., and Than, M. E. (2014). The structural biology of the amyloid precursor protein APP—a complex puzzle reveals its multi-domain architecture. Biol. Chem. 395, 485–498. doi: 10.1515/hsz-2013-0280

11) Delaglio, F., Grzesiek, S., Vuister, G. W., Zhu, G., Pfeifer, J., and Bax, A. (1995). NMRPipe: a multidimensional spectral processing system based on UNIX pipes. J. Biomol. NMR 6, 277–293. doi: 10.1007/bf00197809

12) Dietl, A., Wild, K., and Simon, B. (2014). 1H, 13C, and 15N chemical shift assignments of the phosphotyrosine binding domain 2 (PTB2) of human FE65. Biomol. NMR Assign. 8, 93–95. doi: 10.1007/s12104-013-9460-z

13) Eggert, S., Midthune, B., Cottrell, B., and Koo, E. H. (2009). Induced dimerization of the amyloid precursor protein leads to decreased amyloid-b protein production. J. Biol. Chem. 284, 28943–28952. doi: 10.1074/jbc.M109.038646

14) Emsley, P., Lohkamp, B., Scott, W. G., and Cowtan, K. (2010). Features and development of Coot. Acta Crystallogr. D Biol. Crystallogr. 66, 486–501. doi: 10.1107/S0907444910007493

15) Ermekova, K. S., Zambrano, N., Linn, H., Minopoli, G., Gertler, F., Russo, T., et al. (1997). The WW domain of neural protein FE65 interacts with proline-rich motifs in Mena, the mammalian homolog of Drosophila enabled. *J. Biol. Chem.* 272, 32869–32877. doi: 10.1074/jbc.272.52.32869

16) Evans, P. R., and Murshudov, G. N. (2013). How good are my data and what is the resolution? *Acta Crystallogr. D Biol. Crystallogr.* 69, 1204–1214. doi: 10.1107/S0907444913000061

17) Fukumoto, H., Cheung, B. S., Hyman, B. T., and Irizarry, M. C. (2002). *b*-secretase protein and activity are increased in the neocortex in Alzheimer disease. *Arch. Neurol.* 59, 1381–1389. doi: 10.1001/archneur.59.9.1381

18) Goodger, Z. V., Rajendran, L., Trutzel, A., Kohli, B. M., Nitsch, R. M., and Konietzko, U. (2009). Nuclear signaling by the APP intracellular domain occurs predominantly through the amyloidogenic processing pathway. *J. Cell Sci.* 122, 3703–3714. doi: 10.1242/jcs.048090

19) Guenette, S., Chang, Y., Hiesberger, T., Richardson, J. A., Eckman, C. B., Eckman, E. A., et al. (2006). Essential roles for the FE65 amyloid precursor

protein-interacting proteins in brain development. *EMBO J.* 25, 420–431. doi: 10.1038/sj.emboj.7600926

20) Haass, C., Kaether, C., Thinakaran, G., and Sisodia, S. (2012). Trafficking and proteolytic processing of APP. *Cold Spring Harb. Perspect. Med.* 2:a006270. doi: 10.1101/cshperspect.a006270

21) Hu, Q., Cool, B. H., Wang, B., Hearn, M. G., and Martin, G. M. (2002). A candidate molecular mechanism for the association of an intronic polymorphism of FE65 with resistance to very late onset dementia of the Alzheimer type. *Hum. Mol. Genet.* 11, 465–475. doi: 10.1093/hmg/11.4.465

22) Johnson, B. A., and Blevins, R. A. (1994). NMR view: a computer program for the visualization and analysis of NMR data. *J. Biomol. NMR* 4, 603–614. doi: 10.1007/BF00404272

23) Kabsch, W. (2010). XDS. *Acta Crystallogr. D Biol. Crystallogr.* 66, 125–132. doi: 10.1107/S0907444909047337

24) Koistinen, N. A., Edlund, A. K., Menon, P. K., Ivanova, E. V., Bacanu, S., Iverfeldt, K., et al. (2017). Nuclear localization of amyloid-*b* precursor protein-binding protein Fe65 is dependent on regulated intramembrane proteolysis. *PLoS One* 12:e0173888. doi: 10.1371/journal.pone.0173888

25) Kohli, B. M., Pflieger, D., Mueller, L. N., Carbonetti, G., Aebersold, R., Nitsch, R. M., et al. (2012). Interactome of the amyloid precursor protein APP in brain reveals a protein network involved in synaptic vesicle turnover and a close association with Synaptotagmin-1. *J. Proteome Res.* 11, 4075–4090. doi: 10.1021/pr300123g

26) Krissinel, E., and Henrick, K. (2007). Inference of macromolecular assemblies from crystalline state. *J. Mol. Biol.* 372, 774–797. doi: 10.1016/j.jmb.2007. 05.022

27) Lichtenthaler, S. F., Haass, C., and Steiner, H. (2011). Regulated intramembrane proteolysis—lessons from amyloid precursor protein processing. *J. Neurochem.* 117, 779–796. doi: 10.1111/j.1471-4159.2011.07248.x

28) McLoughlin, D. M., and Miller, C. C. (2008). The FE65 proteins and Alzheimer's disease. *J. Neurosci. Res.* 86, 744–754. doi: 10.1002/jnr.21532

29) Meiyappan, M., Birrane, G., and Ladias, J. A. (2007). Structural basis for polyproline recognition by the FE65 WW domain. *J. Mol. Biol.* 372, 970–980. doi: 10.1016/j.jmb.2007.06.064

30) Minopoli, G., Gargiulo, A., Parisi, S., and Russo, T. (2012). Fe65 matters: new light on an old molecule. *IUBMB Life* 64, 936–942. doi: 10.1002/iub.1094

31) Müller, T., Meyer, H. E., Egensperger, R., and Marcus, K. (2008). The amyloid precursor protein intracellular domain (AICD) as modulator of gene expression, apoptosis, and cytoskeletal dynamics-relevance for Alzheimer's disease. *Prog. Neurobiol.* 85, 393–406. doi: 10.1016/j.pneurobio.2008.05.002

32) Müller, U. C., and Zheng, H. (2012). Physiological functions of APP family proteins. *Cold Spring Harb. Perspect. Med.* 2:a006288. doi: 10.1101/cshperspect. a006288

33) Pardossi-Piquard, R., and Checler, F. (2012). The physiology of the *b*-amyloid precursor protein intracellular domain AICD. *J. Neurochem.* 120, 109–124. doi: 10.1111/j.1471-4159.2011.07475.x

34) Pernot, P., Round, A., Barrett, R., De Maria Antolinos, A., Gobbo, A., Gordon, E., et al. (2013). Upgraded ESRF BM29 beamline for SAXS on macromolecules in solution. *J. Synchrotron Radiat.* 20, 660–664. doi: 10.1107/S0909049513010431 Petoukhov, M. V., Franke, D., Shkumatov, A. V., Tria, G., Kikhney, A. G., Gajda, M., et al. (2012). New developments in the ATSAS program package for small-angle scattering data analysis. *J. Appl. Crystallogr.* 45, 342–350. doi: 10.1107/S0021889812007662

35) Radzimanowski, J., Beyreuther, K., Sinning, I., and Wild, K. (2008a). Overproduction, purification, crystallization and preliminary X-ray analysis of human Fe65-PTB2 in complex with the amyloid precursor protein intracellular domain. *Acta Crystallogr. Sect. F Struct. Biol. Cryst. Commun.* 64, 409–412. doi: 10.1107/S1744309108009524

36) Radzimanowski, J., Ravaud, S., Schlesinger, S., Koch, J., Beyreuther, K., Sinning, I., et al. (2008b). Crystal structure of the human Fe65-PTB1 domain. *J. Biol. Chem.* 283, 23113–23120. doi: 10.1074/jbc.M800861200

37) Radzimanowski, J., Simon, B., Sattler, M., Beyreuther, K., Sinning, I., and Wild, K. (2008c). Structure of the intracellular domain of the amyloid precursor protein in complex with Fe65-PTB2. *EMBO Rep.* 9, 1134–1140. doi: 10.1038/embor. 2008.188

38) Ramelot, T. A., Gentile, L. N., and Nicholson, L. K. (2000). Transient structure of the amyloid precursor protein cytoplasmic tail indicates preordering of structure for binding to cytosolic factors. *Biochemistry* 39, 2714–2725. doi: 10.1021/bi992580m

39) Russo, T., Faraonio, R., Minopoli, G., De Candia, P., De Renzis, S., and Zambrano, N. (1998). Fe65 and the protein network centered around the cytosolic

domain of the Alzheimer's *b*-amyloid precursor protein. *FEBS Lett.* 434, 1–7. doi: 10.1016/s0014-5793(98)00941-7

40) Selkoe, D. J., and Hardy, J. (2016). The amyloid hypothesis of Alzheimer's disease at 25 years. *EMBO Mol. Med.* 8, 595–608. doi: 10.15252/emmm.201606210

41) Shen, Y., and Bax, A. (2010). SPARTA+: a modest improvement in empirical NMR chemical shift prediction by means of an artificial neural network. *J. Biomol. NMR* 48, 13–22. doi: 10.1007/s10858-010-9433-9

42) Shen, Y., Delaglio, F., Cornilescu, G., and Bax, A. (2009). TALOS+: a hybrid method for predicting protein backbone torsion angles from NMR chemical shifts. *J. Biomol. NMR* 44, 213–223. doi: 10.1007/s10858-009-9333-z

43) Simon, B., Madl, T., Mackereth, C. D., Nilges, M., and Sattler, M. (2010). An efficient protocol for NMR-spectroscopy-based structure determination of protein complexes in solution. *Angew. Chem. Int. Ed Engl.* 49, 1967–1970. doi: 10.1002/anie.200906147

44) Strecker, P., Ludewig, S., Rust, M., Mundinger, T. A., Görlich, A., Krächan, E. G., et al. (2016). FE65 and FE65L1 share common synaptic functions and genetically interact with the APP family in neuromuscular junction formation. *Sci. Rep.* 6:25652. doi: 10.1038/srep25652

45) Telese, F., Bruni, P., Donizetti, A., Gianni, D., D'Ambrosio, C., Scaloni, A., et al. (2005). Transcription regulation by the adaptor protein Fe65 and the nucleosome assembly factor SET. *EMBO Rep.* 6, 77–82. doi: 10.1038/sj.embor. 7400309

46) Uhlik, M. T., Temple, B., Bencharit, S., Kimple, A. J., Siderovski, D. P., and Johnson, G. L. (2005). Structural and evolutionary division of phosphotyrosine binding (PTB) domains. *J. Mol. Biol.* 345, 1–20. doi: 10.1016/j.jmb.2004. 10.038

47) von Rotz, R. C., Kohli, B. M., Bosset, J., Meier, M., Suzuki, T., Nitsch, R. M., et al. (2004). The APP intracellular domain forms nuclear multiprotein complexes and regulates the transcription of its own precursor. *J. Cell Sci.* 117, 4435–4448. doi: 10.1242/jcs.01323

48) Winkler, E., Julius, A., Steiner, H., and Langosch, D. (2015). Homodimerization protects the amyloid precursor protein C99 fragment from cleavage by *g*-secretase. *Biochemistry* 54, 6149–6152. doi: 10.1021/acs.biochem.5b00986

49) Winn, M. D., Ballard, C. C., Cowtan, K. D., Dodson, E. J., Emsley, P., Evans, P. R., et al. (2011). Overview of the CCP4 suite and current developments. *Acta*

Crystallogr. D Biol. Crystallogr. 67, 235–242. doi: 10.1107/S0907444910045749

Xu, X., Zhou, H., and Boyer, T. G. (2011). Mediator is a transducer of amyloid-precursor-protein-dependent nuclear signalling. *EMBO Rep.* 12, 216–222. doi: 10.1038/embor.2010.210

50) Yang, Z., Cool, B. H., Martin, G. M., and Hu, Q. (2006). A dominant role for FE65 (APBB1) in nuclear signaling. *J. Biol. Chem.* 281, 4207–4214. doi: 10.1074/jbc. m508445200

51) Yang, L. B., Lindholm, K., Yan, R., Citron, M., Xia, W., Yang, X. L., et al. (2003). Elevated *b*-secretase expression and enzymatic activity detected in sporadic Alzheimer disease. *Nat. Med.* 9, 3–4. doi: 10.1038/nm0103-3

52) Zambrano, N., Bimonte, M., Arbucci, S., Gianni, D., Russo, T., and Bazzicalupo, P. (2002). *feh-1* and *apl-1*, the *Caenorhabditis elegans* orthologues of mammalian Fe65 and *b*-amyloid precursor protein genes, are involved in the same pathway that controls nematode pharyngeal pumping. *J. Cell Sci.* 115, 1411–1422.

53) Zambrano, N., Minopoli, G., de Candia, P., and Russo, T. (1998). The Fe65 adaptor protein interacts through its PID1 domain with the transcription factor CP2/LSF/LBP1. *J. Biol. Chem.* 273, 20128–20133. doi: 10.1074/jbc.273.32. 20128

Chapter III

Analysis of LRP1 and APP transport and its dependence on the

Fe65 protein family

Background

Generation of the toxic amyloid β (Aβ) peptide, which is one of the hallmark of AD (Masters et al. 1985) or non-toxic fragments depends mainly on the processing of APP by the α-, β- and ɣ-secretases (Jacobsen & Iverfeldt 2009). The localization of the secretases differs within the cell, while the α- and ɣ-secretases are prominently localized at the cell surface (Chow et al. 2010) the β-secretase primary cleaves APP within the Trans Golgi Network (TGN) (Huse et al. 2002). Hence, intracellular sorting and transport of APP is crucial for its processing and Aβ generation. Sorting proteins like SorLA, SorCS1 and LRP1 have been implicated to play an import role in APP allocation and thereby potentially influencing the Aβ generation (Pietrzik 2002, Waldron et al. 2008, Schmidt et al. 2012, Hermey et al. 2015). Furthermore, it was shown that mutated LRP1 which retains in the endoplasmic reticulum (ER) leads to a decrease in Aβ secretion and C-terminal fragments of APP at the plasma membrane (Waldron et al. 2008).

LRP1 belongs to the low density lipoprotein receptor (LDLR) family (Krieger 1994) and interacts with APP via the N- and C-terminus assuming to have an impact on endocytosis (Ulery et al. 2000, Pietrzik et al. 2004). Interestingly, this C-terminal interaction of LRP1 and APP is mediated by Fe65 whose PTB domains consolidate both proteins leading to increased APP secretion which was only detectable in the presence of LRP1 indicating that Fe65 forms a functional linker between APP and LRP1 (Pietrzik et al. 2004).

In addition, it was shown that APP is able to interact in *cis*- as well as in *trans*-orientation (Soba et al. 2005) which also has an influence on its processing and thereby the formation of Aβ (Eggert et al. 2009, Jung et al. 2014). Interaction of APP in *trans*-orientation is supposed to modulate synapse formation (Wang et al. 2009, Klevanski et al. 2014, Stahl et al. 2014) while *cis*-dimerization, which already occurs in the ER (Isbert et al. 2012), seems to affect the processing of APP by α-, β- and ɣ-secretases (Eggert et al. 2009, Jung et al. 2014).

The precise mechanism of APP intracellular processing and transport in dependence of its monomeric or dimeric state and which role LRP1 and Fe65 might play in these processes remained until yet elusive and were addressed in this study.

Methods

Analysis of monomeric and dimeric APP was conducted by comparing the generation and processing of APP in Human Embryonic Kidney cells (HEK) and primary cortical neurons (PCN). Transport characteristics of monomeric or dimeric APP and LRP1 as well as co-expressed APP and LRP1 were quantitated via live cell imaging of transfected PCN or primary hypocampal neurons (PHN), respectively, followed by analysis of corresponding kymographs. Following constructs were used to obtain live cell imaging data: APP-GFP, LRP1-GFP, APP-RFP and APP-F1 (see below). Furthermore, the influence of the Fe65 protein family was analyzed by using neurons of Fe65 KO, Fe65 KO and Fe65/Fe65L1 DKO mice. In addition, we examined the loss of LRP1 on APP transport rates by treating PCN of Lrp1$^{flox/flox}$ mice with Cre-recombinase fused to a basic protein translocation peptide derived from HIV-TAT (Tat-Cre). In human brain APP is present 30-50% in its dimerized form (Schmidt et al. 2011) and we therefor increased the dimerization ratio by using an APP construct with inducible FK501-binding-protein (FKBP) – tag (APP-F1) (Eggert et al. 2009) or by using stable transfected Chinese Hamster Ovary (CHO) cells expressing mutated human APP bearing an amino acid exchange (Lysin to Cystein at position 587 of APP695, APP695 K587C). The influence of LRP1 on generated APP dimers was determined based on pulse chase experiments using CHO cells lacking LRP1 (CHO 13-5-1 (Pietrzik 2002)). Further, the amount of processed dimeric and monomeric soluble APP (sAPP) in absence of LRP1 was studied using CHO 13-5-1 cells overexpressing APP695 K587C or PCN of 5xFAD/Lrp1$^{flox/flox}$ mice treated with Tat-Cre, respectively. In HEK APP695 K587C or CHO 13-5-1 APP695 K587C cells we determined cleavage properties of meprin β and the α-secretase depending on the dimerization status of APP as well as in absence of LRP. Finally, we checked the amount of sAPP dimers in 5xFAD/Lrp1$^{BE-/-}$ mice (Storck et al. 2015) lacking LRP1 in brain endothelial and choroid plexus epithelial cells.

Results and Conclusion

Analysis of the dimerization and processing properties of APP in HEK cells as well as in PCN revealed that disulfide-bound sAPP dimers are present in the conditioned media indicating that sAPP dimers, probably already formed in the ER, are transported and cleaved by secretases in a dimerized status. Interestingly, quantification of kymographs of our live cell imaging data showed no influence of APP dimerization on transport characteristic. We found no significant difference in vesicle distribution or mean velocities of monomeric or dimeric APP. Both forms were transported by the same kinesin-dependent transport machinery at an average speed of 1.5µm/s, which is line with previous findings (Hermey et al. 2015). Via pulse chase experiments using CHO 13-5-1 cells lacking LRP1 and stably overexpressing APP695 K587C we could demonstrate that LRP1 is important for the transport of dimeric APP to the cell surface, as it was shown for monomeric APP before (Waldron et al. 2008). Since LRP1 influences the transport of APP, we wondered how LRP1 itself is transported and how APP might affect LRP1 transport. We studied LRP1 transport in PHN again by usage of live cell imaging. LRP1 positive vesicles were transported with a velocity of 1-2µm/s in anterograde as well as retrograde direction. In contrast, APP containing vesicles moved with velocities >2µm/s assuming that LRP1 and APP are mostly transported in distinct transport vesicles, associated with different fast axonal transport machineries. Most interestingly, co-expression of LRP1 and APP altered the transport velocities of APP containing vesicles both in anterograde and retrograde direction to velocities similar to LRP1 containing vesicles. However, reduced levels of LRP1 in PCN of Lrp1$^{flox/flox}$ mice treated with Tat-Cre increased the transport velocities of moving APP containing vesicles and the vesicle distribution to decreased amounts of stationary vesicles which underline the assumption that LRP1 causes a sorting of APP into LRP1 membrane bound organelles (Waldron et al. 2008). Furthermore, we compared the transport properties of APP and LRP in dependence of the Fe65 protein family utilizing PHN of Fe65 KO, Fe65L1 KO and Fe65/Fe65L1 DKO mice. Surprisingly, we found no consistent influence of the Fe65 protein family neither on LRP1 nor APP transport expressing LRP1 or APP alone (Figure 3.1) or co-expressing LRP1 and APP (Figure 3.2). These data are currently difficult to understand and require more detailed analysis, including

deletion of Fe65L2. Therefore, we decided to not include these data in this manuscript.
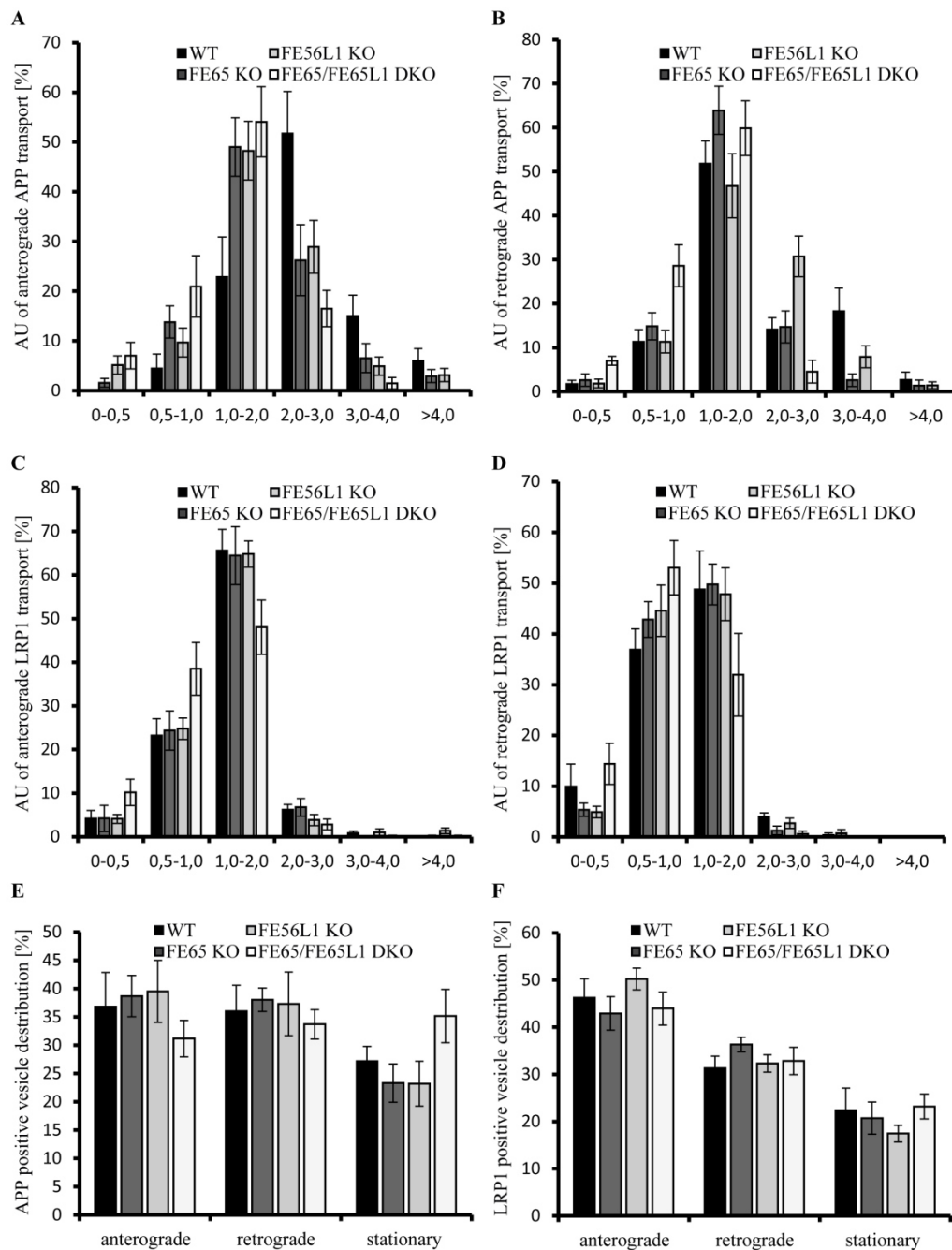

Figure 3.1: No influence of the Fe65 protein family on APP or LRP1 transport characteristics.

Primary hippocampal neurons (PHN) (DIV6) of C57BL/6J wild type (WT), Fe65 KO, Fe65L1 KO or Fe65/Fe65L1 DKO mouse embryos expressing APP or LRP1 were subjected for live cell imaging 18–20 h post transfection. Time lapse series were plotted as kymographs and used for determination of individual transport vesicle velocities. (A) Anterograde and (B) retrograde transport velocity profiles and (E) vesicle distribution of APP-RFP in WT (black columns), Fe65 KO (dark grey columns), Fe65L1 KO (light grey columns) and Fe65/Fe65L1 DKO (white columns) neurons. (C) Anterograde and (D) retrograde transport velocity profiles and (F) vesicle distribution of LRP1-GFP in WT

Figure 3.1 continued

(black columns), Fe65 KO (dark grey columns), Fe65L1 KO (light grey columns) and Fe65/Fe65L1 DKO (white columns) neurons. For quantification of transport velocities 7 kymographs from different cells were analyzed (APP-RFP in WT neurons: n = 254 vesicles; in Fe65 KO neurons: n = 378 vesicles; in Fe65L1 KO neurons: n = 410 vesicles; in Fe65/Fe65L1 DKO neurons: n = 228 vesicles; LRP1-GFP in WT neurons: n = 534 vesicles; in Fe65 KO neurons: n = 746 vesicles; in Fe65L1 KO neurons: n = 708vesicles; in Fe65/Fe65L1 DKO neurons: n = 675 vesicles). Bars represent mean values ± SEM; Kruskal-Wallis-Test followed by Dunn's Multiple Comparison Test.
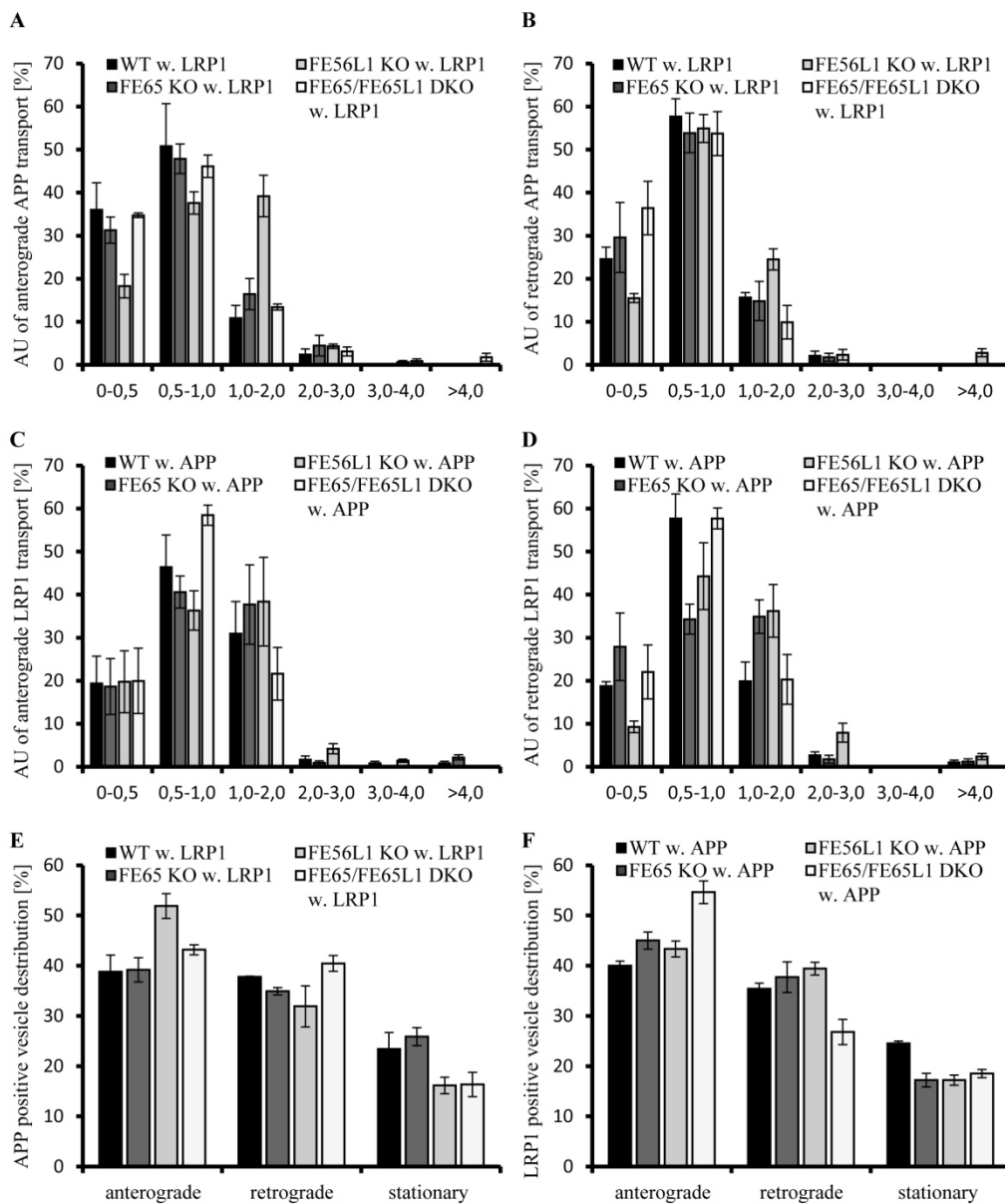
Figure 3.2: No influence of the Fe65 protein family on APP and LRP1 co-transport characteristics.

Primary hippocampal neurons (PHN) (DIV6) of C57BL/6J wild type (WT), Fe65 KO, Fe65L1 KO or Fe65/Fe65L1 DKO mouse embryos expressing APP and LRP1 were subjected for live cell imaging 18–20 h post transfection. Time lapse series were plotted

Figure 3.2 continued

as kymographs and used for determination of individual transport vesicle velocities. (A) Anterograde and (B) retrograde transport velocity profiles and (E) vesicle distribution of APP-RFP in WT (black columns), Fe65 KO (dark grey columns), Fe65L1 KO (light grey columns) and Fe65/Fe65L1 DKO(white columns) neurons co-expressing LRP1-GFP. (C) Anterograde and (D) retrograde transport velocity profiles and (F) vesicle distribution of LRP1-GFP in WT (black columns), Fe65 KO (dark grey columns), Fe65L1 KO (light grey columns) and Fe65/Fe65L1 DKO (white columns) neurons co-expressing APP-RFP. For quantification of transport velocities >3 kymographs from different cells were analyzed (APP-RFP in WT neurons: n = 175 vesicles; in Fe65 KO neurons: n = 161 vesicles; in Fe65L1 KO neurons: n = 228 vesicles; in Fe65/Fe65L1 DKO neurons: n = 199 vesicles; LRP1-GFP in WT neurons: n = 196 vesicles; in Fe65 KO neurons: n = 201 vesicles; in Fe65L1 KO neurons: n = 253 vesicles; in Fe65/Fe65L1 DKO neurons: n = 228 vesicles). Bars represent mean values ± SEM; Kruskal-Wallis-Test followed by Dunn's Multiple Comparison Test

After revealing via live cell imaging analysis that LRP1 overexpression leads to a shift of APP containing transport vesicles towards retrograde transport direction we further hypothesised that a partial reduction of LRP1 might increase dimeric sAPP secretion due to reduced internalization and in turn providing more APP dimers at the plasma membrane. To test this assumption, we first analyzed the sAPP dimer formation in CHO 13-5-1 cells and CHO wt cells stably overexpressing APP K587C. After comparing the sAPP dimer to total APP dimer ratio we could show that in cells lacking LRP1 the sAPP dimer secretion is increased. Further examination of sAPP dimer secretion in cells overexpressing the internalization deficient APP K587C NGYE construct (with mutated NPTY internalization motif) in presence or absence of LRP1 leaded to an interesting finding. In wt CHO cells transfected with the internalization deficient APP construct, the sAPP dimer level were increased and which have also been shown for monomeric APP (Perez et al. 1999), while the internalization deficiency showed no significant increase in sAPP in cells lacking LRP1. To investigate wheather LRP1 has a similiar effect in neuronal cells, we analyzed PCN of Lrp1$^{flox/flox}$ mice treated with Tat-Cre and found a comparable increase in sAPP dimer secretion after reducing LRP1 levels. The increased sAPP secretion is mainly mediated by shedding of APP by meprin β as further analyzed in transfected HEK cells expressing APP K587C alone or co-expressing meprin β. Interestingly, meprin β shows a higher affinity to dimeric APP whereas the α-secretase cleaves preferentially monomeric APP, which is in line with previous findings exhibiting that α-secretase is mainly involved in cleavage of monomeric APP (Jorissen et al. 2010, Kuhn et al. 2010). The higher affinity of meprin β to dimeric

APP is not well understood but might be linked to the fact that the secretase itself exists in form of a dimer (Kruse et al. 2004).

Several results exhibited that in brain a large fraction of APP is present as a dimer (Munter et al. 2007, Schmidt et al. 2012). To determine the possibility that LRP1 also may have a regulatory effect on APP dimer processing *in vivo* we analyzed the cerebrospinal fluid (CSF) of 5xFAD mutant mice and 5xFAD/Lrp1$^{BE-/-}$ mice lacking LRP1 in the brain endothelial and choroid plexus epithelial cells. Quantification of the western blot analysis showed indeed an increase of sAPP dimers in the CSF of 5xFAD/Lrp1$^{BE-/-}$ mice which is likely caused by the reduced internalization of APP.

Conclusion

Intracellular sorting of APP determines the fate of generating pathogenic Aβ peptides initiated by the cleavage of the β-secretase or non-pathogenic fragments by meprin β or α-secretase cleavage. Here we could show that the sorting protein LRP1 modulates APP distribution intracellularly independently of its monomeric or dimeric state. Interestingly, LRP1 expression shifts APP in a different slow moving transport vesicle type, indicating that it acts as an APP sorting molecule, recruiting APP in LRP1 positive transport vesicles. Consistently decreased levels of LRP1 accelerated the secretion rate of APP. In turn its increased availability at the surface leads to elevated cleavage by meprin β and the α-secretase. Further, in context of this thesis, it is worth mentioning, that Fe65 is not required for the LRP1 mediated recruitment of APP.

References

Chow, V.W. et al., 2010. An Overview of APP Processing Enzymes and Products. Neuromolecular medicine, 12(1), pp.1–12.

Eggert, S. et al., 2009. Induced dimerization of the amyloid precursor protein leads to decreased amyloid-?? protein production. Journal of Biological Chemistry, 284(42), pp.28943–28952.

Hermey, G. et al., 2015. SorCS1 variants and amyloid precursor protein (APP) are co-transported in neurons but only SorCS1c modulates anterograde APP transport. Journal of Neurochemistry, 135(1), pp.60–75.

Huse, J.T. et al., 2002. ??-secretase processing in the trans-Golgi network preferentially generates truncated amyloid species that accumulate in Alzheimer's disease brain. Journal of Biological Chemistry, 277(18), pp.16278–16284.

Jacobsen, K.T. & Iverfeldt, K., 2009. Amyloid precursor protein and its homologues: a family of proteolysis-dependent receptors. Cellular and molecular life sciences : CMLS, 66(14), pp.2299–318.

Jorissen, E. et al., 2010. The disintegrin/metalloproteinase ADAM10 is essential for the establishment of the brain cortex. The Journal of neuroscience : the official journal of the Society for Neuroscience, 30(14), pp.4833–44.

Jung, J.I. et al., 2014. Independent relationship between amyloid precursor protein (APP) dimerization and γ-secretase processivity. PLoS ONE, 9(10).

Klevanski, M. et al., 2014. Differential role of APP and APLPs for neuromuscular synaptic morphology and function. Molecular and Cellular Neuroscience, 61, pp.201–210.

Krieger, M., 1994. Structures and Functions of Multiligand Lipoprotein Receptors: Macrophage Scavenger Receptors and LDL Receptor-Related Protein (LRP). Annual Review of Biochemistry, 63(1), pp.601–637.

Kruse, M.-N. et al., 2004. Human meprin alpha and beta homo-oligomers: cleavage of basement membrane proteins and sensitivity to metalloprotease inhibitors. The Biochemical journal, 378(Pt 2), pp.383–389.

Kuhn, P.-H. et al., 2010. ADAM10 is the physiologically relevant, constitutive alpha-secretase of the amyloid precursor protein in primary neurons. The EMBO journal, 29(17), pp.3020–32.

Masters, C.L. et al., 1985. Amyloid plaque core protein in Alzheimer disease and Down syndrome. Proceedings of the National Academy of Sciences of the United States of America, 82(12), pp.4245–9.

Pietrzik, C. et al., 2004. FE65 constitutes the functional link between the low-density lipoprotein receptor-related protein and the amyloid precursor protein. The Journal of neuroscience : the official journal of the Society for Neuroscience, 24, pp.4259–4265.

Pietrzik, C.U., 2002. The cytoplasmic domain of the LDL receptor-related protein regulates multiple steps in APP processing. The EMBO Journal, 21(21), pp.5691–5700.

Schmidt, V. et al., 2011. Quantitative modelling of amyloidogenic processing and its influence by SORLA in Alzheimer's disease. The EMBO Journal, 31(1), pp.187–200.

Soba, P. et al., 2005. Homo- and heterodimerization of APP family members promotes intercellular adhesion. The EMBO journal, 24(20), pp.3624–3634.

Stahl, R. et al., 2014. Shedding of APP limits its synaptogenic activity and cell adhesion properties. Frontiers in cellular neuroscience, 8(December), p.410.

Storck, S.E. et al., 2015. Endothelial LRP1 transports amyloid- β 1 – 42 across the blood-brain barrier. Journal of Clinical Investigation, 126(21), pp.1–14.

Ulery, P.G. et al., 2000. Modulation of Amyloid Precursor Protein Processing by the Low Density Lipoprotein Receptor-related Protein (LRP). Journal of Biological Chemistry, 275(10), pp.7410–7415.

Waldron, E. et al., 2008. LRP1 modulates APP trafficking along early compartments of the secretory pathway. Neurobiology of Disease, 31(2), pp.188–197.

LRP1 Modulates APP Intraneuronal Transport and Processing in Its Monomeric and Dimeric State

Uta-Mareike Herr [1] [†], Paul Strecker [2] [†], Steffen E. Storck [1], Carolin Thomas [2], Verena Rabiej [1], Anne Junker [1], Sandra Schilling [2], Nadine Schmidt [2], C. Marie Dowds [2], Simone Eggert [2], Claus U. Pietrzik [1*†] and Stefan Kins [2*†]

[1] Institute of Pathobiochemistry, Molecular Neurodegeneration, University Medical Center of the Johannes Gutenberg-University Mainz, Mainz, Germany, [2] Division of Human Biology and Human Genetics, Technical University of Kaiserslautern, Kaiserslautern, Germany

†These authors have contributed equally to this work.

Uta-Mareike Herr [1†], **Paul Strecker** [2†] et al. (2017)

ABSTRACT

The low-density lipoprotein receptor-related protein 1, LRP1, interacts with APP and affects its processing. This is assumed to be mostly caused by the impact of LRP1 on APP endocytosis. More recently, also an interaction of APP and LRP1 early in the secretory pathway was reported whereat retention of LRP1 in the ER leads to decreased APP cell surface levels and in turn, to reduced Aβ secretion. Here, we extended the biochemical and immunocytochemical analyses by showing via live cell imaging analyses in primary neurons that LRP1 and APP are transported only partly in common (one third) but to a higher degree in distinct fast axonal transport vesicles. Interestingly, co-expression of LRP1 and APP caused a change of APP transport velocities, indicating that LRP1 recruits APP to a specific type of fast axonal transport vesicles. In contrast lowered levels of LRP1 facilitated APP transport. We further show that monomeric and dimeric APP exhibit similar transport characteristics and that both are affected by LRP1 in a similar way, by slowing down APP anterograde transport and increasing its endocytosis rate. In line with this, a knockout of LRP1 in CHO cells and in primary neurons caused an increase of monomeric and dimeric APP surface localization and in turn accelerated shedding by meprin β and ADAM10. Notably, a choroid plexus specific LRP1 knockout caused a much higher secretion of sAPP dimers into the cerebrospinal fluid compared to sAPP monomers. Together, our data show that LRP1 functions as a sorting receptor for APP, regulating its cell surface localization and thereby its processing by ADAM10 and meprin β, with the latter exhibiting a preference for APP in its dimeric state.

INTRODUCTION

The amyloid precursor protein (APP) is a type I transmembrane protein that has first been identified related in association with Alzheimer's disease (AD) as representing the precursor of amyloid β (Aβ) peptides (Kang et al., 1987). Those peptides generated by sequential cleavage of APP by β- and γ-secretases were shown to be a major component of senile plaques found in the brains of AD patients (Merz et al., 1983; Masters et al., 1985). Besides its role in AD pathogenesis, APP has been implicated in physiological functions including intracellular signaling, trophic activity in neurons and synapses as well as in synaptic and cell adhesion processes (Baumkötter et al., 2012; Müller and Zheng, 2012). Recent studies revealed that APP can dimerize or oligomerize in cis- as well as in trans-orientation (Scheuermann et al., 2001; Soba et al., 2005; Munter et al., 2007; Kaden et al., 2009; Wang et al., 2009; Isbert et al., 2012; Baumkötter et al., 2014; Klevanski et al., 2014; Stahl et al., 2014). Remarkably, APP dimers were detected in mouse brains (Soba et al., 2005; Schmidt et al., 2012), indicating that dimer formation occurs in vivo under physiological conditions. Trans-cellular APP dimerization is assumed to modulate synapse organization (Soba et al., 2005; Wang, 2005; Wang et al., 2009; Isbert et al., 2012; Baumkötter et al., 2014; Klevanski et al., 2014; Stahl et al., 2014). In contrast, APP cis-dimerization, that has been shown to occur as early as in the endoplasmic reticulum (ER) (Isbert et al., 2012), has been implicated in processing of APP by α-, β-, and γ-secretases (Munter et al., 2007, 2010; Kaden et al., 2008; Eggert et al., 2009; Libeu et al., 2012; Schmidt et al., 2012; So et al., 2012; Jung et al., 2014). Recently, it has been claimed that efficient processing of APP by α- and β-secretases may depend on its oligomerization state that results in cooperative effects for these allosteric enzymes, influenced by SorLA and possibly also LRP1 (Schmidt et al., 2012). However, whether sAPP dimers are generated in vivo in neurons, which secretases are required and what might be the role of LRP1 in this context, is unknown yet.

LRP1, a member of the low density lipoprotein receptor (LDLR) family (Krieger and Herz, 1994), was shown to interact with APP via the N- and C-terminal domain and to affect its processing (Ulery et al., 2000; Pietrzik et al., 2002, 2004). This effect is presumably based on the impact of LRP1 on APP endocytosis (Knauer et al., 1996; Ulery et al., 2000; Pietrzik et al., 2002; Cam et al., 2005). In addition, APP can

interact with LRP1 before it is cleaved by furin in the TGN, implying an interaction of APP with LRP1 early in the secretory pathway (Pietrzik et al., 2004). This hypothesis was confirmed in 2008 (Waldron et al., 2008), by using a truncated LRP1-construct (LRP-CT) (Pietrzik et al., 2002) containing a dilysine ER-retention motif (KKAA) capable of binding to APP. The retention of LRP1 in the ER leads to a decrease in Aβ secretion as well as to a decrease in full length APP and CTF levels at the plasma membrane (Waldron et al., 2008).

Here, we extend the analysis of APP transport characteristics and show that LRP1 plays a crucial role in trafficking and processing of monomeric as well as dimeric APP.

MATERIALS AND METHODS

Cell Culture

Human Embryonic Kidney cells (HEK 293T) were cultured in Dulbecco's Modified Eagle's Medium (DMEM; Thermo Fisher Scientific) supplemented with 10% fetal calf serum (FCS), 1 mM sodium pyruvate (Sigma-Aldrich), 100 units/ml penicillin and 0.1 mg/ml streptomycin (Thermo Fisher Scientific).

Chinese Hamster Ovary cells, either CHO K1 or LRP-deficient CHO 13-5-1 (FitzGerald et al., 1995), were grown in Alpha Minimum Essential Medium (α-MEM; Lonza) supplemented equally.

Primary neurons were extracted from cortices of C57BL/6J or 5xFAD/Lrp1[flox/flox] mouse embryos at embryonic day 14 as described previously (Maier et al., 2013). Cells were seeded on poly-L-ornithine (100 µg/ml; Sigma-Aldrich) coated 6-well plates or 6 cm dishes, respectively, in a density of 600,000 cells per well or 1,000,000 cells per dish. They were cultured in Neurobasal Medium (Thermo Fisher Scientific) complemented with 100 units/ml penicillin and 0.1 mg/ml streptomycin, 1 x B27 supplement and 1 x GlutaMAX (all Thermo Fisher Scientific).

Primary cortical neurons (PCN) were prepared using E14 embryos from C57BL/6J mice (Janvier) or 5xFAD/Lrp1[flox/flox] mice as described before (Stahl et al., 2014; Hermey et al., 2015). PCN dissolved in DB1 medium [DMEM with 10% FBS, 0.79% D-glucose and 1 x GlutaMAX (Thermo Fisher Scientific)] were plated on poly-L-lysine (Sigma-Aldrich) coated fluorodishes in a density of $6*105/cm^2$. Six hour post plating DB1 was changed and PCN were cultivated in neurobasal medium supplemented with B27 and GlutaMAX (Thermo Fisher Scientific).

Primary hippocampal neurons (PHN), used for APP/LRP live cell imaging, were prepared from P0 pups of C57BL/6J mice and treated in the same way as described for PCN.

All cell types were cultivated at 37°C in an incubator maintaining a relative humidity of over 80% and a CO_2 level of 5%.

DNA Constructs and Cloning

For analyzing the properties of APP cis-dimers a human APP695 construct with a dimer-bearing amino acid exchange from lysine (K) to cysteine (C) at position 587 (APP695 K587C) was generated for transient and stable transfections. The plasmid consisting of the human APP695 CDS with the triplet mutation (AAG to TGT) at position 1,761 as well as a C-terminal myc-tag in the vector pLBCX was developed by an overlap extension PCR as described by Isbert et al. (2012). The restriction sites for HindIII and ClaI, which are flanking the myc-tagged, mutated APP sequence, enabled the subcloning of this DNA fragment into the vector pLHCX resulting in the pLHCX-APP695 K587C construct. Hence this construct has the same vector backbone as the also used pLHCX-APP695 wt plasmid (Jäger et al., 2009). APP dimer constructs exhibiting a mutation in the APP internalization motif "YENPTY" (Lai et al., 1995; MarquezSterling et al., 1997) were generated performing a standard PCR followed by restriction and ligation into the pLHCX vector backbone. The plasmid pLHCX-APP695 K587C served as template for PCR using the forward primer 5′-CCCAAGCTTATGCTGCCCGGTTTG-3′, which contains a 5′ HindIII restriction site and the reverse primer 5′-CCATCGATGGTTACAGATCCTCTTCTGAGATGAGTTTTTGTTCGTTCTGCATCTG CTCAAAGAACTTTTCGTAGCCGTTTTCGTAG-3′ exhibiting the mutation in the internalization motif, the myc-epitope and a 3′ ClaI restriction site. The described mutation results in an amino acid exchange from NPTY to NGYE at the C-terminus of the expressed APP695 K587C protein. The amplified DNA fragment was subcloned in frame into the pLHCX vector backbone via the HindIII and ClaI restriction sites. Sequencing of the generated construct authenticated its accuracy. To study the processing of monomeric and dimeric APP by meprin β, HEK 293T cells were co-transfected with either APP695 wt or APP695 K587C and the meprin β HA construct in pLBCX (Schönherr et al., 2016).

For generation of the expression construct encoding the LRP1-GFP fusion protein, the EGFP cDNA was amplified from pcDNA3.1 APP-GFP (Szodorai et al., 2009) using the oligos 5′-TGAGCAGATGCAGAACGTCG-3′ and 5′-GCACAGTCGAGGCTGATCAGC-3′. The PCR product was cloned via flanking BamHI/NotI sites in frame into pLBCX myc-LRP1 and the resulting construct, pLBCX-myc-LRP1-GFP, was validated by sequencing.

Infections and Transfections

The infection of primary cortical neurons (PCN) with an adenoviral vector encoding human APP695 (Yuan et al., 1999) was performed at DIV 7. Cells were incubated with 100 plaque-forming units per cell for 6 h. In contrast, for live cell imaging, PCN or PHN were transiently transfected at DIV 6 using calcium phosphate transfection. A neurobasal medium containing 2% B27 (transfection medium) was prepared and incubated for at least 30 min at 37°C and 5% CO_2. Meanwhile, the following transfection mix was pipetted (sufficient for two fluorodishes): Solution A containing 75 µl H_2O dd, 9.5 µl 2.5 M $CaCl_2$ and 20 µg DNA; Solution B containing 75 µl 2 × HBS pH 7.07 (274 mM NaCl, 10 mM KCl, 1.4 mM Na_2HPO_4, 15 mM D-Glucose, 42 mM HEPES pH 7.1). Solution A was added to Solution B, immediately vortexed for 10 s at maximum speed and incubated for 20 min at RT. Meanwhile, the medium of the cultured neurons was replaced by 2 ml of the previously prepared transfection medium. The old medium was collected for later usage. Afterwards, 89.75 µl of the transfection mix were added per neuronal culture dish. The neuronal cells were incubated for 3 h at 37°C until precipitates were formed. To remove the precipitates, the cells were washed twice with 2 × HBS. Therefore 1 ml prewarmed 2 x HBS was added to the transfected neurons before 1 ml was removed. This step was repeated once and the medium-HBS mix was afterwards removed completely. To provide important growth factors for neuronal growth, 2 ml of the collected old medium were added to each dish. The cells were incubated at 37°C for 18–20 h and analyzed by live cell imaging. For transient transfection of HEK and CHO cells with different APP695 constructs or the meprin β construct a transfection mixture containing 8 µg polyethylenimine (PEI) and 2 µg DNA in 120 µl serum-free medium was added to the cells for 4 h. Stable CHO cells were generated as described previously (Isbert et al., 2012) using pLHCX-APP695 K587C and 350 µg/ml Hygromycin B (Thermo Fisher Scientific) for selection.

Antibodies

The antibody mix 1G75A3 of the two monoclonal antibodies 1G7 and 5A3, both directed against the APP ectodomain, was provided by Dr. Koo (UC San Diego School of Medicine, USA) and enabled the detection of all forms of full-length APP (mature, immature or dimerized) in cell lysates as well as soluble APP in the conditioned medium. This antibody mix was used for Western Blotting and for

immunoprecipitation of APP. For detection of LRP1 in Western Blotting the polyclonal antibody 1704 (Pietrzik et al., 2002) directed against the C-terminus of LRP1 was used. Y188 (Abcam) directed against the C-terminus of APP was used to detect monomeric and dimeric APP in Blue Native Gel Electrophoresis. Aβ was detected by IC16, a monoclonal antibody recognizing the amino acids 1 to 16 of the human Aβ sequence (Jäger et al., 2009). The polyclonal anti-actin antibody and the secondary HRP-conjugated goat anti-rabbit antibody were purchased from Sigma-Aldrich. The secondary donkey antibody against mouse, also HRP-conjugated, was obtained from Jackson ImmunoResearch

Western Blotting

After collecting the conditioned medium cells were harvested and lysed either in RIPA (50 mM Tris-Cl (pH 8), 150 mM NaCl, 0.1% SDS, 1% Nonidet P-40, 10 mM NaF, 1 mM β-glycerophosphate, 0.5% sodium deoxycholate) regarding neurons or, concerning HEK and CHO cells, in NP-40 lysis buffer (500 mM Tris (pH 7.4), 150 mM NaCl, 5 mM EDTA, 1% Nonidet P-40, 0.02% NaN_3) both containing 1 x protease inhibitor cocktail (PI; Roche). Debris were pelleted by centrifugation with 18,600 × g for 20 min at 4°C. The protein concentrations were measured using the PierceTM BCA Protein Assay Kit (Thermo Fisher Scientific) to determine equal amounts of total protein for lysate analysis. For comparable protein amounts of the conditioned media volumes were adjusted to the protein concentration in the corresponding lysates. After addition of 4 x SDS sample buffer with (Roti R -Load 1; Roth) or without (40% glycerol, 200 mM Tris-HCl (pH 6.8), 0.08% bromphenol blue, 8% SDS in VE-H_2O) β-mercaptoethanol (βME) samples were boiled for 5 min at indicated temperatures. Proteins were separated by gel electrophoresis in 6 or 7% Bis-Tris gels and transferred onto nitrocellulose membranes (GE Healthcare Life Sciences) via wet blot. To block non-specific binding membranes remained for 1 h in 5% (w/v) non-fat dry milk dissolved in TBS containing 0.05% Tween 20 (Roth) before incubation with the appropriate primary and secondary antibodies. The protein detection was carried out using the Immobilon Western HRP Substrate (Millipore) resulting in chemiluminescence, which was recorded by the LAS-3000 mini (Fujifilm).

Immunoprecipitation and Detection of Aβ

The immunoprecipitation of Aβ peptides was performed as described by Schönherr et al. (2016). Proteins were separated by Urea SDS-PAGE corresponding to the approach of Klafki et al. (1996) and transferred to PVDF membranes via semi-dry Western Blotting (Biorad) at 47 mA per gel. Afterwards membranes were boiled for 3 min in 1 x PBS before blocking non-specific binding in 5% (w/v) non-fat dry milk in TBST for 30 min. Membranes were incubated over night at 4°C with IC16 antibody (1:500). After washing with TBST the secondary HRP-conjugated mouse antibody was added for 1 h at room temperature. Protein detection and recording were performed as described above.

Blue Native Gel Electrophoresis

Blue native gel electrophoresis was performed as described before (Eggert et al., 2009). Briefly, transfected cells were resuspended in 1 ml of homogenization buffer (250 mM sucrose in 20 mM HEPES, pH 7.4, with protease inhibitors) and then sheared by passing through a 27 gauge needle. Postnuclear supernatant was collected after a centrifugation step at 1,000 × g for 15 min. After sedimentation at 100,000 × g for 1 h the membrane fraction was washed once with 200 μl of homogenization buffer followed by another centrifugation at 100,000 × g. The pellet was resuspended in 200 μl homogenization buffer. 100 μg of protein were solubilized with Blue Native sample buffer (1.5 M amino caproic acid, 0.05 M Bis-Tris, 10% *n*-dodedecyl-D-maltoside, and protease inhibitor at pH 7). The samples were separated on gradient gels. Thyroglobulin (669 kDa), apoferritin (443 kDa), catalase (240 kDa), aldolase (158 kDa), and bovine serum albumin (66 kDa) were used as molecular weight standards.

Live Cell Imaging

Fluorophore tagged LRP1 and APP fusion proteins were tracked by imaging of living cells, as described before (Szodorai et al., 2009; Hermey et al., 2015). Briefly, during live cell imaging transfected cells were temperature-controlled (37°C) and CO2-controlled (5%). Images were taken every 200 ms over a period of 30 s. GFP-tagged proteins were excited with 470 nm and RFP fusion proteins with 550 nm wave length using a matching filter and fast changing LED's. Kymographs were created using Image J software (1.46r) in combination with the Multiple-Kymograph plugin. The

slope of the traces is a direct measure for the velocity of the vesicles (v = cotan(α), where α is the angle relative to the x-axis). Single tracks with an angle $0° < α < 90°$ were defined as anterograde, and tracks with a slope $90° < α < 180°$ were defined as retrograde transport vesicles. Tracks with slopes of $90°$ (parallel to the time axis) were determined as stationary vesicles. For vesicle distribution all lines of one kymograph were counted as individual transport vesicles and the sum of all anterograde, retrograde and stationary vesicles was set to 100% (given as relative amount of vesicles). For calculation of total amount of vesicles per neurite segment, again all traces of individual kymographs were counted as single vesicles (stationary, anterograde and retrograde vesicles) and related to a neurite length of 1 μm.

Immunocytochemistry

Primary cortical neurons (PCN) were differentiated for 7 days in vitro and then subjected for immunocytochemical analysis. PCN were fixed for 10 min at 37∘C in 4% (w/v) PFA with 4% (w/v) sucrose and permeabilized for 10 min with 0.1% (v/v) NP40 in 1 x PBS. For detection of LRP1 and APP we used the polyclonal antibody 1704 and monoclonal antibody C1/6.1, respectively. Secondary antibodies were Alexa Flour 488 and Alexa Flour 594 (1:1,000, Invitrogen). Hoechst (33258, Thermo Fisher Scientific) was used as nuclear counterstaining. Imaging was performed with microscope Axio Observer Z.1 (Zeiss with apotome) and z-stacks were taken in 0.2 μm steps.

Pulse-Chase Assay

To examine the expression and stability of APP dimers, a pulse-chase assay was performed with CHO K1 and CHO 13-5-1 cells 48 h after seeding on 6 cm dishes. Cells were starved in DMEM without methionine and cysteine complemented as described above, which was replaced after 1 h by 1 ml of the same medium containing 150 μCi35S/ml (EasyTag[TM] EXPRESS35S Protein Labeling Mix; PerkinElmer). Following 15 min incubation at 37°C the medium was substituted to 2 ml α-MEM supplemented as outlined above but with addition of 40 mM HEPES (Lonza). Cells were maintained in this medium at 37°C for indicated time spans before being harvested and lysed in NP-40 buffer with 1 x PI as detailed previously. For immunoprecipitation of APP, lysates and conditioned media were incubated over night at 4°C with protein G agarose beads (Roche) and the 1G75A3 antibody mix

against the APP ectodomain. Beads were washed as described above, pelleted and finally boiled in 4 x SDS sample buffer at 80°C for 5 min. The accordingly recovered proteins were separated on 4–12% NuPAGE gradient gels (Invitrogen). After electrophoresis gels were incubated in fixation buffer (10% acetic acid and 20% ethanol in VE-H_2O) for 15 min and washed for 1 h with VE-H_2O thereby renewing the water every 20 min. Gels were dried onto chromatography paper (Whatman) for 2 h at 65°C using the Model 583 Gel Dryer (Bio-Rad). Exposure of the film was carried out over night at room temperature in an exposition cassette. Radioactivity was detected by a phosphor imager (Cyclone Plus Storage Phosphor System; PerkinElmer) and visualized via the OptiQuant software.

Tat-Cre Treatment

PCN of 5xFAD/Lrp1$^{flox/flox}$ mouse embryos (E14) were treated with Cre-recombinase fused to a basic protein translocation peptide derived from HIV-TAT (Tat-Cre) (provided by Dr. Roosmarijn E. Vandenbroucke; Inflammation Research Center, VIB, Ghent, Belgium; Department of Biomedical Molecular Biology, Ghent University, Ghent, Belgium) at DIV 4. Therefore, the culture medium was reduced to 2 ml and the recombinase was added in a final concentration of 200 nM. As control, PCN were treated with the Tat-Cre buffer (20 mM HEPES, 0.6 M NaCl, pH 7.4). Cells were incubated with the Tat-Cre recombinase or the vehicle alone for 48 h at 37°C before cell lysis at DIV 6.

Inhibitor Treatment

The surface levels of APP dimers were examined 24 h after reduction of the medium and inhibitor treatment. After collecting the conditioned medium cells were rinsed 3 times with ice-cold PBS. Surface proteins were biotinylated by addition of 0.25 mg/ml Sulfo-NHS-LC-LC-Biotin (Thermo Fisher Scientific) dissolved in 1 x PBS for 40 min at 4°C thereby refreshing the biotin solution after 20 min. To quench unconjugated biotin, cells were washed 4 times with 50 mM NH_4Cl in ice-cold 1 x PBS. Cells were lysed in NP-40 buffer containing 1 x PI. Equal protein amounts were incubated over night at 4°C with NeutrAvidin Agarose Resin (Pierce). Unbound proteins were removed in 3 washing steps with NP-40 buffer and centrifugation at 4°C with 24 × g for 2 min. Beads were boiled at 80°C in 4 x SDS sample buffer for 5 min to elute proteins, which were separated on 6% Bis-Tris gels.

CSF Isolation

Cerebrospinal fluid (CSF) was harvested from 4 months old 5xFAD/Lrp1$^{flox/flox}$ and 5xFAD/Lrp1BE$^{-/-}$ mice by puncture of the cisterna magna as described previously (Vandenbroucke et al., 2012; Storck et al., 2016). Cell free CSF was obtained by centrifugation at 800 × g for 10 min at 4°C. 2 µl of CSF were diluted in water and mixed with equal amounts of 2 x loading dye (0.72 M Bis-Tris, 0.32 M Bicine, 30% (w/v) sucrose, 2% SDS, 0.02% bromophenol blue without βME). Samples were denatured at 70°C for 5 min to maintain putative dimerization of sAPP. Samples were separated by SDS-PAGE on 7% polyacrylamide SDS gels, transferred onto nitrocellulose membranes (Amersham Hybond ECL) and then blocked in 5% (w/v) non-fat dry milk in TBST (20 mM Tris, 137 mM NaCl, 0.1% (v/v) Tween-20). The antibody mix 1G75A3 (1:300) was used to detect sAPP.

Animals

In vivo analyses were performed with tamoxifen-inducible 5xFAD mice lacking Lrp1 in brain endothelial and choroid plexus epithelial cells (5xFAD/Lrp1BE$^{-/-}$) (described in detail in Storck et al., 2016). 5xFAD mice, which represent a well-established AD model harboring 3 APP mutations and 2 PSEN1 mutations that are linked to FAD, served as LRP1 expressing controls. All animal studies were conducted in compliance with European and German guidelines for the care and use of laboratory animals and were approved by the Central Animal Facility of the University of Mainz and the ethical committee on animal care and use of Rhineland-Palatinate, Germany. Mice were housed on a 12-h-light cycle and had ad libitum access to water and a standard laboratory diet. To induce knock-out of Lrp1 in CSF-secreting epithelial cells of the choroid plexus in 5xFAD/Lrp1BE$^{-/-}$, 12-week-old animals were injected i.p. with 2 mg tamoxifen (T5648, Sigma-Aldrich) for 7 consecutive days as described in Storck et al. (2016). After tamoxifen injection the standard laboratory diet was changed to chow supplemented with 400 mg tamoxifen citrate per kilogram dry weight (CRE Active TAM400, LASvendi) to maintain Cre-mediated recombination.

Quantification and Statistical Analysis

Western Blots and phosphor imager results were quantified by densitometry using ImageJ (1.44 or 1.46r) or Multi Gauge V3.0, respectively. The Graph Pad Prism 4 software (Graph Pad; La Jolla) provided the basis for compilation of the shown graphs and for statistical analysis. Data were analyzed by Student's t-test or one-way ANOVA followed by Tukey's post-hoc test. For live cell analysis at least 5 kymographs were analyzed. Student's t-test was used when comparing only two sets of data or one-way ANOVA followed by Bonferroni post-hoc test when comparing three sets of data and given the data were normaly distributed, respectively. The Kruskal-Wallis-Test followed by Dunn's Multiple Comparison Test was used to assess statistical differences between three sets of data given that data weren't normally distributed or variance was significantly different. The level of significance was set at $p < 0.05$ (∗), $p < 0.01$ (∗∗) and $p < 0.001$ (∗∗∗).

RESULTS

APP Dimers Are Generated and Processed in Cortical Neurons

As described before 30–50% of APP are present in a dimerized form in human brain (Munter et al., 2007; Schmidt et al., 2012). To investigate, whether APP695 dimer formation can be analyzed in a neuronal system, we infected primary cortical neurons of C57BL/6J mouse embryos (E14) with an adenovirus driving expression of human APP695. Indeed, we were able to detect APP dimers in the lysate of DIV 8 mouse neurons (Figure 1A) comparable to the expression of human APP dimers in HEK cells (Figure 1B). Likewise, by analyzing the supernatant of the same cells, we observed soluble APP dimers in the conditioned medium suggesting that APP dimers are not only generated but also processed in neuronal cells as well as in human kidney cells (Figures 1A,B).
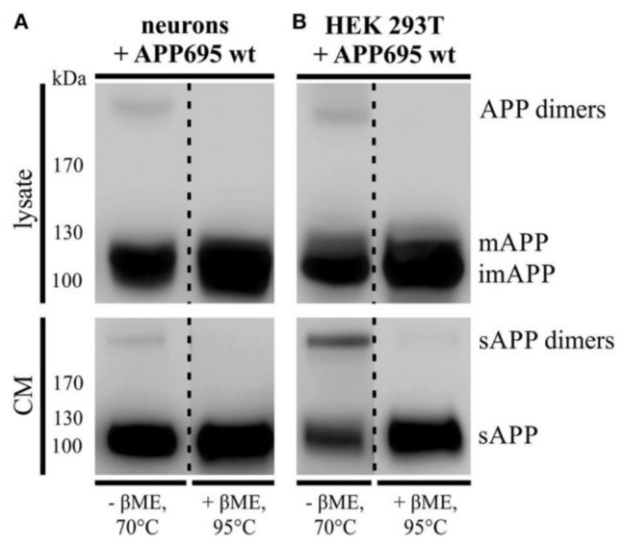
FIGURE 1 | APP dimer generation and processing takes place in primary cortical neurons.

(A) Murine primary cortical neurons (DIV 7) were infected with an adenoviral vector encoding human APP695 while (B) HEK 293T cells were transiently transfected with the pLHCX-APP695 wt construct. 24 h post infection or transfection, respectively, conditioned media (CM) were collected and cells were lysed in RIPA (PCN) or NP-40 (HEK) lysis buffer. Via the antibody mix 1G75A3 (1:3,000) APP was detected in lysates (upper blots) and conditioned media (lower blots). PCN show similar APP dimer expression in the lysate as HEK cells and also generate soluble APP dimers. Under reducing conditions using β-mercaptoethanol (βME) and heating at 95°C the dimer band disappeared. All lanes of lysate or conditioned medium are on the same blot but were rearranged for better presentation.

To verify the existence of APP dimers linked by disulfide bridges as we have described before (Isbert et al., 2012), the samples were boiled in sample buffer containing β-mercaptoethanol (βME). Note, that in the samples under reducing conditions the disulfide bonds were dissolved and the dimer band signal decreased, whereas the signal intensity for monomeric APP increased (Figures 1A,B). These data show that disulfide-bound sAPP dimers, formed most likely in the ER, are anterogradely transported and shed by secretases in a dimerized status.

Monomeric and Dimeric APP Show Similar Transport Characteristics

As we found that neurons secrete disulfide-bound dimerized sAPP, we wondered if monomeric and dimeric APP are transported along the secretory pathway in the same or diverse types of transport vesicles. For this purpose we used an inducible FK501-binding-protein (FKBP) -based dimerization system (Rollins et al., 2000), previously used for analysis of APP processing in dependence of APP dimerization (Eggert et al., 2009). For live cell imaging expression constructs encoding for C-terminal tagged GFP APP-FKBP fusion proteins were generated (APP-F1-GFP) (Video in Supplementary Material 1). For control, we first verified that APP-GFP and non-dimerized APP-F1-GFP exhibit identical transport characteristics (Figure 2A). Furthermore, as GFP has a weak tendency to self-dimerize (Chalfie and Kain, 2005), we tested if APP-GFP might exhibit in comparison to APP altered dimerization properties, by using the blue-native gel system (Eggert et al., 2009). Notably, we observed for APP-GFP no increase in dimerization properties (Supplementary Figure 1). In the next step, the transport of non-dimerized (APP-F1-GFP + EtOH) and dimerized APP (APP-F1-GFP + dim.) was compared (Figure 2A). Surprisingly, the induction of APP dimerization had no significant influence on APP transport velocities in anterograde or retrograde direction, respectively (Figures 2B,C). The majority of APP vesicles moved with a velocity between 0.5 and 2.5 μm/s in both directions, independent of their dimerization status. These data suggest that monomeric and dimeric APP are transported by the same kinesin dependent transport machinery.
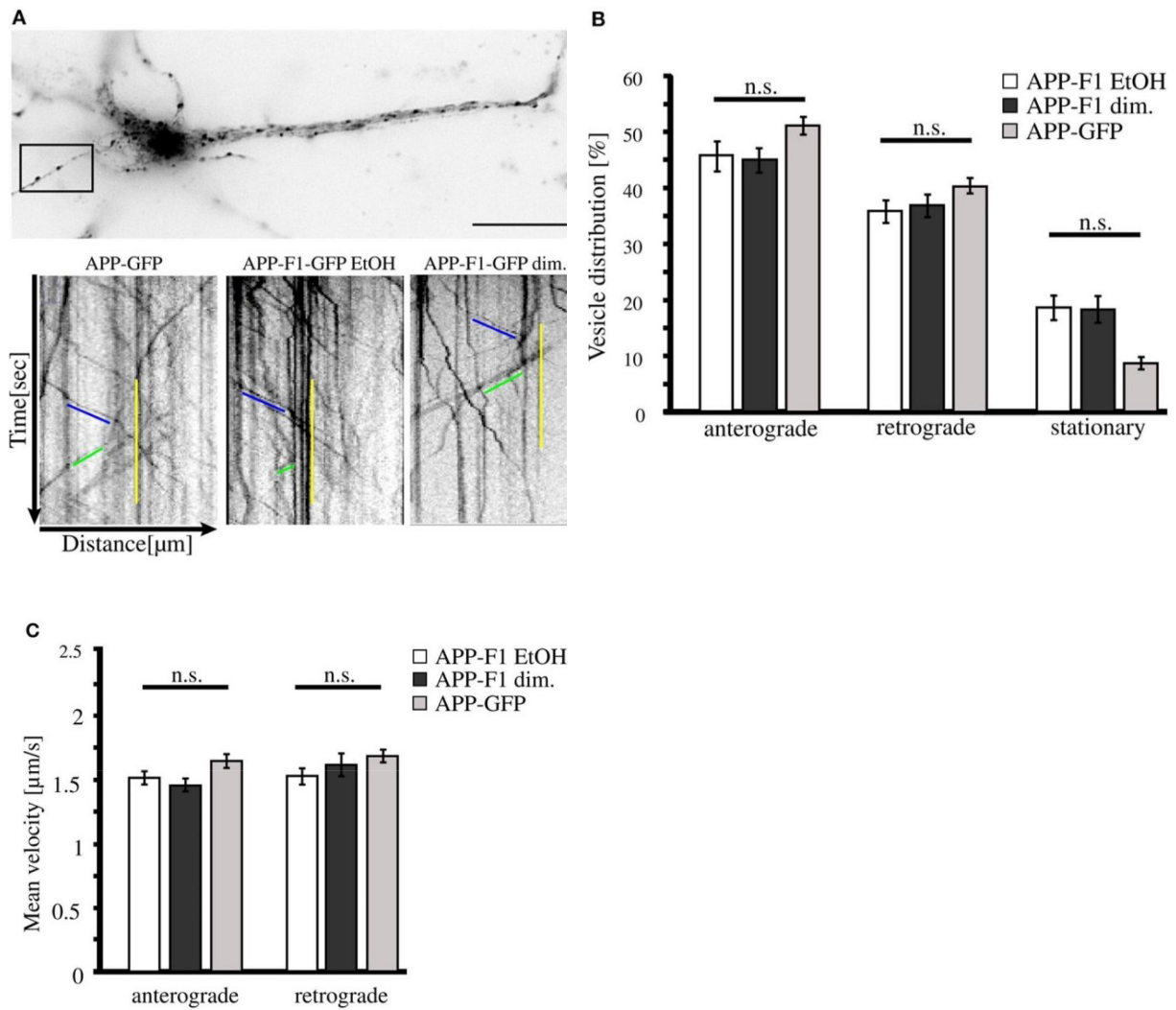
FIGURE 2 | APP dimerization does not affect its transport characteristics.

Murine cortical primary neurons (DIV 6) were transiently transfected with expression constructs encoding APP-GFP or APP-F1-GFP. After 18–20 h and 1 h prior live cell recording of axonal vesicle movements, APP-F1-GFP expressing neurons were either treated with 100 nM AP20187 (dimerizer) or for control with the vehicle of the dimerizer, ethanol (negative control). (A) Representative primary neuron and kymographs of cells expressing APP GFP or APP-F1-GFP treated with dimerizer or ethanol respectively. The ROI is marked by a rectangle. Bar: 20 µm. (B) Vesicle distribution and (C) anterograde and retrograde transport velocities of APP-GFP, non-dimerized APP-F1-GFP (ethanol control) and APP-F1-GFP dimerized vesicles. No differences among APP variants could be observed (one-way ANOVA followed by Bonferroni post hoc test). Bars represent mean values ± SEM, n = 3 (≥16 cells per approach).

LRP1 Deficiency Leads to Accelerated Trafficking of APP Dimers

Since APP cis-homodimers and monomers show similar transport characteristics, we assumed that both follow the same principle. Previously, we demonstrated that LRP1 influences monomeric APP transport along the secretory pathway (Waldron et al., 2008). Therefore, we wanted to analyze now, whether a lack of LRP1 may also affect trafficking of APP dimers. For this purpose, we generated a cDNA construct providing the continuous expression of SDS-stable APP cis-dimers. The expression construct exhibits a triplet mutation in the coding sequence of APP695, which leads to an amino acid exchange from lysine (K) to cysteine (C) at position 587 (APP695 K587C) (Figure 3A). This mutation enabled the formation of APP cis-dimers by disulfide bridges between the cysteine residues in the E2 domain of two mutant APP molecules. According to our expectation a stepwise increase of temperature up to 95°C showed only a slight decrease of APP K587C dimers, indicating that most of the APP K587C dimers are stabilized by intramoleclular disulfide bonds (Figures 3B,C). To get further insights on the generation and processing of APP cis-dimers in regard to LRP1, we performed a pulse-chase assay with CHO K1 and LRP1-deficient CHO 13-5-1 cells stably expressing APP695 K587C dimers. This assay revealed that sAPP dimers were already immunoprecipitated after a 30 min chase in CHO 13-5-1 cells while in CHO K1 cells shed APP dimer fragments were first detectable after a 1 h chase (Figure 3D). Quantification of the sAPP dimer/APP dimer ratio showed an increase of this ratio in LRP1-deficient cells (Figure 3E) suggesting an earlier availability of APP dimers for shedding at the cell surface. Thus, these results point to an accelerated trafficking of APP dimers in the absence of LRP1
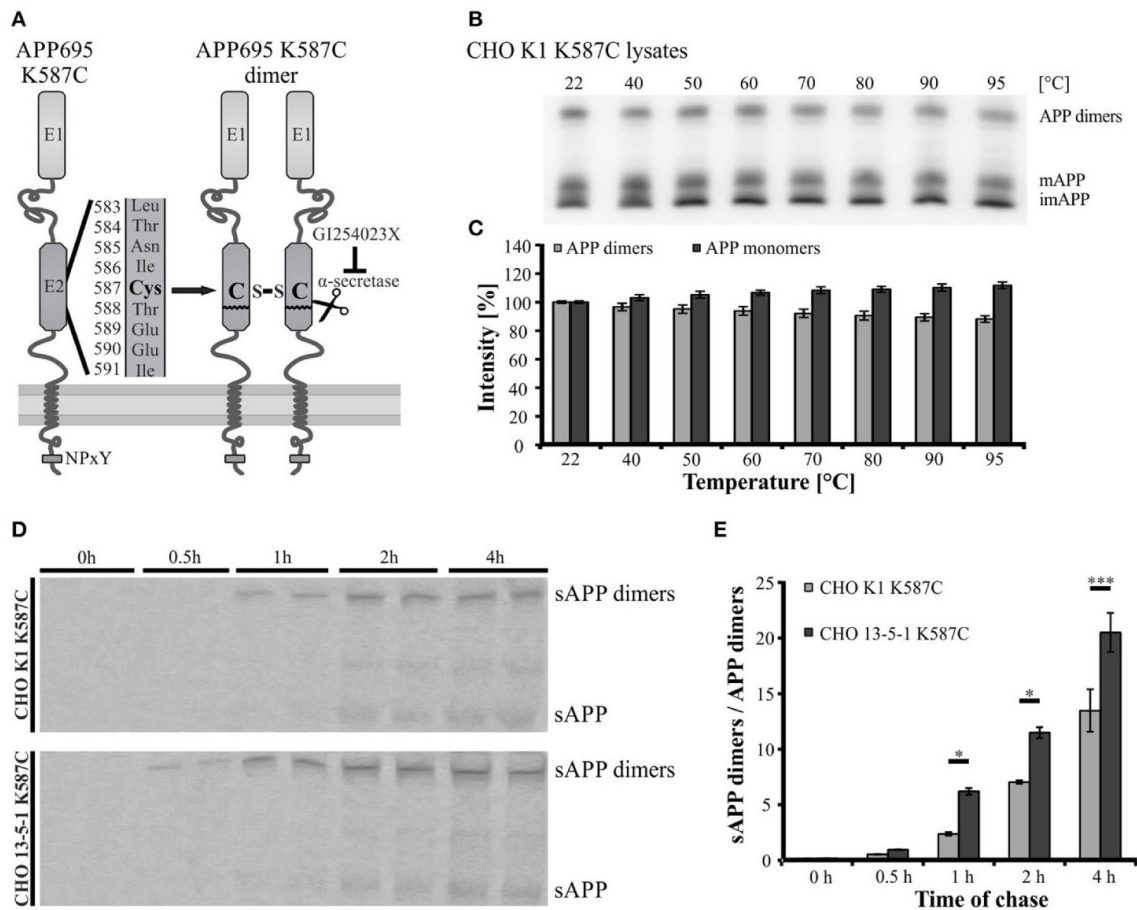
FIGURE 3 | Faster trafficking of SDS- and heat-stable APP cis-dimers in LRP1-deficient cells.

(A) Schematic representation of the APP Cys-mutant encoded by the pLHCX-APP695 K587C construct and its resulting cis-dimerization state. (B,C) CHO K1 cells were transiently transfected with the APP695 K587C construct. (B) 24 h post transfection monomeric as well as dimerized APP were detected by the antibody mix 1G75A3 (1:3,000) in cell lysates. (B,C) Heating of samples up to 95∘C shows a negligible reduction of the APP dimer signal with a comparable increase in monomeric APP. (D) CHO K1 and LRP1-deficient CHO 13-5-1 cells both stably expressing the dimer bearing APP construct were pulsed with radiolabeled sulfur (35S) for 15 min. Chase was performed after stated time spans prior to immunoprecipitation of APP with the antibody mix 1G75A3 (1:300) and SDS-PAGE. Exposure of the film revealed an earlier occurrence of soluble APP dimers in the conditioned medium of LRP1-deficient CHO 13-5-1 cells (30 min chase) than in CHO K1 cells (1 h chase). (E) Comparison of the sAPP dimer to APP dimer ratio of both cell types shows a significant elevation for CHO 13-5-1 cells beginning after a 1 h chase. Bars represent mean values ± SEM, n = 3; Student's t-test; $p < 0.05$ (*), $p < 0.001$ (***).

LRP1 Alters APP Transport Characteristics

We observed that anterograde transport of monomeric and dimeric APP is affected by LRP1, suggesting that LRP1 and APP might be sorted in common transport vesicles and that LRP1 might be required for APP sorting. To address this hypothesis, we performed co-stainings of endogenous APP and LRP1 in primary cortical neurons (PCN) and used again a live cell imaging approach.

Immuncocytochemical analysis of PCN differentiated for 7 days in vitro using anti-APP and anti-LRP1 antibodies revealed a strong cytoplasmic staining within the cell body and a punctate staining of LRP1 and APP in neurites, at least in part representing transport vesicles (Supplementary Figure 2). Interestingly, we observed only a low co-localization rate, arguing that LRP1 and APP are mostly transported in different transport vesicle types.

An expression construct encoding an N-terminal myc tagged LRP-mini-receptor (Rabiej et al., 2015) was used for generation of a C-terminally GFP tagged LRP-mini-receptor (LRP1-GFP). After verification that the newly generated LRP1-GFP fusion protein was expressed as full-length protein and that the GFP-tag did not alter the subcellular localization (data not shown) the construct was used for live cell imaging. First, we wanted to analyze transport velocities of APP-RFP and LRP1-GFP in single transfected primary hippocampal mouse neurons (PHN). Time lapse series of 30 s were recorded at an interval of 200 ms/frame and vesicle movement was quantified based on the analysis of kymographs (Figures 4A,B; Video in Supplementary Material 2). Quantification showed that the largest fraction (68%) of anterograde LRP1-GFP-positive vesicles was transported with a velocity of 1–2 µm/s in contrast to APP-RFP that was mostly (66%) transported in vesicles faster than 2 µm/s (Figure 4C). Also for retrograde moving vesicles, a clear difference in transport characteristics was observed (Figure 4D). Although most of the retrograde transport vesicles containing APP-RFP and LRP1-GFP moved with a velocity of 1–2 µm, a fraction of APP-RFP positive transport vesicles showed retrograde transport characteristics with velocities >2 µm/s, which was not observed for LRP1-GFP containing vesicles. These data suggest that the majority of LRP1 and APP are transported in distinct anterograde transport vesicles, whereas a larger fraction of LRP1 and APP is co-transported in retrograde transport vesicles.
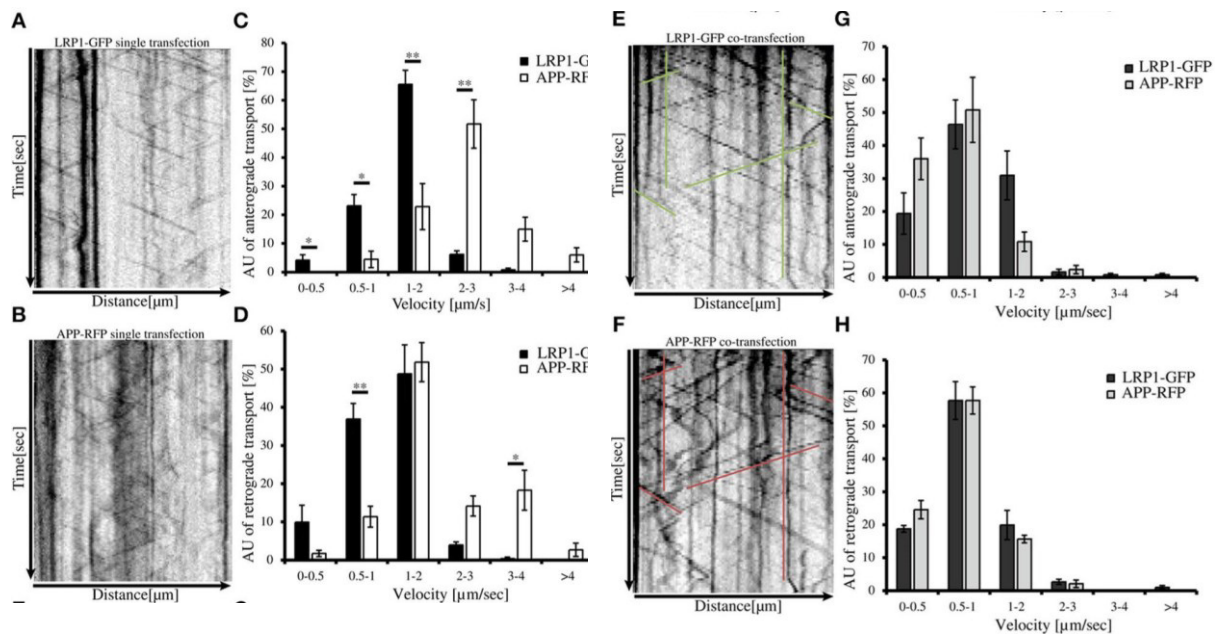
FIGURE 4 | LRP1 recruits APP in common transport vesicles.

Primary hippocampal neurons from mice (P0) were differentiated for 6 days in vitro, expressing either (A) only LRP1-GFP, (B) APP-RFP or (E,F) alternatively co-expressing both, APP-RFP and LRP1-GFP were subjected for live cell imaging 18–20 h post transfection. Time lapse series were plotted as kymographs (representative kymographs, single transfection: A,B; co-transfection: E,F) and used for determination of individual transport vesicle velocities. For quantification of transport velocities >5 kymographs from different cells were analyzed [(C,D) LRP: n = 5 cells, n = 534 vesicles; APP: n = 7 cells, n = 254 vesicles; (G,H) n = 5 cells, n = 371 vesicles]. (C) Anterograde and (D) retrograde transport vesicles containing APP-RFP (white columns) or LRP-GFP (black columns). Note the change of APP-RFP transport characteristcs in (G) anterograde and (H) retrograde direction (light gray columns) upon co-expression of (G,H) LRP1-GFP (dark gray columns). Bars represent mean values ± SEM, n > 5 (≥254 vesicles); Student's t-test, p < 0.05 (*), p < 0.01 (**).

Further, we tested if LRP1 and APP co-expression might affect APP transport characteristics and vice versa. For this purpose, we performed live cell imaging analyses of PHNs co-expressing LRP1-GFP and APP-RFP 18 to 20 h post transfection, as described above (representative kymographs Figures 4E,F). Quantification revealed that LRP1-GFP and APP-RFP are co-transported in common anterograde and retrograde transport vesicles (Figures 4G,H). Most interestingly, co-expression of LRP1-GFP caused a change of APP-RFP transport characteristics, that was highly similar to those observed in single transfected cells for LRP1-GFP (Figures 4A–D), whereas LRP1-GFP transport upon co-expression of APP remained unchanged (Figures 4G,H). This holds true for APP/LRP1 anterograde (Figure 4G) as well as retrograde (Figure 4H) transport. Accordingly, also the mean velocities were strongly reduced upon co-expression of LRP1 (Figure 5E). Notably, the relative

amount of anterograde, retrograde and stationary vesicles remained unchanged, arguing that LRP1 not simply holds back APP in the Golgi. Instead, our data indicate that co-expression of LRP1 may cause a recruitment of APP into common transport vesicles, that exhibit different transport characteristics.

To further validate that LRP1 modifies APP intraneuronal transport, we analyzed APP-RFP transport in primary neurons with reduced LRP1 levels. For this purpose, we used PCN of Lrp1[flox/flox] mouse embryos, treated with 200 nM Cre-recombinase fused to a basic protein translocation peptide derived from HIV-TAT (Tat-Cre) for 48 h prior live cell imaging. Reduced LRP1 expression of about 2-fold was validated by Western Blot analysis (Figures 5A, 7A).
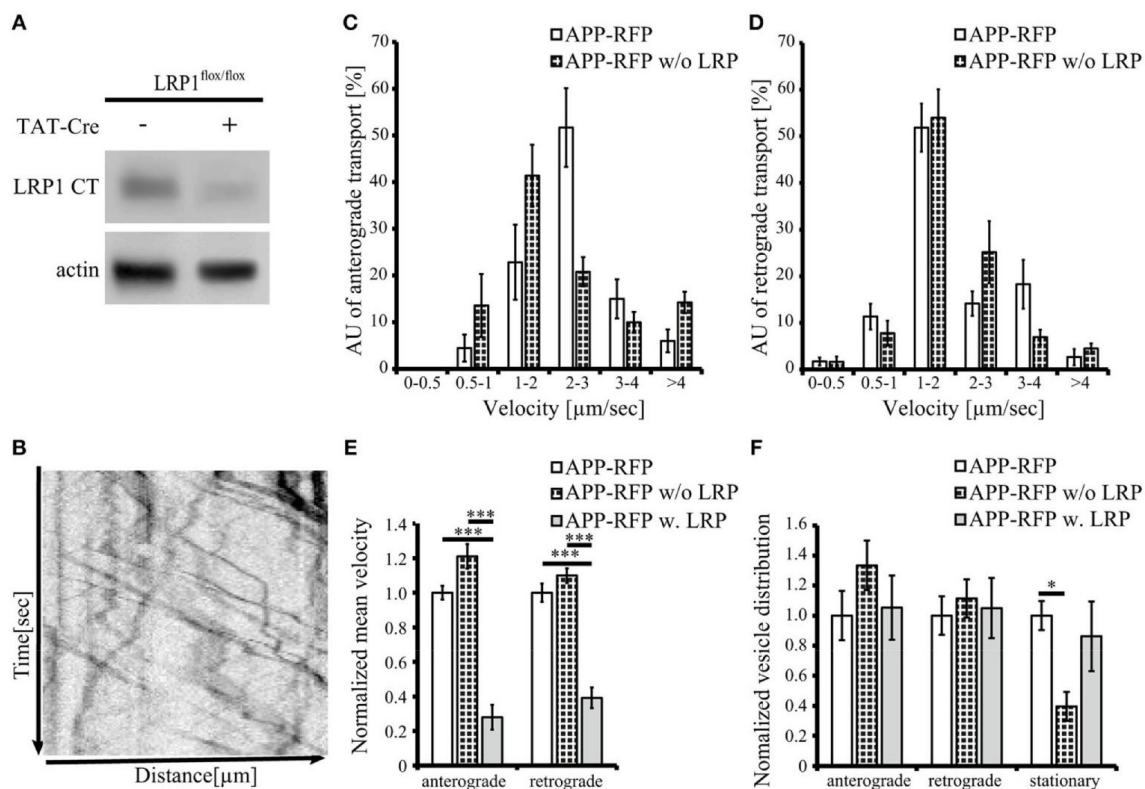
FIGURE 5 | Loss of LRP1 leads to increased transport vesicles rates.

Primary cortical neurons (PCN) (DIV4) of C57BL/6J wild type or Lrp1flox/flox mouse embryos were treated with 200 nM Tat-Cre recombinase or vehicle control for 48 h. (A) Representative blots of PCN from 5xFAD/LRP1flox/flox mouse embryos treated with Tat-Cre showed a decrease in LRP1 CT (1704 antibody) expression by approximately 2-fold compared to vehicle treated control. Anti-actin staining served as loading control. (B) 24 h prior live cell imaging analysis, PCN were transiently transfected with cDNA encoding APP-RFP. Time lapse series from live cell imaging were plotted as kymographs (representative kymograph, B) and used for determination of individual transport vesicle

FIGURE 5 | Continued.

velocities. (C) Anterograde and (D) retrograde transport velocity profiles of APP-RFP in wild type (white columns) and LRP1 deficient PCN (black white columns). Normalized transport velocities (E) and relative distribution (F) of APP-RFP in wild type PCN (white columns), LRP1 deficient PCN (black white columns) and PCN co-expressing LRP1. Note the lower amount of stationary vesicles in LRP1 deficient neurons. For quantification of transport velocities >5 kymographs from different cells were analyzed (APP-RFP in neurons of C57BL/6J mice: n = 7 cells, n = 254 vesicles; APP-RFP in LRP1 deficient neurons: n = 6 cells, n = 573 vesicles; APP-RFP in LRP1-GFP co-expressing neurons: n = 5 cells, n = 371 vesicles). Bars represent mean values ± SEM, n > 5 (≥254 vesicles); (C,D) Student's t-test, (E,F) Kruskal-Wallis-Test followed by Dunn's Multiple Comparison Test, p < 0.05 (*), p < 0.001 (***).

Interestingly, we observed in contrast to LRP1 co-expression only a tendency toward increased APP transport velocity in anterograde direction (p = 0.051) (Figures 5C,F) and no change in retrograde direction or for the amount of stationary vesicles (Figures 5D,F). In contrast, LRP1 deficiency caused a significant (p = 0.011) decrease of stationary and an increase   (p = 0.011) of moving transport vesicles (Figure 5F). Separation of moving vesicle data into anterograde and retrograde transport revealed due to lower n-number not the significance levels (p = 0.06) (Figure 5F).

Together, our data show that elevated LRP1 expression causes a decrease of APP transport rate whereas reduced levels of LRP1 cause an increase of APP transport rates.

LRP1 Expression Affects Processing of APP695 K587C Dimers

Showing that the expression of LRP1 alters trafficking of monomeric as well as dimerized APP, we assumed that LRP1 may also affect processing of APP dimers. We previously demonstrated that internalization of APP (mostly monomeric and possibly also dimeric) from the cell surface is reduced in the absence of LRP1 resulting in an increase in sAPPα secretion (Pietrzik et al., 2002). To investigate, whether a similar effect is obtained also for covalently bound APP homodimers, we used CHO K1 and LRP1-deficient CHO 13-5-1 cells both expressing APP695 K587C exogenously. In Western Blot analyses we first compared APP dimer expression and sAPP dimer secretion of both cell lines (Figure 6A).
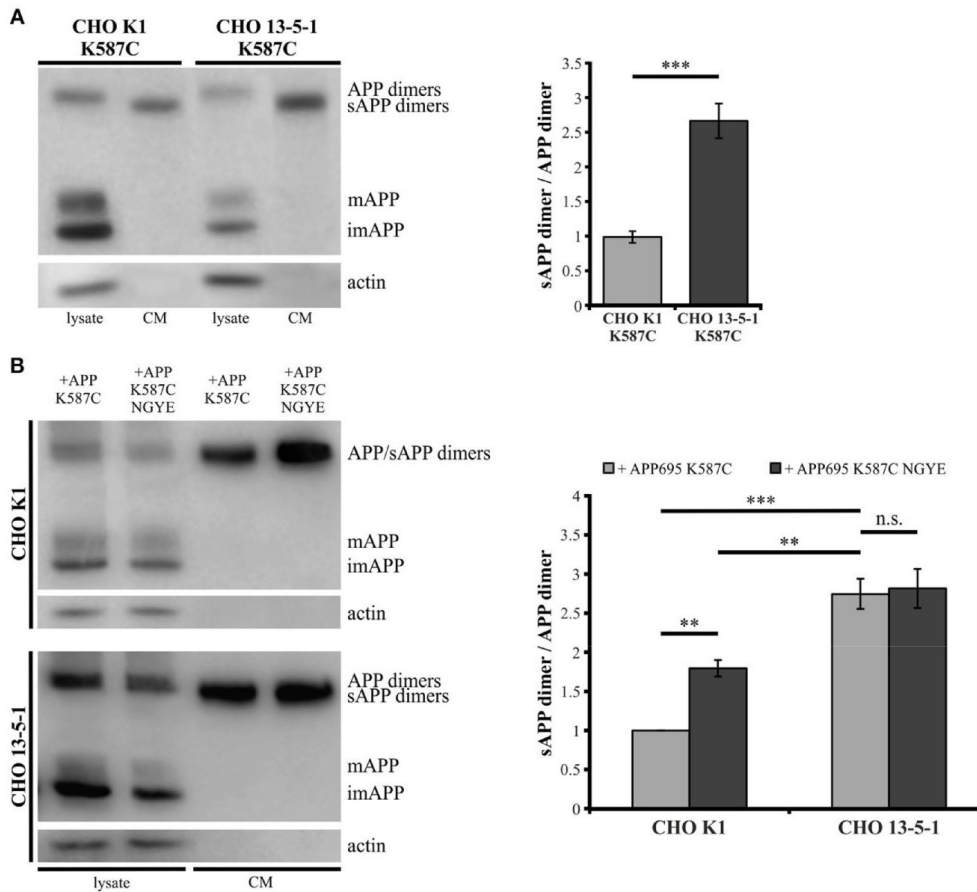
FIGURE 6 | Reduced internalization of APP dimers leads to increased sAPP dimer generation.

Lysates and conditioned media were probed (24 h post transfection, B) with antibodies specific for APP (1G75A3 antibody mix, 1:3,000) or actin (1:1,000). LRP1-deficiency in CHO cells (A) stably or (B) transiently transfected with pLHCX-APP695 K587C lead to increased sAPP dimer production. (A) The ratio of sAPP dimers to APP dimers is significantly increased in CHO 13-5-1 cells (n = 7) compared to CHO K1 cells (n = 5). Bars represent mean values ± SEM; Student's t-test; $p < 0.05$ (*), $p < 0.01$ (**), $p < 0.001$ (***). (B) Expression of the APP dimer construct additionally exhibiting the NGYE mutation in the APP internalization motif partially mimicked the LRP1 deficiency in CHO K1 cells while sAPP dimer secretion in CHO 13-5-1 cells remained unaffected. Note that sAPP dimer to APP dimer ratio increased significantly in CHO K1 cells expressing APP695 K587C NGYE compared to those transfected with APP695 K587C. Bars represent mean values ± SEM, n = 4; one-way ANOVA with Tukey's post-hoc test; $p < 0.01$ (**), $p < 0.001$ (***).

Here, we detected lower APP dimer expression in the lysate of CHO 13-5-1 cells compared to CHO K1 despite a comparable total protein load. However, the ratio of sAPP dimers to dimeric APP of LRP1-deficient CHO cells was approximately 3-fold stronger than in CHO K1 cells. To test, if this difference may be explained by increased processing due to decreased internalization of APP dimers from the cell

surface in LRP1-deficient CHO 13-5-1 cells, we transfected CHO K1 and CHO 13-5-1 cells with an APP695 dimer construct, exhibiting a mutation in the APP internalization motif "YENPTY" (Lai et al., 1995; MarquezSterling et al., 1997). The amino acid exchange from NPTY to NGYE leads to a reduced internalization of APP dimers from the cell surface mimicking LRP1 deficiency. We expected that exogenous expression of APP695 K587C NGYE compared to APP695 K587C should increase sAPP dimer secretion in CHO K1 cells, whereas expression in CHO 13-5-1 cells, that already show reduced APP dimer internalization due to the absence of LRP1, should cause no further increase in sAPP secretion. According to our expectation, we detected higher amounts of soluble APP dimers in the conditioned medium of CHO K1 cells, but no significant difference in sAPP dimer secretion in CHO 13-5-1 cells (Figure 6B). This further supports the hypothesis that LRP1 affects internalization of APP monomers and dimers in a comparable manner.

Lrp1 Knock-Out in PCN Affects APP Dimer Processing

As we could show that APP dimers are formed and processed in primary cortical neurons (Figure 1), we wanted to analyze the effect of a *Lrp1* knock-out on APP dimer processing in neuronal cells. Hence, PCN from 5xFAD/Lrp1$^{flox/flox}$ mouse embryos (E14) were treated with Tat-Cre recombinase to induce the excision of *Lrp1* via recombination of the loxP recognition sites flanking this gene. Western Blot analysis revealed a 2-fold reduction of LRP1 expression in PCN treated with Tat-Cre for 48 h compared to neurons incubated with the vehicle (Figure 7A). We assume that the incomplete reduction of LRP1 was due to its long half-life (24 h) (Reekmans et al., 2010). Interestingly, the sAPP dimer/APP dimer ratio of neurons with a partial *Lrp1* knock-out showed a more than 2-fold increase in comparison to the buffer treated PCN (Figure 7B). These observations are similar to the effects seen in LRP1-deficient CHO 13-5-1 cells and might be explained by a faster transport rate of APP dimers to and/or less internalization from the cell surface. This may result in an elevated APP processing by the active secretases at this site due to earlier and/or prolonged substrate availability.
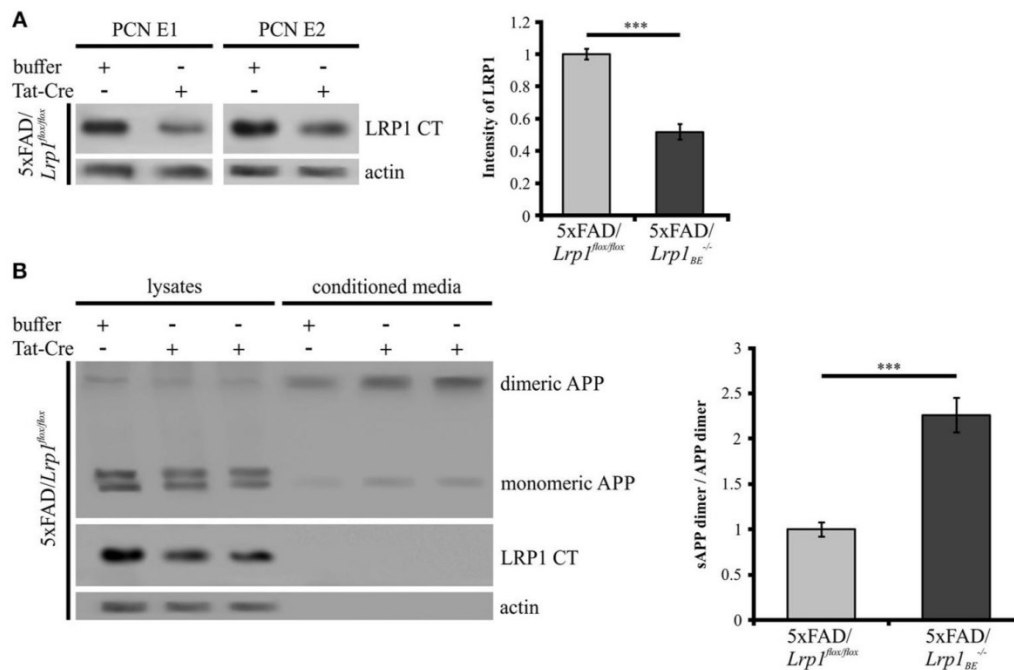
FIGURE 7 | Partial LRP1 knock-out affects APP processing in PCN.

PCN of 5xFAD/LRP1[flox/flox] mouse embryos were treated with either 200 nM Tat-Cre or vehicle for 48 h. Lysates and conditioned media were probed with specific antibodies for APP (1G75A3 antibody mix, 1:300), for LRP1 CT (1704 antibody, 1:10,000) and actin (actin antibody, 1:1,000). (A) Representative blots of PCN from two different 5xFAD/LRP1[flox/flox] mouse embryos (E1 and E2) treated with Tat-Cre showed a decrease in LRP1 CT expression by approximately 2-fold compared to vehicle treated controls (normalized to actin). Bars represent mean values ± SEM, n = 6; Student's t-test; p < 0.001 (***). (B) Representative blot showing a slight APP decrease in lysates and an increase of soluble APP fragments in the conditioned medium of Tat-Cre treated PCN. Partial Lrp1 knock-out resulted in an increased sAPP dimer to APP dimer ratio by more than 2-fold in comparison to buffer treated PCN. Bars represent mean values ± SEM, n = 5; Student's t-test; p < 0.001 (***).

Processing of APP Cis-Dimers by Meprin β and ADAM10

The presence of soluble APP dimers indicates that APP cis-dimers are enzymatically cleaved thereby releasing soluble dimerized fragments. Thus, we wanted to investigate, whether processing of APP cis-dimers can be attributed to the same secretases known to be responsible for cleavage of monomeric APP. Regarding the processing of monomeric APP at the cell surface, the metalloproteinases ADAM10 (Weidemann et al., 1989; Lammich et al., 1999) and meprin β (Jefferson et al., 2011; Bien et al., 2012; Schönherr et al., 2016) are implicated. As the metalloproteinase meprin β itself occurs in a dimerized form (Bertenshaw et al., 2003; Kruse et al., 2004), we first focused on the role of meprin β in APP dimer cleavage. To address

this point, we co-transfected HEK 293T cells with either APP695 K587C or APP695 wt and the meprin β construct to analyze processing of APP cis-dimers in comparison to monomeric APP cleavage by this secretase. As a control for meprin β activity, cells were solely transfected with the wt APP or the dimer-bearing APP construct. As expected, analysis of the conditioned medium of transfected HEK 293T cells revealed higher sAPP dimer levels in cells expressing the dimer-bearing APP construct, compared to those transfected with wildtype APP695 (Figure 8A). Co-transfection with meprin β resulted in a decrease in the signal for monomeric as well as dimerized soluble APP irrespective of the APP construct used for transfection. Interestingly, the reduction of sAPP dimers was considerably stronger than that of monomeric sAPP.
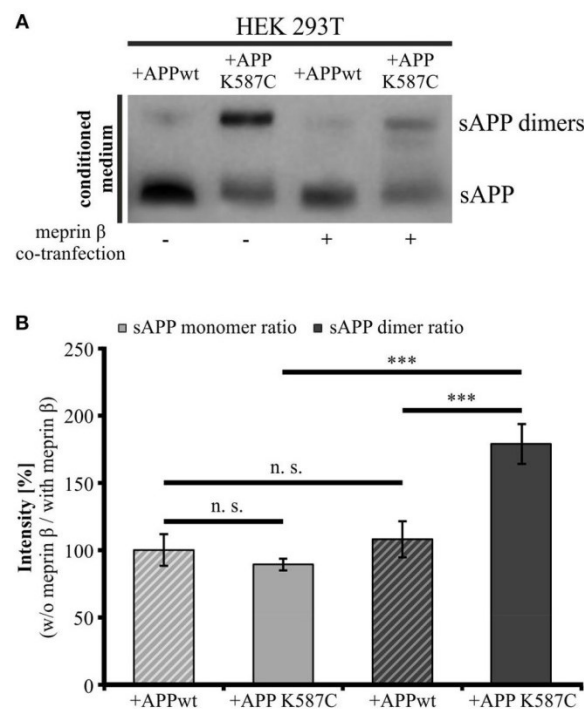
FIGURE 8 | Meprin β cleaves sAPP dimers with a higher affinity than monomeric sAPP.

HEK 293T cells were transiently transfected with the APP695 wt or the APP695 K587C construct either alone or in co-transfection with meprin β. (A) Conditioned medium was probed 24 h post transfection with the antibody mix 1G75A3 (1:3,000) directed against the APP ectodomain. Meprin β expression resulted in a reduced signal intensity of soluble APP, especially prominent for sAPP dimers in cells expressing the APP Cys-mutant (APP695 K587C). (B) For quantification the ratio of sAPP monomers and sAPP dimers, respectively, was calculated as the quotient of signal intensities in cells just transfected with an APP construct (w/o meprin β) to appropriate cells co-expressing meprin β (with meprin β). This analysis revealed a similar reduction in dimerized and monomeric sAPP for cells transfected with APP695 wt. In contrast, HEK cells expressing the dimer bearing construct show a significant increase in the sAPP dimer ratio

FIGURE 8 continued

compared to sAPP monomer ratio. Bars represent mean values ± SEM, n = 4; one-way ANOVA with Tukey's post-hoc test; $p < 0.001$ (***).

To quantify these observations, we calculated the ratio of sAPP dimers secreted from APP/meprin β expressing cells to sAPP dimer secretion of solely APP expressing cells as well as APP K587C/meprin β to APP K587C expressing cells. APP695 wt expressing cells showed no significant difference in the ratio for monomeric and dimerized sAPP, possibly due to the weak signal for sAPP dimers (Figures 8A,B).

In contrast, processing of APP695 K587C by meprin β was significantly increased compared to cleavage of monomeric sAPP (Figures 8A,B). In line with this, meprin β co-transfection resulted also in an increase of Aβ secretion (Supplementary Figure 3). Together, these data suggest a higher affinity of meprin β for dimerized than for monomeric APP695.

To investigate the role of α-secretase cleavage in APP cis-dimer processing, CHO K1 and CHO 13-5-1 cells expressing APP695 K587C were treated with the ADAM10 inhibitor GI254023X (Ludwig et al., 2005). Quantification of APP dimer expression in the lysates of CHO K1 and CHO 13-5-1 cells after incubation with GI254023X revealed an increase of APP dimers of 50 or 56%, respectively (Figure 9A). In line with this, we detected an average decrease in sAPP dimer secretion of 38% for inhibitor treated CHO K1 cells compared to those incubated with the vehicle DMSO alone (Figure 9B). A similar result (55% reduction of sAPP dimers after ADAM10 inhibition) was observed in CHO 13-5-1 cells (Figure 9B). As ADAM10 cleaves APP at the cell surface (Lammich et al., 1999), we expected an accumulation of the mature cell surface exposed APP, after treatment with GI254023X. Indeed, cell surface biotinylation assays using APP695 K587C expressing CHO cells revealed after ADAM10 inhibition an increase of mature cell surface APP dimers of 43% in comparison to DMSO controls (Figure 9C). In CHO 13-5-1 cells treated with GI254023X the surface expression of APP dimers was increased by 54% compared to DMSO controls (Figure 9C), underlining our assumption that LRP1 deficiency accelerates availability of APP dimers for processing by ADAM10.
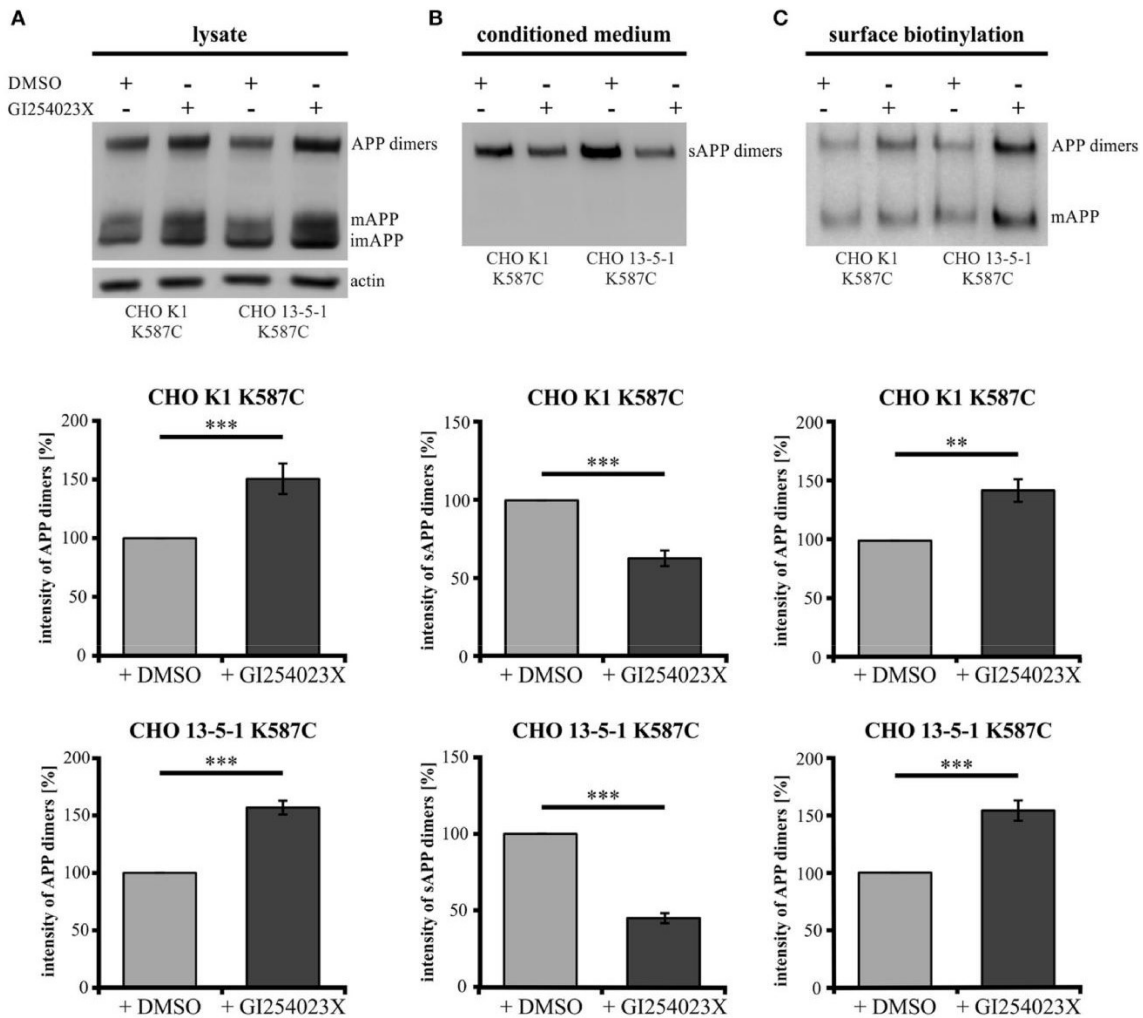
FIGURE 9 | LRP1 deficiency affects APP dimer processing at the cell surface by ADAM10.

Treatment of APP695 K587C-stable CHO cells (CHO K1 and LRP1-deficient CHO 13-5-1) with the ADAM10-inhibiting compound GI254023X or DMSO (control) was performed 24 h prior to surface biotinylation (sbio) and analysis of lysates and conditioned media (CM) with the APP specific antibody mix 1G75A3 (1:3,000) or the actin antibody (1:1,000), respectively. Bars represent mean values ± SEM, Student's t-test; $p < 0.01$ (**), $p < 0.001$ (***). (A) Inhibition of ADAM10 resulted in an increase of APP dimers in the lysate by 50% for CHO K1 (n = 7) and by 56% for CHO 13-5-1 (n = 7) cells compared to the corresponding DMSO controls. (B) In the conditioned medium the decrease of sAPP dimers by ADAM10 inhibition in comparison to DMSO treatment was more substantial in LRP1-deficient cells (55%; n = 7) than in CHO K1 cells (38%; n = 7). (C) The inhibitory effect of the GI254023X compound resulted in an elevation comparing surface expression of APP dimers to DMSO controls. This increase amounted to 43% for CHO K1 and 54% for CHO 13-5-1 cells.

Together, these data indicate that processing of APP cis-dimers can be attributed to the same secretases (meprin β and ADAM10) with meprin β shedding APP preferentially in the dimeric form.

LRP1 Expression Affects sAPP Dimer Secretion *In vivo#*

As secretion of monomeric sAPP fragments into the cerebrospinal fluid (CSF) of AD patients has been shown previously (Van Nostrand et al., 1992; Sennvik et al., 2000; Olsson et al., 2003; Brinkmalm et al., 2013), we wanted to study the generation of dimeric sAPP in vivo. To investigate, whether LRP1 expression also affects processing of APP dimers in vivo, we analyzed the cerebrospinal fluid of 5xFAD mice expressing LRP1 and of 5xFAD mice with a tissue-specific Lrp1 knock-out in brain endothelial cells and the choroid plexus epithelial cells. In 5xFAD mice only very little amounts of sAPP dimers could be detected (Figure 10A). However, in 5xFAD mice lacking LRP1 in CSF-secreting epithelial cells of the choroid plexus an about 4-fold stronger immunoreactivity for sAPP dimers was observed (Figure 10B). In line with our previous results showing preferred clavage of APP dimers by meprin β (Figure 8), the immense increase in dimerized APP fragments may be explained by the involvement of meprin β besides ADAM10 in APP cleavage at the surface of epithelial cells. These in vivo data underline that LRP1 preferentially affects sAPP dimer secretion.
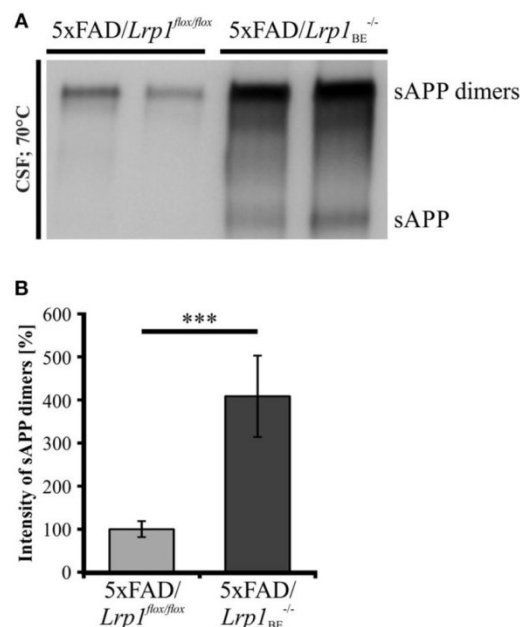
FIGURE 10 | sAPP dimers in CSF of 5xFAD/Lrp1^flox/flox and 5xFAD/Lrp1BE⁻/⁻ mice.

(A) Representative Western Blot of 2 µl CSF from 5xFAD/Lrp1^flox/flox and 5xFAD/Lrp1BE⁻/⁻ mice. Immunostaining with the 1G75A3 antibody mix (1:3,000) revealed (B) an about 4-fold stronger immunoreactivity for sAPP dimers in the CSF of 5xFAD mice exhibiting an *Lrp1* knock-out in brain endothelial and choroid plexus epithelial cells (n = 3) than in 5xFAD mice expressing LRP1 (n = 5). p < 0.001 (***).

DISCUSSION

Our data show that LRP1 recruits APP into common fast axonal transport (FAT) membrane bound organelles (MBOs), suggesting that LRP1 functions as a sorting receptor. Thereby, increased levels of LRP1 slow down APP anterograde transport and decrease its endocytosis rate. This in turn causes an increase of surface APP and thus accelerates secretion of sAPP. Interestingly, we observed the same influence for APP monomers and dimers. However, *Lrp1* knock-out in choroid plexus cells increased sAPP monomer secretion, but much more pronounced sAPP dimer secretion in the CSF. This is likely explained by different processing properties of cell surface APP monomers/dimers, as we found that meprin β preferentially cleaves APP dimers.

Our live cell imaging analyses in primary neurons show that LRP1 is anterogradely transported with a median velocity of 1–2 µm/s, (Figure 4), indicating that LRP1 anterograde transport is mediated by the fast axonal kinesin dependent transport (FAT) machinery. Time lapse analysis of APP from our group and others revealed transport velocities of 2–10 µm/s (Figures 2, 4; Kaether et al., 2000; Szodorai et al., 2009; Hermey et al., 2015). Those types of transport vesicles with velocities above 2 µm/s have only been observed very rarely for LRP1 positive vesicles. In line with the low extend of co-localization of LRP1 and APP in neurites, these data indicate that APP and LRP1 are transported in distinct membrane bound organelles (MBO), associated with different FAT machineries. Interestingly, reduced levels of LRP1 in primary neurons caused an increase of APP transport vesicles (Figure 5), whereas co-expression of LRP1 and APP caused an approximation of both transport characteristics, changing APP transport toward velocities observed for LRP1. These data corroborate our previous assumption that LRP1 causes a sorting of APP into LRP1 bearing MBOs (Waldron et al., 2008). As monomeric and dimeric APP are transported with very similar transport characteristics (Figure 2), and as a knock-out of *Lrp1* caused an increase of monomeric as well as dimeric sAPP (Waldron et al., 2008; Figure 3) we assume that LRP1 affects monomeric and dimeric APP in a similar way. In contrast, other sorting receptors of APP, such as SorLA are assumed to affect the equilibrium of APP dimerization, causing different processing kinetics of monomeric and dimeric APP, as indicated by elegant mathematical modeling

(Schmidt et al., 2012). Notably, these analyses were performed in cells lacking LRP1. Thus, it would be interesting for future studies to investigate the interplay of LRP1, SorLA and APP dimerization in more detail.

Since LRP1 recruits APP to transport vesicles and the velocity of vesicles carrying APP dimers is similar to APP monomer carrying vesicles we wondered whether APP dimers are released in a similar LRP1 dependent manner as APP monomers (Waldron et al., 2008). In a pulse-chase analysis of LRP1 expressing CHO K1 and LRP1-deficient CHO 13-5-1 cells both stably expressing APP dimers, we detected faster sAPP dimer release in LRP1-deficient cells (Figure 3D). As APP dimerization already takes place in the ER and as those dimers remain stable throughout their transport to the plasma membrane (Isbert et al., 2012; Khalifa et al., 2012), an interaction of dimeric APP with LRP1 early in the secretory pathway may lead to a decelerated APP dimer trafficking, similar as shown for monomeric APP (Waldron et al., 2008). Thus, cell surface processing may be affected, resulting in the delayed occurrence of dimerized sAPP in LRP1 expressing cells.

The interaction of APP with LRP1 also plays an important role at the cell surface as monomeric APP is internalized in a complex with LRP1 by clathrin-mediated endocytosis, thereby affecting its processing (Knauer et al., 1996; Ulery et al., 2000; Pietrzik et al., 2002, 2004; Cam et al., 2005). Hence, we estimated that the accelerated generation of soluble APP dimers in LRP1 deficient cells compared to LRP1 expressing cells (Figure 6A) may result from a reduced APP dimer internalization due to LRP1 deficiency that in turn causes higher APP levels for processing at the cell surface. This assumption is strengthened by the fact that APP dimer constructs, harboring a mutated internalization motif caused an increase in sAPP levels (Figure 6B), as shown before for internalization deficient monomeric APP (Perez et al., 1999). Importantly, the sAPP dimer levels of the internalization deficient mutant were not increased in LRP1 lacking cells. To investigate, whether the LRP1 regulatory effects are similar in neuronal cells, we analyzed PCN with a knock-out of *Lrp1* by Cre recombination. Similar as shown for LRP1-deficient CHO 13-5-1 cells we observed a decrease of APP in the lysates accompanied by an accelerated sAPP generation for monomeric as well as dimeric APP (Figure 7), when LRP1 expression was knocked out in primary neurons. The more than 2-fold increase of the sAPP dimer to APP dimer ratio further supports our hypothesis that LRP1

regulated effects on APP dimer transport and internalization take place in neuronal cells. A resulting earlier and/or prolonged availability of APP may therefore provide more substrate for the cell surface-active shaddases ADAM10 and meprin β. Thus, our data strongly suggest that monomeric and dimeric APP trafficking is equally affected by LRP1 (Ulery et al., 2000; Pietrzik et al., 2002; Cam et al., 2005) and that this process is also important in the neuronal system.

Due to the similar characteristics of monomeric and dimeric APP transport we assumed that APP dimers might also be processed by the same secretases as monomeric APP. Here, we concentrated on cell surface APP. It has been well documented over the last decade that ADAM10 is the most prominent sheddase of APP at the cell surface (Weidemann et al., 1989; Lammich et al., 1999; Jorissen et al., 2010; Kuhn et al., 2010). Recently, the metalloproteinase meprin β was identified to be also capable to process APP at the cell surface (Jefferson et al., 2011; Bien et al., 2012; Schönherr et al., 2016). Here, we show that meprin β as well as ADAM10 are implicated in dimer processing (Figures 8, 9). Inhibition of ADAM10 resulted in a surface accumulation of APP dimers as shown by protein surface biotinylation. This was accompanied by an increase of APP dimers in the lysate and a decrease in soluble APP dimers in the conditioned medium of the tested cells (Figures 9A–C) as shown for monomeric sAPPα (Woods and Padmanabhan, 2013). The role of LRP1 in APP dimer processing is again highlighted by ADAM10 inhibition in LRP1-deficient cells as the demonstrated effects (in CHO K1 cells) were considerably stronger in CHO 13-5-1 cells (Figures 9A–C).

To investigate the role of meprin β in cleavage of APP dimers, we analyzed the sAPP monomer and dimer ratios of HEK cells transfected with APP alone to cells co-expressing meprin β. Interestingly, the sAPP dimer ratio was significantly increased compared to the sAPP monomer ratio (Figure 8) when the stabilized APP homodimer was generated. This indicates that meprin β processes APP, with a preference for APP dimers. Although we do not understand the underlying molecular mechanism yet, it appears reasonable that the higher affinity of meprin β for dimeric vs. monomeric APP is connected to the fact that this secretase itself exists in form of a dimer (Bertenshaw et al., 2003; Kruse et al., 2004). Thus, dimerized APP may offer a cooperative effect on enzymatic activity of meprin β, as recently postulated for α- and β-secretase for APP dimer processing (Schmidt et al., 2012).

Due to the fact that a large fraction of APP occurs in a dimerized form in the brain (Munter et al., 2007; Schmidt et al., 2012) and that APP dimers are processed in PCN of C57BL/6J mice (Figures 1, 7), we asked whether the regulatory effect of LRP1 in APP dimer processing does also play a role *in vivo*. Therefore, we analyzed the CSF of 5xFAD mice and 5xFAD mice with an induced Lrp1 knock-out in brain endothelial and choroid plexus epithelial cells. Indeed, we were able to detect sAPP dimers to an about 4-fold greater extent in the CSF of mice with the tissue-specific *Lrp1* knock-out than of 5xFAD control littermates (Figures 10A,B). As the choroid plexus epithelial cells express APP (Kalaria et al., 1996; Bergen et al., 2015) and are the main producers of CSF (Brown et al., 2004), sAPP dimers in the CSF presumably originate from these cells. Thus, the increased amount of sAPP dimers in the CSF of 5xFAD/Lrp1BE^{−/−} mice is likely due to reduced internalization of APP from the surface of the choroid plexus epithelial cells. This may provide more APP dimers for enzymatic cleavage at the cell surface. We could show that ADAM10, the main sheddase of APP at the cell surface (Weidemann et al., 1989; Lammich et al., 1999; Jorissen et al., 2010; Kuhn et al., 2010), is also implicated in the cleavage of APP dimers (Figure 9). Thus, the processing of APP dimers in epithelial cells of the choroid plexus may be at least partially performed by this secretase. Furthermore, the especially high levels of sAPP dimers may point to a prominent role of meprin β in this context as we could show that this protease exhibits a preferred activity for dimeric vs. monomeric APP (Figure 8).

Altogether, our studies show that LRP1 affects trafficking of APP monomers and dimers and that APP dimers are preferentially cleaved by ADAM10 and meprin β. Hence, dimerized APP may affect physiological as well as pathogenic functions of APP by different transport and processing characteristics and should be included in future studies regarding the interplay with other sorting receptors than LRP1 or the generation of Aβ species.

REFERENCES

1) Baumkötter, F., Schmidt, N., Vargas, C., Schilling, S., Weber, R., Wagner, K., et al. (2014). Amyloid precursor protein dimerization and synaptogenic function depend on copper binding to the growth factor-like domain. J. Neurosci. 34, 11159–11172. doi: 10.1523/JNEUROSCI.0180-14.2014

2) Baumkötter, F., Wagner, K., Eggert, S., Wild, K., and Kins, S. (2012). Structural aspects and physiological consequences of APP/APLP trans-dimerization. Exp. Brain Res. 217, 389–395. doi: 10.1007/s00221-011-2878-6

3) Bergen, A. A., Kaing, S., Ten Brink, J. B., Netherlands, B. B., Gorgels, T. G., and Janssen, S. F. (2015). Gene expression and functional annotation of human choroid plexus epithelium failure in Alzheimer's disease. BMC Genomics 16:956. doi: 10.1186/s12864-015-2159-z

4) Bertenshaw, G. P., Norcum, M. T., and Bond, J. S. (2003). Structure of homo- and hetero-oligomeric meprin metalloproteases: dimers, tetramers, and high molecular mass multimers. J. Biol. Chem. 278, 2522–2532. doi: 10.1074/jbc.M208808200

5) Bien, J., Jefferson, T., Cauševic, M., Jumpertz, T., Munter, L., Multhaup, G., et al. (2012). The metalloprotease meprin β generates amino terminal-truncated amyloid β peptide species. J. Biol. Chem. 287, 33304–33313. doi: 10.1074/jbc.M112.395608

6) Brinkmalm,G., Brinkmalm, A., Bourgeois, P., Persson, R., Hansson, O., Portelius,E., et al. (2013). Soluble amyloid precursor protein α and β in CSF in Alzheimer's disease. Brain Res. 1513, 117–126. doi: 10.1016/j.brainres.2013.03.019

7) Brown, P. D., Davies, S. L., Speake, T., and Millar, I. D. (2004). Molecular mechanisms of cerebrospinal fluid production. Neuroscience 129, 957–970. doi: 10.1016/j.neuroscience.2004.07.003

8) Cam, J. A., Zerbinatti, C. V., Li, Y., and Bu, G. (2005). Rapid endocytosis of the low density lipoprotein receptor-related protein modulates cell surface

distribution and processing of the β-amyloid precursor protein. J. Biol. Chem. 280, 15464–15470. doi: 10.1074/jbc.M500613200

9) Chalfie, M., and Kain, S. R. (eds.). (2005). Green Fluorescent Protein: Properties, Applications and Protocols, 2nd Edn. John Wiley & Sons. doi: 10.1002/0471739499.ch1

10) Eggert, S., Midthune, B., Cottrell, B., and Koo, E. H. (2009). Induced dimerization of the amyloid precursor protein leads to decreased amyloid-β protein production. J. Biol. Chem. 284, 28943–28952. doi: 10.1074/jbc.M109. 038646

11) FitzGerald, D. J., Fryling, C. M., Zdanovsky, A., Saelinger, C. B., Kounnas, M., Winkles, J. A., et al. (1995). Pseudomonas exotoxin-mediated selection yields cells with altered expression of low-density lipoprotein receptor-related protein. Mol. Microbiol. 16, 1171–1181. doi: 10.1083/jcb.129.6.1533

12) Hermey, G., Schmidt, N., Bluhm, B., Mensching, D., Ostermann, K., Rupp, C., et al. (2015). SorCS1 variants and amyloid precursor protein (APP) are co-transported in neurons but only SorCS1c modulates anterograde APP transport. J. Neurochem. 135, 60–75. doi: 10.1111/jnc.13221

13) Isbert, S., Wagner, K., Eggert, S., Schweitzer, A., Multhaup, G., Weggen, S., et al. (2012). APP dimer formation is initiated in the endoplasmic reticulumand differs between APP isoforms. Cell. Mol. Life Sci. 69, 1353–1375. doi: 10.1007/s00018-011-0882-4

14) Jäger, S., Leuchtenberger, S., Martin, A., Czirr, E., Wesselowski, J., Dieckmann, M., et al. (2009). α-secretase mediated conversion of the amyloid precursor protein derived membrane stub C99 to C83 limits Aβ generation. J. Neurochem. 111, 1369–1382. doi: 10.1111/j.1471-4159.2009.06420.x

15) Jefferson, T., Causevic,´ M., Auf Dem Keller, U., Schilling, O., and Isbert, S., Geyer, R., et al. (2011). Metalloprotease meprin β generates nontoxic N-terminal amyloid precursor protein fragments in vivo. J. Biol. Chem. 286, 27741–27750. doi: 10.1074/jbc.M111.252718

16) Jorissen, E., Prox, J., Bernreuther, C., Weber, S., Schwanbeck, R., Serneels, L., et al. (2010). The disintegrin/metalloproteinase ADAM10 is essential for the establishment of the brain cortex. J. Neurosci. 30,b4833–4844. doi: 10.1523/JNEUROSCI.5221-09.2010

17) Jung, J. I., Premraj, S., Cruz, P. E., Ladd, T. B., Kwak, Y., Koo, E. H., et al. (2014). Independent relationship between amyloid precursor protein (APP) dimerization and γ-secretase processivity. PLoS ONE 9:111553. doi: 10.1371/journal.pone.0111553

18) Kaden, D., Munter, L. M., Joshi, M., Treiber, C., Weise, C., Bethge, T., et al. (2008). Homophilic interactions of the amyloid precursor protein (APP) ectodomain are regulated by the loop region and affect β-secretase cleavage of APP. J. Biol. Chem. 283, 7271–7279. doi: 10.1074/jbc.M708046200

19) Kaden, D., Voigt, P., Munter, L.-M., Bobowski, K. D., Schaefer, M., and Multhaup, G. (2009). Subcellular localization and dimerization of APLP1 are strikingly different from APP and APLP2. J. Cell Sci. 122, 368–377. doi: 10.1242/jcs.034058

20) Kaether, C., Skehel, P., and Dotti, C. G. (2000). Axonal membrane proteins are transported in distinct carriers: a two-color video microscopy study in cultured hippocampal neurons. Mol. Biol. Cell 11, 1213–1224. doi: 10.1091/mbc.11.4.1213

21) Kalaria, R. N., Premkumar, D. R. D., Pax, A. B., Cohen, D. L., and Lieberburg, I. (1996). Production and increased detection of amyloid β protein and amyloidogenic fragments in brain microvessels, meningeal vessels and choroid plexus in Alzheimer's disease. Mol. Brain Res. 35, 58–68. doi: 10.1016/0169-328X(95)00180-Z

22) Kang, J., Lemaire, H.-G., Unterbeck, A., Salbaum, J. M., Masters, C. L., Grzeschik, Karl, H., et al. (1987). The precursor of Alzheimer's disease amyloid A4 protein resembles a cell-surface receptor. Nature 325, 733–736. doi: 10.1038/325733a0

23) Khalifa, B. N., Tyteca, D., Marinangeli, C., Depuydt, M., Collet, J.-F., Courtoy, P. J., et al. (2012). Structural features of the KPI domain control APP dimerization, trafficking, and processing. FASEB J. 26, 855–867. doi: 10.1096/fj.11-190207

24) Klafki, H. W., Wiltfang, J., and Staufenbiel, M. (1996). Electrophoretic separation of betaA4 peptides (1-40) and (1-42). Anal. Biochem. 237, 24–29. doi: 10.1006/abio.1996.0195

25) Klevanski, M., Saar, M., Baumkötter, F., Weyer, S. W., Kins, S., and Müller, U. C. (2014). Differential role of APP and APLPs for neuromuscular synaptic morphology and function. Mol. Cell. Neurosci. 61, 201–210. doi: 10.1016/j.mcn.2014.06.004

26) Knauer, M. F., Orlando, R. A., and Glabe, C. G. (1996). Cell surface APP751 forms complexes with protease nexin 2 ligands is internalized via the low density lipoprotein receptor-related protein (LRP). Brain Res. 740, 6–14. doi: 10.1016/S0006-8993(96)00711-1

27) Krieger, M., and Herz, J. (1994). Structures and functions of multiligand lipoprotein receptors: macrophage scavenger receptors and LDL receptor-related protein (LRP). Annu. Rev. Biochem. 63, 601–637. doi: 10.1146/annurev.bi.63.070194.003125

28) Kruse, M.-N., Becker, C., Lottaz, D., Köhler, D., Yiallouros, I., Krell, H.-W., et al. (2004). Human meprin alpha and beta homo-oligomers: cleavage of basement membrane proteins and sensitivity to metalloprotease inhibitors. Biochem. J. 378, 383–389. doi: 10.1042/bj20031163

29) Kuhn, P.-H., Wang, H., Dislich, B., Colombo, A., Zeitschel, U., Ellwart, J. W., et al. (2010). ADAM10 is the physiologically relevant, constitutive alpha-secretase of the amyloid precursor protein in primary neurons. EMBO J. 29, 3020–3032. doi: 10.1038/emboj.2010.167

30) Lai, A., Sisodia, S. S., and Trowbridge, I. S. (1995). Characterization of sorting signals in the β-amyloid precursor protein cytoplasmic domain. J. Biol. Chem. 270, 3565–3573. doi: 10.1074/jbc.270.8.3565

31) Lammich, S., Kojro, E., Postina, R., Gilbert, S., Pfeiffer, R., Jasionowski, M., et al. (1999). Constitutive and regulated alpha-secretase cleavage of Alzheimer's amyloid precursor protein by a disintegrin metalloprotease. Proc. Natl. Acad. Sci. U.S.A. 96, 3922–3927. doi: 10.1073/pnas.96.7.3922

32) Libeu, C. A. P., Descamps, O., Zhang, Q., John, V., and Bredesen, D. E. (2012). Altering APP proteolysis: Increasing sAPPalpha production by targeting dimerization of the APP Ectodomain. PLoS ONE 7:27. doi: 10.1371/journal.pone.0040027

33) Ludwig, A., Hundhausen, C., Lambert, M. H., Broadway, N., Andrews, R.C., Bickett, D. M., et al. (2005). Metalloproteinase inhibitors for the disintegrin-like metalloproteinases ADAM10 and ADAM17 that differentially block constitutive and phorbol ester-inducible shedding of cell surface molecules. Comb. Chem. High Throughput Screen 8, 161–171. doi: 10.2174/1386207053258488

34) Maier, W., Bednorz, M., Meister, S., Roebroek, A., Weggen, S., Schmitt, U., et al. (2013). LRP1 is critical for the surface distribution and internalization of the NR2B NMDA receptor subtype. Mol. Neurodegener. 8:25. doi: 10.1186/1750-1326-8-25

35) MarquezSterling, N. R., Lo, A. C. Y., Sisodia, S. S., and Koo, E. H. (1997). Trafficking Of cell-surface β-amyloid precursor protein - evidence that a sorting intermediate participates in synaptic vesicle recycling. J. Neurosci. 17, 140–151.

36) Masters, C. L., Simms, G., Weinman, N. A., Multhaup, G., McDonald, B. L., and Beyreuther, K. (1985). Amyloid plaque core protein in Alzheimer disease and down syndrome. Proc. Natl. Acad. Sci. U.S.A. 82, 4245–4249. doi: 10.1073/pnas.82.12.4245

37) Merz, P. A., Wisniewski, H. M., Somerville, R. A., Bobin, S. A., Masters, C. L., and Iqbal, K. (1983). Ultrastructural morphology of amyloid fibrils from neuritic and amyloid plaques. Acta Neuropathol. 60, 113–124. doi: 10.1007/BF00685355

38) Müller, U. C., and Zheng, H. (2012). Physiological functions of APP family proteins. Cold Spring Harb Perspect. Med. 2, 1–17. doi: 10.1101/cshperspect.a006288

39) Munter, L. M., Botev, A., Richter, L., Hildebrand, P. W., Althoff, V., Weise, C., et al. (2010). Aberrant amyloid precursor protein (APP) processing in hereditary forms of Alzheimer disease caused by APP familial Alzheimer disease mutations can be rescued by mutations in the APP GxxxG motif. J. Biol. Chem. 285, 21636–21643. doi: 10.1074/jbc.M109.088005

40) Munter, L.-M., Voigt, P., Harmeier, A., Kaden, D., Gottschalk, K. E., Weise, C., et al. (2007). GxxxG motifs within the amyloid precursor protein transmembrane sequence are critical for the etiology of Abeta42. EMBO J. 26, 1702–1712. doi: 10.1038/sj.emboj.7601616

41) Olsson, A., Höglund, K., Sjögren, M., Andreasen, N., Minthon, L., Lannfelt, L., et al. (2003). Measurement of α- and β-secretase cleaved amyloid precursor protein in cerebrospinal fluid from Alzheimer patients. Exp. Neurol. 183, 74–80. doi: 10.1016/S0014-4886(03)00027-X

42) Perez, R. G., Soriano, S., Hayes, J. D., Ostaszewski, B., Xia, W., Selkoe, D. J., et al. (1999). Mutagenesis identifies new signals for β-amyloid precursor protein endocytosis, turnover, and the generation of secreted fragments, including Aβ42. J. Biol. Chem. 274, 18851–18856. doi: 10.1074/jbc.274.27.18851

43) Pietrzik, C. U., Busse, T., Merriam, D. E., Weggen, S., and Koo, E. H. (2002). The cytoplasmic domain of the LDL receptor-related protein regulates multiple steps in APP processing. EMBO J. 21, 5691–5700. doi: 10.1093/emboj/cdf568

44) Pietrzik, C. U., Yoon, I.-S., Jaeger, S., Busse, T., Weggen, S., and Koo, E. H. (2004). FE65 constitutes the functional link between the low-density lipoprotein receptor-related protein and the amyloid precursor protein. J. Neurosci. 24, 4259–4265. doi: 10.1523/JNEUROSCI.5451-03.2004

45) Rabiej, V. K., Pflanzner, T., Wagner, T., Goetze, K., Storck, S. E., Eble, J. A., et al. (2015). Low density lipoprotein receptor-related protein 1 mediated

endocytosis of β1-integrin influences cell adhesion and cell migration. Exp. Cell Res. 340, 102–115. doi: 10.1016/j.yexcr.2015.11.020

46) Reekmans, S. M., Pflanzner, T., Gordts, P. L. S. M., Isbert, S., Zimmermann, P., Annaert, W., et al. (2010). Inactivation of the proximal NPXY motif impairs early steps in LRP1 biosynthesis. Cell. Mol. Life Sci. 67, 135–145. doi: 10.1007/s00018-009-0171-7

47) Rollins, C. T., Rivera, V. M., Woolfson, D. N., Keenan, T., Hatada, M., Adams, S. E., et al. (2000). A ligand-reversible dimerization system for controlling protein-protein interactions. Proc. Natl. Acad. Sci. U.S.A. 97, 7096–7101. doi: 10.1073/pnas.100101997

48) Scheuermann, S., Hambsch, B., Hesse, L., Stumm, J., Schmidt, C., Beher, D., et al. (2001). Homodimerization of amyloid precursor protein and its implication in the amyloidogenic pathway of Alzheimer's Disease. J. Biol. Chem. 276, 33923–33929. doi: 10.1074/jbc.M105410200

49) Schmidt, V., Baum, K., Lao, A., Rateitschak, K., Schmitz, Y., Teichmann, A., et al. (2012). Quantitative modelling of amyloidogenic processing and its influence by SORLA in Alzheimer's disease. EMBO J. 31, 187–200. doi: 10.1038/emboj.2011.352

50) Schönherr, C., Bien, J., Isbert, S., Wichert, R., Prox, J., Altmeppen, H., et al. (2016). Generation of aggregation prone N- terminally truncated amyloid β peptides by meprin β depends on the sequence specificity at the cleavage site. Mol. Neurodegener. 11:19. doi: 10.1186/s13024-016-0084-5

51) Sennvik, K., Fastbom, J., Blomberg, M., Wahlund, L. O., Winblad, B., and Benedikz, E. (2000). Levels of α- and β-secretase cleaved amyloid precursor protein in the cerebrospinal fluid of Alzheimer's disease patients. Neurosci. Lett. 278, 169–172. doi: 10.1016/S0304-3940(99)00929-5

52) So, P. P., Zeldich, E., Seyb, K. I., Huang, M. M., Concannon, J. B., King, G. D., et al. (2012). Lowering of amyloid beta peptide production with a small molecule inhibitor of amyloid-β precursor protein dimerization. Am. J. Neurodegener. Dis. 1, 75–87.

53) Soba, P., Eggert, S., Wagner, K., Zentgraf, H., Siehl, K., Kreger, S., et al. (2005). Homo- and heterodimerization of APP family members promotes intercellular adhesion. EMBO J. 24, 3624–3634. doi: 10.1038/sj.emboj.76 00824

54) Stahl, R., Schilling, S., Soba, P., Rupp, C., Hartmann, T., Wagner, K., et al. (2014). Shedding of APP limits its synaptogenic activity and cell adhesion properties. Front. Cell. Neurosci. 8:410. doi: 10.3389/fncel.2014.00410

55) Storck, S. E., Meister, S., Nahrath, J., Meibner, J. N., Schubert, N., Di Spiezio, A., et al. (2016). Endothelial LRP1 transports amyloid-β1-42 across the blood-brain barrier. J. Clin. Invest. 126, 123–136. doi: 10.1172/JCI81108

56) Szodorai, A., Kuan, Y.-H., Hunzelmann, S., Engel, U., Sakane, A., Sasaki, T., et al. (2009). APP anterograde transport requires Rab3A GTPase activity for assembly of the transport vesicle. J. Neurosci. 29, 14534–14544. doi: 10.1523/JNEUROSCI.1546-09.2009

57) Ulery, P. G., Beers, J., Mikhailenko, I., Tanzi, R. E., Rebeck, G. W., Hyman, B. T., et al. (2000). Modulation of amyloid precursor protein processing by the low density Lipoprotein Receptor-related Protein (LRP). J. Biol. Chem. 275, 7410–7415. doi: 10.1074/jbc.275.10.7410

58) Vandenbroucke, R. E., Dejonckheere, E., Van Lint, P., Demeestere, D., Van Wonterghem, E., Vanlaere, I., et al. (2012). Matrix metalloprotease 8-dependent extracellular matrix cleavage at the blood-CSF barrier contributes to lethality during systemic inflammatory diseases. J. Neurosci. 32, 9805–9816. doi: 10.1523/JNEUROSCI.0967-12.2012

59) Van Nostrand, W. E., Wagner, S. L., Shankle, W. R., Farrow, J. S., Dick, M., Rozemuller, J. M., et al. (1992). Decreased levels of soluble amyloid beta-protein precursor in cerebrospinal fluid of live Alzheimer disease patients. Proc. Natl. Acad. Sci. U.S.A. 89, 2551–2555. doi: 10.1073/pnas.89.7.2551

60) Waldron, E., Heilig, C., Schweitzer, A., Nadella, N., Jaeger, S., Martin, A. M., et al. (2008). LRP1 modulates APP trafficking along early compartments of the secretory pathway. Neurobiol. Dis. 31, 188–197. doi:

10.1016/j.nbd.2008.04.006 Wang, P. (2005). Defective Neuromuscular synapses in mice lacking Amyloid Precursor Protein (APP) and APP-Like protein 2. J. Neurosci. 25, 1219–1225. doi: 10.1523/JNEUROSCI.4660-04.2005

61) Wang, Z., Wang, B., Yang, L., Guo, Q., Aithmitti, N., Songyang, Z., et al. (2009). Presynaptic and postsynaptic interaction of the amyloid precursor protein promotes peripheral and central synaptogenesis. J. Neurosci. 29, 10788–10801. doi: 10.1523/JNEUROSCI.2132-09.2009

62) Weidemann, A., König, G., Bunke, D., Fischer, P., Salbaum, J. M., Masters, C. L., et al. (1989). Identification, biogenesis, and localization of precursors of Alzheimer's disease A4 amyloid protein. Cell 57, 115–26. doi: 10.1016/0092-8674(89)90177-3

63) Woods, N. K., and Padmanabhan, J. (2013). Inhibition of amyloid precursor protein processing enhances gemcitabine-mediated cytotoxicity in pancreatic cancer cells. J. Biol. Chem. 288, 30114–30124. doi: 10.1074/jbc.M113.459255

64) Yuan, H., Zhai, P., M., Anderson, L., Pan, J., Thimmapaya, B., H., Koo, E., et al. (1999). Recombinant adenovirus is an appropriate vector for endocytotic protein trafficking studies in cultured neurons. J. Neurosci. Methods 88, 45–54. doi: 10.1016/S0165-0270(99)00011-4

Conclusions and Outlook

The results of this thesis provide deeper insights into the Fe65 protein family function by giving clear *in vivo* evidence for a role of Fe65/Fe65L1 in synaptic plasticity in the CNS and development of the neuromuscular junction. Furthermore, the results of this thesis allowed insights in the structural features of Fe65, relevant for a better understanding of its pathophysiological function. Finally, the influence of LRP1 on monomeric and dimeric APP trafficking was analyzed which might affect physiological and pathogenic properties of APP regarding its interplay with LRP1.

The results described in the first chapter of my thesis demonstrate that the Fe65 Fe65 and Fe65L1 are important for learning and memory as well as locomotor activity in mice by utilizing different behavioral approaches. Furthermore, Fe65 and Fe65L1 are necessary for synaptic plasticity and neuromuscular junction formation as shown by electrophysiological and histochemical examinations. Similar phenotypes have already been described for several APP protein family KO mice leading to the assumption that the Fe65 protein family is the main interaction partner of the APP protein family in the central as well as peripheral nervous system acting downstream of the latter. Further, I could show that Fe65 and Fe65L1 have partly overlapping or redundant function, but are also involved in distinct signaling pathways, as revealed from analyses of Fe65 and Fe65L1 KO mice in short term plasticity paradigms.

With an interdisciplinary team we could reveal the intramolecular structure of the PTB2 domain of Fe65 forming an intermolecular dimer which is provided in chapter II. Thereby I could verify the dimer formation *in vivo* and analyzed the influence of APP. Co-immunoprecipitation experiments and Blue Native Gel analysis further exhibited evidence for a trimeric complex, composed of two Fe65 and one APP molecule. An interesting finding of the study is that dimerization of Fe65, which most likely occur in the cytosol, effectively shields the APP binding region of Fe65-PTB2 by mimicking the AICD/Fe65-PTB2 interaction. This mimicking might be of peculiar interest in developing new therapeutic approaches in up- or down regulating APP signaling in the case of AD.

Although it has been shown in previous studies that Fe65 links APP and LRP1, a member of the low density lipoprotein receptor family, i couldn´t reveal any influence of Fe65 and/or Fe65L1 on fast axonal transport of solely expressed LRP1 or APP or co-expressed LRP1 and APP in primary neurons. However, these data encompassed

a detailed analysis of LRP1 transport characteristics, documented in chapter III. Importantly, these data showed that LRP1 is transported in axonal membrane organelles distinct from APP bearing transport vesicles and further show that LRP1 causes a recruitment of APP in LRP1 transport vesicles. Nevertheless, a possible participation of the Fe65 protein family on LRP1 mediated APP endocytosis has to be considered as it was shown to interact with ARF6, which is an important protein in endocytosis. Furthermore, the influence of Fe65L2 on APP endocytosis should be incorporated, which might compensate the loss of Fe65 and Fe65L1 and has not been addressed in course of this thesis.

In conclusion, the three chapters of this thesis extend our understanding of the Fe65 protein family function by different *in vivo, in vitro and ex vivo* analyses as well as its intra- and intermolecular binding properties with possible affect on physiological and pathogenic function regarding its interplay with APP and LRP1 in Alzheimers Disease research.

Summary/Zusammenfassung

The cytosolic Fe65 adaptor protein family, consisting of Fe65, Fe65L1 and Fe65L2 is involved in many intracellular signaling pathways linking via its three interaction domains a continuously growing list of proteins by facilitating functional interactions. One of the most important binding partners of Fe65 family proteins is the amyloid precursor protein (APP), which plays an important role in Alzheimer Disease.

To gain deeper insights in the function of the ubiquitously expressed Fe65 and the brain enriched Fe65L1, the goal of my study was I) to analyze their putative synaptic function *in vivo*, II) to examine structural analysis focusing on a putative dimeric complex of Fe65, III) to consider the involvement of Fe65 in mediating LRP1 and APP intracellular trafficking in murine hippocampal neurons. By utilizing several behavioral analyses of Fe65 KO, Fe65L1 KO and Fe65/Fe65L1 DKO mice I could demonstrate that the Fe65 protein family is essential for learning and memory as well as grip strength and locomotor activity. Furthermore, immunohistological as well as protein biochemical analysis revealed that the Fe65 protein family is important for neuromuscular junction formation in the peripheral nervous system, which involves binding of APP and acting downstream of the APP signaling pathway. Via Co-immunoprecipitation analysis I could verify that Fe65 is capable to form dimers *ex vivo*, which exclusively occur in the cytosol and upon APP expression are shifted to membrane compartments forming trimeric complexes. The influence of the loss of Fe65 and/or Fe65L1 on APP and/or LRP1 transport characteristics in axons could not be verified, possibly conditioned by the compensatory effect of Fe65L2. However, I could demonstrate that LRP1 affects the APP transport independently of Fe65 by shifting APP into slower types of vesicles leading to changed processing and endocytosis of APP.

The outcome of my thesis advanced our understanding of the Fe65 protein family, especially its interplay with APP physiological function in synapse formation and synaptic plasticity.

Die zytosolische Fe65 Adapterprotein Familie, zu der Fe65, Fe65L1 und Fe65L2 gehören, ist an einer Vielzahl an intrazellulären Signalwegen beteiligt, wobei sie durch ihre drei Interaktionsdomänen eine stetig wachsenden Anzahl an Proteinen verbindet und deren funktionelle Wechselwirkung erleichtert. Einer der wichtigsten Bindungspartner der Fe65 Protein Familie ist das Amyloid-Vorläuferprotein (*engl.:Amyloid-Precursor-Protein*, APP), dass in der Alzheimer Demenz eine bedeutende Rolle spielt.

Um einen tieferen Einblick in die Funktion des ubiquitär exprimierten Fe65 und des hauptsächlich im Gehirn vorkommenden Fe65L1 zu erhalten, war das Ziel dieser Arbeit I) die Untersuchung ihrer putativen synaptischen Funktion *in vivo*, II) strukturelle Analysen durchzuführen mit dem Fokus auf einen möglichen dimeren Komplex von Fe65, III) die Beteiligung von Fe65 am intrazellulären Transport von LRP1 und APP in murinen hippocampalen Neuronen zu überprüfen. Unter Anwendung verschiedener Verhaltensanalysen an Fe65 KO, Fe65L1 KO and Fe65/Fe65L1 DKO Mäusen konnte ich zeigen, dass die Fe65 Protein Familie für das Lern- sowie das Gedächtnisvermögen als auch für die (Greif-)Kraft und die lokomotorische Aktivität essentiell ist. Weiterhin haben immunhistologische als auch protein-biochemische Untersuchungen gezeigt, dass die Fe65 Protein Familie für die Bildung der neuromuskulären Endplatte im peripheren Nervensystem entscheidend ist, wobei Fe65 an APP bindet und unterhalb der APP Signalkaskade wirkt. Anhand von Co-Immunpräzipitationsstudien konnte ich nachweisen, dass Fe65 in der Lage ist *ex vivo* Dimere zu bilden, welche ausschließlich im Zytosol enstehen, bei APP Expression in Membrankompartimente verlagert werden und dabei trimere Komplexe bilden. Ein Einfluss bei Fehlen von Fe65 und/oder Fe65L1 auf die axonalen Transporteigenschaften von APP und/oder LRP1 konnte nicht nachgewiesen werden, welcher wahrscheinlich durch den kompensatorischen Effekt von Fe65L2 bedingt ist. Allerdings konnte ich zeigen, dass LRP1, unabhängig von Fe65, einen Einfluss auf das Transportverhalten von APP aufweist. APP wird dabei in langsamere Vesikel umverteilt und es findet eine Veränderung in der Prozessierung und Endozytose statt.

Die Erkenntnisse meiner Doktorarbeit erweitern unser Verständnis über die Fe65 Proteinfamilie, insbesondere dessen Wechselwirkung mit der physiologischen Funktion von APP bei der Synapsenbildung und Synapsenplastizität.

References

Adams, P. D., Afonine, P. V., Bunkóczi, G., Chen, V. B., Davis, I. W., Echols, N., et al. (2010). PHENIX: a comprehensive Python-based system for macromolecular structure solution. Acta Crystallogr. D Biol. Crystallogr. 66, 213–221. doi: 10.1107/S0907444909052925

Aleksis, R. et al., 2017. Structural studies of amyloid-β peptides: Unlocking the mechanism of aggregation and the associated toxicity. Biochimie, 140, pp.176–192.

Alvira-Botero, X. et al., 2010. Megalin interacts with APP and the intracellular adapter protein FE65 in neurons. Molecular and Cellular Neuroscience, 45(3), pp.306–315.

Ando, K., Iijima, K. I., Elliott, J. I., Kirino, Y., and Suzuki, T. (2001). Phosphorylation-dependent regulation of the interaction of amyloid precursor protein with Fe65 affects the production of b-amyloid. J. Biol. Chem. 276, 40353–40361. doi: 10.1074/jbc.M104059200

Auerbach, W. et al. The HD mutation causes progressive lethal neurological disease in mice expressing reduced levels of huntingtin. Human molecular genetics 10, 2515–2523 (2001).

Barbagallo, A. P., Wang, Z., Zheng, H. & D'Adamio, L. A single tyrosine residue in the amyloid precursor protein intracellular domain is essential for developmental function. J Biol Chem 286, 8717–8721, doi: 10.1074/jbc.C111.219873 (2011).

Bassez, G. et al., 2008. Type 2 Myotonic Dystrophy Can Be Predicted by the Combination of Type 2 Muscle Fiber Central Nucleation and Scattered Atrophy. Journal of Neuropathology & Experimental Neurology, 67(4), pp.319–325.

Baumkotter, F., Schmidt, N., Vargas, C., Schilling, S., Weber, R., Wagner, K., et al. (2014). Amyloid precursor protein dimerization and synaptogenic function depend on copper binding to the growth factor-like domain. J. Neurosci. 34, 11159–11172. doi: 10.1523/JNEUROSCI.0180-14.2014

Baumkötter, F., Wagner, K., Eggert, S., Wild, K., and Kins, S. (2012). Structural aspects and physiological consequences of APP/APLP trans-dimerization. Exp. Brain Res. 217, 389–395. doi: 10.1007/s00221-011-2878-6

Bergen, A. A., Kaing, S., Ten Brink, J. B., Netherlands, B. B., Gorgels, T. G., and Janssen, S. F. (2015). Gene expression and functional annotation of human choroid plexus epithelium failure in Alzheimer's disease. BMC Genomics 16:956. doi: 10.1186/s12864-015-2159-z

Berlin, K., Longhini, A., Dayie, T. K., and Fushman, D. (2013). Deriving quantitative dynamics information for proteins and RNAs using ROTDIF with a graphical user interface. J. Biomol. NMR 57, 333–352. doi: 10.1007/s10858-013-9791-1

Bertenshaw, G. P., Norcum, M. T., and Bond, J. S. (2003). Structure of homo- and hetero-oligomeric meprin metalloproteases: dimers, tetramers, and high molecular mass multimers. J. Biol. Chem. 278, 2522–2532. doi: 10.1074/jbc.M208808200

Bien, J., Jefferson, T., Causevic, ́ M., Jumpertz, T., Munter, L., Multhaup, G., et al. (2012). The metalloprotease meprin β generates amino terminal-truncated amyloid β peptide species. J. Biol. Chem. 287, 33304–33313. doi: 10.1074/jbc.M112.395608

Blanco, G. et al., 1998. Mapping of the human and murine X11-like genes (APBA2 and Apba2), the murine Fe65 gene (Apbb1), and the human Fe65-like gene (APBB2): Genes

encoding phosphotyrosine-binding domain proteins that interact with the Alzheimer's disease amyloid precursor prote. Mammalian Genome, 9(6), pp.473–475.

Borg, J. P., Ooi, J., Levy, E., and Margolis, B. (1996). The phosphotyrosine interaction domains of X11 and FE65 bind to distinct sites on the YENPTY motif of amyloid precursor protein. Mol. Cell. Biol. 16, 6229–6241. doi: 10.1128/mcb.16.11.6229

Bork, P. & Margolis, B., 1995. A phosphotyrosine interaction domain. Cell, 80(5), pp.693–694.

Bork, P. & Sudol, M., 1994. The WW domain: A signalling site in dystrophin? Trends in Biochemical Sciences, 19(12), pp.531–533.

Bressler, S.L. et al., 1996. cDNA cloning and chromosome mapping of the human Fe65 gene: interaction of the conserved cytoplasmic domains of the human beta-amyloid precursor protein and its homologues with the mouse Fe65 protein. Human molecular genetics, 5(10), pp.1589–98.

Brinkmalm,G., Brinkmalm, A., Bourgeois, P., Persson, R., Hansson, O., Portelius,E., et al. (2013). Soluble amyloid precursor protein α and β in CSF in Alzheimer's disease. Brain Res. 1513, 117–126. doi: 10.1016/j.brainres.2013.03.019

Brown, P. D., Davies, S. L., Speake, T., and Millar, I. D. (2004). Molecular mechanisms of cerebrospinal fluid production. Neuroscience 129, 957–970. doi: 10.1016/j.neuroscience.2004.07.003

Bruni, P. et al., 2002. Fe65, a ligand of the Alzheimer's Aβ-amyloid precursor protein, blocks cell cycle progression by down-regulating thymidylate synthase expression. Journal of Biological Chemistry, 277(38), pp.35481–35488.

Bukhari, H. et al., 2017. Small things matter: Implications of APP intracellular domain AICD nuclear signaling in the progression and pathogenesis of Alzheimer's disease. Progress in Neurobiology, 156(Supplement C), pp.189–213.

Bukhari, H., Kolbe, K., Leonhardt, G., Loosse, C., Schröder, E., Knauer, S., et al. (2016). Membrane tethering of APP c-terminal fragments is a prerequisite for T668 phosphorylation preventing nuclear sphere generation. Cell Signal. 28, 1725–1734. doi: 10.1016/j.cellsig.2016.08.007

Caldwell, J.H. et al., 2012. Roles of the amyloid precursor protein family in the peripheral nervous system. Mechanisms of development, 130(6–8), pp.433–46.

Cam, J. A., Zerbinatti, C. V., Li, Y., and Bu, G. (2005). Rapid endocytosis of the low density lipoprotein receptor-related protein modulates cell surface distribution and processing of the β-amyloid precursor protein. J. Biol. Chem. 280, 15464–15470. doi: 10.1074/jbc.M500613200

Cao, X. & Sudhof, T. C. A transcriptionally [correction of transcriptively] active complex of APP with Fe65 and histone acetyltransferase Tip60. Science 293, 115–120 (2001).

Cao, X., and Südhof, T. C. (2004). Dissection of amyloid-b precursor protein-dependent transcriptional transactivation. J. Biol. Chem. 279, 24601–24611. doi: 10.1074/jbc.m402248200

Chalfie, M., and Kain, S. R. (eds.). (2005). Green Fluorescent Protein: Properties, Applications and Protocols, 2nd Edn. John Wiley & Sons. doi: 10.1002/0471739499.ch1

Chang, Y. et al., 2003. Generation of the beta-amyloid peptide and the amyloid precursor protein C-terminal fragment gamma are potentiated by FE65L1. The Journal of biological chemistry, 278(51), pp.51100–7.

Chang, Y. et al., 2006. Essential roles for the FE65 amyloid precursor protein-interacting proteins in brain development. The EMBO journal, 25(2), pp.420–31.

Chen, G. et al., 2017. Amyloid beta: structure, biology and structure-based therapeutic development. Acta Pharmacol Sin, 38(9), pp.1205–1235.

Cheung, H. N. et al. FE65 interacts with ADP-ribosylation factor 6 to promote neurite outgrowth. FASEB journal: official publication of the Federation of American Societies for Experimental Biology 28, 337–349, doi: 10.1096/fj.13-232694 (2014).

Choi, H. Y. et al. APP interacts with LRP4 and agrin to coordinate the development of the neuromuscular junction in mice. eLife 2, e00220, doi: 10.7554/eLife.00220 (2013).

Chow, V.W. et al., 2010. An Overview of APP Processing Enzymes and Products. Neuromolecular medicine, 12(1), pp.1–12.

Chow, W. N., Cheung, H. N., Li, W. & Lau, K. F. FE65: Roles beyond amyloid precursor protein processing. Cell Mol Biol Lett 20, 66–87, doi: 10.1515/cmble-2015-0002 (2015).

Clore, G. M. (2015). Practical aspects of paramagnetic relaxation enhancement in biological macromolecules. Meth. Enzymol. 564, 485–497. doi: 10.1016/bs.mie. 2015.06.032

Coburger, I., Hoefgen, S., and Than, M. E. (2014). The structural biology of the amyloid precursor protein APP—a complex puzzle reveals its multi-domain architecture. Biol. Chem. 395, 485–498. doi: 10.1515/hsz-2013-0280

Cool, B. H., Zitnik, G., Martin, G. M. & Hu, Q. Structural and functional characterization of a novel FE65 protein product upregulated in cognitively impaired FE65 knockout mice. J Neurochem 112, 410–419, doi: 10.1111/j.1471-4159.2009.06456.x (2010).

Delaglio, F., Grzesiek, S., Vuister, G. W., Zhu, G., Pfeifer, J., and Bax, A. (1995). NMRPipe: a multidimensional spectral processing system based on UNIX pipes. J. Biomol. NMR 6, 277–293. doi: 10.1007/bf00197809

Dietl, A., Wild, K., and Simon, B. (2014). 1H, 13C, and 15N chemical shift assignments of the phosphotyrosine binding domain 2 (PTB2) of human FE65. Biomol. NMR Assign. 8, 93–95. doi: 10.1007/s12104-013-9460-z

Domingues, S.C. et al., 2011. Identification and characterization of a neuronal enriched novel transcript encoding the previously described p60Fe65 isoform. Journal of neurochemistry, 119(5), pp.1086–98.

Duilio, A. et al., 1991. A Rat Brain mRNA Encoding a Transcriptional Activator Homologous to the DNA Binding Domain of Retroviral Integrases. Nucleic Acids Research, 19(19), pp.5269–5274.

Duilio, A. et al., 1998. Fe65L2: a new member of the Fe65 protein family interacting with the intracellular domain of the Alzheimer's beta-amyloid precursor protein. The Biochemical journal, 330 Pt 1, pp.513–9.

Dumanis, S. B. et al. FE65 as a link between VLDLR and APP to regulate their trafficking and processing. Molecular neurodegeneration 7, 9, doi: 10.1186/1750-1326-7-9 (2012).

Eggert, S. et al., 2004. The proteolytic processing of the amyloid precursor protein gene family members APLP-1 and APLP-2 involves α-, β-, γ-, and ε-Like cleavages: Modulation of APLP-1 processing by N-glycosylation. Journal of Biological Chemistry, 279(18), pp.18146–18156.

Eggert, S., Midthune, B., Cottrell, B., and Koo, E. H. (2009). Induced dimerization of the amyloid precursor protein leads to decreased amyloid-β protein production. J. Biol. Chem. 284, 28943–28952. doi: 10.1074/jbc.M109. 038646

Emsley, P., Lohkamp, B., Scott, W. G., and Cowtan, K. (2010). Features and development of Coot. Acta Crystallogr. D Biol. Crystallogr. 66, 486–501. doi: 10.1107/S0907444910007493

Ermekova, K.S. et al., 1997. The WW domain of neural protein FE65 interacts with proline-rich motifs in Mena, the mammalian homolog of Drosophila enabled. Journal of Biological Chemistry, 272(52), pp.32869–32877.

Esposito, F. et al., 1990. Isolation of cDNA fragments hybridizing to rat brain-specific mRNAs. Developmental neuroscience, 12(6), pp.373–381.

Evans, P. R., and Murshudov, G. N. (2013). How good are my data and what is the resolution? Acta Crystallogr. D Biol. Crystallogr. 69, 1204–1214. doi: 10.1107/S0907444913000061

Fiore, F. et al., 1995. The Regions Of the Fe65 Protein Homologous to the Phosphotyrosine Interaction Phosphotyrosine Binding Domain Of Shc Bind the Intracellular Domain Of the Alzheimers Amyloid Precursor Protein. Journal of Biological Chemistry, 270(52), pp.30853–30856.

FitzGerald, D. J., Fryling, C. M., Zdanovsky, A., Saelinger, C. B., Kounnas, M., Winkles, J. A., et al. (1995). Pseudomonas exotoxin-mediated selection yields cells with altered expression of low-density lipoprotein receptor-related protein. Mol. Microbiol. 16, 1171–1181. doi: 10.1083/jcb.129.6.1533

Fukumoto, H., Cheung, B. S., Hyman, B. T., and Irizarry, M. C. (2002). b-secretase protein and activity are increased in the neocortex in Alzheimer disease. Arch. Neurol. 59, 1381–1389. doi: 10.1001/archneur.59.9.1381

Gersbacher, M.T. et al., 2013. Turnover of Amyloid Precursor Protein Family Members Determines Their Nuclear Signaling Capability. PLoS ONE, 8(7).

Goh, K.L. et al., 2002. Ena/VASP Proteins Regulate Cortical Neuronal Positioning. Current Biology, 12(7), pp.565–569.

Golanska, E. et al., 2013. APBB2 genetic polymorphisms are associated with severe cognitive impairment in centenarians. Experimental Gerontology, 48(4), pp.391–394.

Goodger, Z. V., Rajendran, L., Trutzel, A., Kohli, B. M., Nitsch, R. M., and Konietzko, U. (2009). Nuclear signaling by the APP intracellular domain occurs predominantly through the amyloidogenic processing pathway. J. Cell Sci. 122, 3703–3714. doi: 10.1242/jcs.048090

Guenette, S., Chang, Y., Hiesberger, T., Richardson, J. A., Eckman, C. B., Eckman, E. A., et al. (2006). Essential roles for the FE65 amyloid precursor protein-interacting proteins in brain development. EMBO J. 25, 420–431. doi: 10.1038/sj.emboj.7600926

Guénette, S., Strecker, P. & Kins, S., 2017. APP Protein Family Signaling at the Synapse: Insights from Intracellular APP-Binding Proteins. Frontiers in Molecular Neuroscience, 10(March), p.87.

Guénette, S.Y. et al., 1996. Association of a novel human FE65-like protein with the cytoplasmic domain of the beta-amyloid precursor protein. Proceedings of the National Academy of Sciences of the United States of America, 93(20), pp.10832–7.

Gunther, R. et al. Clinical testing and spinal cord removal in a mouse model for amyotrophic lateral sclerosis (ALS). J Vis Exp, doi: 10.3791/3936 (2012).

Haass, C., Kaether, C., Thinakaran, G., and Sisodia, S. (2012). Trafficking and proteolytic processing of APP. Cold Spring Harb. Perspect. Med. 2:a006270. doi: 10.1101/cshperspect.a006270

Haditsch, U. et al., 2009. A central role for the small GTPase Rac1 in hippocampal plasticity and spatial learning and memory. Molecular and cellular neurosciences, 41(4), pp.409–419.

Harrison, M. et al. Vertebral landmarks for the identification of spinal cord segments in the mouse. Neuroimage 68, 22–29, doi: 10.1016/j.neuroimage.2012.11.048 (2013).

Hayward, L. J. et al. Targeted mutation of mouse skeletal muscle sodium channel produces myotonia and potassium-sensitive weakness. J Clin Invest 118, 1437–1449, doi: 10.1172/JCI32638 (2008).

Heber, S. et al., 2000. Mice with combined gene knock-outs reveal essential and partially redundant functions of amyloid precursor protein family members. The journal of neuroscience, 20(21), pp.7951–7963.

Hebert, S. et al., 2006. Regulated intramembrane proteolysis of amyloid precursor protein and regulation of expression of putative target genes. EMBO reports.

Hermey, G., Schmidt, N., Bluhm, B., Mensching, D., Ostermann, K., Rupp, C., et al. (2015). SorCS1 variants and amyloid precursor protein (APP) are co-transported in neurons but only SorCS1c modulates anterograde APP transport. J. Neurochem. 135, 60–75. doi: 10.1111/jnc.13221

Herms, J. et al., 2004. Cortical dysplasia resembling human type 2 lissencephaly in mice lacking all three APP family members. The EMBO journal, 23(20), pp.4106–15.

Ho, A. et al. Genetic analysis of Mint/X11 proteins: essential presynaptic functions of a neuronal adaptor protein family. J Neurosci 26, 13089–13101, doi: 10.1523/JNEUROSCI.2855-06.2006 (2006).

Hoe, H. S. et al. FE65 interaction with the ApoE receptor ApoEr2. J Biol Chem 281, 24521–24530, doi: 10.1074/jbc.M600728200 (2006).

Hoe, H.-S. et al., 2006. FE65 Interaction with the ApoE Receptor ApoEr2. Journal of Biological Chemistry, 281(34), pp.24521–24530.

Hsu, C.H., Park, S., Mortenson, D.E., Foley, B.L., Wang, X., Woods, R.J., Case, D.A., Powers, E.T., Wong, C.H., Dyson, H.J. , et al. (2016). The Dependence of Carbohydrate-Aromatic Interaction Strengths on the Structure of the Carbohydrate. J Am Chem Soc 138, 7636-7648.

Hu, Q. ai et al., 1999. Alternatively spliced isoforms of FE65 serve as neuron-specific and non- neuronal markers. Journal of Neuroscience Research, 58(5), pp.632–640.

Hu, Q. et al., 2002. A candidate molecular mechanism for the association of an intronic polymorphism of FE65 with resistance to very late onset dementia of the Alzheimer type. Human molecular genetics, 11(4), pp.465–475.

Hu, Q. et al., 2005. Endoproteolytic cleavage of FE65 converts the adaptor protein to a potent suppressor of the sAPP?? pathway in primates. Journal of Biological Chemistry, 280(13), pp.12548–12558.

Huse, J.T. et al., 2002. ß-secretase processing in the trans-Golgi network preferentially generates truncated amyloid species that accumulate in Alzheimer's disease brain. Journal of Biological Chemistry, 277(18), pp.16278–16284.

Ikin, A. F., Sabo, S. L., Lanier, L. M. & Buxbaum, J. D. A macromolecular complex involving the amyloid precursor protein (APP) and the cytosolic adapter FE65 is a negative regulator of axon branching. Molecular and cellular neurosciences 35, 57–63, doi: 10.1016/j.mcn.2007.02.003 (2007).

Irizarry, M.C. et al., 2004. Apolipoprotein E modulates γ-secretase cleavage of the amyloid precursor protein. Journal of Neurochemistry, 90(5), pp.1132–1143.

Isbert, S., Wagner, K., Eggert, S., Schweitzer, A., Multhaup, G., Weggen, S., et al. (2012). APP dimer formation is initiated in the endoplasmic reticulumand differs between APP isoforms. Cell. Mol. Life Sci. 69, 1353–1375. doi: 10.1007/s00018-011-0882-4

Jacobsen, K.T. & Iverfeldt, K., 2009. Amyloid precursor protein and its homologues: a family of proteolysis-dependent receptors. Cellular and molecular life sciences : CMLS, 66(14), pp.2299–318.

Jäger, S., Leuchtenberger, S., Martin, A., Czirr, E., Wesselowski, J., Dieckmann, M., et al. (2009). α-secretase mediated conversion of the amyloid precursor protein derived membrane stub C99 to C83 limits Aβ generation. J. Neurochem. 111, 1369–1382. doi: 10.1111/j.1471-4159.2009.06420.x

Jefferson, T., Caušević,´ M., Auf Dem Keller, U., Schilling, O., and Isbert, S., Geyer, R., et al. (2011). Metalloprotease meprin β generates nontoxic N-terminal amyloid precursor protein fragments in vivo. J. Biol. Chem. 286, 27741–27750. doi: 10.1074/jbc.M111.252718

John, A. & Gerald, A., 1992. Alzheimers Disease : The Amyloid Cascade Hypothesis.

Johnson, B. A., and Blevins, R. A. (1994). NMR view: a computer program for the visualization and analysis of NMR data. J. Biomol. NMR 4, 603–614. doi: 10.1007/BF00404272

Jorissen, E., Prox, J., Bernreuther, C., Weber, S., Schwanbeck, R., Serneels, L., et al. (2010). The disintegrin/metalloproteinase ADAM10 is essential for the establishment of the brain cortex. J. Neurosci. 30,b4833–4844. doi: 10.1523/JNEUROSCI.5221-09.2010

Jung, J. I., Premraj, S., Cruz, P. E., Ladd, T. B., Kwak, Y., Koo, E. H., et al. (2014). Independent relationship between amyloid precursor protein (APP) dimerization and γ-secretase processivity. PLoS ONE 9:111553. doi: 10.1371/journal.pone.0111553

Kabsch, W. (2010). XDS. Acta Crystallogr. D Biol. Crystallogr. 66, 125–132. doi: 10.1107/S0907444909047337

Kaden, D., Munter, L. M., Joshi, M., Treiber, C., Weise, C., Bethge, T., et al. (2008). Homophilic interactions of the amyloid precursor protein (APP) ectodomain are regulated by the loop region and affect β-secretase cleavage of APP. J. Biol. Chem. 283, 7271–7279. doi: 10.1074/jbc.M708046200

Kaden, D., Voigt, P., Munter, L.-M., Bobowski, K. D., Schaefer, M., and Multhaup, G. (2009). Subcellular localization and dimerization of APLP1 are strikingly dfferent from APP and APLP2. J. Cell Sci. 122, 368–377. doi: 10.1242/jcs.034058

Kaether, C., Skehel, P., and Dotti, C. G. (2000). Axonal membrane proteins are transported in distinct carriers: a two-color video microscopy study in cultured hippocampal neurons. Mol. Biol. Cell 11, 1213–1224. doi: 10.1091/mbc.11.4.1213

Kalaria, R. N., Premkumar, D. R. D., Pax, A. B., Cohen, D. L., and Lieberburg, I. (1996). Production and increased detection of amyloid β protein and amyloidogenic fragments in brain microvessels, meningeal vessels and choroid plexus in Alzheimer's disease. Mol. Brain Res. 35, 58–68. doi: 10.1016/0169-328X(95)00180-Z

Kang, J., Lemaire, H.-G., Unterbeck, A., Salbaum, J. M., Masters, C. L., Grzeschik, Karl, H., et al. (1987). The precursor of Alzheimer's disease amyloid A4 protein resembles a cell-surface receptor. Nature 325, 733–736. doi: 10.1038/325733a0

Kerschensteiner, M., Reuter, M. S., Lichtman, J. W. & Misgeld, T. Ex vivo imaging of motor axon dynamics in murine triangularis sterni explants. Nat Protoc 3, 1645–1653, doi: 10.1038/nprot.2008.160 (2008).

Kesavapany, S., Banner, S.J., et al., 2002. Expression of the Fe65 adapter protein in adult and developing mouse brain. Neuroscience, 115(3), pp.951–60.

Khalifa, B. N., Tyteca, D., Marinangeli, C., Depuydt, M., Collet, J.-F., Courtoy, P. J., et al. (2012). Structural features of the KPI domain control APP dimerization, trafficking, and processing. FASEB J. 26, 855–867. doi: 10.1096/fj.11-190207

Kim, M. L. et al. O-fucosylation of muscle agrin determines its ability to cluster acetylcholine receptors. Molecular and cellular neurosciences 39, 452–464, doi: 10.1016/j.mcn.2008.07.026 (2008).

Kimberly, W. T., Zheng, J. B., Guenette, S. Y. & Selkoe, D. J. The intracellular domain of the beta-amyloid precursor protein is stabilized by Fe65 and translocates to the nucleus in a notch-like manner. J Biol Chem 276, 40288–40292 (2001).

Klafki, H. W., Wiltfang, J., and Staufenbiel, M. (1996). Electrophoretic separation of betaA4 peptides (1-40) and (1-42). Anal. Biochem. 237, 24–29. doi: 10.1006/abio.1996.0195

Klevanski, M. et al. The APP Intracellular Domain Is Required for Normal Synaptic Morphology, Synaptic Plasticity, and Hippocampus-Dependent Behavior. J Neurosci 35, 16018-16033, doi: 10.1523/JNEUROSCI.2009-15.2015 (2015).

Klevanski, M., Saar, M., Baumkötter, F., Weyer, S. W., Kins, S., and Müller, U. C. (2014). Differential role of APP and APLPs for neuromuscular synaptic morphology and function. Mol. Cell. Neurosci. 61, 201–210. doi: 10.1016/j.mcn.2014.06.004

Knauer, M. F., Orlando, R. A., and Glabe, C. G. (1996). Cell surface APP751 forms complexes with protease nexin 2 ligands is internalized via the low density lipoprotein receptor-related protein (LRP). Brain Res. 740, 6–14. doi: 10.1016/S0006-8993(96)00711-1

Kohli, B. M., Pflieger, D., Mueller, L. N., Carbonetti, G., Aebersold, R., Nitsch, R. M., et al. (2012). Interactome of the amyloid precursor protein APP in brain reveals a protein network involved in synaptic vesicle turnover and a close association with Synaptotagmin-1. J. Proteome Res. 11, 4075–4090. doi: 10.1021/pr300123g

Koistinen, N. A., Edlund, A. K., Menon, P. K., Ivanova, E. V., Bacanu, S., Iverfeldt, K., et al. (2017). Nuclear localization of amyloid-b precursor protein-binding protein Fe65 is dependent on regulated intramembrane proteolysis. PLoS One 12:e0173888. doi: 10.1371/journal.pone.0173888

Konietzko, U. AICD nuclear signaling and its possible contribution to Alzheimer's disease. Curr Alzheimer Res 9, 200–216 (2012).

Krieger, M., 1994. Structures and Functions of Multiligand Lipoprotein Receptors: Macrophage Scavenger Receptors and LDL Receptor-Related Protein (LRP). Annual Review of Biochemistry, 63(1), pp.601–637.

Krissinel, E., and Henrick, K. (2007). Inference of macromolecular assemblies from crystalline state. J. Mol. Biol. 372, 774–797. doi: 10.1016/j.jmb.2007. 05.022

Kruse, M.-N., Becker, C., Lottaz, D., Köhler, D., Yiallouros, I., Krell, H.-W., et al. (2004). Human meprin alpha and beta homo-oligomers: cleavage of basement membrane proteins and sensitivity to metalloprotease inhibitors. Biochem. J. 378, 383–389. doi: 10.1042/bj20031163

Kuhn, P.-H., Wang, H., Dislich, B., Colombo, A., Zeitschel, U., Ellwart, J. W., et al. (2010). ADAM10 is the physiologically relevant, constitutive alpha-secretase of the amyloid precursor protein in primary neurons. EMBO J. 29, 3020–3032. doi: 10.1038/emboj.2010.167

Lai, A., Sisodia, S. S., and Trowbridge, I. S. (1995). Characterization of sorting signals in the β-amyloid precursor protein cytoplasmic domain. J. Biol. Chem. 270, 3565–3573. doi: 10.1074/jbc.270.8.3565

Lalonde, R. & Strazielle, C. Brain regions and genes affecting limb-clasping responses. Brain Res Rev 67, 252–259, doi: 10.1016/j. brainresrev.2011.02.005 (2011).

Lambrechts, A. et al. cAMP-dependent protein kinase phosphorylation of EVL, a Mena/VASP relative, regulates its interaction with actin and SH3 domains. J Biol Chem 275, 36143–36151, doi: 10.1074/jbc.M006274200 (2000).

Lammich, S., Kojro, E., Postina, R., Gilbert, S., Pfeiffer, R., Jasionowski, M., et al. (1999). Constitutive and regulated alpha-secretase cleavage of Alzheimer's amyloid precursor protein by a disintegrin metalloprotease. Proc. Natl. Acad. Sci. U.S.A. 96, 3922–3927. doi: 10.1073/pnas.96.7.3922

Lane-Donovan, C.E., Philips, G.T. & Herz, J., 2014. More Than Cholesterol Transporters: Lipoprotein Receptors in CNS Function and Neurodegeneration. Neuron, 83(4), pp.771–787.

Lau, K. F. et al. Dexras1 interacts with FE65 to regulate FE65-amyloid precursor protein-dependent transcription. J Biol Chem 283, 34728–34737, doi: 10.1074/jbc.M801874200 (2008).

Li, H. et al. Genetic dissection of the amyloid precursor protein in developmental function and amyloid pathogenesis. J Biol Chem 285, 30598–30605, doi: M110.137729/jbc.M110.137729 (2010).

Li, H. et al. Soluble amyloid precursor protein (APP) regulates transthyretin and Klotho gene expression without rescuing the essential function of APP. Proc Natl Acad Sci USA 107, 17362–17367, doi: 1012568107 (2010).

Libeu, C. A. P., Descamps, O., Zhang, Q., John, V., and Bredesen, D. E. (2012). Altering APP proteolysis: Increasing sAPPalpha production by targeting dimerization of the APP Ectodomain. PLoS ONE

Lichtenthaler, S. F., Haass, C., and Steiner, H. (2011). Regulated intramembrane proteolysis—lessons from amyloid precursor protein processing. J. Neurochem. 117, 779–796. doi: 10.1111/j.1471-4159.2011.07248.x

Ludwig, A., Hundhausen, C., Lambert, M. H., Broadway, N., Andrews, R.C., Bickett, D. M., et al. (2005). Metalloproteinase inhibitors for the disintegrin-like metalloproteinases ADAM10 and ADAM17 that differentially block constitutive and phorbol ester-inducible shedding of cell surface molecules. Comb. Chem. High Throughput Screen 8, 161–171. doi: 10.2174/1386207053258488

Lynch, M. A. Long-term potentiation and memory. Physiol Rev 84, 87–136, doi: 10.1152/physrev.00014.2003 (2004).

Maier, W., Bednorz, M., Meister, S., Roebroek, A., Weggen, S., Schmitt, U., et al. (2013). LRP1 is critical for the surface distribution and internalization of the NR2B NMDA receptor subtype. Mol. Neurodegener. 8:25. doi: 10.1186/1750-1326-8-25

MarquezSterling, N. R., Lo, A. C. Y., Sisodia, S. S., and Koo, E. H. (1997). Trafficking Of cell-surface β-amyloid precursor protein - evidence that a sorting intermediate participates in synaptic vesicle recycling. J. Neurosci. 17, 140–151.

Masin, M. et al., 2006. Fe65 interacts with P2X2 subunits at excitatory synapses and modulates receptor function. Journal of Biological Chemistry, 281(7), pp.4100–4108.

Masters, C. L., Simms, G., Weinman, N. A., Multhaup, G., McDonald, B. L., and Beyreuther, K. (1985). Amyloid plaque core protein in Alzheimer disease and down syndrome. Proc. Natl. Acad. Sci. U.S.A. 82, 4245–4249. doi: 10.1073/pnas.82.12.4245

McLoughlin, D. M., and Miller, C. C. (2008). The FE65 proteins and Alzheimer's disease. J. Neurosci. Res. 86, 744–754. doi: 10.1002/jnr.21532

McLoughlin, D.M. & Miller, C.C., 1996. The intracellular cytoplasmic domain of the Alzheimer's disease amyloid precursor protein interacts with phosphotyrosine-binding domain proteins in the yeast two-hybrid system. FEBS Lett, 397(2–3), pp.197–200. Meiyappan, M., Birrane, G. & Ladias, J.A.A., 2007. Structural Basis for Polyproline Recognition by the FE65 WW Domain. Journal of Molecular Biology, 372(4), pp.970–980.

Meiyappan, M., Birrane, G., and Ladias, J. A. (2007). Structural basis for polyproline recognition by the FE65 WW domain. J. Mol. Biol. 372, 970–980. doi: 10.1016/j.jmb.2007.06.064

Merz, P. A., Wisniewski, H. M., Somerville, R. A., Bobin, S. A., Masters, C. L., and Iqbal, K. (1983). Ultrastructural morphology of amyloid fibrils from neuritic and amyloid plaques. Acta Neuropathol. 60, 113–124. doi: 10.1007/BF00685355

Minopoli, G., Gargiulo, A., Parisi, S., and Russo, T. (2012). Fe65 matters: new light on an old molecule. IUBMB Life 64, 936–942. doi: 10.1002/iub.1094

Morris, R., 1984. Developments of a water-maze procedure for studying spatial learning in the rat. Journal of Neuroscience Methods, 11(1), pp.47–60.

Müller, T. et al., 2008. The amyloid precursor protein intracellular domain (AICD) as modulator of gene expression, apoptosis, and cytoskeletal dynamics-Relevance for Alzheimer's disease. Progress in Neurobiology, 85(4), pp.393–406.

Müller, U. C., and Zheng, H. (2012). Physiological functions of APP family proteins. Cold Spring Harb. Perspect. Med. 2:a006288. doi: 10.1101/cshperspect. a006288

Müller, U. et al., 1994. Behavioral and anatomical deficits in mice homozygous for a modified beta-amyloid precursor protein gene. Cell, 79(5), pp.755–765.

Munter, L. M., Botev, A., Richter, L., Hildebrand, P. W., Althoff, V., Weise, C., et al. (2010). Aberrant amyloid precursor protein (APP) processing in hereditary forms of Alzheimer disease caused by APP familial Alzheimer disease mutations can be rescued by mutations in the APP GxxxG motif. J. Biol. Chem. 285, 21636–21643. doi: 10.1074/jbc.M109.088005

Munter, L.-M., Voigt, P., Harmeier, A., Kaden, D., Gottschalk, K. E., Weise, C., et al. (2007). GxxxG motifs within the amyloid precursor protein transmembrane sequence are critical for the etiology of Abeta42. EMBO J. 26, 1702–1712. doi: 10.1038/sj.emboj.7601616

Nakajima, C. et al., 2013. Low Density Lipoprotein Receptor-related Protein 1 (LRP1) Modulates N-Methyl-d-aspartate (NMDA) Receptor-dependent Intracellular Signaling and NMDA-induced Regulation of Postsynaptic Protein Complexes. The Journal of Biological Chemistry, 288(30), pp.21909–21923.

Nensa, F. M. et al. Amyloid beta a4 precursor protein-binding family B member 1 (FE65) interactomics revealed synaptic vesicle glycoprotein 2A (SV2A) and sarcoplasmic/endoplasmic reticulum calcium ATPase 2 (SERCA2) as new binding proteins in the human brain. Molecular & cellular proteomics : MCP 13, 475–488, doi: 10.1074/mcp.M113.029280 (2014).

Newbern, J. M. et al. Specific functions for ERK/MAPK signaling during PNS development. Neuron 69, 91–105, doi: 10.1016/j. neuron.2010.12.003 (2011).

Oku, Y. & Huganir, R.L., 2013. AGAP3 and Arf6 Regulate Trafficking of AMPA Receptors and Synaptic Plasticity. The Journal of Neuroscience, 33(31), pp.12586–12598.

Olsson, A., Höglund, K., Sjögren, M., Andreasen, N., Minthon, L., Lannfelt, L., et al. (2003). Measurement of α- and β-secretase cleaved amyloid precursor protein in cerebrospinal fluid from Alzheimer patients. Exp. Neurol. 183, 74–80. doi: 10.1016/S0014-4886(03)00027-X

Pardossi-Piquard, R., and Checler, F. (2012). The physiology of the b-amyloid precursor protein intracellular domain AICD. J. Neurochem. 120, 109–124. doi: 10.1111/j.1471-4159.2011.07475.x

Penna, I. et al., 2013. A novel snRNA-like transcript affects amyloidogenesis and cell cycle progression through perturbation of Fe65L1 (APBB2) alternative splicing. Biochimica et Biophysica Acta - Molecular Cell Research, 1833(6), pp.1511–1526.

Perez, R. G., Soriano, S., Hayes, J. D., Ostaszewski, B., Xia, W., Selkoe, D. J., et al. (1999). Mutagenesis identifies new signals for β-amyloid precursor protein endocytosis, turnover, and the generation of secreted fragments, including Aβ42. J. Biol. Chem. 274, 18851–18856. doi: 10.1074/jbc.274.27.18851

Perkinton, M.S. et al., 2004. The c-Abl tyrosine kinase phosphorylates the Fe65 adaptor protein to stimulate Fe65/amyloid precursor protein nuclear signaling.

Pernot, P., Round, A., Barrett, R., De Maria Antolinos, A., Gobbo, A., Gordon, E., et al. (2013). Upgraded ESRF BM29 beamline for SAXS on macromolecules in solution. J. Synchrotron Radiat. 20, 660–664. doi: 10.1107/S0909049513010431 Petoukhov, M. V., Franke, D., Shkumatov, A. V., Tria, G., Kikhney, A. G., Gajda, M., et al. (2012). New developments in the ATSAS program package for small-angle scattering data analysis. J. Appl. Crystallogr. 45, 342–350. doi: 10.1107/S0021889812007662

Pietrzik, C. U., Busse, T., Merriam, D. E., Weggen, S., and Koo, E. H. (2002). The cytoplasmic domain of the LDL receptor-related protein regulates multiple steps in APP processing. EMBO J. 21, 5691–5700. doi: 10.1093/emboj/cdf568

Pietrzik, C. U., Yoon, I.-S., Jaeger, S., Busse, T., Weggen, S., and Koo, E. H. (2004). FE65 constitutes the functional link between the low-density lipoprotein receptor-related protein and the amyloid precursor protein. J. Neurosci. 24, 4259–4265. doi: 10.1523/JNEUROSCI.5451-03.2004

Pohlkamp, T., Wasser, C.R. & Herz, J., 2017. Functional Roles of the Interaction of APP and Lipoprotein Receptors. Frontiers in Molecular Neuroscience, 10(March), pp.1–22.

Rabiej, V. K., Pflanzner, T., Wagner, T., Goetze, K., Storck, S. E., Eble, J. A., et al. (2015). Low density lipoprotein receptor-related protein 1 mediated endocytosis of β1-integrin influences cell adhesion and cell migration. Exp. Cell Res. 340, 102–115. doi: 10.1016/j.yexcr.2015.11.020

Radzimanowski, J., Beyreuther, K., Sinning, I., and Wild, K. (2008a). Overproduction, purification, crystallization and preliminary X-ray analysis of human Fe65-PTB2 in complex with the amyloid precursor protein intracellular domain. Acta Crystallogr. Sect. F Struct. Biol. Cryst. Commun. 64, 409–412. doi: 10.1107/S1744309108009524

Radzimanowski, J., Ravaud, S., Schlesinger, S., Koch, J., Beyreuther, K., Sinning, I., et al. (2008b). Crystal structure of the human Fe65-PTB1 domain. J. Biol. Chem. 283, 23113–23120. doi: 10.1074/jbc.M800861200

Radzimanowski, J., Simon, B., Sattler, M., Beyreuther, K., Sinning, I., and Wild, K. (2008c). Structure of the intracellular domain of the amyloid precursor protein in complex with Fe65-PTB2. EMBO Rep. 9, 1134–1140. doi: 10.1038/embor. 2008.188

Ramelot, T. A., Gentile, L. N., and Nicholson, L. K. (2000). Transient structure of the amyloid precursor protein cytoplasmic tail indicates preordering of structure for binding to cytosolic factors. Biochemistry 39, 2714–2725. doi: 10.1021/bi992580m

Reekmans, S. M., Pflanzner, T., Gordts, P. L. S. M., Isbert, S., Zimmermann, P., Annaert, W., et al. (2010). Inactivation of the proximal NPXY motif impairs early steps in LRP1 biosynthesis. Cell. Mol. Life Sci. 67, 135–145. doi: 10.1007/s00018-009-0171-7

Ring, S. et al. The secreted beta-amyloid precursor protein ectodomain APPs alpha is sufficient to rescue the anatomical, behavioral, and electrophysiological abnormalities of APP-deficient mice. J Neurosci 27, 7817–7826 (2007).

Rogers, D.C. et al., 1997. Behavioral and functional analysis of mouse phenotype: SHIRPA, a proposed protocol for comprehensive phenotype assessment. Mammalian genome : official journal of the International Mammalian Genome Society, 8(10), pp.711–3.

Rollins, C. T., Rivera, V. M., Woolfson, D. N., Keenan, T., Hatada, M., Adams, S. E., et al. (2000). A ligand-reversible dimerization system for controlling protein-protein interactions. Proc. Natl. Acad. Sci. U.S.A. 97, 7096–7101. doi: 10.1073/pnas.100101997

Russo, T., Faraonio, R., Minopoli, G., De Candia, P., De Renzis, S., and Zambrano, N. (1998). Fe65 and the protein network centered around the cytosolic domain of the Alzheimer's b-amyloid precursor protein. FEBS Lett. 434, 1–7. doi: 10.1016/s0014-5793(98)00941-7

Sabo, S. et al., 2001. The Alzheimer amyloid precursor protein (APP) and FE65, an APP-binding protein, regulate cell movement. The Journal of Cell Biology, 153(7), pp.1403–1414.

Sabo, S.L. et al., 1999. Regulation of beta-amyloid secretion by FE65, an amyloid protein precursor-binding protein. Journal of Biological Chemistry, 274(12), pp.7952–7957.

Sabo, S.L. et al., 2003. The amyloid precursor protein and its regulatory protein, FE65, in growth cones and synapses in vitro and in vivo. The Journal of neuroscience : the official journal of the Society for Neuroscience, 23(13), pp.5407–5415.

Saeki, K. et al., 2011. Amyloid precursor protein binding protein Fe65 is cleaved by caspases during DNA damage-induced apoptosis. Biological & pharmaceutical bulletin, 34(2), pp.290–294.

Santiard-Baron, D. et al., 2005. Expression of human FE65 in amyloid precursor protein transgenic mice is associated with a reduction in beta-amyloid load. Journal of neurochemistry, 93(2), pp.330–8.

Sasaguri, H. et al., 1994. APP mouse models for Alzheimer's disease preclinical studies. The EMBO Journal, 36(17), pp.2473–2487.

Scheuermann, S., Hambsch, B., Hesse, L., Stumm, J., Schmidt, C., Beher, D., et al. (2001). Homodimerization of amyloid precursor protein and its implication in the amyloidogenic pathway of Alzheimer's Disease. J. Biol. Chem. 276, 33923–33929. doi: 10.1074/jbc.M105410200

Schilling, S. et al., 2017. APLP1 Is a Synaptic Cell Adhesion Molecule, Supporting Maintenance of Dendritic Spines and Basal Synaptic Transmission. The Journal of Neuroscience, 37(21), p.5345 LP-5365.

Schmidt, V., Baum, K., Lao, A., Rateitschak, K., Schmitz, Y., Teichmann, A., et al. (2012). Quantitative modelling of amyloidogenic processing and its influence by SORLA in Alzheimer's disease. EMBO J. 31, 187–200. doi: 10.1038/emboj.2011.352

Scholz, J., Niibori, Y., Frankland, P. W. & Lerch, J. P. Rotarod training in mice is associated with changes in brain structure observable with multimodal MRI. Neuroimage 107, 182–189, doi: 10.1016/j.neuroimage.2014.12.003 (2015).

Scholz, R. et al., 2017. AMPA Receptor Signaling through BRAG2 and Arf6 Critical for Long-Term Synaptic Depression. Neuron, 66(5), pp.768–780.

Schönherr, C., Bien, J., Isbert, S., Wichert, R., Prox, J., Altmeppen, H., et al. (2016). Generation of aggregation prone N- terminally truncated amyloid β peptides by meprin β depends on the sequence specificity at the cleavage site. Mol. Neurodegener. 11:19. doi: 10.1186/s13024-016-0084-5

Seabrook, G.R. et al., 1999. Mechanisms contributing to the deficits in hippocampal synaptic plasticity in mice lacking amyloid precursor protein. Neuropharmacology, 38(3), pp.349–359.

Selkoe, D. J., and Hardy, J. (2016). The amyloid hypothesis of Alzheimer's disease at 25 years. EMBO Mol. Med. 8, 595–608. doi: 10.15252/emmm.201606210

Sennvik, K., Fastbom, J., Blomberg, M., Wahlund, L. O., Winblad, B., and Benedikz, E. (2000). Levels of α- and β-secretase cleaved amyloid precursor protein in the cerebrospinal fluid of Alzheimer's disease patients. Neurosci. Lett. 278, 169–172. doi: 10.1016/S0304-3940(99)00929-5

Shen, Y., and Bax, A. (2010). SPARTA+: a modest improvement in empirical NMR chemical shift prediction by means of an artificial neural network. J. Biomol. NMR 48, 13–22. doi: 10.1007/s10858-010-9433-9

Shen, Y., Delaglio, F., Cornilescu, G., and Bax, A. (2009). TALOS+: a hybrid method for predicting protein backbone torsion angles from NMR chemical shifts. J. Biomol. NMR 44, 213–223. doi: 10.1007/s10858-009-9333-z

Simon, B., Madl, T., Mackereth, C. D., Nilges, M., and Sattler, M. (2010). An efficient protocol for NMR-spectroscopy-based structure determination of protein complexes in solution. Angew. Chem. Int. Ed Engl. 49, 1967–1970. doi: 10.1002/anie.200906147

So, P. P., Zeldich, E., Seyb, K. I., Huang, M. M., Concannon, J. B., King, G. D., et al. (2012). Lowering of amyloid beta peptide production with a small molecule inhibitor of amyloid-β precursor protein dimerization. Am. J. Neurodegener. Dis. 1, 75–87.

Soba, P., Eggert, S., Wagner, K., Zentgraf, H., Siehl, K., Kreger, S., et al. (2005). Homo- and heterodimerization of APP family members promotes intercellular adhesion. EMBO J. 24, 3624–3634. doi: 10.1038/sj.emboj.76 00824

Sosa, L.J. et al., 2017. "The physiological role of the Amyloid Precursor Protein (APP) as an adhesion molecule in the developing nervous system." Journal of Neurochemistry, pp.11–29.

Stahl, R., Schilling, S., Soba, P., Rupp, C., Hartmann, T., Wagner, K., et al. (2014). Shedding of APP limits its synaptogenic activity and cell adhesion properties. Front. Cell. Neurosci. 8:410. doi: 10.3389/fncel.2014.00410

Storck, S. E., Meister, S., Nahrath, J., Meibner, J. N., Schubert, N., Di Spiezio, A., et al. (2016). Endothelial LRP1 transports amyloid-β1-42 across the blood-brain barrier. J. Clin. Invest. 126, 123–136. doi: 10.1172/JCI81108

Strecker, P., Ludewig, S., Rust, M., Mundinger, T. A., Görlich, A., Krächan, E. G., et al. (2016). FE65 and FE65L1 share common synaptic functions and genetically interact with the APP family in neuromuscular junction formation. Sci. Rep. 6:25652. doi: 10.1038/srep25652

Suh, J. et al. FE65 and FE65L1 amyloid precursor protein-binding protein compound null mice display adult-onset cataract and muscle weakness. FASEB journal : official publication of the Federation of American Societies for Experimental Biology, doi: 10.1096/ fj.14-261453 (2015).

Suh, J., Lyckman, A., Wang, L., Eckman, E. A. & Guenette, S. Y. FE65 proteins regulate NMDA receptor activation-induced amyloid precursor protein processing. J Neurochem 119, 377–388, doi: 10.1111/j.1471-4159.2011.07419.x (2011).

Sumioka, A. et al. Role of 14-3-3gamma in FE65-dependent gene transactivation mediated by the amyloid beta-protein precursor cytoplasmic fragment. J Biol Chem 280, 42364–42374 (2005).

Szodorai, A., Kuan, Y.-H., Hunzelmann, S., Engel, U., Sakane, A., Sasaki, T., et al. (2009). APP anterograde transport requires Rab3A GTPase activity for assembly of the transport vesicle. J. Neurosci. 29, 14534–14544. doi: 10.1523/JNEUROSCI.1546-09.2009

Tanahashi, H. & Tabira, T., 1999. Molecular cloning of human Fe65L2 and its interaction with the Alzheimer's beta-amyloid precursor protein. Neuroscience Letters, 261(3), pp.143–146.

Tanahashi, H. & Tabira, T., 2002. Characterization of an amyloid precursor protein-binding protein Fe65L2 and its novel isoforms lacking phosphotyrosine-interaction domains. The Biochemical journal, 367(Pt 3), pp.687–95.

Tang, W. et al., 2015. Arf6 controls beta-amyloid production by regulating macropinocytosis of the Amyloid Precursor Protein to lysosomes. Molecular Brain, 8(1), p.41.

Telese, F., Bruni, P., Donizetti, A., Gianni, D., D'Ambrosio, C., Scaloni, A., et al. (2005). Transcription regulation by the adaptor protein Fe65 and the nucleosome assembly factor SET. EMBO Rep. 6, 77–82. doi: 10.1038/sj.embor. 7400309

Trommsdorff, M., Borg, J. P., Margolis, B. & Herz, J. Interaction of cytosolic adaptor proteins with neuronal apolipoprotein E receptors and the amyloid precursor protein. J Biol Chem 273, 33556–33560 (1998).

Uhlik, M. T., Temple, B., Bencharit, S., Kimple, A. J., Siderovski, D. P., and Johnson, G. L. (2005). Structural and evolutionary division of phosphotyrosine binding (PTB) domains. J. Mol. Biol. 345, 1–20. doi: 10.1016/j.jmb.2004. 10.038

Ulery, P. G., Beers, J., Mikhailenko, I., Tanzi, R. E., Rebeck, G. W., Hyman, B. T., et al. (2000). Modulation of amyloid precursor protein processing by the low density Lipoprotein Receptor-related Protein (LRP). J. Biol. Chem. 275, 7410–7415. doi: 10.1074/jbc.275.10.7410

Van Nostrand, W. E., Wagner, S. L., Shankle, W. R., Farrow, J. S., Dick, M., Rozemuller, J. M., et al. (1992). Decreased levels of soluble amyloid beta-protein precursor in cerebrospinal fluid of live Alzheimer disease patients. Proc. Natl. Acad. Sci. U.S.A. 89, 2551–2555. doi: 10.1073/pnas.89.7.2551

Vandenbroucke, R. E., Dejonckheere, E., Van Lint, P., Demeestere, D., Van Wonterghem, E., Vanlaere, I., et al. (2012). Matrix metalloprotease 8-dependent extracellular matrix cleavage at the blood-CSF barrier contributes to lethality during systemic inflammatory diseases. J. Neurosci. 32, 9805–9816. doi: 10.1523/JNEUROSCI.0967-12.2012

Von Arnim, C.A.F. et al., 2005. The low density lipoprotein receptor-related protein (LRP) is a novel β-secretase (BACE1) substrate. Journal of Biological Chemistry, 280(18), pp.17777–17785.

von Einem, B. et al., 2010. The role of low-density receptor-related protein 1 (LRP1) as a competitive substrate of the amyloid precursor protein (APP) for BACE1. Experimental Neurology, 225(1), pp.85–93.

von Koch, C.S. et al., 1997. Generation of APLP2 KO Mice and Early Postnatal Lethality in APLP2/APP Double KO Mice. Neurobiology of Aging, 18(6), pp.661–669. Available at: http://dx.doi.org/10.1016/S0197-4580(97)00151-6.

von Rotz, R. C., Kohli, B. M., Bosset, J., Meier, M., Suzuki, T., Nitsch, R. M., et al. (2004). The APP intracellular domain forms nuclear multiprotein complexes and regulates the transcription of its own precursor. J. Cell Sci. 117, 4435–4448. doi: 10.1242/jcs.01323

Wagner, T. & Pietrzik, C.U., 2012. The role of lipoprotein receptors on the physiological function of APP. Experimental Brain Research, 217(3), pp.377–387.

Waldron, E. et al., 2008. Increased AICD generation does not result in increased nuclear translocation or activation of target gene transcription. Experimental Cell Research, 314(13), pp.2419–2433.

Waldron, E., Heilig, C., Schweitzer, A., Nadella, N., Jaeger, S., Martin, A. M., et al. (2008). LRP1 modulates APP trafficking along early compartments of the secretory pathway. Neurobiol. Dis. 31, 188–197. doi: 10.1016/j.nbd.2008.04.006

Wang, B. et al. Isoform-specific knockout of FE65 leads to impaired learning and memory. J Neurosci Res 75, 12–24, doi: 10.1002/ jnr.10834 (2004).

Wang, B. et al., 2017. The Amyloid Precursor Protein Is a Conserved Receptor for Slit to Mediate Axon Guidance. eNeuro, 4(3), p.ENEURO.0185-17.2017.

Wang, P. et al., 2005. Defective neuromuscular synapses in mice lacking amyloid precursor protein (APP) and APP-Like protein 2. The Journal of neuroscience : the official journal of the Society for Neuroscience, 25(5), pp.1219–25.

Wang, P.-L. et al., 2011. Functional and molecular interactions between Rac1 and FE65. Neuroreport, 22(14), pp.716–20.

Wang, Y. et al. The APP-interacting protein FE65 is required for hippocampus-dependent learning and long-term potentiation. Learning & memory 16, 537–544, doi: 10.1101/lm.1499309 (2009).

Wang, Z., Wang, B., Yang, L., Guo, Q., Aithmitti, N., Songyang, Z., et al. (2009). Presynaptic and postsynaptic interaction of the amyloid precursor protein promotes peripheral and central synaptogenesis. J. Neurosci. 29, 10788–10801. doi: 10.1523/JNEUROSCI.2132-09.2009

Wasser, C.R. et al., 2014. Differential splicing and glycosylation of Apoer2 alters synaptic plasticity and fear learning. Science Signaling, 7(353), p.ra113--ra113.

Weidemann, A., König, G., Bunke, D., Fischer, P., Salbaum, J. M., Masters, C. L., et al. (1989). Identification, biogenesis, and localization of precursors of Alzheimer's disease A4 amyloid protein. Cell 57, 115–26. doi: 10.1016/0092-8674(89)90177-3

Weyer, S. W. et al. APP and APLP2 are essential at PNS and CNS synapses for transmission, spatial learning and LTP. The EMBO journal 30, 2266–2280, doi: 10.1038/emboj.2011.119 (2011).

Weyer, S.W. et al., 2014. Comparative analysis of single and combined APP/APLP knockouts reveals reduced spine density in APP-KO mice that is prevented by APPsα expression. Acta Neuropathologica Communications, 2, p.36.

Winkler, E., Julius, A., Steiner, H., and Langosch, D. (2015). Homodimerization protects the amyloid precursor protein C99 fragment from cleavage by g-secretase. Biochemistry 54, 6149–6152. doi: 10.1021/acs.biochem.5b00986

Winn, M. D., Ballard, C. C., Cowtan, K. D., Dodson, E. J., Emsley, P., Evans, P. R., et al. (2011). Overview of the CCP4 suite and current developments. Acta Crystallogr. D Biol. Crystallogr. 67, 235–242. doi: 10.1107/S0907444910045749 Xu, X., Zhou, H., and Boyer, T. G. (2011). Mediator is a transducer of amyloid-precursor-protein-dependent nuclear signalling. EMBO Rep. 12, 216–222. doi: 10.1038/embor.2010.210

Woods, N. K., and Padmanabhan, J. (2013). Inhibition of amyloid precursor protein processing enhances gemcitabine-mediated cytotoxicity in pancreatic cancer cells. J. Biol. Chem. 288, 30114–30124. doi: 10.1074/jbc.M113.459255

Wu, H. et al. Distinct roles of muscle and motoneuron LRP4 in neuromuscular junction formation. Neuron 75, 94–107, doi: 10.1016/j.neuron.2012.04.033 (2012).

Yang, L. B., Lindholm, K., Yan, R., Citron, M., Xia, W., Yang, X. L., et al. (2003). Elevated b-secretase expression and enzymatic activity detected in sporadic Alzheimer disease. Nat. Med. 9, 3–4. doi: 10.1038/nm0103-3

Yang, Z., Cool, B. H., Martin, G. M., and Hu, Q. (2006). A dominant role for FE65 (APBB1) in nuclear signaling. J. Biol. Chem. 281, 4207–4214. doi: 10.1074/jbc. m508445200

Yuan, H., Zhai, P., M., Anderson, L., Pan, J., Thimmapaya, B., H., Koo, E., et al. (1999). Recombinant adenovirus is an appropriate vector for endocytotic protein trafficking studies in cultured neurons. J. Neurosci. Methods 88, 45–54. doi: 10.1016/S0165-0270(99)00011-4

Zambrano, N. et al., 2001. The β-Amyloid Precursor Protein APP is Tyrosine-Phosphorylated in Cells Expressing a Constitutively Active Form of the Abl Protoncogene. The Journal of Biological Chemistry, 276(23), pp.19787–19792.

Zambrano, N., Bimonte, M., Arbucci, S., Gianni, D., Russo, T., and Bazzicalupo, P. (2002). feh-1 and apl-1, the Caenorhabditis elegans orthologues of mammalian Fe65 and b-amyloid precursor protein genes, are involved in the same pathway that controls nematode pharyngeal pumping. J. Cell Sci. 115, 1411–1422.

Zambrano, N., Minopoli, G., de Candia, P., and Russo, T. (1998). The Fe65 adaptor protein interacts through its PID1 domain with the transcription factor CP2/LSF/LBP1. J. Biol. Chem. 273, 20128–20133. doi: 10.1074/jbc.273.32. 20128

Zhang, W., Coldefy, A. S., Hubbard, S. R. & Burden, S. J. Agrin binds to the N-terminal region of Lrp4 protein and stimulates association between Lrp4 and the first immunoglobulin-like domain in muscle-specific kinase (MuSK). J Biol Chem 286, 40624–40630, doi: 10.1074/jbc.M111.279307 (2011).

Zheng, H. et al., 1995. Beta-Amyloid Precursor Protein-Deficient Mice Show Reactive Gliosis and Decreased Locomotor Activity. Cell, 81(4), pp.525–531.

Zimmermann, A. M. et al. Attention-Deficit/Hyperactivity Disorder-like Phenotype in a Mouse Model with Impaired Actin Dynamics. Biol Psychiatry, doi: 10.1016/j.biopsych.2014.03.011 (2014).

Zurhove, K. et al., 2008. γ-Secretase Limits the Inflammatory Response Through the Processing of LRP1. Science Signaling, 1(47), p.ra15 LP-ra15.

Appendix

Supplemental Material: Chapter I

FE65 and FE65L1 share common synaptic functions and genetically interact with the APP family in neuromuscular junction formation

Paul Strecker[1], Susann Ludewig[3], Marco Rust[2,4], Tabea A. Mundinger[5], Andreas Görlich[2], Elisa G. Krächan[2], Christina Mehrfeld[1], Joachim Herz[6], Martin Korte[3], SuzanneY. Guénette[7,*] & Stefan Kins[1,5,*]

[1]Division of Human Biology and Human Genetics, Erwin-Schrödinger-Straße13, 67663 Kaiserslautern, Germany. [2]Division of Animal Physiology, University of Kaiserslautern, Erwin-Schrödinger-Straße 13, 67663 Kaiserslautern, Germany. [3]Department of Cellular Neurobiology, Technical University of Braunschweig, Spielmannstraße 7, 38106 Braunschweig, Germany. [4]Institute of Physiological Chemistry, University of Marburg, Karl-von-Frisch-Straße 1, 35032 Marburg, Germany. [5]Centre for Molecular Biology (ZMBH) University of Heidelberg, Im Neuenheimer Feld 282, 69120 Heidelberg, Germany. [6]Center for Translational Neurodegeneration Research, UT Southwestern, Dallas, TX, USA. [7]Genetics and Aging Research Unit, MassGeneral Institute for Neurodegenerative Disease, Department of Neurology, Massachusetts General Hospital, Harvard Medical School, Boston, MA, USA.

[*]These authors contributed equally to this work.

Supplementary Figure S1: Morris Water Maze analysis of FE65/FE65L1-DKO mice.

(**a**) Mice were trained for five days in a pool filled with opaque water. The platform was located 0.5 cm beneath the water surface and the time to find the platform was measured. (**b**) On the 6th day the hidden-platform probe trial was performed by removing the platform and measuring the time of residence in each quadrant. (**c**) After one day without training, the platform was placed in the opposite quadrant and the mice were trained in this new setting for four days. (**d**) On the last day the platform was removed for the reversal learning probe trial and the time of residence in each quadrant was measured. The number of mice is given in brackets. Data from learning phases (Hidden Platform and Reverse Hidden Platform) were analyzed by two-way repeated measures ANOVA (Greenhouse-Geisser correction). Probe trial data were analyzed by two-way ANOVA followed by Bonferroni´s post-hoc test. Error bars are given as s.e.m.. * p< 0,05; ** p< 0,01; *** p< 0,001; n.s. for not significant.

a

b
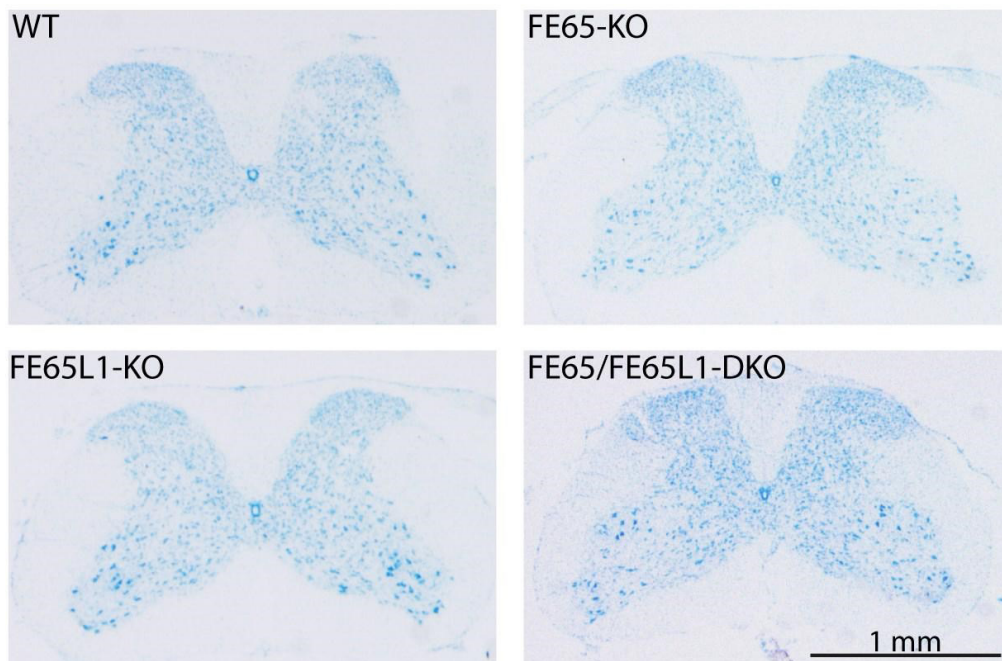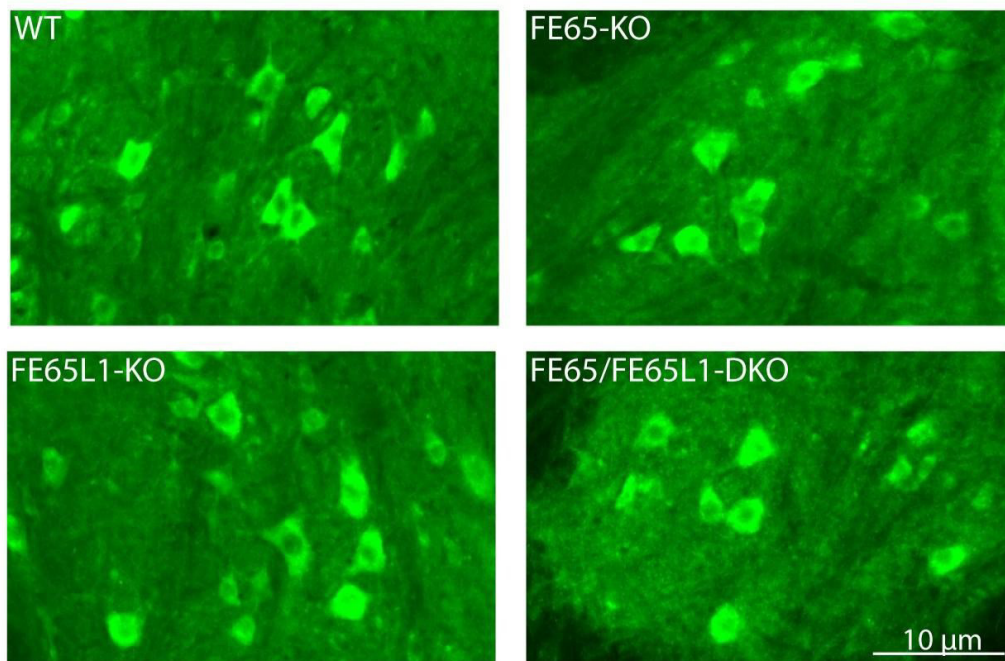
Supplementary Figure S2: No obvious morphological and neuronal changes in spinal cord stainings of FE65 family KO mice.

(a) Nissl staining of coronal sections of spinal cord segment ~C8-C6 of 6-8 month old WT, FE65-KO, FE65L1-KO and FE65/FE65L1-DKO mice. **(b)** Choline acetyltransferase staining (#178850, Abcam) of motor neurons in the anterior horn of coronal sections of spinal cord segment ~C8-C6 of 6-8 month old WT, FE65-KO, FE65L1-KO and FE65/FE65L1-DKO mice.

Supplementary Video S1: Open-field behavior of WT and FE65/FE65L1-DKO mice.

The behavior of WT, FE65-KO, FE65L1-KO and FE65/FE65L1-DKO mice was recorded for 1h. In this video several sequences (after 30 seconds as well as 10, 30 and 50 minutes) of the recording (1h) from a representative WT and FE65/FE65L1-DKO mouse in the open field is shown.

Supplementary Video S2: Behavior of WT and FE65/FE65L1-DKO mice in the visible platform version of the Morris water maze test.

FE65-KO, FE65L1-KO and FE65/FE65L1-DKO mice (4-6 months-old) were trained using a platform placed 0.5 cm beneath the water surface and marked with a black pencil in a pool filled with opaque water. This video shows behavior of a representative WT and FE65/FE65L1-DKO mouse in the visible platform version of the MWM test during the 4th trial. Notable, FE65/FE65L1-DKO mice appeared disoriented.

Supplementary Video S1 and S2 are provided in the supplemental CD-ROM of this thesis.

Supplemental Material: Chapter II

Fe65-PTB2 Dimerization Mimics Fe65-APP Interaction

Lukas P. Feilen [1†], Kevin Haubrich [1,2†], **Paul Strecker** [3], Sabine Probst [4], Simone Eggert [3], Gunter Stier [1], Irmgard Sinning [1], Uwe Konietzko [4], Stefan Kins [3], Bernd Simon [2] and Klemens Wild [1*]

[1]Heidelberg University Biochemistry Center (BZH), University of Heidelberg, Heidelberg, Germany, [2]European Molecular Biology Laboratory (EMBL), Structural and Computational Biology, Heidelberg, Germany, [3]Division of Human Biology and Human Genetics, University of Kaiserslautern, Kaiserslautern, Germany, [4]Institute for Regenerative Medicine (IREM), University of Zurich, Zurich, Switzerland

†These authors have contributed equally to this work.

A

SEC of Fe65-PTB2
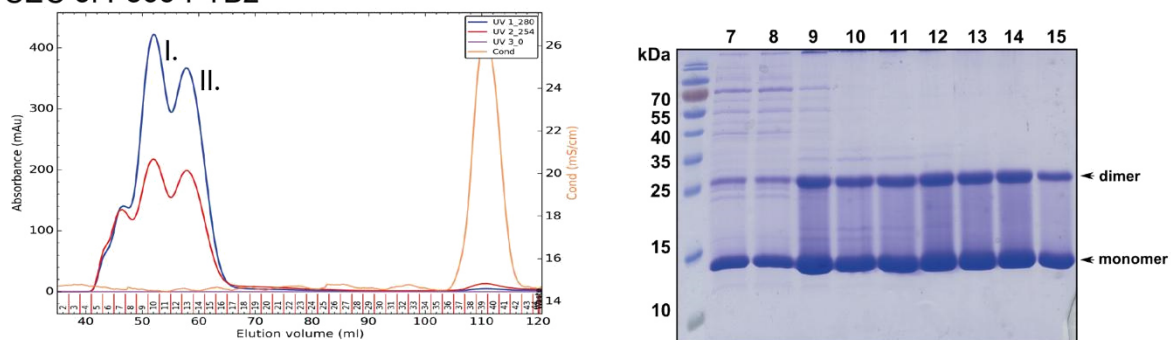
B

MALS:

peak I.

peak II.
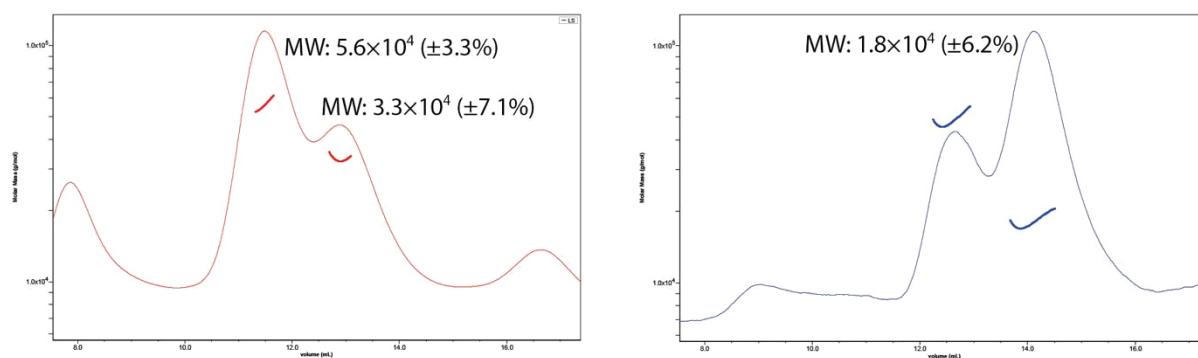
Figure S1. Biochemical evidence for Fe65 oligomerization.

(**A**) Elution diagrams for size exclusion chromatography (SEC, S75 16/600) of Fe65-PTB2 and according SDS-PAGE. The protein elutes in two major peaks and appears in the gel as partially detergent-resistant dimer indicating a very hydrophobic interaction of the subunits. (**B**) Re-chromatographed peaks I. and II. (S75 10/300 coupled with multi-angle light scattering (MALS)) reveal partitioning in monomeric (MW: 18 kDa, theoretical: 15.4 kDa), dimeric (MW: 33 kDa), and tetrameric (MW: 56 kDa) species.
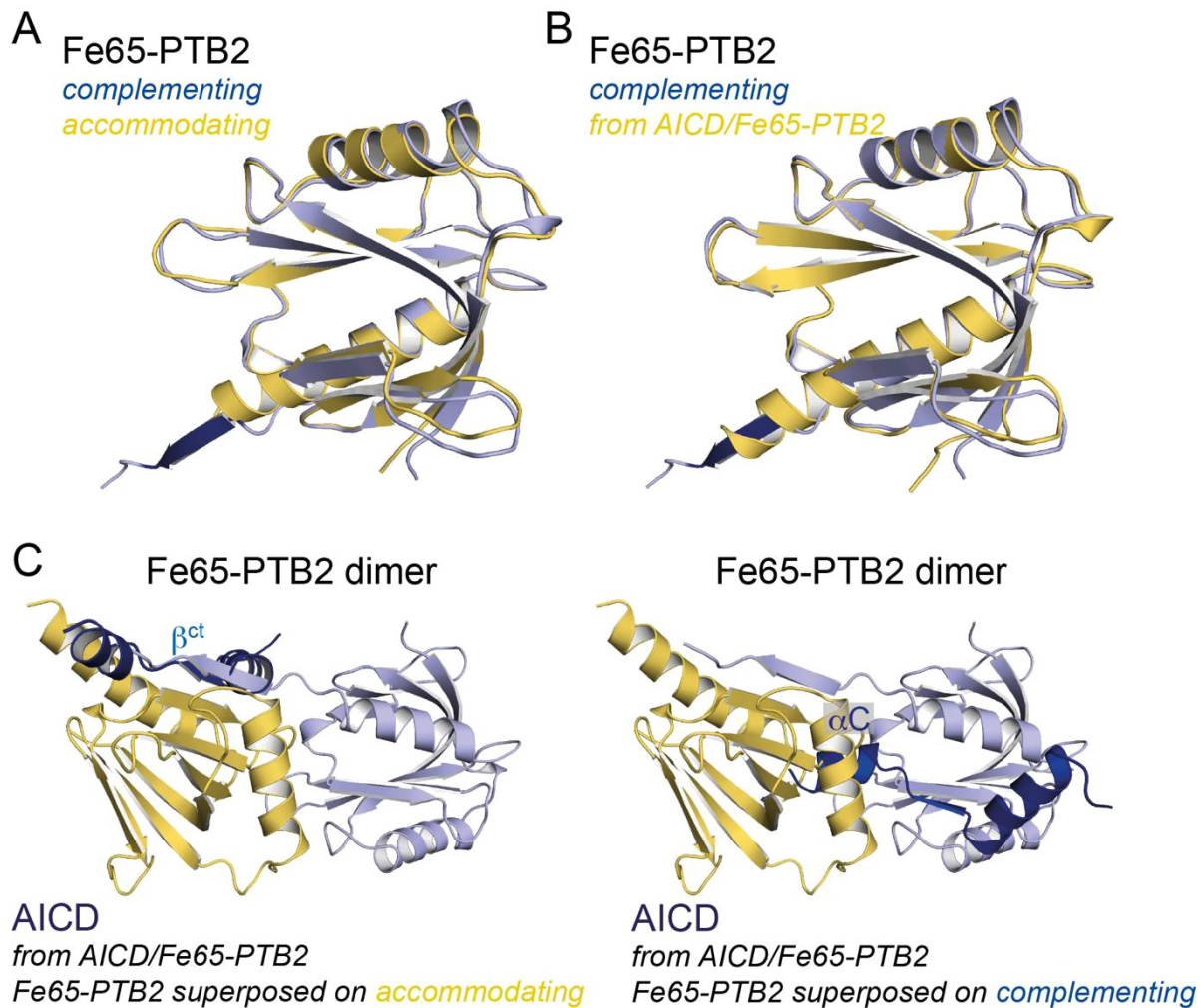
Figure S2. Structural superpositions.

(**A**) The two subunits of the Fe65-PTB2 dimer. The subunits adopt identical conformations except the C-terminus. The C-terminus is flexible and in the complementing subunit forms strand β^{ct} (dark blue). (**B**) The accommodating Fe65-PTB2 subunit superposed on Fe65-PTB2 from the AICD/Fe65-PTB2 complex (PDB code 3dxc; (Radzimanowski et al., 2008)). In the complex, the C-terminal helix is fully formed and stabilized by the AICD (not shown). (**C**) The AICD and the Fe65-PTB2 dimer. Left panel: The binding site for the central β-strand of the AICD (GYE sequence) in the accommodating subunit is blocked by strand β^{ct} of the complementing subunit. Right panel: The binding site for helix αC of the AICD in the complementing subunit is blocked by the accommodating subunit. The superpositions are based on the respective Fe65-PTB2 subunits with Fe65-PTB2 (not shown for clarity) of the AICD/Fe65-PTB2 complex.
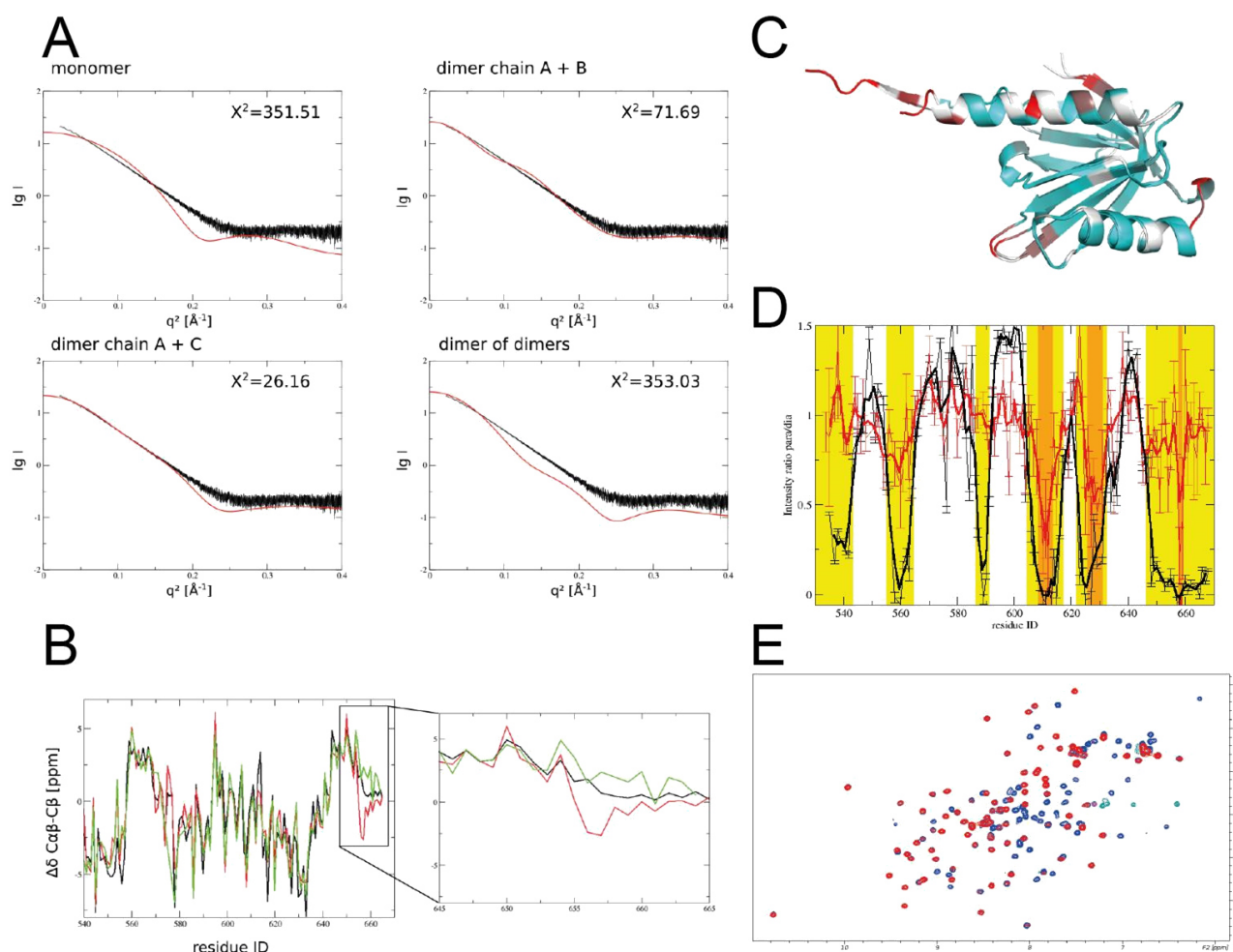
Figure S3. Biophysical characterization of the Fe65-PTB2 dimer in solution.

(**A**) Fit of the experimental SAXS data extrapolated to infinite dilution to monomer (chain A, complementing), dimers (chain A+C, C: accommodating; A+B, B: alternative accommodating subunit) or dimer of dimers of the X-ray structure suggest that the protein is not monomeric in solution. The best fit is achieved for dimer (A+C). The experimental radius of gyration of 24.4±3.4 Å compares to theoretical values of 17.1 Å (monomer chain A), 23.2 Å (dimer chain A+C), 29.6 Å (dimer chain A+B) and 25.7 Å (dimer of dimers). (**B**) Secondary chemical shift differences of carbon Cα and Cβ atoms ($\Delta\delta$Cαβ-Cβ). The experimental values for the C-terminal helix (black) are in between the values predicted from the coordinates of the complementing and accommodating subunits. (**C**) Color representation of the ^{15}N spin-relaxation data derived backbone order parameters S^2 (Fig. 2C) on the structure of the superimposed chains A and C of the X-ray structure, with a color gradient from cyan (high S^2) to red (low S^2) and residues with no experimental data in gray. Fast timescale backbone motions are present for the N-terminus, two loop regions and the C-terminal helix. (**D**) Plot of the peak intensity ratios of ^{1}H-^{15}N HSQC spectra with reduced and oxidized nitroxide spin label for the ^{15}N/nitroxide labeled sample (yellow) and the mixed ^{15}N-only and nitroxide proteins (orange). The continuous line corresponds to a three-point average of the data points and the colored boxes correspond to the colors used for the protein surface plot in Fig. 2D. (**E**) Typical HSQC spectra of Fe65-PTB2 C633E with reduced (blue) and oxidized (red) spin labels.
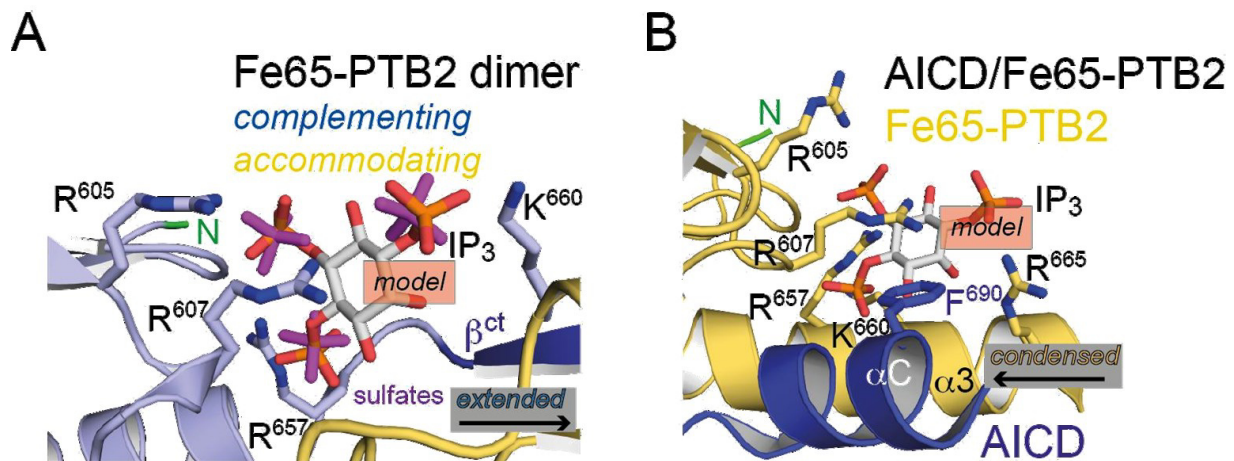
Figure S4. A basic patch for PIP$_2$ binding.

(A) The spatial arrangement of three sulfate ions bound to a highly basic surface patch in the Fe65-PTB2 dimer interface perfectly match to the three phosphoryl-moieties of the IP$_3$ head-group of phosphatidyl-inositol-4,5-bisphosphate (PIP$_2$). In the complementing subunit, strand β^{ct} is part of the extended patch. Of note, also the N-terminus of Fe65-PTB2 (green) and thus the PTB1-PTB2 linker region locates next to the basic cluster. (B) Within the AICD/Fe65-PTB2 complex, the C-terminal AICD helix αC would complement the now condensed PIP$_2$-binding binding site. A solvent exposed phenylalanine (F^{690}) of the AICD would be perfectly located to interact with the inositol ring, a structural motif characteristic for protein-carbohydrate complexes (Hsu et al., 2016). Condensing of the patch results in the contribution of in total three charges (R^{657}, K^{660}, and R^{665}) from the C-terminal helix α3 of Fe65-PTB2 to the cluster. While in the extended patch arginine R^{665} is involved in the intramolecular salt-bridge in strand β^{ct} (Fig. 3a, right panel), it would contribute to PIP$_2$-binding in the condensed state.

References

Hsu, C.H., Park, S., Mortenson, D.E., Foley, B.L., Wang, X., Woods, R.J., Case, D.A., Powers, E.T., Wong, C.H., Dyson, H.J. *, et al.* (2016). The Dependence of Carbohydrate-Aromatic Interaction Strengths on the Structure of the Carbohydrate. J Am Chem Soc *138*, 7636-7648.

Radzimanowski, J., Simon, B., Sattler, M., Beyreuther, K., Sinning, I., and Wild, K. (2008). Structure of the intracellular domain of the amyloid precursor protein in complex with Fe65-PTB2. EMBO Rep *9*, 1134-1140.

Supplemental Material: Chapter III

LRP1 Modulates APP Intraneuronal Transport and Processing in Its Monomeric and Dimeric State

Uta-Mareike Herr [1][†], Paul Strecker [2][†], Steffen E. Storck [1], Carolin Thomas [2], Verena Rabiej [1], Anne Junker [1], Sandra Schilling [2], Nadine Schmidt [2], C. Marie Dowds [2], Simone Eggert [2], Claus U. Pietrzik [1][*][†] and Stefan Kins [2][*][†]

[1] Institute of Pathobiochemistry, Molecular Neurodegeneration, University Medical Center of the Johannes Gutenberg-University Mainz, Mainz, Germany, [2] Division of Human Biology and Human Genetics, Technical University of Kaiserslautern, Kaiserslautern, Germany

†These authors have contributed equally to this work.

Y188, α-APP CT

Supplementary Figure 1: Blue native gel analysis of APP-GFP in comparison to APP-F1.

APP-GFP or APP-F1 (containing one FKBP domain fused to the C-terminus of APP) were heterologously expressed in N2a cells. 18-20 hours after transfection and 1 hour prior harvesting, APP-F1 expressing cells were treated with 100 nM AP20187 (dimerizer), which binds two FKBP molecules to induce dimerization of APP as described in Eggert et al. (2009). Treatment with the vehicle of the dimerizer, ethanol, served as a negative control. Membrane fractions of indicated cells were analyzed via blue native gel analysis (Eggert et al., 2009). Antibody Y188 (Abcam) directed against the C-terminus of APP was used to detect monomeric and dimeric APP. Note the predominantly monomeric state of APP-GFP and ethanol treated APP-F1 cells in comparison to APP-F1 cells treated with dimerizer.
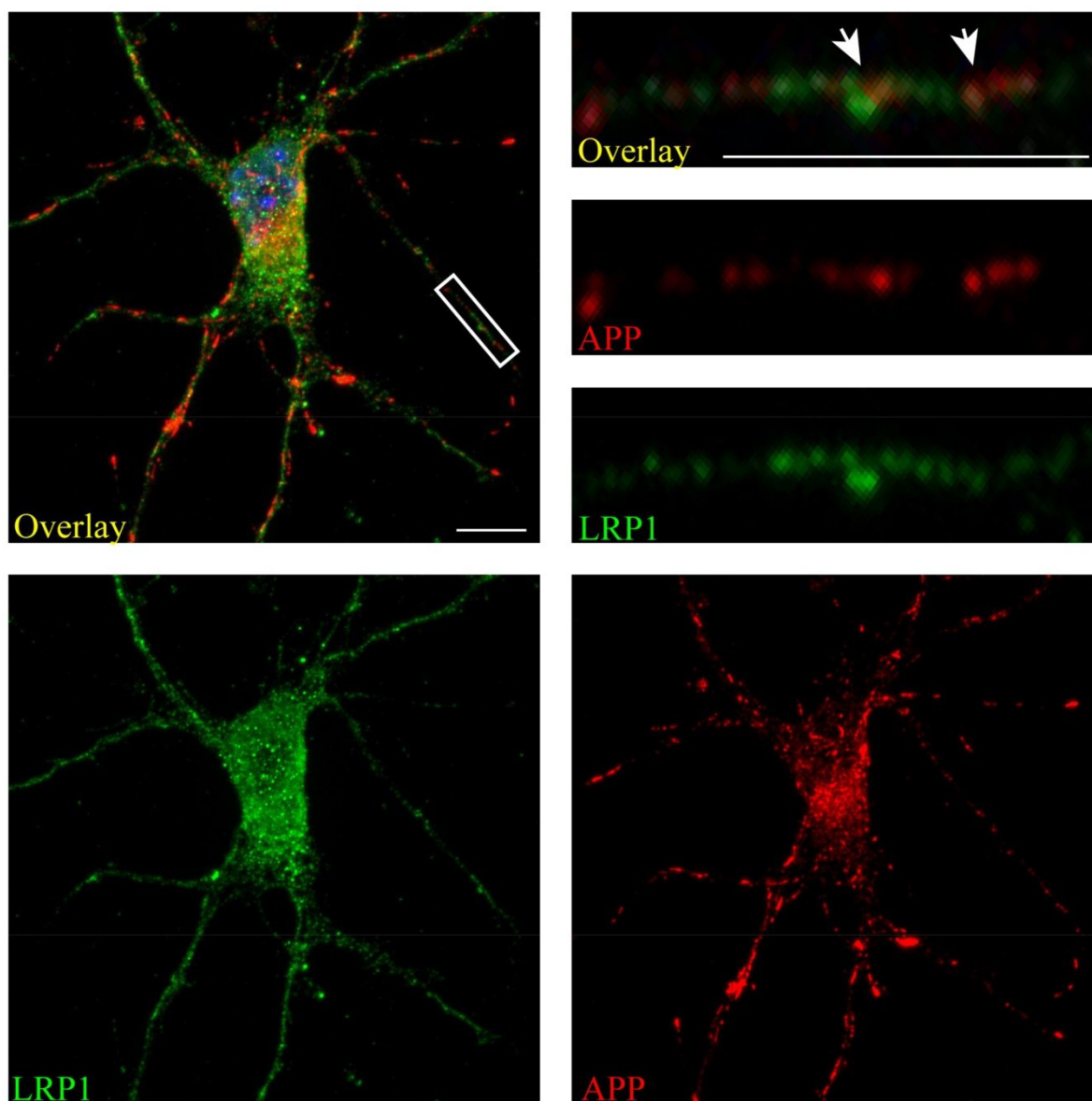
Supplementary Figure 2: Co-localization of LRP1 and APP in primary cortical neurons.

Immunocytochemical analysis of primary cortical neurons differentiated for 7 days in vitro. Endogenous APP (red) and LRP1 (green) were stained with C1/6.1 and 1704 (Pietrzik et al., 2002), respectively. Hoechst 33258 was used for nuclear counterstaining (blue). Co-localization is indicated in yellow. The outlined region in the overlay is enlarged in the upper right panels. Please note the high degree of co-localization of APP and LRP1 immunoreactivity in the cytoplasmic region and the low partial overlap in neurites (indicated by arrow heads). Scale bar: 5 µm.
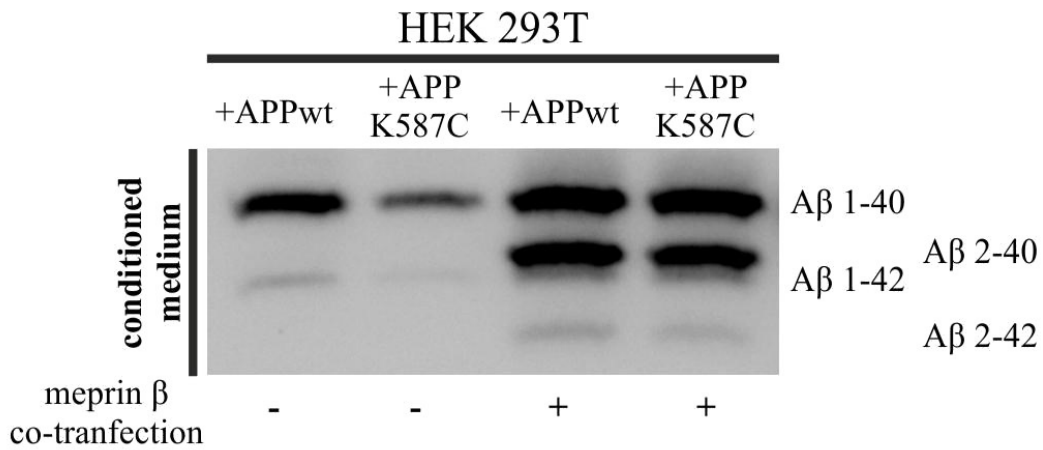
Supplementary Figure 3: Meprin β overexpression affects Aβ generation.

Urea SDS-PAGE of immunoprecipitated Aβ from the conditioned medium of HEK 293T cells 24 hours after transfection. Peptides were detected by the IC16 antibody (1:500). Cells were transiently transfected with either APP695 wt or APP695 K587C or co-transfected with meprin β. Transfections with the APP constructs alone served as controls. In APP695 K587C transfected cells additionally expressing meprin β, levels of truncated Aβ species (2-40 and 2-42) were raised to the same amount as deserved for cells transfected with APP695 wt and meprin β. Note, that in the corresponding controls Aβ generation from the APP dimer bearing construct was reduced compared to that derived from wildtype APP.

Supplementary Video 1: Live Cell imaging of APP-F1-GFP transfected primary cortical neuron.

Murine cortical primary neurons (DIV 6) were transiently transfected with an expression construct encoding APP-F1-GFP. After 18–20 h live cell recording of vesicle movements were performed.

Supplementary Video 2: Live Cell imaging of LRP1-GFP transfected primary hippocampal neuron.

Murine hippocampal primary neurons (DIV 6) were transiently transfected with an expression construct encoding LRP1-GFP. After 18–20 h live cell recording of vesicle movements were performed.

Supplementary Video 1 and 2 are provided in the supplemental CD-ROM of this thesis.

References

Eggert, S., Midthune, B., Cottrell, B., and Koo, E. H. (2009). Induced dimerization of the amyloid precursor protein leads to decreased amyloid-β protein production. J. Biol. Chem. 284, 28943–28952. doi: 10.1074/jbc.M109. 038646

Pietrzik, C. U., Busse, T., Merriam, D. E., Weggen, S., and Koo, E. H. (2002). The cytoplasmic domain of the LDL receptor-related protein regulates multiple steps in APP processing. EMBO J. 21, 5691–5700. doi: 10.1093/emboj/cdf568

Acknowledgements

Curriculum vitae

Personal Data

Name   Paul Strecker

Eduaction

04/2013 – today   Ph.D. student, Department of Human Biology and Human Genetics, University of Kaiserslautern
Topic: Analyse von Fe65/Fe65L1 an Knockout Mausmodellen

10/2005 – 12/2012 Diploma, Department of Human Biology and Human Genetics, University of Kaiserslautern
Topic: Analyse der Fe65-Proteinfamilie; Auswirkungen auf die neuromuskuläre Endplatte des Triangularis sterni, sowie die Synaptosomenzusammensetzung im Gehirn und das Aktinzytoskelett in MEF-Zellen

Scientific Presentation

July 2016	10th FENS, Forum of Neuroscience; Copenhagen, Denmark
	poster title: FE65 and FE65L1 share common synaptic functions and genetically interact with the APP family
January 2016	8th Tschagguns Meeting 'Cellular and molecular processes in neurodegenerative diseases'; Tschagguns, Austria
	oral presentation: The role of Fe65 in CNS development.
March 2015	12th AD/PD, International Conference on Alzheimer`s and Parkinsons Disease; Nice, France
	poster title: The APP adaptor proteins Fe65 and Fe65L1 are essential for locomotor activity, NMJ formation and learning
December 2014	Annual seminar of the Faculty of Biology, University of Kaiserslautern, Thallichtenberg, Germany
	oral presentation: Fe65 matters -Behavioral analysis of KO mice-
July 2014	3rd Biennial Meeting of the Rhine Main Neuroscience Network RMN^2; Oberwesel, Germany
	poster title: The APP adaptor proteins Fe65 and Fe65L1 are essential for locomotor activity, NMJ formation and learning
January 2014	6th Tschagguns Meeting 'Cellular and molecular processes in neurodegenerative diseases'; Tschagguns, Austria
	oral presentation: Analysis of the Fe65 protein family.
January 2014	'Current topics in neurobiology'; Kaiserslautern, Germany
	oral presentation: Analysis of the Fe65 protein family; Influence on Neuromuscular Junction (NMJ) and behavioral/locomotor studies of KO mice

Publications

Eggert, S., Gonzalez, A.C., Thomas, C., Schilling, S., Schwarz, S.M., Tischer, C., Adam, V., **Strecker, P.**, Schmidt, V., Willnow, T.E., Hermey, G., Pietrzik, C.U., Koo, E.H., Kins, S., (2017) Dimerziation leads to changes in APP (Amyloid Precursor Protein) trafficking mediated by LRP1 and SorLA. Journal of Cellular and Molecular Life Scienc: DOI 10.1007/s00018-017-2625-7

Sandra Schilling, Annika Mehr, Susann Ludewig, Jonathan Stephan, Marius Zimmermann, Alexander August, **Paul Strecker**, Martin Korte, Edward H. Koo, Ulrike C. Müller, Stefan Kins and Simone Eggert. APLP1 Is a Synaptic Cell Adhesion Molecule, Supporting Maintenance of Dendritic Spines and Basal Synaptic Transmission. Journal of Neuroscience 24 May 2017, 37 (21) 5345-5365

Lukas P. Feilen, Kevin Haubrich, **Paul Strecker**, Sabine Probst, Simone Eggert, Gunter Stier, Irmgard Sinning, Uwe Konietzko, Stefan Kins, Bernd Simon and Klemens Wild. Fe65-PTB2 Dimerization Mimics Fe65-APP Interaction. Front. Mol. Neurosci., 11 May 2017

Uta-Mareike Herr[†], **Paul Strecker**[†], Steffen E. Storck, Carolin Thomas, Verena Rabiej, Anne Junker, Sandra Schilling, Nadine Schmidt, C. Marie Dowds, Simone Eggert, Claus U. Pietrzik and Stefan Kins. LRP1 Modulates APP Intraneuronal Transport and Processing in Its Monomeric and Dimeric State. Front. Mol. Neurosci., 27 April 2017

Suzanne Guénette, **Paul Strecker** and Stefan Kins. APP Protein Family Signaling at the Synapse: Insights from Intracellular APP-Binding Proteins. Front. Mol. Neurosci., 30 March 2017

Paul Strecker, Susann Ludewig, Marco Rust, Tabea A. Mundinger, Andreas Görlich, Elisa G. Krächan, Christina Mehrfeld, Joachim Herz, Martin Korte, Suzanne Y. Guénette & Stefan Kins. FE65 and FE65L1 share common synaptic functions and genetically interact with the APP family in neuromuscular junction formation. Scientific Reports 6, Article number: 25652 (2016)